9 July 2010 | $10

Science

HIV/AIDS

Eastern Europe

AAAS

Efficiency Expert.

3500 Series Genetic Analyzer

Every lab needs one.

Are you that type? Always looking for ways to simplify and streamline lab processes—like, for example, the cumbersome and imprecise chores of handling and tracking consumables? Well, with a revolutionary new suite pre-formulated, ready-to-use, RFID-trackable consumables, the 3500 Series Genetic Analyzer *is* that type, too. Just snap in and run.

Make it Yours.

Easy-to-Use Consumables

Control at Your Fingertips

Quality-Assured Data

www.appliedbiosystems.com/3500Series

applied biosystems™
by life technologies™

cell sciences®

Buy two - Get three!

Buy two recombinant proteins and get an additional protein free for a limited time on any of our popular items listed below. Mention offer code RP342 when ordering. Visit www.cellsciences.com for details.

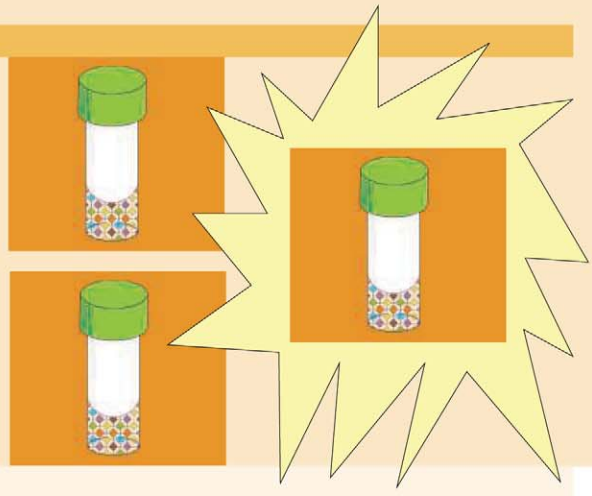

www.cellsciences.com

Recombinant human proteins

BD1 (47 aa)
BD2
BD3
BD4
BLC/BCA1/CXCL13
BMP2
BMP4
CCL14
CD40 Ligand
CNTF
CXCL1
CXCL10/IP10
CXCL11/I-TAC
CXCL2
CXCL3/MIP2 beta
EGF
ENA78/CXCL5
Eotaxin
Eotaxin-2
Exodus-2
FGF1 (aa 141)
FGF7
FGF10/KGF2
FLT3 Ligand
Fractalkine
GCSF
GH1
GM-CSF
IFN alpha 2b
IFN beta 1b
IFN gamma
IGF1
IGFBP3
IL1 alpha
IL1 beta
IL1RA
IL2
IL3
IL4
IL6
IL8 (72 aa)
IL8 (77 aa)
IL10
IL11
IL12
IL13
IL15
IL17
IL21
IL31
IL33
LEC
MCP1
MCP2
MCP4
M-CSF
MEC/CCL28
MIA-2
MICA
MIF
MIG
MIP-1 alpha
MIP-1 beta
MIP-3 alpha/CCL20
MIP-3/CCL23
MIP-4/CCL18
MIP-5/CCL15
NAP-2/CXCL7
Noggin
NRG1
NT4
RANTES
SCF
SDF-1 alpha
TARC/CCL17
TNF alpha
TPO
VEGF

Recombinant mouse proteins

CXCL2
CXCL16
EGF
FGF2
GM-CSF
IFN gamma
IL2
IL3
IL4
IL11
IL33
LIX/CXCL5
MCP2
Noggin
SDF-1 beta
SF20
TNF alpha
VEGF

Recombinant rat proteins

EGF
FGF2
IFN gamma
SDF-1a/CXCL12
SDF-1b/CXCL12

Other recombinant proteins

Protein A/G
Staphylokinase
Streptokinase

Offer good for any combination of three items on the list above. Products are for research use only. Not for human use. Not for use in diagnostic or therapeutic procedures.

CELL SCIENCES INC • 480 NEPONSET STREET, BUILDING 12A, CANTON, MA 02021 • INFO@CELLSCIENCES.COM

TOLL FREE: (888) 769-1246 • TEL: (781) 828-0610 • FAX: (781) 828-0542 • WEB: WWW.CELLSCIENCES.COM

Submission deadline August 1

Your name here.

The GE & Science Prize for Young Life Scientists. Because brilliant ideas build better realities.

Imagine standing on the podium at the Grand Hotel in Stockholm, making your acceptance speech for the GE & Science Prize for Young Life Scientists. Imagine having your essay read by your peers around the world. Imagine discussing your work in a seminar with other prize winners and Nobel Laureates. Imagine what you could do with the $25,000 prize money. Now stop imagining. If you were awarded your Ph.D. in molecular biology in 2009, then submit your 1000-word essay by August 1, and you can make it reality.

Want to build a better reality? Go to www.gescienceprize.org

GE & Science Prize for Young Life Scientists

imagination at work

Science AAAS

* For the purpose of this prize, molecular biology is defined as "that part of biology which attempts to interpret biological events in terms of the physico-chemical properties of molecules in a cell".

(McGraw-Hill Dictionary of Scientific and Technical Terms, 4th Edition).

28-9402-06AB

SPECIAL SECTION

HIV/AIDS

INTRODUCTION

NEWS

REVIEW

>> Editorial p. 120, Policy Forums pp. 145 and 147, Science *Express Research Article by T. Zhou* et al., Science *Express Report by X. Wu* et al., *and* Science *Careers and* Science *Translational Medicine p. 117 and www.sciencemag.org/special/aids2010/*

page 132

EDITORIAL

NEWS OF THE WEEK

NEWS FOCUS

LETTERS

BOOKS *ET AL.*

POLICY FORUMS

PERSPECTIVES

CONTENTS continued >>

COVER

Sergey Nenov gives thanks at a church in Odessa, Ukraine. HIV, tuberculosis, and injecting drug use are tightly linked in Eastern Europe, the only region in the world with a growing HIV/AIDS epidemic. Nenov is one of the few people with access to treatment for both infections and opiate dependency. See the special section on HIV/AIDS beginning on page 159 and at www.sciencemag.org/special/aids2010/.

Photo: Malcolm Linton

DEPARTMENTS

Rotor-Gene Q — pure detection

- Enjoy a real-time PCR cycler with outstanding thermal and optical performance
- Perform multiple real-time PCR applications and optional high-resolution melting
- Benefit from a variety of state-of-the-art analyses
- Experience unrivaled robustness and minimal maintenance
- Count on reliable results from QIAGEN kits and assays

Discover more at www.qiagen.com/goto/PureDetection.

QIAGEN®

AUTORGQ01105 1WW

Sample & Assay Technologies

CONTENTS continued >>

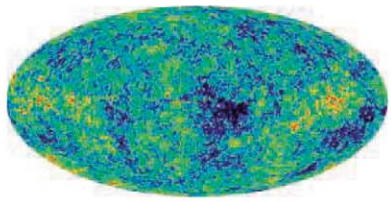

page 144

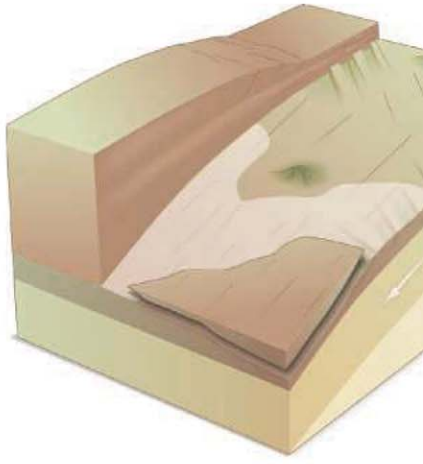

pages 152, 207, & 210

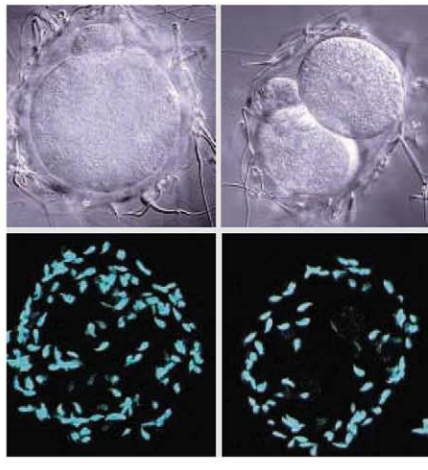

page 216

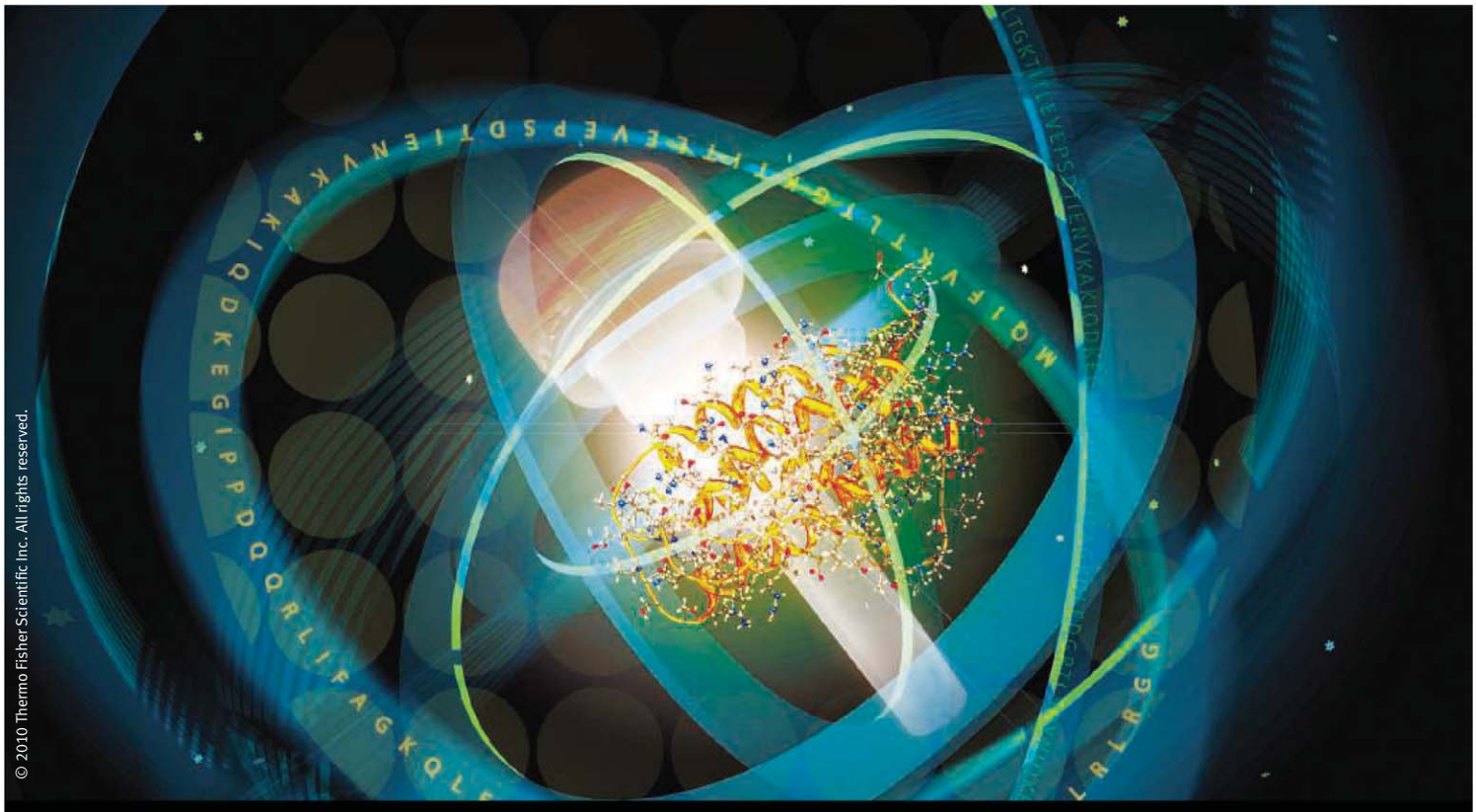

An exceptional spin on high-performance desalting.

Thermo Scientific Zeba Desalting Products provide a flexible platform for desalting multiple samples across a range of protein concentrations and sample volumes. The high-performance Zeba™ Resin offers exceptional desalting and protein recovery results, requiring no chromatographic system, cumbersome column preparation or equilibration.

- › 95% removal of contaminants
- Process 2 µl to 4 ml of sample in only 6 minutes with exceptional protein recovery
- Sample collection in one fraction eliminates dilution
- Wide product offering meeting your sample needs – 0.5, 2, 5 and 10 ml spin columns and 96-well spin plates
- Available with 7K and 40K MWCOs

For more information, visit www.thermoscientific.com/pierce

Quick desalting with exceptional recovery.
Easy-to-use spin column format, 96-well spin plates and chromatography cartridges dramatically improve results over standard drip-column methodologies.

Moving science forward

Thermo SCIENTIFIC
Part of Thermo Fisher Scientific

SCIENCEONLINE

SCIENCEXPRESS
www.sciencexpress.org

Global Convergence in the Temperature Sensitivity of Respiration at Ecosystem Level
M. D. Mahecha et al.
The long-standing discrepancy between modeled and empirical measures of ecosystem temperature sensitivity is resolved.
10.1126/science.1189587

Terrestrial Gross Carbon Dioxide Uptake: Global Distribution and Covariation with Climate
C. Beer et al.
A combination of data and models provides an estimate of how much photosynthesis by all the world's plants occurs each year.
10.1126/science.1184984

Structural Basis for Broad and Potent Neutralization of HIV-1 by Antibody VRC01
T. Zhou et al.
10.1126/science.1192819

Rational Design of Envelope Identifies Broadly Neutralizing Human Monoclonal Antibodies to HIV-1
X. Wu et al.
A human antibody achieves broad neutralization by binding the viral site of recognition for the primary host receptor, CD4.
10.1126/science.1187659
>> HIV/AIDS section p. 159

High-Resolution Analysis of Parent-of-Origin Allelic Expression in the Mouse Brain
C. Gregg et al.
A large repertoire of genes shows preferential expression of the paternally or maternally inherited allele.
10.1126/science.1190830

Sex-Specific Parent-of-Origin Allelic Expression in the Mouse Brain
C. Gregg et al.
The relative contributions of the paternal and maternal genomes differ in distinct brain regions and also in males and females.
10.1126/science.1190831

Long Noncoding RNA as Modular Scaffold of Histone Modification Complexes
M.-C. Tsai et al.
The long noncoding RNA HOTAIR binds two distinct protein complexes that modify chromatin and repress transcription.
10.1126/science.1192002

TECHNICALCOMMENTS

Comment on "Differential Sensitivity to Human Communication in Dogs, Wolves, and Human Infants"
S. Fiset
Full text at www.sciencemag.org/cgi/content/full/329/5988/142-b

Comment on "Differential Sensitivity to Human Communication in Dogs, Wolves, and Human Infants"
S. Marshall-Pescini et al.
Full text at www.sciencemag.org/cgi/content/full/329/5988/142-c

Response to Comments on "Differential Sensitivity to Human Communication in Dogs, Wolves, and Human Infants"
J. Topál et al.
Full text at www.sciencemag.org/cgi/content/full/329/5988/142-d

SCIENCENOW
www.sciencenow.org
Highlights From Our Daily News Coverage

Moon's Craters Hold Clues to the Lunar Interior
The Kaguya lunar orbiter finds possible similarities between the moon's and Earth's mantles.

Did Mammoth Extinction Warm Earth?
A sudden surge in northern birch forests 15,000 years ago is linked to climate change.

Friendly Baboons Live Longer
Study shows that people are not the only ones to benefit from having many friends.

SCIENCESIGNALING
www.sciencesignaling.org
The Signal Transduction Knowledge Environment

RESEARCH ARTICLE: Error Minimization in Lateral Inhibition Circuits
O. Barad et al.

PODCAST
N. Barkai and A. M. VanHook
Lateral inhibition in proneuronal clusters in the fruit fly relies on competition between cis and trans Notch signaling.

MEETING REPORT: Zinc Bells Rang in Jerusalem!
M. Hershfinkel et al.
Researchers met to discuss zinc signaling in health and disease.

SCIENCECAREERS
www.sciencecareers.org/career_magazine
Free Career Resources for Scientists

Getting to Know the Enemy
E. Pain
Russian epidemiologist Elena Dukhovlinova studies genetic diversity and transmission of HIV circulating in St. Petersburg.
>>HIV/AIDS section p. 159 and www.sciencemag.org/special/aids2010/

Taken for Granted: The Immigration Guru
B. L. Benderly
In a debate long dominated by industry voices, statistician and technology expert Norman Matloff speaks up for the little people.

SCIENCETRANSLATIONAL MEDICINE
www.sciencetranslationalmedicine.org
Integrating Medicine and Science

EDITORIAL: Recombinant Innovation and Translational Science Trainees
F. J. Meyers
Diversely trained young scholars form the center of an innovation network in translational medicine.

PERSPECTIVE: Twenty-Five Years of Translational Medicine in Antiretroviral Therapy—Promises to Keep
S. Broder

PODCAST
S. Broder and A. M. VanHook
Early translational research on dideoxynucleoside drugs set HIV-1/AIDS on a hopeful path.
>>HIV/AIDS section p. 159 and www.sciencemag.org/special/aids2010/

RESEARCH ARTICLE: A Generalized Linear-Quadratic Model for Radiosurgery, Stereotactic Body Radiation Therapy, and High–Dose Rate Brachytherapy
J. Z. Wang et al.
A mathematical model enables better treatment planning for current high-dose cancer therapies.

SCIENCEPODCAST
www.sciencemag.org/multimedia/podcast
Free Weekly Show

Download the 9 July *Science* Podcast to hear about HIV/AIDS in Eastern Europe, adaptation to parasites via symbiosis, why fireflies synchronize, and more.

SCIENCEINSIDER
news.sciencemag.org/scienceinsider
Science Policy News and Analysis

SCIENCE (ISSN 0036-8075) is published weekly on Friday, except the last week in December, by the American Association for the Advancement of Science, 1200 New York Avenue, NW, Washington, DC 20005. Periodicals Mail postage (publication No. 484460) paid at Washington, DC, and additional mailing offices. Domestic individual membership and subscription (51 issues): $146 ($74 allocated to subscription). Domestic institutional subscription (51 issues): $910; Foreign postage extra: Mexico, Caribbean (surface mail) $55; other countries (air assist delivery) $85. First class, airmail, student, and emeritus rates on request. Canadian rates with GST available upon request, GST #1254 88122. Publications Mail Agreement Number 1069624. **Printed in the U.S.A.**

Change of address: Allow 4 weeks, giving old and new addresses and 8-digit account number. **Postmaster:** Send change of address to AAAS, P.O. Box 96178, Washington, DC 20090–6178. **Single-copy sales:** $10.00 current issue, $15.00 back issue prepaid includes surface postage; bulk rates on request.

AAAS
ADVANCING SCIENCE, SERVING SOCIETY

EDITED BY STELLA HURTLEY

Going Multicellular >>

The volvocine algae include both the unicellular *Chlamydomonas* and the multicellular *Volvox*, which diverged from one another 50 to 200 million years ago. **Prochnik *et al.*** (p. 223) compared the *Volvox* genome with that of *Chlamydomonas* to identify any genomic innovations that might have been associated with the transition to multicellularity. Size changes were observed in several protein families in *Volvox*, but, overall, the *Volvox* genome and predicted proteome were highly similar to those of *Chlamydomonas*. Thus, biological complexity can arise without major changes in genome content or protein domains.

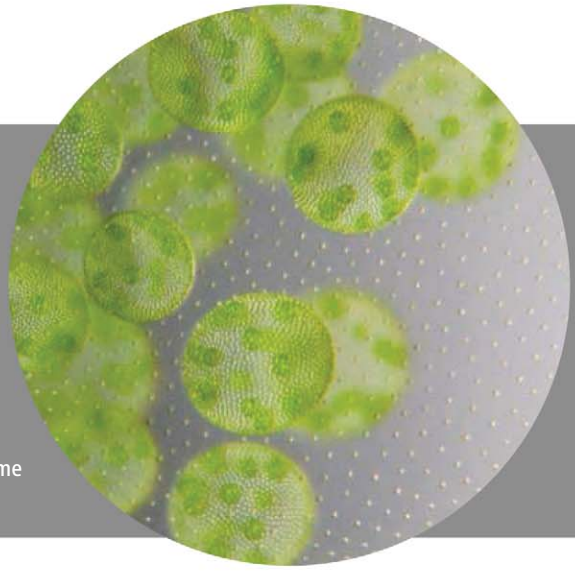

Out of the Oort Cloud

Long-period comets originate from the Oort cloud, a vast reservoir of icy bodies that surrounds the solar system. These bodies are thought to be remnants from the formation of the solar system. But did they all form in the Sun's protoplanetary disk, or could they have been generated in the protoplanetary disks of other stars in the cluster where the Sun probably formed? **Levison *et al.*** (p. 187, published online 10 June) used detailed numerical simulations to investigate what fraction of comets might transfer from the outer reaches of one stellar system to another. The simulations suggest that a substantial number of comets can be captured through this mechanism, which may explain why the number of bodies in the Oort cloud is larger than models predict.

BK Channel Cytoplasmic Domain

BK channels are potassium ion channels found on the surface of a variety of cell types that are essential for the regulation of several key physiological processes, including smooth muscle tone and neuronal excitability. BK channels are regulated by both membrane voltage and intracellular Ca^{2+}. The channel comprises an integral membrane pore, an integral membrane voltage sensor domain, and a large cytoplasmic region that confers Ca^{2+} sensitivity. Now **Yuan *et al.*** (p. 182, published online 27 May; see the Perspective **Weyand and Iwata**) have determined the crystal structure of the cytoplasmic domain of the human BK channel. Four cytoplasmic regions form a gating ring at the intracellular membrane surface with four Ca^{2+} binding sites on the outer perimeter.

Elucidating Turbulent Flow

When needing to mix two fluids rapidly, turbulent flow can be beneficial. However, in most cases, the churning and tumbling motions of a fluid during turbulent flow reduce the efficiency of a device or process. When fluid flows past a solid object, the bulk of the turbulent motion is concentrated at the surface boundary, but it is unclear to what extent these inner motions are influenced by flow far from the boundary. **Marusic *et al.*** (p. 193; see the Perspective by **Adrian**) demonstrate a nonlinear connection between inner-layer motions and the large-scale outer-layer motions in wind tunnel experiments. A simple model was able to describe the relationship mathematically while accurately mapping the experimental data.

Switching Basins

Most of the densest, deepest water at the bottom of the oceans comes from two regions, the North Atlantic and the circum-Antarctic. Have other regions been able to produce significant quantities of deep water in the past? For decades, researchers have looked, with limited success, for evidence of deepwater formation in the North Pacific since the time of the Last Glacial Maximum, about 23,000 years ago. **Okazaki *et al.*** (p. 200) combine published observational evidence from the North Pacific with model simulations to suggest that deep water did form in the North Pacific during the early part of the Last Glacial Termination, between about 17,500 and 15,000 years ago. The switch between deep-water formation in the North Atlantic and the North Pacific is likely to have had an important effect on heat transport and climate.

Nanorod Polymers

Nanoparticles and colloids have been used to model crystallization and melting phenomena. **Liu *et al.*** (p. 197) studied the polymerization kinetics of nanoparticles. Functionalized arrowhead nanorods acted as linkable units that joined together in solvent-tuned assembly. The results resembled common processes of chemical polymerization: Growth was controlled kinetically and could be interpreted by formulas for step-growth polymerization and branching. Furthermore, some isomerization phenomena were observed, as was the formation of cyclic "macromolecules."

Quake Control

Large earthquakes occur at the margins of two colliding plates, where one plate subducts beneath the other at a shallow angle. These megathrust earthquakes often cause destructive tsunamis owing to the displacement of large volumes of water at the fault along the plate boundary. Two related studies of the seismic structure of subduction zones attempt to reveal the underlying mechanisms of megathrust earthquakes (see the Perspective by **Wang**). **Kimura *et al.*** (p. 210) compared seismic reflection images and microearthquake locations at the Philippine Sea plate where it subducts obliquely beneath Japan. The locations of repeating microearthquakes correspond to active transfer of material from the subducting plate to the continent—a process only previously assumed from exhumed metamorphic rocks. **Dean *et al.*** (p. 207) observe an expansive structure in the sea-floor sediment near the location of the 2004 and 2005 Sumatra earthquakes in Indonesia that suggests sediment properties may influence the magnitude of megathrust ruptures and their subsequent tsunamis.

CREDITS (TOP TO BOTTOM): ARMIN HALLMANN; YUAN *ET AL.*

Offsetting the Cost of Parasitism

Fruit flies, like most animals, are vulnerable to infection by a range of organisms, which, in co-infections, can interact with sometimes surprising effects. **Jaenike *et al.*** (p. 212) discovered that a species of *Spiroplasma* bacterium that is sometimes found in flies, and that is transmitted from mother to offspring, protects its host from the effects of a nematode worm parasite, *Howardula aoronymphium*. The worm sterilizes the female flies and shortens their lives, but when flies were experimentally infected with *Spiroplasma*, their fertility was rescued. Similarly, in wild populations of fruit flies infected with worms, those also infected with *Spiroplasma* had more eggs in their ovaries. The bacterium inhibits the growth of the adult female worms, but such is the advantage of this bacterial infection in offsetting the burden of nematodes on reproductive fitness, *Spiroplasma* appears to be spreading rapidly through populations of fruit flies in North America.

Separating Under Strain

Complex oxides, such as cuprate superconductors and perovskites, often exhibit microscopic phase separation, where two or more phases coexist on the macroscopic scale but are spatially separated on the microscopic scale. **Lai *et al.*** (p. 190) studied a configuration often found in technological applications, a strained manganite thin film placed on a substrate. Microwave impedance microscopy, which differentiates between conducting and insulating areas on the thin film, allowed visualization of the phase separation as the magnetic field was varied. A network of conducting domains was observed whose orientation and characteristic length scales suggest that the substrate-exerted strain was involved in network formation.

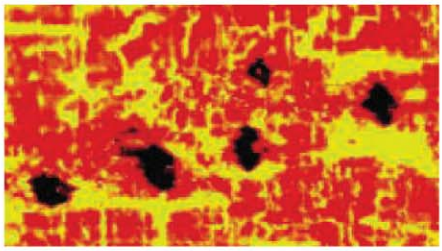

Getting Gametes Together

Despite decades of research, the molecular basis of sperm-egg recognition in mammals remains unresolved. Models in which a glycan ligand in the zona pellucida (ZP) surrounding ovulated eggs binds to a sperm surface receptor have been widely embraced. A more recent model proposes that the cleavage status of a ZP protein, ZP2, renders the structure of the zona matrix either permissive or nonpermissive for sperm binding. **Gahlay *et al.*** (p. 216) tested predictions of each model by replacing endogenous zona proteins with either a mutant form of ZP2 that could not be cleaved or of ZP3 that lacked O glycan attachment sites. Sperm-egg recognition depended on the cleavage status of ZP2 rather than on glycan ligands released following fertilization.

Righting Repair Pathways

The genetic disease Fanconi anemia (FA) results from mutations in a series of genes involved in a DNA repair pathway that helps process the damage caused by erroneous chemical cross-links between the two strands of the DNA double helix. The double-stranded breaks in DNA that arise from such cross-links can be repaired in an error-free manner or through an error-prone repair pathway. **Pace *et al.*** (p. 219, published online 10 June) show that the FA pathway can drive repair through the error-free pathway. The FA *FANCC* gene shows a genetic interaction with a component of the error-prone repair pathway, Ku70, inhibiting its action and thereby promoting the error-free pathway.

Correcting a Liver Problem

The classical form of α_1-antitrypsin (AT) deficiency is caused by a point mutation that alters the folding and causes intracellular aggregation of AT—an abundant liver-derived plasma glycoprotein. AT deficiency is the most common genetic cause of liver disease in childhood and can also lead to cirrhosis and/or hepatocellular carcinoma in adulthood. Carbamazepine is a drug known to be well tolerated in humans that enhances the intracellular degradation process known as autophagy. Now, **Hidvegi *et al.*** (p. 229, published online June 3; see the Perspective by **Sifers**) show that carbamazepine can reduce the severity of liver disease in a mouse model of AT deficiency by enhancing the degradation of misfolded accumulated AT.

CREDIT: LAI *ET AL.*

AIDS Response at a Crossroads

LATER THIS MONTH, THE XVIII INTERNATIONAL AIDS CONFERENCE WILL BE HELD IN VIENNA, AUSTRIA. Now the largest conference dedicated to a single disease, it will bring together more than 20,000 attendees. Over the past several years, however, attendance by the basic science and clinical research communities at this conference has waned. This raises the question of whether their absence threatens the success of the overall response to AIDS.

The evolution of this conference frames a history of the AIDS epidemic and suggests reasons for the decreased interest of these scientists. The initial conferences were small, bringing together basic scientists with clinicians who were witnessing the manifestations of HIV, spurring research to understand the virus and its pathology. In the 1990s, conference themes widened as the breadth of the impact of HIV and its global dimension were appreciated. During this time, individuals living with HIV pushed relentlessly for increased funding for basic and clinical research. Key interactions between scientists and AIDS activists occurred at International AIDS Conferences, motivating a vibrant research agenda. Newly discovered protease inhibitors—the eventual cornerstone of effective therapy in the developed world—were announced at the 1996 conference, a breakthrough discovery that transformed HIV from a death sentence to a chronic and manageable condition.

The past decade of the International AIDS Conference has reflected frustration over a growing divide between those with and without access to HIV treatment, particularly as millions continued to die of HIV in Africa. The challenges of preventing mother-to-child transmission of HIV and providing mothers with lifesaving treatment were among the most critical issues debated. But during this same period of promoting wider access to treatment, basic and clinical researchers became increasingly reluctant to attend the conference. Rather, many chose to attend highly focused meetings in their specific interest areas (for example, those on HIV resistance, HIV vaccine development, or metabolic complications during HIV infection) or general meetings perceived as "more scientific," such as the Conference on Retroviruses and Opportunistic Infections. As a result, the only forum emphasizing dialogue between those engaged in generating new scientific knowledge, those tackling the epidemic in a practical manner, and those dealing with its very personal impact, has been weakened.

The response to the HIV epidemic is at a crossroads. Major scientific challenges remain. There is still no cure for HIV and no vaccine for its prevention. Although antiretroviral therapy has now reached about 40% of those in urgent need in Africa, this scale-up has generated new questions about mechanisms underlying increased early mortality after the initiation of antiretroviral therapy, diagnostics for use at the lowest health facility level, and distinguishing recent from chronic HIV infections at individual and population levels. These critical questions must be informed not only by clinical, behavioral, and operations research, but by progress in basic research. The International AIDS Conference provides the opportunity for this critical interchange. Scientists, clinicians, advocates, policy-makers, community members, and governmental leaders can sit side by side and debate issues from their own perspective and learn from each other. The basic scientists need to discern how to translate their discoveries into practice and learn of new pathogenesis dilemmas. The clinical and behavioral scientists need to recognize key challenges faced by those affected by HIV that should inform their research. The work of operation researchers should guide policy and implementation. And policy-makers and community members should express their needs and gain access to knowledge to assist their actions.

For all of these reasons, the scientists who have abandoned this conference must fully reengage, by helping to build future agendas and recruiting the most distinguished HIV scientists to present state-of-the art research that will advance the global agenda for conquering AIDS. Only by bringing science back to the center of the dialogue and bridging the divide across interests can we truly hope to achieve a world without AIDS. **– Jessica Justman and Wafaa M. El-Sadr**

10.1126/science.1193218

Jessica Justman and Wafaa M. El-Sadr are with the International Center for AIDS Care and Treatment Programs and are professors in the Departments of Medicine and Epidemiology at Columbia University, New York, NY, USA. E-mail: jj2158@columbia.edu (J.J.); wme1@columbia.edu (W.M.E.)

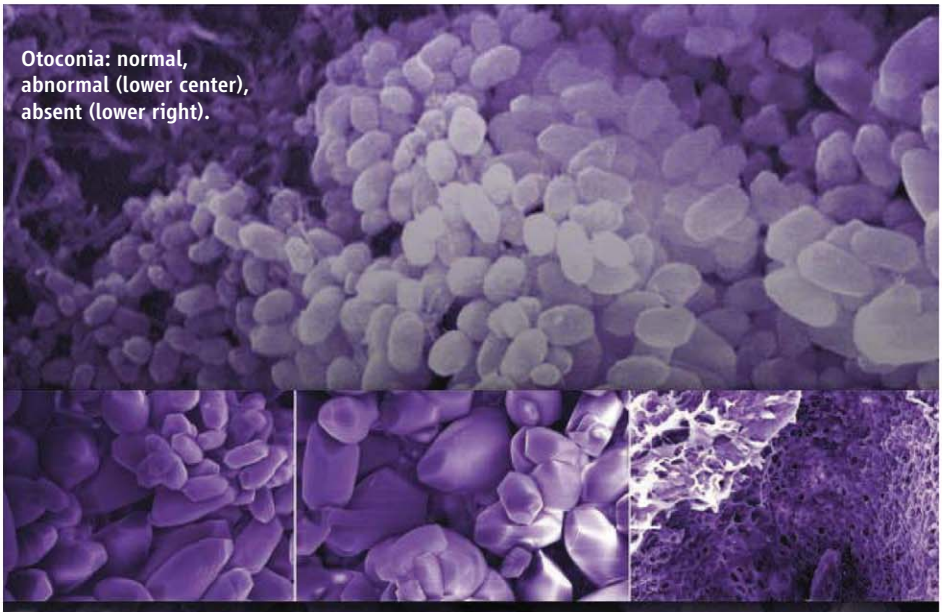

Otoconia: normal, abnormal (lower center), absent (lower right).

CELL BIOLOGY

Caught Off Balance

An episode of dizziness, no matter how brief, reminds us that our body performs important physiological functions that we take for granted. Our sense of balance is dependent on small crystals in the inner ear called otoconia. These crystals are embedded within a fibrous extracellular matrix that couples the force of gravity to the cilia of sensory cells, which in turn send signals to the nervous system. The biosynthesis of otoconia occurs during fetal development when core proteins secreted by vestibular epithelial cells form a proteinaceous matrix that sequesters calcium carbonate. Little is known about the genes and cellular processes involved in otoconial assembly and maintenance.

Mariño *et al.* have discovered that a degradative cellular process called autophagy is essential for otoconial biogenesis. Mice genetically deficient in a protein that plays a key role in autophagy, Atg4b, showed behaviors consistent with inner ear defects, such as head tilting, circling movements, and disorientation in swimming tests. These behaviors were accompanied by the absence of otoconia or by the presence of morphologically abnormal otoconia. Similar abnormalities were seen in mice deficient in Atg5, which like Atg4 appears to be important in the secretion and assembly of otoconial core proteins. Further mechanistic investigation of how these small but critical crystals are made and maintained throughout life may yield new treatments for balance-related disorders, which are common in the elderly and can also be a side effect of certain antibiotics. — PAK

J. Clin. Invest. **120**, 10.1172/JCI42601 (2010).

MICROBIOLOGY

Restricting Promiscuity

Although it might seem that many species of bacteria swap DNA promiscuously, in reality, the transfer of genetic information is curtailed by sequence-specific restriction systems. Several such systems have been characterized; the core component is an endonuclease that cleaves unmodified DNA (the host's own DNA is protected against digestion, usually by methylation). Corvaglia *et al.* have discovered a new endonuclease in *Staphylococcus aureus*, which is a potentially pathogenic bacterium carried by up to half the human population. Methicillin-resistant strains of *S. aureus* (MRSA) were found to carry mutations in this restriction endonuclease, which has tentatively been assigned to the type III family; these mutations probably render these strains hypersusceptible to the uptake of antibiotic-resistance genes from gut bacteria. — CA

Proc. Natl. Acad. Sci. U.S.A. **107**, 10.1073/pnas.1000489107 (2010).

CHEMISTRY

Ironing Out Formic Acid

Some biomass transformations, such as pathways that deoxygenate sugars, produce formic acid as a by-product, and the options for downstream use of large amounts of it have been limited. Boddien *et al*. now report a photocatalytic route for liberating hydrogen from formic acid. Previous catalysts for this reaction used noble metals, but after screening a range of more abundant transition metals, the authors discovered that effective catalysts formed in situ from an iron carbonyl cluster [$Fe_3(CO)_{12}$], a polydentate nitrogen-donating ligand, and triphenylphosphine. Under irradiation with the visible light from a 300-W xenon arc lamp, these catalysts generated hydrogen from formic acid solutions stabilized with triethylamine; the best examples had turnover frequencies up to 200 per hour and turnover numbers exceeding 100. Extensive spectroscopic studies implicated photogenerated iron hydrides as active species. — PDS

J. Am. Chem. Soc. **132**, 10.1021/ja100925n (2010).

PHYSICS

Running in Circles

While the debate about the origin of high-temperature superconductivity in the cuprates has been raging since their discovery more than 20 years ago, many of these materials have found practical use, most commonly as superconducting magnets and wires. However, a serious limitation exists, especially pronounced in the yttrium barium copper oxide (YBCO) family: Grain boundaries (interfaces between mismatched neighboring crystal orientations), present in the technologically interesting polycrystals, limit the observed supercurrent to values considerably below that attainable in a perfect single crystal. Graser *et al.* use molecular dynamics simulations and an effective tight binding model to simulate the flow of a supercurrent through a grain boundary in YBCO. They find that, even away from the boundary, the flow is disrupted and can run in closed loops (see arrows in the figure) and even backwards (blue lines). The experimentally established exponential dependence of the supercurrent on the angle of misorientation is recovered; the authors identify the accumulation of charge at the boundary as the primary cause, with the d-wave symmetry of the superconducting gap having, surprisingly, little effect. There are indications that similar behavior might occur in other complex superconductors, such as the ferropnictides. — JS

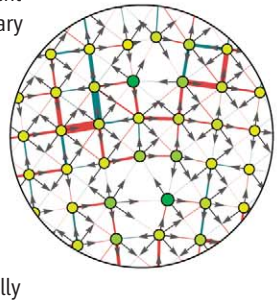

Nat. Phys. **6**, 10.1038/nphys1687 (2010).

CREDITS (TOP TO BOTTOM): MARIÑO *ET AL.*, *J. CLIN. INVEST.* **120**, 10.1172/JCI42601 (2010); GRASER *ET AL.*, *NAT. PHYS.* **6**, 10.1038/NPHYS1687 (2010)

www.sciencemag.org

Science

1200 New York Avenue, NW
Washington, DC 20005
Editorial: 202-326-6550, FAX 202-289-7562
News: 202-326-6581, FAX 202-371-9227
Bateman House, 82-88 Hills Road
Cambridge, UK CB2 1LQ
+44 (0) 1223 326500, FAX +44 (0) 1223 326501

Subscription Services For change of address, missing issues, new orders and renewals, and payment questions: 866-434-AAAS (2227) or 202-326-6417, FAX 202-842-1065. Mailing addresses: AAAS, P.O. Box 96178, Washington, DC 20090-6178 or AAAS Member Services, 1200 New York Avenue, NW, Washington, DC 20005

Institutional Site Licenses please call 202-326-6755 for any questions or information

Reprints: Author Inquiries 800-635-7181
Commercial Inquiries 803-359-4578

Permissions 202-326-7074, FAX 202-682-0816

Member Benefits AAAS/Barnes&Noble.com bookstore www.aaas.org/bn; AAAS Online Store www.apisource.com/aaas/ code MKB6; AAAS Travels: Betchart Expeditions 800-252-4910; Apple Store www.apple.com/eppstore/aaas; Bank of America MasterCard 1-800-833-6262 priority code FAA3YU; Cold Spring Harbor Laboratory Press Publications www.cshlpress.com/affiliates/aaas.htm; GEICO Auto Insurance www.geico.com/landingpage/go51.htm?logo=17624; Hertz 800-654-2200 CDP#343457; Office Depot https://bsd.officedepot.com/portalLogin.do; Seabury & Smith Life Insurance 800-424-9883; Subaru VIP Program 202-326-6417; VIP Moving Services www.vipmayflower.com/domestic/index.html; Other Benefits: AAAS Member Services 202-326-6417 or www.aaasmember.org.

science_editors@aaas.org	(for general editorial queries)
science_letters@aaas.org	(for queries about letters)
science_reviews@aaas.org	(for returning manuscript reviews)
science_bookrevs@aaas.org	(for book review queries)

Published by the American Association for the Advancement of Science (AAAS), *Science* serves its readers as a forum for the presentation and discussion of important issues related to the advancement of science, including the presentation of minority or conflicting points of view, rather than by publishing only material on which a consensus has been reached. Accordingly, all articles published in *Science*—including editorials, news and comment, and book reviews—are signed and reflect the individual views of the authors and not official points of view adopted by AAAS or the institutions with which the authors are affiliated.

AAAS was founded in 1848 and incorporated in 1874. Its mission is to advance science, engineering, and innovation throughout the world for the benefit of all people. The goals of the association are to: enhance communication among scientists, engineers, and the public; promote and defend the integrity of science and its use; strengthen support for the science and technology enterprise; provide a voice for science on societal issues; promote the responsible use of science in public policy; strengthen and diversify the science and technology workforce; foster education in science and technology for everyone; increase public engagement with science and technology; and advance international cooperation in science.

Information for Authors
See pages 352 and 353 of the 15 January 2010 issue or access www.sciencemag.org/about/authors

EDITOR-IN-CHIEF **Bruce Alberts**
EXECUTIVE EDITOR **Monica M. Bradford**
NEWS EDITOR **Colin Norman**
MANAGING EDITOR, RESEARCH JOURNALS **Katrina L. Kelner**
DEPUTY EDITORS **R. Brooks Hanson, Barbara R. Jasny, Andrew M. Sugden**

Editorial senior editors/commentary Lisa D. Chong, Brad Wible; **senior editors** Gilbert J. Chin, Pamela J. Hines, Paula A. Kiberstis (Boston), Marc S. Lavine (Toronto), Beverly A. Purnell, L. Bryan Ray, Guy Riddihough, H. Jesse Smith, Phillip D. Szuromi (Tennessee), Valda Vinson, Jake S. Yeston; **associate editors** Kristen L. Mueller, Jelena Stajic, Nicholas S. Wigginton, Laura M. Zahn; **research associate** Alexis Wynne Mogul; **book review editor** Sherman J. Suter; **associate letters editor** Jennifer Sills; **editorial manager** Cara Tate; **senior copy editors** Jeffrey E. Cook, Cynthia Howe, Harry Jach, Lauren Kmec, Barbara P. Ordway, Trista Wagoner; **copy editor** Chris Filiatreau; **editorial coordinators** Carolyn Kyle, Beverly Shields; **publications assistants** Ramatoulaye Diop, Joi S. Granger, Emily Guise, Jeffrey Hearn, Michael Hicks, Lisa Johnson, Scott Miller, Jerry Richardson, Jennifer A. Seibert, Brian White, Anita Wynn; **editorial assistants** Emily C. Horton, Patricia M. Moore, Miriam Weinberg; **executive assistant** Alison Crawford; **administrative support** Maryrose Madrid; **editorial fellow** Melissa R. McCartney

Editorial director, web and new media Stewart Wills; **senior web editor** Tara S. Marathe; **web editor** Robert Frederick; **web development manager** Martyn Green; **web developer** Andrew Whitesell

News deputy news editors Robert Coontz, Eliot Marshall, Jeffrey Mervis, Leslie Roberts; **contributing editors** Elizabeth Culotta, Polly Shulman; **news writers** Yudhijit Bhattacharjee, Adrian Cho, Jennifer Couzin, David Grimm, Jocelyn Kaiser, Richard A. Kerr, Eli Kintisch, Greg Miller, Elizabeth Pennisi, Robert F. Service (Pacific NW), Erik Stokstad, Jue Wang; **interns** Lauren Schenkman, Nezile Mthembu, Dolly Krishnaswamy; **contributing correspondents** Jon Cohen (San Diego, CA), Daniel Ferber, Ann Gibbons, Sam Kean, Robert Koenig, Andrew Lawler, Mitch Leslie, Charles C. Mann, Virginia Morell, Gary Taubes; **copy editors** Linda B. Felaco, Melvin Gatling, Melissa Raimondi; **administrative support** Scherraine Mack; **bureaus** San Diego, CA: 760-942-3252, FAX 760-942-4979; Pacific Northwest: 503-963-1940

Production director James Landry; **senior manager** Wendy K. Shank; **assistant manager** Rebecca Doshi; **senior specialists** Steve Forrester, Chris Redwood, Anthony Rosen; **Preflight director** David M. Tompkins; **manager** Marcus Spiegler; **specialist** Jason Hillman

Art director Yael Kats; **associate art director** Laura Creveling; **senior illustrators** Chris Bickel, Katharine Sutliff; **illustrator** Yana Greenman; **senior art associates** Holly Bishop, Preston Huey, Nayomi Kevitiyagala; **art associates** Kay Engman, Matthew Twombly; **photo editor** Leslie Blizard

***Science* International**

Europe (science@science-int.co.uk) **editorial: international managing editor** Andrew M. Sugden; **senior editor/commentary** Julia Fahrenkamp-Uppenbrink; **senior editors** Caroline Ash, Stella M. Hurtley, Ian S. Osborne, Peter Stern; **associate editor** Maria Cruz; **locum editor** Helen Pickersgill; **editorial support** Rachel Roberts, Alice Whaley; **administrative support** John Cannell, Janet Clements, Louise Hartwell; **news: europe news editor** John Travis; **deputy news editor** Daniel Clery; **contributing correspondents** Michael Balter (Paris), John Bohannon (Vienna), Martin Enserink (Amsterdam and Paris), Gretchen Vogel (Berlin); **intern** Sarah Reed

Latin America contributing correspondent Antonio Regalado

Asia Japan Office: Asca Corporation, Tomoko Furusawa, Rustic Bldg. 7F, 77 Tenjin-cho, Shinjuku-ku, Tokyo 162-0808, Japan; +81 3 6802 4616, FAX +81 3 6802 4615, inquiry@sciencemag.jp; **asia news editor** Richard Stone (Beijing: rstone@aaas.org); **contributing correspondents** Dennis Normile [Japan: +81 (0) 3 3391 0630, FAX +81 (0) 3 5936 3531; dnormile@gol.com]; Hao Xin [China: cindyhao@gmail.com]; Pallava Bagla [South Asia: +91 (0) 11 2271 2896; pbagla@vsnl.com]

EXECUTIVE PUBLISHER **Alan I. Leshner**
PUBLISHER **Beth Rosner**

Fulfillment Systems and Operations (membership@aaas.org); **director** Waylon Butler; **customer service supervisor** Pat Butler; **specialists** Latoya Casteel, LaVonda Crawford, Vicki Linton, April Marshall; **data entry supervisor** Cynthia Johnson; **specialists** Shirlene Hall, Tarrika Hill, William Jones

Business Operations and Administration director Deborah Rivera-Wienhold; **business systems and financial analysis director** Randy Yi; **manager, business analysis** Eric Knott; **manager, business operations** Jessica Tierney; **financial analysts** Priti Pamnani, Celeste Troxler; **rights and permissions: administrator** Emilie David; **associate** Elizabeth Sandler; **marketing director** Ian King; **marketing managers** Allison Pritchard, Alison Chandler, Julianne Wielga; **marketing associates** Aimee Aponte, Mary Ellen Crowley, Wendy Wise; **senior marketing executive** Jennifer Reeves; **director, site licensing** Tom Ryan; **director, corporate relations** Eileen Bernadette Moran; **publisher relations, eresources specialist** Kiki Forsythe; **senior publisher relations specialist** Catherine Holland; **publisher relations, east coast** Phillip Smith; **publisher relations, west coast** Philip Tsolakidis; **fulfillment supervisor** Iquo Edim; **fulfillment coordinator** Carrie MacDonald; **marketing manager** Christina Schlecht; **marketing associate** Laura Tutino; **electronic media: manager** Lizabeth Harman; **project manager** Trista Snyder; **assistant manager** Lisa Stanford; **senior production specialists** Ryan Atkins, Christopher Coleman, **computer specialist** Walter Jones; **production specialists** Nichele Johnston, Kimberly Oster; **director, web and new media** Will Collins

advertising director, worldwide ad sales Bill Moran
commercial editor Sean Sanders: 202-326-6430
assistant commercial editor Tianna Hicklin 202-326-6463
project director, outreach Brianna Blaser

Product (science_advertising@aaas.org); **midwest** Rick Bongiovanni: 330-405-7080, FAX 330-405-7081; **east coast/e. canada** Laurie Faraday: 508-747-9395, FAX 617-507-8189; **west coast/w. canada** Lynne Stickrod: 415-931-9782, FAX 415-520-6940; **uk/europe/asia** Roger Goncalves: TEL/FAX +41 43 243 1358; **japan** ASCA Corporation, Nanako Ide +81 (0) 3 6802 4616, FAX +81 (0) 3 6802 4615; ads@sciencemag.jp; **senior traffic associate** Deiandra Simms

worldwide associate director of *Science* Careers Tracy Holmes: +44 (0) 1223 326525, FAX +44 (0) 1223 326532

Classified (advertise@sciencecareers.org); **u.s.: midwest/west coast/south central/canada** Tina Burks: 202-326-6577; **east coast/industry** Elizabeth Early: 202-326-6578; **sales coordinators** Rohan Edmonson, Shirley Young; **europe/row sales:** Susanne Kharraz, Dan Pennington, Alex Palmer; **sales assistant** Lisa Patterson; **japan** ASCA Corporation, Jie Chin +81 (0) 3 6802 4616, FAX +81 (0) 3 6802 4615; careerads@sciencemag.jp; **advertising support manager** Karen Foote: 202-326-6740; **advertising production operations manager** Deborah Tompkins; **senior production specialist/graphic designer** Amy Hardcastle; **senior production specialist** Robert Buck; **senior traffic associate** Christine Hall

AAAS Board of Directors retiring president, chair Peter C. Agre; **president** Alice Huang; **president-elect** Nina Fedoroff; **treasurer** David E. Shaw; **chief executive officer** Alan I. Leshner; **board** Linda P. B. Katehi, Nancy Knowlton, Stephen Mayo, Cherry A. Murray, Julia M. Phillips, Sue V. Rosser, David D. Sabatini, Thomas A. Woolsey

AAAS
ADVANCING SCIENCE, SERVING SOCIETY

re:sponsibility

Toward a smaller footprint:

extending "reduce, reuse, and recycle"

Reduce, reuse, and recycle—three basic principles that help guide responsible actions toward our environment. These principles are as relevant today as ever, and at Life Technologies, we put them to work at all levels of our business operations. However, with the serious environmental threats we now face, reaching toward a state of genuine sustainability will challenge us to step outside our comfort zone in search of truly innovative ways to lessen our impact.

We're up to the challenge. In addition to continuing to get the most we can out of "reduce, reuse, and recycle," Life Technologies is further committed to:

re:think	Take a fresh look at what we do, why we do it, and how it impacts the environment
re:search	Find better materials, more efficient processes, and greener partnerships
re:solve	Make the decisions that bring sustainable solutions into practice and offer greener product alternatives

Life Technologies—looking for new ways to tread lightly in our world.

To learn more, visit **www.lifetechnologies.com/responsibility**

life technologies™

applied biosystems™ | invitrogen™

AAAS is here – bringing educational infrastructure to the developing world.

AAAS is helping the Rwandan government rebuild its educational infrastructure as a way to help drive economic growth and development. By providing materials such as the Project 2061 *Atlas of Science Literacy*, lesson plans from Science NetLinks, and access to *Science* digital libraries, AAAS is helping the people of Rwanda work toward a future built around science and technology. As a AAAS member your dues support these efforts. If you're not yet a AAAS member, join us. Together we can make a difference.

To learn more, visit **aaas.org/plusyou/rwanda**

AAAS + U = Δ

EDITED BY LAUREN SCHENKMAN

Out of the Ice

Three years ago, Craig Lee spied what looked like a tree branch in a small water channel streaming from a melting ice patch high in the Rocky Mountains near Yellowstone National Park. Walking over for a better look, Lee, an archaeologist at the University of Colorado, Boulder, realized it was the 107-centimeter-long foreshaft of a wooden dart, shaped by an ancient hunter and later trampled by an animal and deformed by flowing slush. Now, radiocarbon dating has revealed that the weapon is 10,400 years old—the earliest artifact ever discovered melting out of ancient ice. "I was just flabbergasted," says Lee, who presented the results at a meeting in April and is preparing a paper for publication.

With global temperatures rising, archaeologists have collected hundreds of ancient artifacts melting out from alpine ice patches in Alaska, northern Canada, and Norway. By feeding data from satellite images and aerial photographs into a computerized geographical information system, Lee is identifying sites for finds much farther south in North America. His new find, says Canadian Yukon government archaeologist Greg Hare, shows that "the potential for ice-patch archaeology exists almost anywhere there is persistent snow cover."

Lee thinks a Paleoindian hunter lost the ancient dart while hunting bighorn sheep. The dart's icy grave was a boon. "Most of our archaeological record from this period consists of chipped stone artifacts," he says. "The ice patches preserve organic materials, so they are giving us a huge window into more perishable technology."

Doom on the Moon

You're an astronaut on a lunar base, and a meteorite knocks out the oxygen generator. You've got 20 minutes of air left. What to do?

Click the mouse! You're playing Moonbase Alpha, a free, commercial-quality video game NASA released this week (http://bit.ly/moonbase). Graphics draw from engineers' models for future lunar habitats and rovers, says project manager Daniel Laughlin, an educator at

the University of Maryland, Baltimore County. How does it rate as a game? "I'm a gamer, and plenty of times I've been gritting my teeth … in frustration," Laughlin says. "That's what I tend to call hard fun."

Lucky Genes

Finding the gene that makes four-leaf clovers has been as hard as spotting the lucky plants themselves. For one thing, white clover has two complete genomes, probably from two ancestors that hybridized to make the species. Plus, the four-leaf trait is recessive, and it's expressed more in some seasons than others.

Now a team of researchers has pinned down the gene. Rebecca Tashiro, then a graduate student at the University of Georgia, Athens (UGA), crossed a plant that had been bred to make multipart leaves with another white clover, took tissue samples from the offspring, and checked their leaves. "Three years of looking for a four-leaf clover on 200, 400 plants each time, you get pretty good at spotting them," says Tashiro, who mapped the four-leaf trait and others onto the genome. The map is published in the July-August issue of *Crop Science*.

The new map should make it easier for other breeders to get the clover they want, says Tashiro. The map could also be relevant to alfalfa, clover's relative and a vital feed for livestock, says E. Charles Brummer, a plant breeder at UGA who did not work on the project. "Any time you learn something in clover, it's almost trivial to apply that to an alfalfa question," he says. "It just helps fill in the whole puzzle."

EVOLUTION FOR BARTENDERS

While sipping a Bloody Mary at a party in graduate school, evolutionary biologist James Harriman had an idea. "Everyone has a different recipe for Bloody Marys, so there occur these little differences. Like someone says, 'I want more hot sauce,' " he says. Harriman wondered whether such personal quirks evolve into popular cocktails much as mutations give rise to new species, through a sort of taste-based natural selection.

So Harriman, now a visiting scientist at Cornell University, fired up a computer program for generating phylogenetic trees. Instead of genes, he plugged in the ingredients of 100 cocktails, taking vodka as the tree's common ancestor. The program divided cocktails into several distinct families—drinks based on champagne or Irish cream, for example, or punch bowl drinks—and served up a few surprises. A cocktail called 110 in the shade (lager and tequila) is "sort of the platypus of the drink family," Harriman says, "because it has nothing in common with anything else." A poster of the tree, which doubles as a mixology guide, is available online from ThinkGeek (www.thinkgeek.com).

CREDITS (TOP TO BOTTOM): CASEY A. CASS/UNIVERSITY OF COLORADO; JAMES HARRIMAN; NASA LEARNING TECHNOLOGIES; PHOTOS.COM

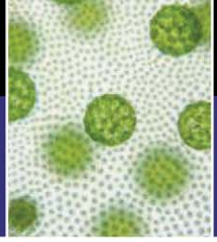

Few genetic clues to multicellularity 128

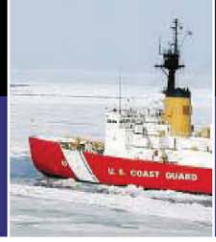

The icebreaking crunch 128

U.S. SCIENCE POLICY

Panel Explores What It'll Take To Keep Universities Strong

U.S. research universities may be the envy of the world, but they are under increasing stress. Endowments have shrunk, state support has declined, and operating costs are rising. University administrators say they also need help in complying with an increasing number of federal rules covering research topics that include bioweapons and financial conflicts of interest.

Now, at the behest of Congress, the National Academies has convened a blue-ribbon committee to examine these concerns and recommend ways to keep research universities healthy. But universities are likely to be disappointed if they are hoping that the committee will conclude that money is the solution: "If we simply turn out a report that says, 'Spend more money on research universities,' we won't have done our job," says the panel's chair, Charles "Chad" Holliday, retired CEO of DuPont.

"I'm an industrial engineer. … And I haven't seen a system yet that can't be improved."

—CHARLES HOLLIDAY, PANEL CHAIR

Holliday, now chair of the board of Bank of America, said in an interview with *Science* that he intends to push the 21-member committee to take a close look at the way the universities themselves operate. "I'm an industrial engineer. We try to make systems work more efficiently. And I haven't seen a system yet that can't be improved," says Holliday.

"We know what a research university is supposed to do, and I don't think we're going to [recommend] changing that drastically," he adds. "But if we could come up with different ways to accomplish that mission, I think it might be helpful." The list of possible study topics, he says, includes everything from reducing the time to degree to making better use of new technology.

The roots of the problem lie in an unwritten agreement between the academic community and the government that was struck after World War II. In return for receiving federal support for research, universities promised to create new knowledge that ultimately benefits society and to educate the next generation of scientists and engineers. But academic leaders say that historic partnership is fraying at both ends. "The quality of our research can only be as strong as the foundation upon which it rests," Robert Berdahl, president of the Association of American Universities in Washington, D.C., explained last fall in a talk to the new committee's parent body, the Board on Higher Education and Workforce. "And if the fundamental operations of our research universities are deteriorating, the [country's] research superstructure will inevitably decline as well."

The university lobbyists who pushed for the new study took a page from an improbably influential 2006 academies' report on ways to strengthen the U.S. research enterprise that was requested by a bipartisan group of legislators with influence over science policy. That report, titled *Rising Above the Gathering Storm*, helped persuade Congress and the White House to embrace a 10-year doubling of federal spending on basic research, a goal enshrined in the 2007 America COMPETES Act.

Similarly, the new committee grows out of a request 1 year ago by four legislators to the presidents of the three academies asking them to suggest the "top 10 actions that Congress, state governments, research universities, and others could take" so that U.S. research universities could continue to help the country "compete, prosper, and achieve national goals in health, energy, the environment, and global security." Last month, after the Alfred P. Sloan Foundation put up most of the $1.5 million needed, the academies formally announced that the study was under way.

The committee expects to meet for the first time in September and complete its work by next summer. Holliday is trying to speed up the process by talking with individual panel members before the initial meeting, for example, and using teleconferencing as much as possible. He hopes those strategies could be a model for other studies run by the academies' National Research Council.

The *Gathering Storm* report actually made 20 recommendations in four areas, including for a massive boost in scholarships to train more science and math teachers and for changes to tax and immigration policies that would promote innovation. But its call for increased spending drowned out other proposals. Holliday, who was a member of that panel chaired by Norman Augustine, says that the new committee plans to revisit some of those issues that pertain to research universities. "Maybe we'll have the opportunity to make a more compelling argument the second time around," he says.

Asking universities to use existing resources in the most efficient manner is part of a larger trend, Holliday notes: "We're reducing the time it takes to do things across society, so the question is whether we are doing that in academia, too." For example, he wonders, "Are there steps in the process [of earning a Ph.D.] that aren't adding value? If there's a way to speed up the process without sacrificing quality, it could ease the financial burden on students and also free up capacity to train more students."

Holliday says he understands the concerns surrounding unfunded mandates but only to a point. "My first reaction [to those complaints] is, 'Join the club.' I've been on the business side for 35 years, and that's how we feel, too."

Improving how universities work with industry to commercialize the fruits of academic research is another topic on the com-

CREDIT: COURTESY OF BANK OF AMERICA

Yunnan's medical mystery solved?
132

Orphaned tissue banks
135

mittee's plate. Holliday cites the position of "opportunity broker" that DuPont created when it moved into biotechnology—"someone who knew how to talk to leading-edge scientists in their labs and also the people who know how to apply their research to the market"—as a possible model. "My feeling is that research universities probably need the same sort of person," he says.

Holliday says his concerns about current academic practices don't undermine his conviction that "our research universities have got to remain strong." Lawrence Summers, the former Harvard University president who is now director of the National Economic Council in the White House, agrees that the country's competitive edge derives in part from the "staying power" of its research universities. But universities should not rest on their laurels, Summers told *Science*. "At Harvard, I would often say that not having any failures would be the biggest failure of all," he says. "Because it would mean that we didn't take enough chances." **–JEFFREY MERVIS**

CLIMATE MONITORING

Solar Sensor Grounded on Revamped Satellite Program

U.S. climate scientists were hoping that the restructuring of a troubled $14 billion environmental satellites program would elevate the importance of climate sensors among instruments scheduled to fly over the next decade. But last week's announcement that the first spacecraft of the reconfigured National Polar-orbiting Operational Environmental Satellite System (NPOESS) wouldn't be able to measure the intensity of sunlight has left them feeling out in the cold again.

"It's terrible news" that the Total and Spectral Irradiance Sensor (TSIS) has lost its ride to space, says solar physicist Judith Lean of the Naval Research Laboratory in Washington, D.C. Officials with NASA and the National Oceanic and Atmospheric Administration (NOAA) say they're committed to maintaining solar measurements, either by adding TSIS to future missions or dedicating one to it. In a tight budget environment, however, Lean says, "to not be a part of the satellite makes it more likely the sensors won't fly" anytime soon.

The omission of TSIS flows from the Obama Administration's efforts to reform NPOESS. The massive weather and climate-monitoring program, under joint management by NASA, NOAA, and the Pentagon during the Bush Administration, has seen its cost double and its schedule fall 5 years behind since 2002 (*Science*, 5 February, p. 629). To reduce infighting and simplify the effort, the White House announced earlier this year that NPOESS would be broken into separate but cooperating components. NASA and NOAA would build and operate the Joint Polar Satellite System (JPSS), focused on weather and climate, while the Pentagon would build and run satellites aimed primarily at weather observations. The total number of satellites has yet to be decided.

Last week, NOAA announced that the first craft, JPSS-1, scheduled for 2014, will fly the same four sensors currently scheduled to go up next year on a preliminary mission known as NPP. That decision, which NOAA's Mary Kicza said is meant to "reduce risk" of future schedule or budget slips, leaves no room for TSIS, now under construction.

That delay could cause a gap in the continuous record of solar brightness, crucial for calculating global warming, that has been maintained since 1978. The only current climate-relevant brightness sensor is on an orbiting NASA craft called SORCE, which is 5 years beyond its design life. A similar sensor is due to fly this fall on Glory. Because calibrating the sensors requires missions that overlap in time, however, scientists wanted TSIS to go up no later than 2014.

TSIS program manager Tom Sparn, an engineer at the University of Colorado, Boulder, says the latest twist might actually be an opportunity. The original plan to keep TSIS focused on the sun while orbiting as part of a suite of instruments looking down at Earth requires hardware that adds vibration, increasing the engineering challenges and total cost. Sparn hopes that TSIS and other outward-facing sensors can fly on a dedicated solar JPSS solar platform. "We still have faith that in a timely fashion there will be a ride found" for TSIS, he says.

Climate scientist Judith Curry of the Georgia Institute of Technology in Atlanta worries that the TSIS decision sends the wrong message about the state of climate monitoring in the latest configuration of environmental satellites. "We can probably survive in the interim without TSIS on JPSS," she says. But "somebody somewhere needs to clean up this mess with NPOESS. Its new incarnation doesn't seem to be much better."

–ELI KINTISCH

Flying free? Scientists are mulling a dedicated sun-monitoring mission similar to SORCE, launched in 2003.

CREDIT: NASA

GENETICS

Volvox Genome Shows It Doesn't Take Much to Be Multicellular

How a single cell made the leap to a complex organism is one of life's great mysteries. Biologists have thought that new genes and gene networks would be needed to make possible the move to multicellularity. But, at least in green algae, that turns out not to be the case. On page 223, a comparison between the genomes of the 2000-cell *Volvox carteri* and a single-celled green alga, *Chlamydomonas reinhardtii*, has revealed surprisingly few differences in their gene makeup. "Even major evolutionary transitions can be accomplished via relatively subtle genetic changes," says David Kirk, a developmental biologist at Washington University in St. Louis. As a result, solving this mystery "is going to take a lot more work."

Ever since the Dutch microbiologist Antonie van Leeuwenhoek discovered a multicellular *Volvox* in 1700, biologists have thought it would be a good model for studying how complex organisms arose. It belongs to a group that includes single-celled and multicellular species of varying degrees of complexity. *Chlamydomonas reinhardtii*, for example, is a single cell powered by two flagella that lives in soil and fresh water.

By contrast, *Volvox carteri*, which is found in temporary and permanent ponds, has a much more complex life cycle. Adults consist of 2000 flagellated cells embedded in a spherical extracellular matrix, with 16 larger germ cells inside. Germ cells give rise to embryos in which dividing cells remain connected by cytoplasmic bridges from one cell interior to another, forming a hollow ball. At first all of the embryo's flagella face inward, but soon the newly formed embryo turns itself inside out, putting the flagella on the outside. Now called juveniles, these balls begin expanding by adding to their extracellular matrix and eventually burst out of the parental sphere. Soon after the juveniles leave the sphere, the rest of the cells die.

In 2005, James Umen, a cell and developmental biologist at the Salk Institute for Biological Studies in San Diego, California, teamed up with Simon Prochnik and Daniel Rokhsar of the U.S. Department of Energy Joint Genome Institute (JGI) in Walnut Creek, California, and others to sequence the *Volvox* genome. JGI had already deciphered the genome of the single-celled *Chlamydomonas*.

The 138-million-base *Volvox* genome proved to be 17% bigger than the *Chlamydomonas* genome, but not because of new genes. Instead, it contained more repetitive DNA, Prochnik, Umen, Rokhsar, and their colleagues report. Moreover, it has roughly the same number of genes—about 14,500—as *Chlamydomonas*. The researchers found few, if any, *Volvox* genes coding for novel proteins or protein subunits that could account for the difference in morphology between the two species. The gene networks that likely underlie the cytoplasmic bridges, the inversion of the sphere, and asymmetric cell division were quite similar

POLAR RESEARCH

Broken-Down Icebreakers Hamstring U.S. Science

Biologist Carin Ashjian is hoping that her research cruise next winter will fill in some of the many blanks about how the Arctic ecosystem behaves during that forbidding season. But to do so, she'll need help from a good mechanic.

That's how it works these days for scientists whose access to the polar regions depends on an over-the-hill and increasingly fragile U.S. icebreaking fleet. A 2006 report from the National Academies called for building two new icebreakers (*Science*, 6 October 2006, p. 33), but Congress has so far been unwilling to pony up the estimated $2 billion or more that would be needed to upgrade the fleet. The most that supporters have achieved to date is a Senate-backed call for a cost-benefit analysis of the nation's icebreaking needs.

Crunch time. Neither of the U.S. Coast Guard's two polar-class icebreakers, shown operating in Antarctica in 2002, are currently serviceable.

CREDIT: PETER WEST/NATIONAL SCIENCE FOUNDATION

Such an analysis won't help Ashjian, a scientist at the Woods Hole Oceanographic Institution in Massachusetts. Her 6-week cruise aboard the Coast Guard cutter *Polar Sea*, the world's most powerful icebreaker, would be the first such scientific exploration of the Bering and Chukchi seas in January, Ashjian says. The goal is to provide information on water temperature, nutrient chemistry, and other biological and physical characteristics of this poorly understood ecosystem.

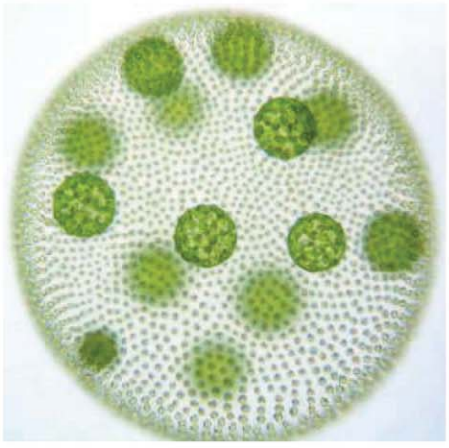

Complex cousin. The juvenile *Volvox* (*above*), with its sphere of flagellated cells and 16 germ cells, is not much different genewise from the single-celled *Chlamydomonas* (*left*).

in both species as well, says Umen.

"It's surprising how few differences were found," says Arthur Grossman, a plant biologist at the Carnegie Institution for Science in Stanford, California. "The findings suggest that it doesn't take very large changes in gene content to transition from a single-cell to a multicellular lifestyle." He suspects that some genes have altered their function in *Volvox* to account for the changes, and he calls for a more in-depth look for small changes in gene—and protein—sequence.

The findings parallel what Nicole King of the University of California, Berkeley, and her colleagues saw when they compared the genomes of a choanoflagellate—a close single-celled relative to animals—and several animals. The choanoflagellate had protein subunits, or domains, previously thought to be unique to metazoans, leading her to conclude that multicellularity in that part of the tree of life arose not so much from new genes but from a shuffling and recombining of existing genes and parts of genes.

"What we found was even more similarities between the unicellular and multicellular organism," says Umen. "The key transition is not inventing a whole bunch of genes and proteins; you just have to change the way you use what you have."

–ELIZABETH PENNISI

"Right now, when we run our Arctic models, we don't know what to do with the winters because we know so little about what happens during that season," she says.

But the *Polar Sea* may not be available. In May, the 32-year-old ship limped into its home port of Seattle, Washington, after suffering engine trouble during a spring Arctic cruise. On 25 June, the Coast Guard announced that a 3-month scheduled maintenance had turned into a $3 million repair job that will stretch until "at least January 2011." The Coast Guard has already canceled two fall events—one in support of a simulated oil spill in Arctic waters—and has told the National Science Foundation that the ship won't be able to provide backup support for the annual clearing of a winter passage through McMurdo Sound to the main U.S. research station in Antarctica.

There's no other vessel in the U.S. icebreaking fleet that can do those jobs. The *Polar Sea*'s older twin, the *Polar Star*, has been out of the water since 2006, and its $62 million "life extension" won't be finished until 2013. A third—and slightly younger—Coast Guard cutter, the *Healy*, is much less powerful, and a fourth, newer vessel operated by NSF, the *Nathaniel B. Palmer*, is a research ship with limited icebreaking capability. That thin bench is why NSF has relied in recent years on Swedish and Russian icebreakers to clear a passage to McMurdo (*Science*, 19 August 2005, p. 1164).

Coast Guard officials have tried unsuccessfully to win approval for new polar icebreakers from both the Bush and Obama administrations. Legislators from maritime states aren't happy with the status quo. "On a national level, this eliminates the nation's only heavy icebreaking capability and seriously imperils our ability to respond to emergencies in ice-covered and ice-diminished waters," said Senator Lisa Murkowski (R–AK), in response to the latest breakdown. "This could clearly impact our ability to preserve and protect U.S. interests in the Arctic."

A reauthorization bill now awaiting a House-Senate conference would require the Coast Guard to carry out a study by outside advisers "with extensive experience in the analysis of military procurements" of the cost of improving or adding to the fleet as well as the implications of not upgrading the nation's icebreaking capacity. "This subject's been studied to death," says a Senate aide who follows the issue. "We'd like to see more, but right now it may be the best we can do."

–JEFFREY MERVIS

CREDITS: S. PROCHNIK *ET AL.*, *SCIENCE*

*Science*Insider

From the *Science* Policy Blog

In the latest twist in a contentious debate about a possible tie between a retrovirus and **chronic fatigue syndrome**, the journal *Retrovirology* last week published a study that failed to find a key virus in blood samples from 51 CFS patients and 56 healthy people. The study, led by federal researchers, was held up in publication because it conflicts with another pending government study that confirms the connection. http://bit.ly/retrovstudy

In what amounts to an unprecedented experiment, scientists are **moving 700 turtle eggs** from the beaches of Alabama and Western Florida to Florida's eastern shores. Protecting the creatures from the gulf oil spill is worth the risk that the embryos may be damaged or that the species' population genetics may be affected by the move, say scientists. http://bit.ly/eggsmove

For the second time, an investigatory panel at Pennsylvania State University has **cleared climate scientist Michael Mann** of charges of scientific malfeasance. The allegations had arisen after the release last year of hundreds of e-mails between climate scientists. http://bit.ly/mannpanel

In its first action on the 2011 budget for several science agencies, a **House appropriations panel** gave the National Science Foundation, NOAA, and NIST increases roughly matching the White House's request. But an unusually fuzzy budget picture could eventually render the numbers meaningless. http://bit.ly/nsfmoney

A new report by the Massachusetts Institute of Technology calls for a variety of new research efforts to better exploit the large supply of **natural gas** in the United States. http://bit.ly/gasreport

AAAS, which publishes *Science*, has condemned **indictments issued** by an Italian prosecutor against six scientists and a bureaucrat for failing to predict an earthquake that struck L'Aquila, Italy, in April 2009, calling them "unfair and naïve." http://bit.ly/quakeletter

For more science policy news, visit **news.sciencemag.org/scienceinsider**.

BIOMEDICAL RESEARCH

Dream Team Plans a Blitz on Schizophrenia

BALTIMORE, MARYLAND—In a biotechnology park rising from razed rowhouses here, three top neuroscientists are betting big money and their scientific careers on a new approach to studying schizophrenia and other psychiatric diseases. With help from philanthropists, they are launching an institute that will look for treatments by probing early brain development for the origins of mental illness.

The nonprofit Lieber Institute for Brain Development will be led by Daniel Weinberger of the National Institute of Mental Health (NIMH), known for using brain imaging and genetics to study mental illnesses. Ronald McKay of the National Institute of Neurological Disorders and Stroke, whose lab was among the first to use stem cells to treat neurodegenerative diseases in animals, will be director of basic science. Both will leave government jobs for the new institute, which will be an independent affiliate of the adjacent Johns Hopkins University. The institute's third founder and elder statesman is Johns Hopkins neuropharmacologist Solomon Snyder, renowned for his work on brain receptors. Detailed responsibilities are still being worked out.

Brains trust. Solomon Snyder (*left*), Daniel Weinberger, and Ronald McKay are launching an institute to study brain development and search for new schizophrenia drugs.

CREDIT: RONALD MCKAY

The Lieber Institute's research agenda will include basic science and developing treatments for schizophrenia, a disease for which there have been few breakthroughs in the past 50 years. There are other centers dedicated to the brain, but they don't have the same developmental focus, McKay says. "There's no other institute where these areas of science are brought together to solve the problem of mental illness," Weinberger says.

Financing comes from New York City investment banker Stephen A. Lieber and his wife, Connie. The Liebers have a daughter with schizophrenia and for more than 2 decades have led a major charity supporting research on mental illnesses. The couple say they have been struck by studies suggesting that the neural patterns that lead to schizophrenia are present at birth. About 6 years ago, they decided that this area needed "a Manhattan Project." "We want to bring together a gifted group with a common trajectory aimed at finally seeing what happens in neurodevelopment that may lead to these disorders," Stephen Lieber says.

The Liebers talked to Yale, Columbia, and Rockefeller universities and the University of Pennsylvania before deciding to link up with Hopkins, largely because it agreed to allow the institute to be independent, Stephen Lieber says. (Lieber investigators will have appointments to the Johns Hopkins faculty.) Another incentive was the proximity of the National Institutes of Health (NIH), a 50-minute drive away.

Start-up funding includes a $100 million commitment from the Liebers and $20 million from the Maltz Family Foundation in Cleveland, Ohio. There are plans to raise funds for an endowment, Weinberger says.

The institute will begin with a $15 million budget and 30,000 square feet of space for labs. Weinberger expects to recruit 50 to 100 staff members within the next 5 years. Five initial projects will focus on stem cell biology, developmental neurobiology, neurogenetics, imaging, and a drug-discovery unit led by Snyder, who will remain on the Johns Hopkins faculty. McKay starts in late July in temporary space; NIMH neurologist Thomas Hyde will be acting director until Weinberger relocates a year from now.

Another recruit is a prominent medical chemist from the pharmaceutical industry, which has been abandoning research on drugs for brain diseases, says Weinberger, who declined to name the researcher.

Weinberger expects to have guest-researcher exchanges with NIH. He also hopes to partner with the agency to conduct early-phase clinical trials. Companies and universities could do that, but "they won't give up the intellectual property," he says. The Lieber Institute's cell lines and data will be freely available, he says.

The combined firepower of the three leaders, along with recent discoveries of genes that may underlie some cases of schizophrenia, give the institute a good chance at success, say researchers familiar with the Liebers' plans. "They're in the right place at the right time," says psychiatrist Steven Paul, a former NIMH scientific director who recently retired as executive vice president for science and technology at Eli Lilly. "I don't think there are other institutes trying to do this in this holistic manner."

In an interview last week, the Lieber Institute's founders reflected on why they're giving up long-established programs for a new venture. The appeal: the freedom to pursue risky projects that's missing in grant-driven academia and opportunities to interact with industry that aren't possible at NIH. Showing off a vast, empty, glass-walled floor in a new building where their labs will soon take shape, Weinberger says launching the institute feels a lot like starting a biotech company. "But we have this wonderful opportunity not to be worried about profit," he says.

–JOCELYN KAISER

ScienceNOW

From *Science*'s Online Daily News Site

Arctic Bees Still Need Their Beauty Sleep

Even under the midnight sun, bees like their beauty sleep. Researchers have found that both native (*Bombus pascuorum*) and imported (*B. terrestris*) bumblebees in northern Finland, 270 kilometers north of the Arctic Circle, stuck to a regular workday, foraging local flowers from morning until evening and retiring to their nests at "night" despite the sun's 24-hour brightness. Working the graveyard shift would maximize their nests' food supply and boost their chances for survival. The results, published in the journal *BMC Biology*, suggest that, unlike reindeer and other Arctic creatures that lose their 24-hour biological rhythms in summer and winter, bees' internal clocks sync to cues other than light and darkness—perhaps variations in temperature or light quality—and that their nighttime rest confers an advantage even greater than extra food. http://bit.ly/busy-bee

Friendly Baboons Live Longer

Want to live a long life? Have lots of friends. Studies in humans have made clear that people with stronger social networks have greater longevity. Now a new analysis shows the same is true for baboons.

Joan Silk, an anthropologist at the University of California, Los Angeles, studied wild baboons in Botswana's Moremi Game Reserve, teaming up with a long-term project led by University of Pennsylvania biologist Dorothy Cheney and psychologist Robert Seyfarth. From 2001 to 2007, the researchers closely watched 44 female baboons, recording how often they approached each other, how long they groomed each other, and other measures of social interaction.

Silk and colleagues reported in *Current Biology* that females who had the strongest, most stable, and longest-lasting relationships with other baboons lived significantly longer than those whose social ties were more fragile and unpredictable. Such findings in a nonhuman primate, the authors write, "suggest that the human motivation to form close and enduring bonds has a long evolutionary history." The researchers speculate that friendship helps buffer the effects of stress and boost physiological repair mechanisms. http://bit.ly/long-life

Unexpected Downturn for Size of Proton

Perhaps subatomic particles are feeling the pinch of the global recession, too: The highest precision measurement yet shows that the proton is 4% smaller in radius than previously thought. That's a big puzzle, as the theory used to calculate the quantity, quantum electrodynamics, is accurate to a few parts in 10 billion in other circumstances.

Randolf Pohl of the Max Planck Institute for Quantum Optics in Garching, Germany, and 31 colleagues studied hydrogen atoms in which they replaced the electron that whizzes around the proton with a muon, a particle 207 times as heavy that decays in 2 microseconds. They then measured the relative shift in the energies of two of the atom's quantum states, or orbitals (right), caused by quantum fluctuations in the electric field binding the muon and the proton. That "Lamb shift" was bigger than expected, the team reports this week in *Nature*. The shift depends on the proton's radius, so the measurement suggests that the proton is smaller than indicated by similar experiments on ordinary hydrogen. http://bit.ly/smaller-proton

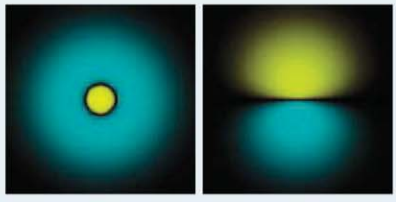

Do Parasites Make You Dumber?

Keeping your kids healthy might make them smarter, according to a new study that finds that countries most heavily affected by infectious diseases generally had the lowest average IQs.

Some scientists have proposed that children who contract "parasites," which includes everything from intestinal worms to bacteria and viruses, devote more energy to fighting off infection and thus have less energy available for brain development. As a result, countries where infectious diseases are prevalent will have lower intelligence, they argue.

To test this idea, Christopher Eppig, a Ph.D. candidate in biology at the University of New Mexico, Albuquerque, and colleagues statistically analyzed the relationship between 2006 data on average IQs in different countries and 2004 data on infectious disease burden from the World Health Organization, which measures potential years of healthy life lost to premature death and illness. The researchers found that this burden was more closely correlated with average IQ than were other variables scientists have linked with IQ, they reported in the *Proceedings of the Royal Society B*. "Parasites alone account for 67% of the worldwide variation in intelligence," Eppig says.

While some scientists say opportunities for enrichment—which might be lacking in countries with low average IQ—are also needed for full brain development, others think Eppig's team, by concentrating on infectious diseases, is on the right track. http://bit.ly/parasite-IQ

Read the full postings, comments, and more at **news.sciencemag.org/sciencenow**.

CREDITS (TOP TO BOTTOM): RALPH STELZER; ANNE ENGH; WOLFGANG CHRISTIAN/DAVIDSON COLLEGE, HTTP://WEBPHYSICS.DAVIDSON.EDU/APPLETS/APPLETS.HTML

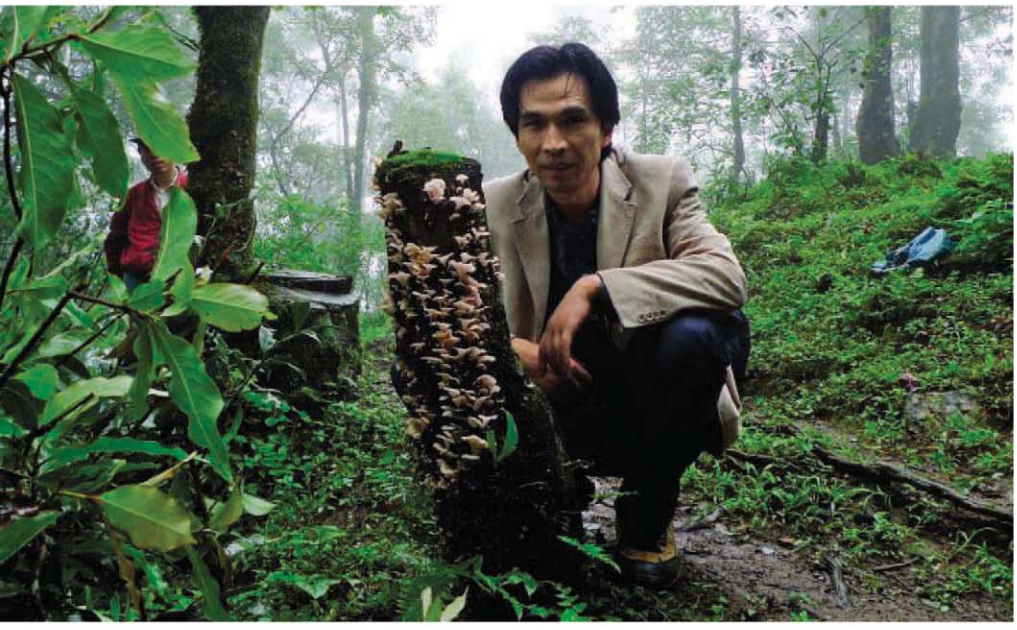

Unassuming. The first time Liu Jikai laid eyes on the small white mushrooms clustered on a tree stump, he didn't believe they could be toxic.

CREDITS: COURTESY OF LIU JIKAI

Will a Midsummer's Nightmare Return?

In southwestern China, people of all ages have been dropping dead suddenly and inexplicably. After a 5-year pursuit, scientists have nabbed a surprising culprit

DALI, CHINA—Every summer, a killer stalks the rugged highlands of Yunnan Province in southwest China. Around the time the monsoon rains begin to fall in late June, "people grow afraid," says Li Guanhui, the sole doctor in Wangjiacun, a village an hour east of the tourist town of Dali in northwestern Yunnan. Li, sitting on a stool in front of a snack shop, cracks a walnut with his bare hand and meticulously picks out the meat. After a while he looks up, brow furrowed. "We wonder," he says, "who will be the first to die? Who will be next?"

For more than 30 years, people of all ages have been dropping dead from sudden cardiac arrest in northern Yunnan. "It's getting everybody across the board: children, adults, older people," says Robert Fontaine, an epidemiologist with the U.S. Centers for Disease Control and Prevention (CDC). The vast majority of deaths occur during the rainy season, from June to August. Yunnan Unknown Cause Sudden Death, as it is called, often strikes in clusters, so the first victim in a village instills dread in the rest of the inhabitants. "It's a fascinating problem," says China's top expert on sudden deaths, cardiologist Zhang Shu of Fuwai Hospital in Beijing. Since 1978, more than 400 deaths and several dozen nonfatal cardiac cases have been attributed to the syndrome.

But this summer, people across Yunnan may be able to rest easy. After a 5-year investigation, a team led by the Chinese CDC in Beijing believes it has uncovered the syndrome's chief cause. CDC and Yunnan Provincial Health Department have embarked on a campaign to warn against eating an innocuous-looking mushroom deemed so trifling that most villages don't even have a name for it. If they have fingered the real culprit—known for lack of a better description as the "little white mushroom"—then this summer could be the first in decades without a death from the syndrome.

The case is not closed, however. Some researchers believe that a substantial percentage of syndrome deaths may be from another cause. Hoping to set lingering doubts to rest, the Chinese CDC–led team will test whether toxins isolated from the fungus, new to science, trigger the heart attacks. But they also acknowledge that some deaths remain unexplained and that other environmental factors may abet the little white scoundrel. "It's a long and complicated story," says Chinese CDC epidemiologist Shi Guoqing.

Portrait of a killer

It dawned gradually on Yunnan health authorities that they had a problem on their hands. The unexplained deaths appear to have started in the late 1970s, largely out of sight in remote villages. As cases piled up, some experts began to suspect that the killer was Keshan disease, a rare heart malady linked to Coxsackie virus and low dietary intake of selenium, a trace element (*Science*, 12 June 2009, p. 1378).

Hoping to cast a wider net, a team led by Huang Wen-li, deputy director of the Yunnan Institute of Endemic Diseases Control and Prevention in Dali, in 2002 compiled a long list of risk factors for the syndrome, including enterovirus infection, drinking water from mountain streams, abusing alcohol, and consuming vegetable oil and mushrooms. "But the evidence for any one factor was not convincing," says Shi Wu-Xiang, an epidemiologist at Dali University who is not affiliated with the team. Two other commonalities were that the syndrome struck almost exclusively during the monsoon season, and in villages at altitudes ranging from 1800 to 2400 meters above sea level. A solution eluded the researchers, however, and the death toll mounted. In 2004, Huang and provincial authorities appealed to Beijing for help. The following spring, the science and health ministries held a conference on the syndrome. "There was a lot of political pressure to solve this mystery," says Zeng Guang, Chinese CDC's top epidemiologist.

The central government ordered the Chinese CDC to join the hunt. The task fell to its China Field Epidemiology Training Program (CFETP), an elite unit formed in 2001 with a mission to crack the toughest cases. The disease sleuths did not immediately warm to the idea of chasing a cardiac killer. Heart attacks are usually brought on by years of poor diet

or lack of exercise. "Normally, I would not touch an investigation of sudden death with a barge pole. The deaths are usually from different causes, and the investigation will lead you nowhere," says Fontaine, who is on assignment as senior adviser to CFETP.

But the case was intriguing, so in June 2005, a team led by Zeng, CFETP's executive director, arrived in Dali and with Huang's group set up a surveillance system. Like clockwork, villagers started dying that July—and CFETP started assembling a vivid picture of their last moments. "We heard amazing stories about how people would drop dead in the middle of a conversation," says Fuwai cardiologist Zhang Jian. But about two-thirds of victims, in the hours before death, experienced symptoms such as heart palpitations, nausea, dizziness, seizures, and fatigue—some of them hard to classify.

At the time, Yunnan investigators were still leaning toward Keshan disease. Genuine Keshan cases had been recorded in areas that reported sudden deaths, and the region's soil is deficient in selenium. Promoting that idea were researchers from the Institute of Keshan Disease in Harbin who had collaborated with Huang's group. "They believed it was Keshan, so that's what they thought they were finding," says Zeng. In August 2005, the government news channel CCTV aired a report on a hard-hit area, Jingdong County, which had tallied at least 40 sudden-death cases from 1993 to 2005. The TV program pinned the blame on Coxsackie virus.

That indictment quickly unraveled. Yunnan researchers had isolated Coxsackie virus from just four villages, and these were strains that are prevalent across China. There was nothing to suggest a new strain spreading, says Fontaine: "The overall pattern was totally inconsistent with Coxsackie virus."

The pathology was more revealing. In Keshan victims, Coxsackie virus ravages heart muscle, riddling the organ with lesions. Some hearts of sudden-death victims showed signs of mild infection, and some looked normal. "It's definitely not Keshan," says Zhang Jian. About half the autopsies and tissue samples revealed severe underlying heart disease. Often the victims had signs of a genetic disorder called arrhythmogenic right ventricular cardiomyopathy, but that was not the answer either. The chronic condition develops slowly, and it's never been known to cause clusters, says Fontaine. Moreover, about two-thirds of cases within clusters were among people who were not related, making a genetic cause exceedingly unlikely.

Lethal locale. The unexplained sudden deaths have occurred in northwest Yunnan.

Then the team caught a lucky break: Local researchers that summer sent the Yunnan investigators pathology slides of heart tissue from three families in which two members of each family died at about the same time. The cardiac lesions were different in each member of each pair, Fontaine says. "And the pathologists said that none of it was enough to kill anybody," he says, indicating that something like a drug or toxin was clearly throwing hearts off kilter. "All the evidence was pointing to a fatal arrhythmia." To probe idea this further, the scientists sought to learn about the electrical activity of victims' hearts, as measured by electrocardiography (ECG). "We needed ECGs on these people before they died," says Zhang Jian. The ECGs confirmed their suspicions.

Shoe-leather epidemiology. After ruling out pathogens as the cause of the sudden deaths, Robert Fontaine (*center*, interviewing villagers) and colleagues at Chinese CDC realized they were on the trail of an unusual toxin.

Reviewing all they had learned, the CFETP team kept circling back to the same suspect. "Mushrooms jumped out at us right away," Fontaine says. But that didn't add up. Yunnan is famed for its wild mushrooms, including matsutake that end up on dinner plates in Japan and *Boletus edulis*, or porcini, that are shipped all the way to Europe. Villagers insisted they knew which are poisonous and which are edible. And it seemed that nobody else in the world was dying after dining on Yunnan mushrooms.

Unlikely villain

In the hills east of Dali, villagers lead a hard-scrabble life, says Shi Wu-Xiang, who over the past 5 years has assessed living standards in places where the syndrome has struck, including Wangjiacun. "This disease is related to poverty" and perhaps influenced by local customs, he says. Mushrooms are a key part of everyone's life. On average, Shi says, one-third of villagers' income is from tobacco farming, one-third is from other crops such as rice and from handcrafts, and one-third is from wild mushrooms.

Mushrooms are gathered in July and August—the height of the rainy season. "Almost the entire village collects," says Li Linmei, a farmer in Wangjiacun bedecked in pale-green bracelets made of local jade, a talisman thought to promote longevity. Families fan out into the countryside, she explains, and will often spend several nights at the mushroom grounds. "Mushroom ladies" go village to village buying up the bounty and moving it to middlemen who sell to restaurants or exporters.

Mushroom picking could explain the syndrome's seasonality and narrow altitude band, says Shi Guoqing. Soon after arriving in Yunnan in 2005, his group had queried villagers about fungi. "We had no idea what kind of mushroom we were looking for. So we asked them what kind they ate," he says. Most villagers, they learned, refrained from eating mushrooms. "They are very poor; they want to earn money. So they don't eat the fat and juicy ones; they sell them," Shi says.

But then in 2006, CFETP began chasing an important new lead. That year, they found curious mushrooms in one home that had experienced sudden deaths. Then a sudden death occurred in another county—and the victim's family members admitted that they had consumed this kind of mushroom. "The mushroom ladies never buy them," Shi says. These mushrooms, little and white and fragile-looking, have no commercial value and turn

CREDITS (TOP TO BOTTOM): M.TWOMBLY/*SCIENCE*; COURTESY OF CFETP

brown quickly after being picked. The CFETP team learned that 3 years earlier, Huang's group, while investigating a case cluster, had collected the nameless mushroom, diced it, and fed it to mice. The animals suffered no ill effects, so the experiment was filed away as a negative result. Dubious, Chinese CDC toxicologists brought samples back to Beijing and did their own mouse-feeding study. They too did not observe an effect.

But in 2007, the circumstantial case against Little White grew stronger. The CFETP team heard about two more sudden-death clusters and raced to the villages. They showed photos of the mushroom to surviving family members and neighbors, who confirmed that the stricken individuals had eaten it. Could the toxicology tests have been misleading? they wondered. "We thought the mushroom might contain a low-level poison," Shi says. "Some people may eat this, no problem. Other people who eat too much, or who have underlying heart disease—they may have trouble." The mice might not have consumed enough of the fresh mushroom to show an effect, Shi says. They had to try again.

The next summer, CFETP asked Liu Jikai, a medicinal chemist at the Kunming Institute of Botany, in Yunnan's capital, to make preparations of the suspicious mushroom for toxicity testing. Liu had recently extracted several antitumor agents from Yunnan mushrooms, including what may be the priciest variety in all of China: *ganbajun*, or groundwart, which can cost up to $100 per kilogram. From that species, his group has identified eight new pigments that are 20 times as potent antioxidants as vitamin E.

The first time Liu laid eyes on Little White, "I didn't believe it could be toxic," he says. His institute colleague, taxonomist Yang Zhuliang, deduced that the mushroom is a new kind of *Trogia*. "Not much is known about this genus," Liu says, apart from the fact that it was not thought to include poisonous species. Little White, which sprouts from downed trees, was by no means rare. Yet numerous surveys had missed it.

In 2008, the Institute of Laboratory Animal Science in Beijing tested Liu's extracts in mice—and all the animals died. With evidence mounting against Little White, CFETP and local health officials began to warn villages to steer clear of it. Shi Guoqing's team went to Jingdong, the blighted county in the CCTV program. Earlier, local investigators had not found the mushroom there. But when CFETP staff showed pictures to villagers, Shi says, "they said, 'Yes, we ate this, but we thought it was safe.' "

Last year, 15 of 16 sudden deaths blamed on the syndrome occurred in areas with no previously reported cases, including 14 in one county. These areas had not been alerted to Little White. Among the deaths were four members of a family: the mother, two daughters, and a son-in-law. Two young children survived. "They could not tell us anything useful," says CFETP's Shen Tao. "But we found dried little white mushrooms in the kitchen. It was quite clear what had happened."

In the meantime, scientists and an army of farmers hit the highlands last summer and "collected a huge amount" of Little White, Liu says. In the months since, his group has attempted to unmask the toxin. First, they zeroed in on ammonia-based cyclic peptides. These proved benign. Then they isolated three unusual amino acids. Most amino acids are building blocks of proteins, but Little White's trio is not associated with any protein, and one is new to science. "All three are toxic but not extremely so," says Liu. Dissections of mice infused with the amino acids revealed intestinal bleeding and edema—but no cardiac lesions. That makes sense, says Fontaine. "If you find a lesion in the heart, then you've got the wrong poison," he says, because human victims also don't have cardiac lesions from the toxin.

The mechanism remains a riddle. "What's happening in Yunnan isn't expected from any other mushroom toxin," says Fontaine. "What we have here is a toxin that's picking off vulnerable people. Anybody who is susceptible and is pushed over the edge will get a fatal arrhythmia."

Going door to door. Epidemiologist Shi Wu-Xiang (*left*) queries a farmer in Wangjiacun about his plans for gathering wild mushrooms this summer. Most villagers can only afford to eat mushrooms that they are unable to sell.

CREDIT: R. STONE/*SCIENCE*

An accomplice—or second killer?

Not everybody buys that explanation. "I don't think it's related to mushrooms," says Wangjiacun's doctor, Li Guanhui. He believes that mountain streams are contaminated with a toxin or pathogen that causes the syndrome. In his experience, he says, "most cases are linked to dirty water." Fuwai's Zhang Jian sees merit in that idea. "People in that area like to drink water from the mountain," he says. "To me it has a very strange taste, but villagers don't like to drink purified water because it has no taste!" His Fuwai colleague Zhang Shu also is not convinced that the little white mushroom is the sole culprit. "I don't think this is the last word," he says.

Indeed, not all sudden-death victims ate the mushroom. But CFTEP researchers think they have the explanation. From the start of the investigation, they had suspected that heavy metal poisoning may play a role in the syndrome. One element seemed most likely: barium, which is used to induce arrhythmias. "If you want to test a drug for antiarrhythmic properties, you give lab animals barium," Fontaine says.

In 2006, the team rushed to two villages that had reported sudden-death clusters and took blood samples from victims and surviving family members. Many had high barium levels; one victim's was highest. Two years later, examining another cluster, they measured high barium levels in the blood, urine, and hair of victims, as well as in local water. In some Yunnan mushrooms—including Little White—barium readings were off the chart. Also pointing to barium are dozens of ECG readings of ill and healthy villagers. A remarkable 40% of exams revealed an abnormal heart electrical pattern called a long QT interval, a major risk factor for sudden death. Barium is known to trigger a long QT.

Putting the strands together, Zeng's team hypothesizes that the little white mushrooms have caused a large share of sudden deaths in Yunnan, perhaps abetted by barium from local foods or untreated water. If a sudden death occurs this year, CFETP researchers hope to detect Little White's amino acids along with barium in the victim's blood. "That would be strong direct evidence," Liu says.

One question may never be answered. "It's still a puzzle why the villagers didn't figure out themselves that the mushrooms are toxic," Fontaine says. But as a public health threat, he says, Yunnan sudden death syndrome may have been vanquished. **–RICHARD STONE**

Nobel-sized attic. Baruch Blumberg has hepatitis B virus samples going back 50 years.

CREDITS: J. COUZIN-FRANKEL/*SCIENCE*

SCIENTIFIC COLLECTIONS

The Legacy Plan

After a long career, you're ready to close the lab and give away a lifetime's worth of specimens. Who will take them?

PHILADELPHIA, PENNSYLVANIA—He never studied history, but Baruch Blumberg is surrounded by it. His home in downtown Philadelphia is steps from an 18th century graveyard that he cuts through to reach the local coffee shop. He presides over the American Philosophical Society, founded by Benjamin Franklin, who, as it happened, died "right down the street," Blumberg says. The walls of his top-floor office are lined with mementos of his nearly 85 years: photos from his time in the U.S. Navy, a certificate marking his induction in 1993 into the National Inventors Hall of Fame, a black-and-white photo of a long-ago field trip to Africa. He even has what appears to be an autographed photo of Albert Einstein that reads, "Congratulations Barry, Al."

"Impressive, eh?" says Blumberg, before confessing that the picture is actually from *Life* magazine, one he tore out and signed himself back in grade school. And saved.

Blumberg has other trophies. Among the most valuable, in his estimation, are those that helped him win a Nobel Prize in 1976 for discovering the hepatitis B virus and inventing a vaccine against it. During the decades he spent studying the liver disease, he collected more than 450,000 blood samples. Although Blumberg remains active, his lab at Philadelphia's Fox Chase Cancer Center closed years ago and his sample collection sits mostly unused, with an uncertain future. No one seems to know quite what to do with it, least of all Blumberg himself.

Scientists don't like to stop working. Yet eventually, at least some do move on and bid their colleagues farewell. And then their collections of blood, DNA, cancer tissue, and more, amassed over the course of their career, need a new steward. But finding one can be difficult, given the cost of archiving and storing samples, as well as concerns about their quality and the suitability of informed consent obtained long ago.

"These samples—they're not easy to separate yourself from," says Anna O'Connell, who retired in February after 51 years at Fox Chase. She spent 40 of those years managing Blumberg's hoard, which eventually took up three and a half giant walk-in freezers, each one measuring 3 meters by 3 meters. For researchers, "it's like their lives are there," O'Connell continues. They've dedicated themselves to the samples, and the samples have helped fuel their career. "But sometimes," says O'Connell, "you have to make a decision" to let go.

There is no academic standard to guide collection bequests, no national repository to hold them. Current studies often include central banks for tissue and DNA, but many researchers, particularly those nearing retirement age, still keep personal repositories in their lab freezers. There's pressure on them to develop contingency plans, but few are willing to confront the toughest issue: whether their collections, which they hold dear, are worth preserving indefinitely.

Winding down

"We've got an aging workforce," says Carolyn Compton, who heads the Office of Biorepositories and Biospecimen Research at the National Cancer Institute (NCI) in Bethesda, Maryland. She knows more than she would like about retiring researchers hunting for a place to stash their samples. "Investigators send these heart-rending pleas to the NCI," begging the institute to "take over these collections. … I can't tell you how common this is." Compton has little sympathy for them. "The NCI has no budget for funding your biospecimen collection for all eternity."

In the last month or so, Compton has had two requests from retiring researchers who amassed large biorepositories and want NCI to adopt them. The answer was the same she gives to all such inquiries: Sorry, but no.

Because tumor tissue is so often banked for research after surgery, NCI struggles with storage more than most. For years, it offered little guidance. Then in 2007, NCI released its "best practices" for biospecimens, urging researchers to develop what Compton calls a "legacy plan." Essentially, she's talking about a will spelling out the fate of specimens if funding evaporates, the study for which they were collected ends, or the researcher holding them retires or dies.

Unlike a traditional will, the options for specimens are more limited and potentially

much more complicated, because the decision isn't the researcher's alone. In a landmark court case in 2006, a Missouri judge ruled that specimens don't belong to the researcher but rather to the institution. The case of *Washington University v. Catalona* pitted the St. Louis school against a prostate cancer specialist, William Catalona, who was moving to Northwestern University in Chicago, Illinois, and wanted to take his vast repository with him. The judge ruled in favor of Washington University, which sought to keep a potentially lucrative blood and tissue bank—a decision upheld the following year on appeal (*Science*, 29 June 2007, p. 1829).

"The NCI has no budget for funding your biospecimen collection for all eternity."

—CAROLYN COMPTON, NATIONAL CANCER INSTITUTE

Human samples come with myriad other issues. Samples collected before the mid-1990s tend to have less stringent terms of informed consent. "Individual consent was not considered necessary" decades ago, Blumberg recalls, when he visited remote communities worldwide—in Africa, South America, the Arctic, the Pacific Islands, and elsewhere. Permission from village leaders and local medical personnel was enough.

Researchers rarely try to predict what future generations will demand of their samples. "It's not something you think about when you're 35 and starting your career," says Kenneth Kidd, a geneticist at Yale University who with his wife, Judith, a physical anthropologist, has amassed 3000 samples from 57 different populations. The Kidds, both 69, developed health problems several years ago. Although now both are doing well and are hard at work, the experience prompted them to consider for the first time the future of a collection they deem both rare and valuable. "We realized that we were not immortal," Kidd says.

The Kidds have strong feeling about how their samples ought to be used by others—or more precisely, not used. Consent forms for samples collected beginning in the 1990s state that they cannot be sold or otherwise generate a profit or patents, and "we are imposing the consent retroactively" on older samples that lacked this clause, because no one considered it at the time, says Kidd. "We realize that if we went to the same population today, they would want that."

Whereas the Kidds are narrowing consent, donors today often give much broader consent than in the past. Samples can be shipped anywhere, for example, or used to study any number of diseases. "The consent [from the past] might preclude you from doing anything, even though you know you have a gold mine in the freezer." says Anna Suk-Fong Lok, a liver disease specialist at the University of Michigan, Ann Arbor.

Quality control and accurate record-keeping are critical, too. Samples might be degraded from having been frozen and thawed many times, or data describing them might have been marked on "sheets of paper that no one else can find," says Lok. Even with good consent, she says, she'd need to know whether the samples are in usable condition and come with reliable clinical information—in other words, if "you don't even know whether sample 1 and sample 101 belong to the same person, then there's really nothing you can learn." Although Lok says Blumberg's collection might be of benefit to her, "I would ask him all these questions" before agreeing to take on any samples.

Golden opportunities

Despite their limitations, decades-old specimens can yield unexpected treasures.

Leonard Seeff, like Blumberg a hepatitis specialist, was making his "liver rounds" at the Walter Reed Army Medical Center in Washington, D.C., back in the 1990s when he overheard a colleague talking about nearly 100,000 blood samples he had recently acquired. "They had been drawn on an air force base in Wyoming" between 1948 and 1954, says Seeff, now 74 and a part-time scientist at the U.S. Food and Drug Administration. "They sat in a basement for 25, 30 years" at least, he says. After the researcher who collected them died, the hospital stacked them in an ice cream truck and sent them to an infectious-disease specialist in Minneapolis, Minnesota, who was willing to take them on. Legend had it that the basement freezers in which they'd been stored were themselves encased in ice, because they sat underneath a leaky air conditioner—meaning the samples were better preserved than one might expect.

Seeff immediately saw an opportunity. He had more than 8000 blood samples tested for hepatitis C, whose origins were uncertain, and found that a handful contained the virus—the earliest it had been detected in the United States. Furthermore, he and some colleagues managed to track down six members of the group who had been infected, and "most of them were doing fine some 45 years later"—providing valuable information on the natural course of the disease. Old samples can answer questions that others cannot, and some argue that

Dream on. Long-term storage in liquid nitrogen, used at the Coriell Institute for Medical Research repository, is not always an option for old collections.

CREDITS (TOP TO BOTTOM): NATIONAL CANCER INSTITUTE; CORIELL INSTITUTE FOR MEDICAL RESEARCH (2)

this makes them worth preserving.

Sitting in his shaded garden on a muggy day, wearing khakis and sandals, Blumberg describes the huge reel-to-reel tapes that hold data on his earliest samples. (Data on newer ones are stored in a secure computer system.) He believes the specimens, which are stripped of names, could be useful in the hunt for new viruses or other microorganisms, or to track the evolving history of hepatitis B and other genomic sequences. The oldest date from 1957, he says. Among other things, he used samples collected from leprosy patients in the Democratic Republic of the Congo to determine that those chronically infected by the retrovirus HTLV-1 were much less likely to survive than were patients who were uninfected.

When it comes to informed consent, says Blumberg, "I haven't looked into it. … One would have to consider each collection independently," for example, those that made up distinct studies. O'Connell says that although any new research project on the samples would need careful vetting, the consent under which they were collected was "always broad" and they can be used for anything.

But even when samples are in good condition, no one else might care as much about them as the person who lovingly collected them. In 2003, Kirsten Fischer Lindahl retired from the University of Texas Southwestern Medical Center at Dallas, where she had worked in mouse genetics. Like almost everyone else, she didn't give much thought to what to do with her vast repository of mouse tissues until she was on her way out the door—and then she started to worry. The Howard Hughes Medical Institute, which had supported Fischer Lindahl's research, offered her a liquid-nitrogen storage tank until she sorted out what to do with the samples.

Four months after she left, the tank malfunctioned. "The whole thing thawed and it had to be thrown out," she recalls. At the time "it seemed terrible." But soon she felt a weight lifted off her shoulders. In retrospect, she says, no one, other than her, was inclined to parse the mouse tissue. In 7 years, she's gotten maybe two requests for the samples.

Although not retired, Lok experienced something similar when she relocated from Hong Kong to the United States. Her university in Hong Kong exerted its right to keep hepatitis samples she'd collected, so Lok divvied up each blood specimen, taking half for herself and leaving half behind. "No one ever touched the samples" in Hong Kong, she says. Meanwhile, "I published 22 papers based on them."

History in vials

Most of Blumberg's samples sit in an old attic on Fox Chase's leafy campus. To reach them, one takes an elevator two stories and then climbs a flight of stairs, with the outdoor heat seeping in. The attic used to house library stacks; now, three massive walk-in freezers take up nearly all the space. They're kept at or below –20°C, and lined with hundreds of boxes filled with vials of serum. Each box is hand-numbered and sometimes labeled with the vials' population of origin: Finnish, Mexican Indians. At the top left of one freezer sits box 0001: the very first samples Blumberg collected.

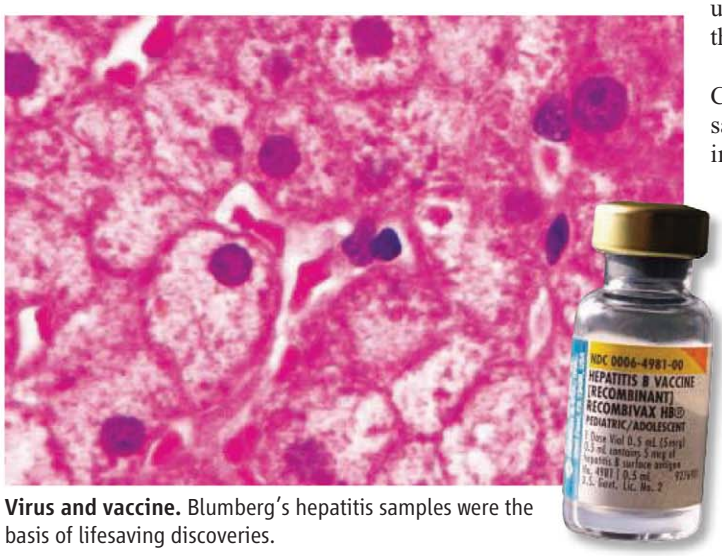

Virus and vaccine. Blumberg's hepatitis samples were the basis of lifesaving discoveries.

Two years ago, more than 40,000 of Blumberg's more recent samples were shipped to the Hepatitis B Foundation in Doylestown, Pennsylvania, for research projects. Now, Fox Chase is likely to take them back. O'Connell thinks the cancer center ought to consider investing in more modern "uprights" for storage—but those cost $8000 to $10,000 each, and Blumberg's collection would occupy 10 of them.

Blumberg believes it would take an archivist 2 to 3 years to sort through his collection to determine the samples' condition. "Some may have evaporated," he says. In the end, an archivist "may decide they're not valuable," although, he says, "I think a lot of them are." Destroying even some of the samples troubles him. "We're sort of stewards of this information that could be used in the future."

Jonathan Chernoff, deputy scientific director at Fox Chase, has been talking with O'Connell and Blumberg about what to do. "I don't think I'm smart enough" to anticipate how the collection could serve science in the future, says Chernoff. He poked around to determine whether the samples were still being used, and the answer was, not often. Ironically, Blumberg's success in developing the vaccine has made his own collection obsolete—at least for hepatitis B work, where, says Chernoff, "the science has moved on" and, although there are still new infections each year, relatively few people work in the area. On the other hand, the samples might come in handy for other projects. "It could be that a few years from now someone could say, 'If only I had samples from Senegal from the '60s and '70s' " to answer a particularly pressing research question, Chernoff points out. "I hate to be the guy to say, 'Well, we used to have those until we threw them out.' "

Given the uncertainty, Chernoff plans to keep the samples at Fox Chase while he's in his current position. But in the long term? "I don't know that I can convince another generation to hold on to these as memory fades," he says. Like Blumberg, Chernoff wishes there were dedicated funding, or a national archive, for historic specimens like these.

Going forward, research institutions are considering their options. The Medical Research Council in the United Kingdom is setting up the UK Brain Banks Network to ensure that samples are carefully preserved and widely available for research. Many universities and cancer centers, including Fox Chase, are establishing their own repositories with consistent standards. One long-term solution for cancer research could lie in "a Match.com for specimens," says Compton. With echoes of the popular dating site, a Web tool called the NCI Specimen Resource Locator matches specimens in need of a home with researchers willing to take them in.

Still, hundreds of investigators maintain personal collections. And, says Compton, they don't think about them "with this kind of seriousness of intent. Their idea of a biorepository … is a freezer in the hallway with an Excel spreadsheet taped to the door." For those, a legacy plan comes only when someone realizes it's missing.

–JENNIFER COUZIN-FRANKEL

CREDITS: WIKIPEDIA; MICHELLE DEL GUERCIO/PHOTO RESEARCHERS INC. (INSET)

PROFILE: JOHN ROGERS

Farewell to Flatland

By creating electronic materials that bend and stretch, a pioneering researcher could change the way we light our homes, treat diseases, and power the planet

In the summer of 2000, at age 33, John Rogers was named as one of the youngest department managers ever at the famed invention shop, Bell Laboratories in Murray Hill, New Jersey. But within months, he was caught in the middle of what he calls "a complete disaster." Shortly after Rogers took the helm of his department, a Bell Labs postdoc and physicist named Jan Hendrik Schön joined the lab's full-time staff. Schön was already a hotshot at Bell Labs and beyond. In a series of high-profile papers, Schön and Bell Labs colleagues reported a steady stream of advances illuminating the way electric charges move through organic crystals. They saw superconductivity, the fractional quantum Hall effect, laserlike behavior—each advance more dramatic than the last. Conference invitations poured in. There were even rumors of a possible Nobel Prize.

Then it all came crashing down. In the autumn of 2002, Schön was found to have faked experimental results in at least 17 published papers (including six in *Science*). "It was off-the-charts awful," Rogers recalls. "I hadn't managed a postdoc before, much less a department, much less a monster." His anger over what he considers Schön's betrayal remains fresh.

To make matters worse, Lucent Technologies—then Bell's parent company—was in the process of imploding financially, forcing managers to shed staff members and talent. Rogers says that at the time he wasn't overly concerned that Schön's misdeeds would contaminate him. "I was more concerned about the taint on the lab. It didn't affect Lucent's decisions [to cut research staff members]. But it didn't help."

Shortly after news of the fraud broke in the summer of 2002, Bell Labs investigated and ultimately fired Schön (*Science*, 4 October 2002, p. 30). And in December 2002, Rogers left Bell Labs to take an academic position at the University of Illinois, Urbana-Champaign, in hopes of giving his career a fresh start.

Rogers hasn't just survived—he has thrived. Running a lab with some 40 students and postdocs and working with colleagues and collaborators around the world, Rogers has pioneered a new approach to patterning conventional flat, rigid semiconductors, such as silicon, atop lightweight, flexible surfaces of nearly any type and shape. That advance is ushering in a new era of lighting, medical equipment, and solar cells that are all quickly moving to commercialization and garnering Rogers plenty of attention. Last fall, Rogers won a MacArthur Fellowship, commonly called a genius grant. And others are offering praise as well. "I've been a fan of John's from the beginning," says Michael McAlpine, a chemist at Princeton University, who also works on novel flexible electronic devices. "He's one of the most creative scientists out there."

Science that works

Rogers's knack for finding novel ways to manipulate semiconductors started early. After earning degrees at the University of Texas, Austin, and the Massachusetts Institute of Technology (MIT), Rogers served as a postdoc with George Whitesides, a chemist at Harvard University. Whitesides, a Renaissance scientist with expertise in fields as far-ranging as nanotechnology and the origins of life, was looking for a cheaper alternative to photolithography, the technique used to pattern computer chips. Rogers helped develop a technique called microcontact printing, capable of patterning tiny features using what amounts to advanced rubber-stamping techniques.

While working at Harvard, Rogers also formed a start-up company to commercialize his doctoral work at MIT: a technique for measuring the thickness of metal films with lasers, still used by chipmakers today. Although commercializing a new technology was difficult, Rogers says that seeing his work succeed commercially gave him a taste not just for pushing scientific boundaries but for inventing technology that affects people's lives. After Harvard, Rogers jumped to Bell Labs, where his approach of coupling science and engineering was strongly encouraged. The company had a reputation for backing revolutionary basic research. But with Lucent struggling, managers were desperate to provide potential products for its business units. Rogers came up with a technique for designing miniature heaters on the surfaces of optical fibers to control the way light propagates through them. The technology quickly moved into products and, like the laser thickness meter, is still sold today.

The ordeal with Schön barely dented Rogers's personal success at Bell, but Rogers says the experience left its mark on his approach to science. "It probably underscored my emphasis on engineering," he says. "If you are making a physical thing and send it to a collaborator, it has to work in other people's hands. It takes the issue of fraud off the table."

Stretchy circuits, bright tattoos

The novel stamping techniques Rogers developed with Whitesides proved ideal for patterning the newly popular flexible organic electronics. Rogers himself devel-

CREDIT: THOMPSON-MCCLELLAN

oped a love-hate relationship with the materials. Their malleability made them ideal for many novel applications, such as lightweight or curved displays. But electrical charges plod through organics, making organic electronics slow. Rogers wanted the best of both worlds: the speed, light-emitting capabilities, and durability of inorganics, and the flexibility of organics.

He found it by turning to nanotechnology. In a series of papers starting in 2005, Rogers and colleagues showed that most flat, rigid, high-performance semiconductors could become flexible if they were merely cut into ribbons just a few tens of nanometers thick. A paper published online in *Science* on 15 December 2005, for example, described a way to pattern silicon nanoribbons on rubber sheets so that the ribbons not only bent when flexed but continued to function as semiconductors. Rogers's team went on to make ever-more-sophisticated designs, including novel ways of making bendable circuitry, solar cells, and lights. Although not alone in this pursuit, "Rogers has been a pioneer in this direction," says Ali Javey, an electrical engineer at the University of California, Berkeley.

More recently, Rogers and his colleagues have begun showing off what they can do with flexible electronics. In a paper published online in *Science* on 27 March 2008, for example, they reported that their printing techniques could make silicon circuitry that not only bends but even folds. Down the road, such pliable circuits could be useful for making paperlike displays that can be folded, or biomedical devices that flex like skin to conform to a person's body.

Such complex devices are a major focus for the Rogers group, says Zhenan Bao, a former colleague of Rogers's at Bell Labs, now a chemist specializing in flexible electronics at Stanford University in Palo Alto, California. "In a lot of his projects, you see not just a single transistor or single solar cell but an array or a medical device," Bao says. "It allows you to start imagining what future technology will look like."

Another recent push for Rogers has been in solar cells. Organic solar cells typically transfer only 5% to 10% of the energy in photons into the electrons that make up an electric current. Silicon does far better, about 20%. Compound semiconductors such as gallium arsenide (GaAs) can top 40%, which is why they are used for generating power in space. But GaAs is very expensive.

Rogers, his Illinois colleague Ralph Nuzzo, and others reported in the 20 May issue of *Nature* a way to make cheap GaAs solar cells by printing tiny flecks of the material on plastic. Starting with an expensive GaAs substrate, they use conventional semiconductor growth techniques to grow stacks of two alternating semiconductor alloys on top of it. The first is the material from which the solar cells will be grown, a combination of GaAs and aluminum gallium arsenide (AlGaAs). The second is a "sacrificial layer" made from a different semiconductor alloy. The researchers cut a grid of lines through these alternating layers and then chemically etch away all the sacrificial layers at once, liberating thousands of flecks of high-quality GaAs/AlGaAs. The GaAs substrate is reused to make a new batch of flecks. Finally, they use their stamping techniques to print the flecks in a regular array on a plastic sheet. The flecks are wired up and topped with glass lenses. The lenses capture light over a large area and focus it on the tiny semiconductor flecks, which convert the light into electricity.

"John has done great work—not only beautiful science, but he takes an approach that can be transitioned to industry," Javey says of the new work. The transition is already taking place. Rogers, Nuzzo, and others recently licensed their GaAs technology to a solar start-up called Semprius. The company has already made photovoltaics that are 37% efficient and recently received its first order for a small system.

Rogers's research has recently veered into biology, with an ambitious goal: integrating electrical and optical devices with living tissue. Other groups have been making a similar push, but Rogers says some of them have used conventional rigid silicon electronics to make what he calls "bricks on straps" and "chips on tapes": devices such as heart monitors that must be strapped or taped to a subject. "Evolution has come up with lots of solutions to challenging problems," Rogers says. "None of those look like a silicon wafer."

Rogers's solution was to change that look. He and his colleagues have made electronic arrays that can be mounted on extremely thin, flexible plastic sheets, or even on a type of silk that slowly dissolves when implanted in tissues. In the 18 April issue of *Nature Materials*, they reported using an electronic array to map the electrical activity on the surface of the brains of cat models. They are now working toward using such implantable arrays to prevent future seizures in patients with epilepsy by disrupting the synchrony characteristic of an epileptic seizure.

In a paper that appeared online 24 March in *Science Translational Medicine*, Rogers and colleagues from the University of Pennsylvania and Northwestern University in Evanston, Illinois, reported implanting an array of 2016 silicon transistors on thin, flexible plastic film to record electrical activity from the beating heart of a live pig. Someday such devices might be used to treat arrhythmia, both by recording electrical activity in heart cells and by delivering bursts of radio-frequency pulses to kill small patches of cells that are triggering irregular heartbeats.

Finally, Rogers and his colleagues have developed low-cost, highly efficient micro light-emitting diodes (LEDs). Not only might such devices revolutionize home lighting, but the group is working on ways to implant them in tissues to make what amount to LED tattoos. Hipster appeal aside, Rogers suggests that micro-LEDs might be integrated with biochemical sensors to warn of dangerous medical conditions. Out there? Perhaps. But if Rogers is right, the next semiconductor revolution could reach far beyond your desktop.

–ROBERT F. SERVICE

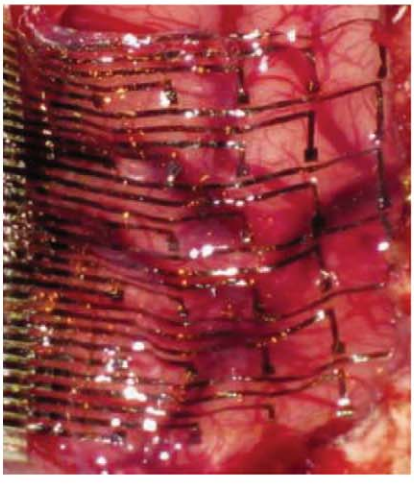

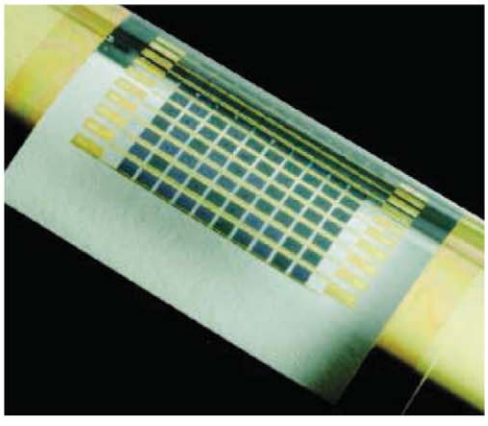

New twist. Flexible devices for monitoring brain activity (*left*) and making cheap solar power (*right*).

CREDIT (LEFT TO RIGHT): D-H. KIM *ET AL.*, *NATURE MATERIALS* **9**, (18 APRIL 2010) ©2010 NATURE PUBLISHING GROUP; J. YOON *ET AL.*, *NATURE* **465**, (20 MAY 2010) ©2010 NATURE PUBLISHING GROUP

LETTERS

edited by Jennifer Sills

Barometer of Life: Sampling

IN THEIR POLICY FORUM "THE BAROMETER OF LIFE" (9 APRIL, P. 177), S. N. Stuart and coauthors report that 160,000 species are required to approach a meaningful indicator of the health of species. Assuming a linear projection, at the current rate of increase and level of investment, this goal will take until 2040. For the barometer to provide trend information (change in status), the 160,000 species assessments will have to be repeated on a regular basis, increasing the time frame for delivery. It is hoped that increased investment and commitment will help accelerate this process, but this will inevitably take many years; the health of the planet's species needs urgently to be better understood.

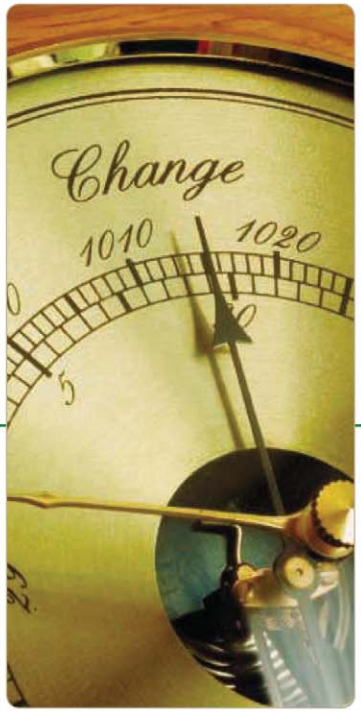

Conducting conservation assessments of a representative sample of a set of species (*1*) can produce robust, meaningful results in a shorter time frame [e.g., (*2*)], setting a baseline from which future change can be measured and indentifying a suite of species whose fate can be tracked over time. By the end of 2010, this new approach will reveal the status of all vertebrates, a large group of plants, and a number of invertebrate groups (*3*).

This technique has important advantages. (i) It enables rapid assessment of groups of species, even those that are comparatively poorly known. (ii) It will add groups of species to the barometer that are more important to ecosystem function (e.g., pollination, water filtration, carbon sequestration) than those that are currently assessed. By using the sampled approach and creating a barometer that is truly representative of biodiversity, we will better equip ourselves to make the right decisions about maintaining life on Earth.

BEN COLLEN* AND JONATHAN E. M. BAILLIE

Zoological Society of London, Regent's Park, London NW1 4RY, UK.

*To whom correspondence should be addressed. E-mail: ben.collen@ioz.ac.uk

References

1. J. E. M. Baillie *et al.*, *Conserv. Lett.* **1**, 18 (2008).
2. V. Clausnitzer *et al.*, *Biol. Conserv.* **142**, 1864 (2009).
3. B. Collen *et al.*, in *Wildlife in a Changing World: An Analysis of the 2008 IUCN Red List of Threatened Species*, J.-C. Vié, C. Hilton-Taylor, S. N. Stuart, Eds. (IUCN, Gland, Switzerland, 2009), pp. 67–76.

Barometer of Life: National Red Lists

IN THEIR POLICY FORUM, S. N. Stuart *et al.* propose "The Barometer of Life" (9 April, p. 177), which would track the conservation status of the global fauna and flora on the basis of the Red List of Threatened Species (*1*). However, restricted knowledge of large sets of organism groups challenges the possibility of true representativeness. To address this problem, Stuart *et al.* argue for investing more resources in global Red List assessment and in accelerating taxonomy and scientific natural history.

In addition to their recommendations, I suggest other ways of speeding up the process. Several national red lists already have a very broad taxonomic scope. For instance, in Nordic countries, more than 40% of all known multicellular species are being assessed every 5 or 10 years, representing all biomes and all major organism groups (*2*–*4*). A number of much more species-rich countries have produced extensive national red lists, such as China, The Philippines, South Africa, Brazil, Venezuela, and Colombia (*5*, *6*). Assessments at a national level could not only complement the Barometer of Life but also serve to explore the extent to which particular organism groups are representative of the biodiversity overall.

With emerging endeavors, such as the Swedish (*7*–*9*) and the Norwegian Taxonomy Initiatives (*10*), aiming at finding and describing every species, we even see the possibility of assessing the conservation status for all species in particular regions. **ULF GÄRDENFORS**

Swedish Species Information Centre (ArtDatabanken), Swedish University of Agricultural Sciences, Uppsala, 750 07, Sweden. E-mail: Ulf.Gardenfors@artdata.slu.se

References and Notes

1. The International Union for Conservation of Nature (IUCN) Red List of Threatened Species (www.iucnredlist.org).
2. U. Gärdenfors, Ed., *The 2010 Red List of Swedish Species* (ArtDatabanken, Uppsala, Sweden, 2010).
3. J. A. Kålås, Å. Viken, T. Bakken, *2006 Norwegian Red List* (Artsdatabanken, Trondheim, Norway, 2006). A 2010 edition is scheduled for the end of 2010.
4. P. Rassi, A. Alanen, T. Kanerva, I. Mannerkoski, Eds., *The 2000 Red List of Finnish Species* (The Ministry of the Environment and the Finnish Environment Institute, Helsinki, Finland, 2001). A 2010 edition is scheduled for the end of 2010.
5. R. M. Miller *et al.*, *Conserv. Biol.* **21**, 684 (2007).
6. T. J. Zamin *et al.*, *Conserv. Biol.*, 10.1111/j.1523-1739.2010.01492.x (2010).
7. F. Ronquist, U. Gärdenfors, *Trends Ecol. Evol.* **18**, 269 (2003).
8. G. Miller, *Science* **307**, 1038 (2005).
9. ArtDatabanken, The Swedish Species Information Centre (www.artdata.slu.se/english/).
10. Artsdatabanken, The Norwegian Biodiversity Information Centre (www.artsdatabanken.no).

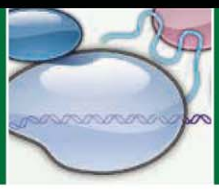

Chromatin repression

150

Stimulating destruction

154

Barometer of Life: More Action, Not More Data

IN THEIR POLICY FORUM, S. N. STUART *ET AL.* called for "The Barometer of Life" (9 April, p. 177) to expand the scope of the IUCN Red List. The barometer would provide more detailed information on the threats, distribution, and extinction risks of 160,000 species considered more representative of the millions of species likely to exist than the 48,000 assessed to date.

We agree that identifying conservation actions to save species depends on knowledge of threats, distribution, and extinction risk, but the conservation benefit of continuing to accumulate such information must be traded off against the benefits of spending the proposed funds on alternative conservation activities, and the return on investment evaluated. Conservation initiatives fail with disturbing regularity (*1*), usually due to a suite of interacting social, economic, and political factors rather than an absence of data (*2*). Conservation plans are unlikely to be significantly improved by increasing the number of taxa upon which they are based, due to the rapidly diminishing returns of biological surveys and the extreme heterogeneity in economic and social influences on decision-making (*3*–*6*).

Although the IUCN Red List has been instrumental in raising global public awareness by documenting the status of threatened species, we question whether its expansion represents a sound return on investment. The US$60 million investment proposed by Stuart *et al*. to expand the Red List could be better spent improving local-scale decision-making and implementing action. For example, the Wildlife Conservation Society spends around US$25 million annually on 1100 staff in 12 countries for its Africa field program, and the New Zealand government plans to spend NZ$30 million a year for the next 50 years on saving 559 threatened species. We have sufficient data to confirm the current unprecedented Anthropocene extinction event. We need to market this fact better and implement action, not add weight to it with more data.

ANDREW T. KNIGHT,[1]* MICHAEL BODE,[2] RICHARD A. FULLER,[3] HEDLEY S. GRANTHAM,[3] HUGH P. POSSINGHAM,[3] JAMES E. M. WATSON,[3] KERRIE A. WILSON[3]

[1]Department of Conservation Ecology and Entomology, Stellenbosch University, Private Bag X1, Matieland 7602, South Africa. [2]Applied Environmental Decision Analysis Group, School of Botany, The University of Melbourne, Melbourne, VIC 3010, Australia. [3]The Ecology Centre and Centre for Applied Environmental Decision Analysis, University of Queensland, St. Lucia, QLD 4072, Australia.

*To whom correspondence should be addressed. E-mail: tawnyfrogmouth@gmail.com

References

1. K. H. Redford, A. Taber, *Conserv. Biol*. **14**, 1567 (2000).
2. A. Jaramillo-Legorreta *et al*., *Conserv. Biol*. **21**, 1653 (2007).
3. M. Bode *et al*., *Proc. Natl. Acad. Sci. U.S.A.* **105**, 6498 (2008).
4. H. Grantham *et al*., *Conserv. Lett*. **1**, 190 (2008).
5. K. Perhans *et al*., *Conserv. Biol.* **22**, 1331 (2008).
6. R. M. Cowling, A. T. Knight, S. D. J. Privett, G. P. Sharma, *Conserv. Biol.* **24**, 633 (2010).

Letters to the Editor

Letters (~300 words) discuss material published in *Science* in the previous 3 months or issues of general interest. They can be submitted through the Web (www.submit2science.org) or by regular mail (1200 New York Ave., NW, Washington, DC 20005, USA). Letters are not acknowledged upon receipt, nor are authors generally consulted before publication. Whether published in full or in part, letters are subject to editing for clarity and space.

Response

COLLEN AND BAILLIE ARGUE THAT EXPANDING the IUCN Red List into a broader Barometer of Life will sometimes require making use of representative samples of sets of species (*1*, *2*). We agree, and indeed the numbers we proposed assumed sampled assessments for many nonchordate taxa, for which assessments of every species are simply not possible in the foreseeable future.

We also agree with Gärdenfors that the barometer must operate at national as well as global levels, and we refer to the importance of national lists (*3*). Increasingly, national and global listing are conducted simultaneously (*4*, *5*), particularly in countries with high levels of endemism. Furthermore, the development of a network of national Red List assessors would increase information availability on the world's species, and strengthen local scientific capacity for generating and using these data to support conservation (*6*).

Our call to invest in the barometer is not an alternative to the good examples of investment in conservation action given by Knight *et al*. The amount spent on data gathering and monitoring should always be a small fraction of the overall conservation budget (noting that donors specialize, some focusing solely on field action, others on research and assessments; funding is often not transferable). What we are calling for is small compared to what must be spent if we are to stop global biodiversity loss. The failure to stem biodiversity loss (*7*) is explained by a widening gap between the mounting pressures on biodiversity and the insufficient responses to those pressures. Consequently, the Organization for Economic Cooperation and Development governments are considering a 10-fold increase by 2020 in international biodiversity assistance [currently US$2 billion annually (*8*)], and IUCN is calling for wealthy countries to invest 0.3% of annual GDP on biodiversity internationally (about US$120 billion) (*9*), making our call for a US$60 million investment in the barometer look small.

Knight *et al*. make the valid point that conservation initiatives do not usually fail because of lack of data. However, they neglect to mention that many essential conservation actions do not happen at all in the absence of data. For example, conservation of globally threatened amphibians was scarcely taking place in 2004 when IUCN first assessed and published the status of nearly 6000 species (*10*), thus stimulating new conservation efforts that otherwise would not have happened [the work of the Amphibian Specialist Group is one example (*11*)]. Thanks to this information, amphibians have joined mammals and birds as species that are considered when evaluating, mitigating, and offsetting the environmental impacts of development projects.

Unfortunately, most of the world's taxa are wholly off the conservation radar, particularly hyperdiverse groups such as plants, fungi, and invertebrates in biodiversity-rich regions where human and financial resources are lacking. Some will be protected by chance through investment in already identified conservation targets, but this will not always be the case. In Madagascar, for example, priorities for expanding the protected area network are very different when considering vertebrates or when integrating data on plants or invertebrates (*12*). And the size and allocation of New Zealand's NZ$30 million yearly budget on threatened species (mentioned by Knight *et al.*) has certainly been influenced

by data on the 92% of their threatened species that are either plants or invertebrates (*13*).

The data in the Red List do much more than confirm the current Anthropocene extinction event, as implied by Knight *et al.*; they are increasingly important in guiding efforts to reduce the severity of biodiversity losses (*14*). For this reason, we believe that a substantial expansion in the taxonomic base of the IUCN Red List would be an excellent conservation investment.

S. N. STUART,[1]* E. O. WILSON,[2] J. A. MCNEELY,[3] R. A. MITTERMEIER,[4] J. P. RODRÍGUEZ[5]

[1]International Union for Conservation of Nature (IUCN) Species Survival Commission, 1196 Gland, Switzerland; United Nations Environmental Programme World Conservation Monitoring Centre, Al Ain Wildlife Park and Resort, Al Ain, United Arab Emirates; and Department of Biology and Biochemistry, University of Bath, Bath BA2 7AY, UK. [2]Museum of Comparative Zoology, Harvard University, Cambridge, MA 02138, USA. [3]IUCN, 1196 Gland, Switzerland. [4]Conservation International, Arlington, VA 22202, USA. [5]Centro de Ecología, Instituto Venezolano de Investigaciones Científicas, Apartado 20632, Caracas 1020-A, Venezuela, and Provita, Apartado 47552, Caracas 1041-A, Venezuela.

*To whom correspondence should be addressed. E-mail: simon.stuart@iucn.or

References

1. J. E. M. Baillie *et al.*, *Conserv. Lett.* **1**, 18 (2008).
2. V. Clausnitzer *et al.*, *Biol. Conserv.* **142**, 1864 (2009).
3. T. J. Zamin *et al.*, *Conserv. Biol.*, 10.1111/j.1523-1739.2010.01492.x (2010).
4. L. R. Minter *et al.*, *Atlas and Red Data Book of the Frogs of South Africa, Lesotho and Swaziland* (SI/MAB Series No. 9, Washington, DC, 2004).
5. R. Valencia, N. Pitman, S. León-Yánez, P. M. Jørgensen, *Libro Rojo de las Plantas Endémicas del Ecuador 2000* (Publications of QCA Herbarium, Pontificia Universidad Católica del Ecuador, Quito, 2000).
6. J. P. Rodríguez, *Endangered Species Res.* **6**, 193 (2008).
7. S. H. M. Butchart *et al.*, *Science* **328**, 1164 (2010); published online 29 April 2010.
8. Convention on Biological Diversity, "Examination of the outcome-oriented goals and targets (and associated indicators) and consideration of their possible adjustment for the period beyond 2010" (2010); www.cbd.int/doc/meetings/sbstta/sbstta-14/official/sbstta-14-10-en.pdf.
9. International Union for Conservation of Nature, "A new vision for biodiversity conservation" (2010); http://cmsdata.iucn.org/downloads/iucn_position_cbd_strategic_plan_and_post_2010_targets_pp_sbstta14_final.pdf.
10. S. N. Stuart *et al.*, *Science* **306**, 1783 (2004).
11. Amphibian Specialist Group projects (www.amphibians.org/ASG/Projects.html).
12. C. Kremen *et al.*, *Science* **320**, 222 (2008).
13. New Zealand Ministry for the Environment, Threatened Species (www.mfe.govt.nz/environmental-reporting/biodiversity/threatened-species.html).
14. A. S. L. Rodrigues, J. D. Pilgrim, J. F. Lamoreux, M. Hoffmann, T. M. Brooks, *Trends Ecol. Evol.* **21**, 71 (2006).

CORRECTIONS AND CLARIFICATIONS

Reports: "Cross-reacting antibodies enhance dengue virus infection in humans" by W. Dejnirattisai *et al*. (7 May, p. 745). On page 747, last paragraph, the following statement was incorrect: "This is the first description, using human monoclonal antibodies, of the serological response in DENV infection." In fact, it had been shown [ ]. S. Schieffelin *et al*., *Virol. J*. **7**, 28 (2010)] that human monoclonal antibodies against DENV E protein were able to recapitulate the serological ADE response of DENV infections.

TECHNICAL COMMENT ABSTRACTS

Comment on "Differential Sensitivity to Human Communication in Dogs, Wolves, and Human Infants"

Sylvain Fiset

Topál *et al*. (Reports, 4 September 2009, p. 1269) reported that dogs' sensitivity to reading and using human signals contributes to the emergence of a spatial perseveration error (the A-not-B error) for locating objects. Here, I argue that the authors' conclusion was biased by two confounding factors: the use of an atypical A-not-B search task and an inadequate nonsocial condition as a control.

Full text at www.sciencemag.org/cgi/content/full/329/5988/142-b

Comment on "Differential Sensitivity to Human Communication in Dogs, Wolves, and Human Infants"

S. Marshall-Pescini, C. Passalacqua, P. Valsecchi, E. Prato-Previde

Topál *et al*. (Reports, 4 September 2009, p. 1269) showed that dogs, like infants but unlike wolves, make perseverative search errors that can be explained by the use of ostensive cues from the experimenter. We suggest that a simpler learning process, local enhancement, can account for errors made by dogs.

Full text at www.sciencemag.org/cgi/content/full/329/5988/142-c

Response to Comments on "Differential Sensitivity to Human Communication in Dogs, Wolves, and Human Infants"

József Topál, Ádám Miklósi, Zsófia Sümegi, Anna Kis

The comments by Fiset and Marshall-Pescini *et al*. raise important methodological issues and propose alternative accounts for our finding of perseverative search errors in dogs. Not denying that attentional processes and local enhancement are involved in such object search tasks, we provide here new evidence and argue that dogs' behavior is affected by a combination of factors, including specific susceptibility to human communicative signals.

Full text at www.sciencemag.org/cgi/content/full/329/5988/142-d

GENOMICS

The View a Decade On

Angela N. H. Creager

Drawing the Map of Life
Inside the Human Genome Project
by Victor K. McElheny
Basic Books (Perseus Books Group), New York, 2010. 383 pp. $28, C$35.50, £16.99. ISBN 9780465043330.

Popular histories of the Human Genome Project (HGP) have appeared since shortly after the enterprise began [early examples include (*1*, *2*)]. Another cluster of books came out after the first draft of the human genome sequence was published, ahead of the original schedule, in 2001 [e.g., (*3*–*7*)]. Victor McElheny's *Drawing the Map of Life* treads a good deal of the same ground but also cuts fresh paths into recent history. McElheny, a science writer best known for his 2003 biography of James Watson (*8*), recounts how particular personalities (not least Watson) and political opportunities shaped the HGP from early proposals vetted at Alta and Santa Cruz to the largely NIH-centered project launched in 1989 and 1990. Although this is familiar territory, McElheny captures vividly the drama of the HGP, particularly once rival Craig Venter threatened to beat the public program to completing a draft of the human sequence. He portrays Francis Collins's steady leadership of the consortium as well as key contributions of researchers such as Maynard Olson and Robert Waterston. Whereas most accounts end with the race to a tie on publishing the human DNA sequence, McElheny follows the story through to the endeavors the HGP has spawned, such as the ENCODE (Encyclopedia of DNA Elements) project and the HapMap Consortium.

The centrality of technology to the era of genomics serves as the book's overarching theme. This leads McElheny to frame the technical origins of the HGP more thoroughly than most previous accounts. His first chapter describes the scientific innovators and techniques that enabled gene cloning and the creation of genomic libraries in the 1970s and 1980s. He makes clear the importance of parallel work on model organisms in the HGP and the focus on mapping, rather than sequencing, in the project's early years. Even this highly planned project had, at times, an unpredictable course. Early opposition to the HGP pivoted on worries that it would industrialize research in molecular biology, which had long been small-scale and hypothesis-driven. McElheny indicates that this did not happen in quite the way critics feared, in part because the technology in the assembly line kept changing and in part because individual contributions continued to matter critically to progress. Moreover, the emerging sequence data on model organisms was indisputably valuable to biologists across fields. In the end, the industrial interface did not lead to mass production so much as to entrepreneurialism. In particular, competition with the private sphere (most visibly represented by Venter's outfit, Celera) inspired many academic sequencers to outperform public goals as well as private rivals. Leaders such as Eric Lander emphasized the need for decentralization, flexibility, and "Just In Time technology decisions" for the project to succeed.

McElheny pays attention (as others have before) to the conflicts that the HGP elicited between the government's commitment to the human genome as a public good and private interests in commercializing the knowledge it produced. He presents the HGP leadership as determined and politically astute, but he does not vilify their private rivals. As he points out,

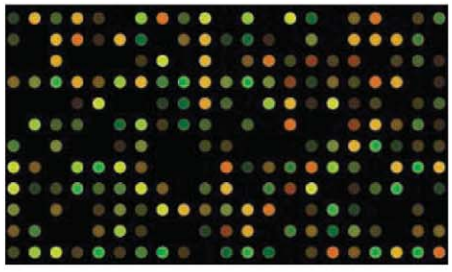

DNA chip microarray.

CREDIT: GUILLAUME PAUMIER/WIKIMEDIA COMMONS

not all of the public-private interactions were combative. In the sequencing of the *Drosophila* genome, for instance, a fruitful collaboration developed between the public project and industry. At the same time, lines were plainly drawn over issues of intellectual property, especially when it came to human sequence data. For the NIH, as well as other national government agencies, philanthropies (such as the Wellcome Trust), some pharmaceutical companies, and university scientists, the Bermuda principle of releasing newly obtained sequence data every day was a defensive tactic to prevent sequences from being patented. As HGP scientists often noted, this meant that those working in the private realm had access to all the public data even as they produced and protected their own. And the defensive tactic was not uncontestable. As McElheny notes, Celera announced in October 1999 that it had provisionally applied for patents on thousands of genes. The consortium's priority of ensuring that the human sequence data remained public became a matter of high politics, with Bill Clinton and Tony Blair calling for "unencumbered access to raw human sequence data." Report of their joint statement, issued 14 March 2000, translated badly on Wall Street, where biotech stocks fell precipitously. Ten years later, the legality of patenting human gene sequences remains to be determined, as evidenced by the recent federal court ruling that invalidated Myriad Genetics patents on two cancer-related genes.

In the last chapters, McElheny appraises the broader shifts in biology and medicine catalyzed by genomics. I found this section of the book the most interesting, in part because the direction and significance of "post-genomics" remain so open to interpretation. As science journalist Nicholas Wade recently observed, the medical advances associated with genomics have been disappointingly modest (*9*, *10*). McElheny details the succession of attempts to relate measurable genetic diversity to disease risk, efforts that have made clear how difficult it is to translate knowledge of an individual's DNA markers into improved health. This does not lead him to be critical of the HGP; on the contrary, the book offers much praise of the technical ingenuity and vision of the molecular biologists that prioritized acquiring sequence data. Nonetheless, the continuing "struggle for medical relevance," as McElheny terms it, does call into question the early claims of rapid cures and benefits that accompanied—and largely justified funding for—the HGP. By contrast, the payoff to biological research has been rapid and extensive. McElheny focuses on the contributions of scientists such as Thomas Gingeras at Cold Spring Harbor Laboratory, who has documented the unexpectedly "pervasive transcription" of the genome.

The book's depiction of current trends in biomedicine, with the decline of "gene-centered" accounts of traits and disease, seems less like a paradigm shift than a new frontier, once again driven by new technologies. The future trajectory, McElheny suggests, is promising though unpredictable. *Drawing the Map of Life* sketches out a more complete history of genomics than previously available, but clearly the story is not yet finished.

The reviewer is at the Department of History, Princeton University, 136 Dickinson Hall, Princeton, NJ 08544–1174, USA. E-mail: creager@princeton.edu

References

1. R. Shapiro, *The Human Blueprint: The Race to Unlock the Secrets of Our Genetic Script* (St. Martin's, New York, 1991).
2. R. Cook-Deegan, *The Gene Wars: Science, Politics, and the Human Genome* (Norton, New York, 1994).
3. K. Davies, *Cracking the Genome: Inside the Race to Unlock Human DNA* (Free Press, New York, 2001).
4. N. Wade, *Life Script: How the Human Genome Discoveries Will Transform Medicine and Enhance Your Health* (Simon and Schuster, New York, 2001).
5. J. Sulston, G. Ferry, *The Common Thread: A Story of Science, Politics, Ethics and the Human Genome* (Bantam, London, 2002).
6. I. Wickelgren, *The Gene Masters: How a New Breed of Scientific Entrepreneurs Raced for the Biggest Prize in Biology* (Holt, New York, 2002).
7. J. Schreeve, *The Genome War: How Craig Venter Tried to Capture the Code of Life and Save the World* (Knopf, New York, 2002).
8. V. K. McElheny, *Watson and DNA: Making a Scientific Revolution* (Perseus, Cambridge, MA, 2003); reviewed in (*11*).
9. N. Wade, *New York Times*, 13 June 2010, p. A1.
10. N. Wade, *New York Times*, 15 June 2010, p. B1.
11. S. Lindee, *Science* **300**, 432 (2003).

10.1126/science.1190992

PHYSICS

How Time Flies

Lisa Jardine-Wright

Time is something that plagues us all; we spend half of our lives wishing it would pass more slowly and the other half wishing events were over. While we all have devices to accurately measure time's passage, we rarely reflect on the fact that time has a direction (except perhaps around birthdays): we all get older, not younger; and we remember the past, not the future. This "arrow of time," Sean Carroll argues in *From Eternity to Here*, is "both a profound feature of the physical universe and a pervasive ingredient of our everyday lives." Once an egg is broken, we cannot reassemble the yolk; once combined, coffee and milk are not to be separated; and an ice cube melted into warm water cannot be reformed—such irreversibility is the hallmark of the arrow of time.

How do we understand this arrow of time or indeed notice its effects? The commonplace examples above, which are used frequently by Carroll, illustrate quite clearly that we identify the arrow of time as order becoming disorder: the continual movement from a lower-entropy state to a higher-entropy state. Because this arrow of time points so emphatically in one direction, perhaps it presents us with a key to understanding the formation and evolution of the universe.

Entropy as defined by Ludwig Boltzmann is the number of microstates equivalent to a single macrostate: More microstates for one given macrostate means higher entropy and a higher likelihood of that state. If we apply this notion to the number of particles in the universe at the Big Bang, the most likely state would be one of high entropy. The incontestable observation that the early universe was in a state of low entropy (isotropic and uniform) provides a further piece in the time-universe puzzle. So our question evolves from why do we experience an arrow of time to why did it all begin with such low entropy? Through persuasive discussions of statistical mechanics and the arrow of time, Carroll (a theoretical physicist at the California Institute of Technology) encourages hope that we can go beyond the Big Bang to formulate a picture of a universe before the beginning.

On a daily basis, it suffices to know the time of day, date, and year as measured from a predefined starting point. Like many cosmologists, I was (before reading this book) happy to consider time as a measurement from the Big Bang to the present day. After all, that is all that really matters from the perspective of our observable universe, isn't it?

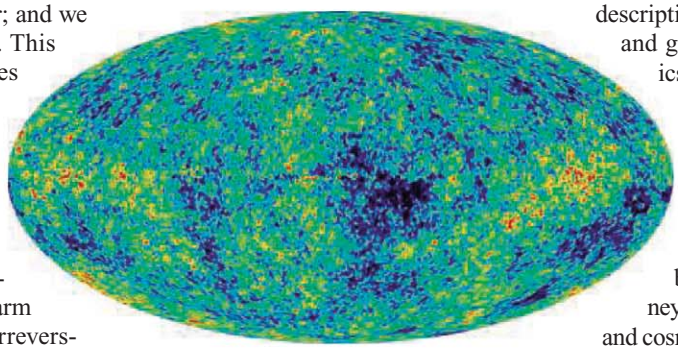

Our universe at 380,000 years. (Wilkinson Microwave Anisotropy Probe)

As Carroll states, "the influence of [the Big Bang] orients us in time, just as the presence of the Earth orients us in space." He notes, however, that in considering the Big Bang as time zero we are avoiding the questions of why its initial state had such low entropy and what came before the Big Bang. Carroll admits that formulations of physical theories of before the Big Bang do not make currently observable predictions. Nonetheless, he discusses how considering the arrow of time can help us piece together a logical, uncontrived, physical picture that explains both why we have a perceived direction of time and how the early universe had such low entropy. There are naturally many uncertainties along the way to constructing such a physically cogent picture, but Carroll is clear about the importance of scientific methodology and honest about his claims—particularly those relating to acceptance of one theory of the universe. While he argues for a multiverse based on a natural high-entropy (de Sitter) space from which baby universes arise, he comments that "we aren't yet able to judge whether this particular [explanation] is sensible, much less part of the ultimately correct answer."

From Eternity to Here
The Quest for the Ultimate Theory of Time
by Sean Carroll
Dutton, New York, 2010. 448 pp. $26.95, C$33.50. ISBN 9780525951339.

As a young, aspiring physics student in the early 1990s, I found Stephen Hawking's *A Brief History of Time* (*1*) essential reading. It introduced me to awe-inspiring concepts and highlighted the important relationships among mathematics, physics, cosmology, and philosophy. Twenty years on, Carroll has gone beyond those revolutionary concepts. He presents a conceivable, coherent picture of the physics of space-time, not just from the Big Bang but through eternity. As one might expect, such a picture encompasses many avenues of physics and philosophy. The author does not shy away from any of them but presents us with clear conceptual descriptions of statistical mechanics, special and general relativity, quantum mechanics, particle physics, and quantum field theory. As an educator and communicator I am interested and enlightened by his descriptions, and as a cosmologist I am invited to challenge my favored explanations.

From Eternity to Here presents both a historical and conceptual journey through the development of physics and cosmology. Although aspects of the book will challenge the interested nonspecialist, it is written in an accessible, conceptual manner rather than through highly mathematical descriptions. Whether a seasoned cosmologist or an enthusiastic apprentice, we are invited to go beyond our comfort zone and confront our preconceptions. Therefore I believe that Carroll's book will appeal equally to both.

References

1. S. Hawking, *A Brief History of Time: From the Big Bang to Black Holes* (Bantam, London, 1988).

10.1126/science.1192247

The reviewer is at Churchill College and the Cavendish Laboratory, University of Cambridge, Cambridge CB3 0HE, UK. E-mail: ljw21@cam.ac.uk

CREDIT: WMAP/NASA

HIV/AIDS

Gender Inequities Must Be Addressed in HIV Prevention

Building gender equity and reducing gender-based violence are vital in the fight against AIDS.

Rachel Jewkes

Worldwide, in excess of 34 million people are living with HIV, with at least 2.7 million new infections occurring annually. For new infections, 71% occur in sub-Saharan Africa. Despite success in expanding treatment, fewer than one in eight people with HIV throughout the world are on antiretroviral therapy (*1*). The expansion of treatment programs is far from keeping pace with increasing numbers of people infected and the changing recommendations for eligibility. Recent failures have shown that avenues of science in which so many hopes have been vested may not provide the key to HIV prevention, at least not in the short and medium term. So the challenge is to deepen our understanding of drivers of the epidemic in different populations and develop a complex multifaceted prevention strategy to address them.

Gender Inequity, Violence and HIV

It is not a new idea that among the key drivers of the HIV/AIDS epidemic in women are gender inequalities—i.e., differences in social value, power, opportunities, and behavioral expectations of men and women—and consequent violence. There has been frustration over the lack of progress, and in 2009, the Action Plan of the Joint United Nations Programme on AIDS (UNAIDS) noted that "Despite … significant commitments to promote and protect the human rights of women and girls, the HIV epidemic continues to reveal a gap between rhetoric and reality" (*1*). I will try to show how the weight of the evidence has grown and how workable interventions are beginning to be found.

Over the last two decades, the evidence for the role of gender-based violence and gender inequity in HIV infection in women has mounted. A recent article shows that women in South Africa who have experienced physical or sexual intimate partner violence or who are in relationships with low equality are at greater risk of incident HIV infections compared with women who do not experience these situations (*2*). In this study, it was concluded that nearly one in seven new HIV infections could have been prevented if the women were not subjected to physical or sexual abuse and a similar proportion if women did not experience very unequal power in their relationships (*2*).

CREDIT: SHERWIN CRASTO/AP PHOTO

Gender inequity in relationships increases HIV. This HIV-positive former prostitute says she feels happy "when people accept condoms from my hands."

Young women who have experienced sexual abuse in childhood are also at two-thirds greater risk of HIV infections (*3*). This new evidence on HIV incidence powerfully supports a decade of cross-sectional research from sub-Saharan Africa and India that has consistently found that women who have experienced physical or sexual partner violence are more likely to be infected with HIV (*4*–*8*) (see the photo, above). Thus, these associations pertain in the generalized epidemics of sub-Saharan African, as well as in the Indian epidemic, which remains substantially driven by contacts with commercial sex workers (*1*).

Is This About Violence, or Gender?

This is an important question, with far-reaching implications for developing responses. Irrespective of exposure to violence, gender inequity in relationships is associated with HIV-seropositive status (*2*, *4*). It is not an either/or, as gender is constructed relationally, and gender-based violence both stems from gender inequity and serves to accentuate gender power differentials.

The research base on this is still limited, but evidence from India shows a greater likelihood of HIV infection among abusive husbands, as well as elevated HIV transmission within abusive relationships (*7*). In South Africa, men who have been physically violent toward partners are more likely to be infected with HIV (*9*). These findings support a wider body of evidence—for example, from India, Bangladesh, and the United States—that men who are violent and rape are much more likely to have sexually transmitted infections (STIs) and risky sexual practices (*10*–*12*).

One piece of evidence suggesting that these associations are not coincidental came from the evaluation of a program in South Africa. Stepping Stones is a 50-hour program of participatory learning that seeks to change the way men and women view themselves as gendered individuals and relationally. In response to the intervention, men significantly changed their sexual behavior, including less perpetration of intimate partner violence (*13*). Male participants achieved a one-third reduction in the incidence of herpes simplex virus 2 (genital herpes) over 2 years, and also significantly reduced transactional sex and problem drinking at 12 months (*13*).

These findings suggest that, when we focus on male behavior and violence, our field of vision is too far downstream. Gender norms and relations and the construction of gender identities constitute the upstream problem. Male sexual behaviors, attitudes, expectations, and violence flow from underlying ideas of masculinity, differential valuation and power of men and women, and culturally based expectations for men to demonstrate their "manhood" in relations with women [reviewed in (*14*)].

The finding that abusive male partners are more likely than other men to be infected is one explanation of the observation that women in the most inequitable relationships and experiencing partner violence have a higher HIV incidence and prevalence. However, it is not the only explanation. Several articles have reviewed evidence for intersections between HIV, sexual risk-taking, and partner violence across global regions (*15*, *16*). In the remainder of this article, I will focus on South Africa, where the mechanisms through which gender

Gender and Health Research Unit, Medical Research Council, Pretoria, 0001, South Africa. E-mail: rjewkes@mrc.ac.za

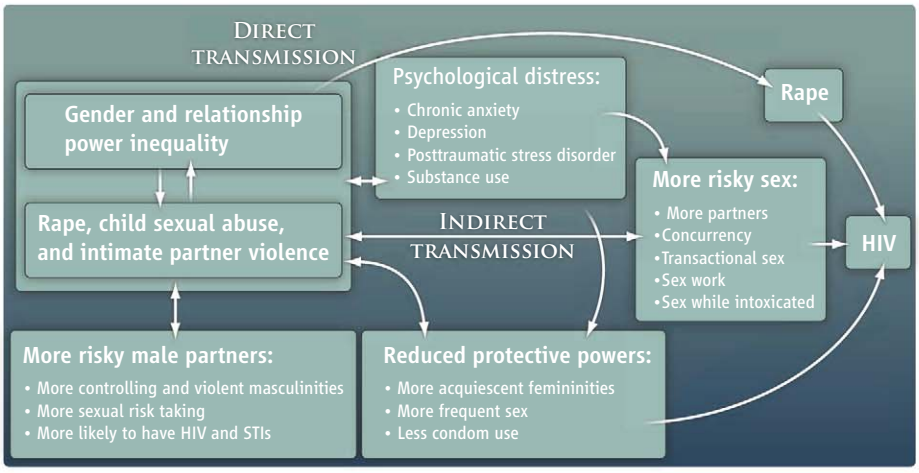

A conceptual model showing intersections of gender-based violence and gender inequity for women.

inequity and gender-based violence result in HIV acquisition in women (see the figure, above) have been closely mapped out (*2*).

The dynamics of gender-inequitable relationships and current, or prior, experience of violence are also important. Experience of male dominance in sexual relationships teaches women the futility of resisting their partners' attempts to control the timing and circumstances of sex. In crude terms, this means that exposed women are less able to protect themselves from HIV; they have more frequent sex and use condoms less (*17*, *18*).

Research also shows that women—whether from, for example, the United States, Ukraine, or South Africa—who have experienced violence (including sexual abuse in childhood) have more risky sex—for example, more partners or older partners—and are more likely to engage in transactional sex or prostitution (*4*, *19*–*21*). Part of the explanation lies in the cycling of risk, whereby vulnerable women and girls are more likely to tolerate partners who are violent and controlling and are also more likely to view engagement in transactional sex or prostitution as a viable choice, in circumstances where their options are severely constrained by poverty and limited opportunities. The latter in turn exposes them to further violence from male partners. Research shows that taking more partners, seeking older partners, and transactional sex may also all be strategies used particularly by more vulnerable women to ensure that their emotional goals are met in relationships and that they feel valued.

A further critical influence on these mechanisms stems from the impact of violence and men's controlling practices on women's mental health. Posttraumatic stress disorder (PTSD) more commonly develops after rape than after any other trauma exposure. Depression, chronic anxiety, and substance abuse are all also common in women exposed to violence, whether as adults or as children (*3*, *22*). Women who are depressed, abusing substances, or dissociating from their PTSD are more likely to engage in risky sex and are much less able to determine the terms of their sexual encounters, as well as being at risk of further violence (*22*). It is important to remember that the problem is a more complex one than just dealing with rape; there are many reasons to stop rape, but stranger or acquaintance rape is not a major driver of HIV prevalence in women.

Given the painful reality of gender-based violence and submission to male controlling behavior, one of the difficult ideas to grasp is the degree to which women acquiesce to these dynamics in relationships, rather than just being coerced into submission. This is most visible among young South African women who are unmarried and not economically supported by male partners (*14*). It is essential to recognize that culturally validated ideals of manhood, which legitimize controlling and sometimes violent practices, are supported by both men and women within a cultural setting, which makes them often more difficult to change. Thus, one of the tasks in building gender equity and reducing violence is to introduce women to the possibility of greater empowerment within their relationships and to justify the idea that these should be based on mutual respect. Furthermore, it is necessary to ensure that women have a structural base (e.g., financial and educational) from which they can assert a degree of independence.

There has been far less research on men, masculinity, and HIV, and so it is not possible to elucidate pathways for them, beyond the broad outline presented in this forum. In reflecting on the model for women, it is important to remember that individual women are affected differently and that the nature of the impact on women's sexual practices will differ according to the cultural context. The severity and frequency of violence, patterns of revictimization, and the extent of men's controlling and abusive practices, as well as financial, educational, and emotional resources available to women, are critical here.

Multifaceted Responses

The task of building gender equity and reducing gender-based violence requires complex policy and programmatic initiatives (*23*). Developing these has been assisted by reviews of evidence, such as that published by the World Health Organization (WHO) in 2009 (*24*). A useful compendium of a range of resources has also been assembled by The Global Coalition on Women and AIDS (*25*). Yet these reviews also highlight how few research resources have been directed to research in this area. As a consequence, very few studies exist that have applied the gold standard of randomized controlled trials with long-term follow up. A further problem in generating the evidence needed for action is that clinical trials are inherently unsuited to evaluating complex interventions. There is a risk that too much emphasis on this gold standard may promote testing of discrete interventions, which are more easily evaluated, over more complex approaches with multifaceted responses. The challenge is that the latter, however, must also be theoretically grounded, evaluated, and evidence-based.

At a national level, we must strengthen the legal framework of gender equity in all areas of social life and must provide protection and redress from rape and partner violence. It is critical that we transform gender dynamics in daily interactions, for example, through implementing effective policies in workplaces and by transforming the management of the education system. Both of these require systems-wide interventions and, in sub-Saharan Africa, cannot be achieved only by sexual harassment policies or isolated curriculum interventions, although both of these are of value.

In the health sector, we need to transform health services so that care provided is patient focused. Services must be shaped around and respond to patients' needs, whether these are for high-quality post-rape care, mental health services, or among women seeking abortions or contraception, or for women in labor.

There have been two community-based, randomized controlled trials of interventions that sought to reduce gender-based violence, to promote gender inequity, and to prevent HIV. Both were undertaken in South Africa and sought to show impact on HIV incidence

but did not achieve this. The Stepping Stones intervention was mentioned above. The IMAGE (Intervention with Microfinance for AIDS and Gender Equity Study) trial was a 3-year study that evaluated the impact of an intervention that included revolving small loans and a participatory gender-based violence intervention. It showed a 55% decrease in partner violence experienced by women (*26*). This study exemplifies the value that may be gained from a combination of prevention—in this case, bringing together a program to economically empower women—with a gender intervention. This warrants considerable further research, as well as exploration of the value that can be accrued by introducing gender interventions to men and women in other contexts, particularly in the workplace.

We need to change the way men come to see themselves as men and they way men and women view unequal gender relations as "normal." All of the national and institutional initiatives contribute to this, but there remains an important role for interventions across society to change such ideas, by using mass media, as well as interventions in schools and communities. Notable efforts are the Soul City mass and multimedia edutainment initiative from South Africa and Sexto Sentido (a multimedia intervention from Nicaragua). These and many other programs and evidence for their effects have been reviewed by WHO (*27*). Leadership at national and international levels and role modeling of respectful, gender-equitable relationships is crucial.

There are other aspects of a gender-based violence-prevention agenda that must be included. Research shows that vulnerability starts from childhood and that the impact is not only on girls. Boys who are exposed to adversity and trauma in childhood are much more likely to develop into more controlling, violent, and antisocial men. The effects of trauma on boys include impact on brain development (*28*). Protecting vulnerable children is a critical element of long-term strategies to prevent gender-based violence and HIV. It is also important in many countries to address alcohol abuse as part of gender-based violence prevention.

After nearly 30 years of the AIDS epidemic, it is welcome that prevention of gender inequities and violence is recognized as important and prevention is considered imperative by the highest level of the U.N. Yet there remains a substantial gulf between these demands and country-level action plans, as well as an even greater distance to implementation. There is enough consensus on what should be done to promote gender equity and reduce violence to include this in national HIV action plans. Implementation requires political will and resources. Governments should be held accountable for implementation. The U.S. President's Emergency Plan for AIDS Relief (PEPFAR) has led the way with its gender-based violence prevention fund; our largest donors must follow suit and ensure that we have more resources, more research, a broader vision, and unswerving commitment. National governments and U.N. agencies must not shy away from the complexity of a comprehensive response to gender inequity. Both the immediate need to scale up HIV prevention and the pursuit of social justice require that we take up the challenge.

References and Notes

1. UNAIDS, *Agenda for Accelerated Country Action for Women, Girls, Gender Equality and HIV* (UNAIDS, Geneva, 2010); http://data.unaids.org/pub/Agenda/2010/20100226_jc1794_agenda_for_accelerated_country_action_en.pdf.
2. R. K. Jewkes, K. Dunkle, M. Nduna, P. N. Shai, *Lancet*, published online 16 June 2010.
3. R. K. Jewkes, K. Dunkle, M. Nduna, P. N. Jama, *Child Abuse Negl.*, in press.
4. K. L. Dunkle *et al.*, *Lancet* **363**, 1415 (2004).
5. A. van der Straten *et al.*, *AIDS Behav.* **2**, 61 (1998).
6. S. Maman *et al.*, *Am. J. Public Health* **92**, 1331 (2002).
7. M. R. Decker *et al.*, *J. Acquir. Immune Defic. Syndr.* **51**, 593 (2009).
8. A. M. Dude, *AIDS Behav.* (2009).
9. R. Jewkes, Y. Sikweyiya, R. Morrell, K. Dunkle, "Understanding men's health and use of violence: Interface of rape and HIV in South Africa" (Technical report, Medical Research Council, Pretoria, 2009).
10. S. L. Martin *et al.*, *JAMA* **282**, 1967 (1999).
11. N. el-Bassel *et al.*, *J. Subst. Abuse* **13**, 29 (2001).
12. J. G. Silverman, M. R. Decker, N. A. Kapur, J. Gupta, A. Raj, *Sex. Transm. Infect.* **83**, 211 (2007).
13. R. Jewkes *et al.*, *BMJ* **337**, a506 (2008).
14. R. Jewkes, R. Morrell, *J. Int. AIDS Soc.* **13**, 6 (2010).
15. J. C. Campbell *et al.*, *Int. J. Inj. Contr. Saf. Promot.* **15**, 221 (2008).
16. A. C. Gielen *et al.*, *Trauma Violence Abuse* **8**, 178 (2007).
17. J. Pulerwitz, S. Gortmaker, W. De Jong, *Sex Roles* **42**, 637 (2000).
18. A. E. Pettifor, D. M. Measham, H. V. Rees, N. S. Padian, *Emerg. Infect. Dis.* **10**, 1996 (2004).
19. G. M. Wingood, R. J. DiClemente, *Am. J. Prev. Med.* **13**, 380 (1997).
20. L. Gilbert, N. el-Bassel, R. F. Schilling, T. Wada, B. Bennet, *AIDS Behav.* **4**, 261 (2000).
21. A. Dude, *Stud. Fam. Plann.* **38**, 89 (2007).
22. S. H. Wang, W. Rowley, *Rape: How Women, the Community and the Health Sector Respond* (Sexual Violence Research Initiative and WHO, Geneva, 2007); www.svri.org/rape.pdf.
23. A. Greig, D. Peacock, R. Jewkes, S. Msimang, *AIDS* **22**, (suppl. 2), S35 (2008).
24. WHO, *Addressing Violence Against Women and HIV/AIDS: What Works?* (WHO, Geneva, 2010).
25. Violence Against Women, The Global Coalition on Women and AIDS, Geneva; www.womenandaids.net/resource-centre/violence-against-women.aspx.
26. P. M. Pronyk *et al.*, *Lancet* **368**, 1973 (2006).
27. G. Barker, C. Ricardo, M. Nascimento, *Engaging Men and Boys to Transform Gender-Based Health Inequities: Is There Evidence of Impact?* (WHO, Geneva and Institute Promundo, Rio de Janiero, 2007).
28. A. Caspi *et al.*, *Science* **297**, 851 (2002).

10.1126/science.1193794

HIV/AIDS

Universal Access in the Fight Against HIV/AIDS

Françoise Girard,[1] Nathan Ford,[2] Julio Montaner,[3] Pedro Cahn,[4] Elly Katabira[5]

Now is not the time to retreat on global commitments to HIV programs.

In 2006, all United Nations member states committed themselves to the goal of universal access to comprehensive programs for HIV prevention, treatment, care, and support by 2010 (*1*). This commitment has inspired national and international responses to achieve impressive results. Unfortunately, it is now clear that the global community has failed to deliver on the universal access pledge. Worse, the global AIDS response is currently under attack. What have we learned, and where should we go from here?

Vertical HIV transmission has been virtually eliminated when antiretroviral therapy (ART) is used appropriately (*2*). Similarly, a strong preventive role of ART in HIV serodiscordant heterosexual couples and among injection drug users has now been documented (*3*, *4*). At the population level, the effect of ART roll out on HIV transmission has been documented in Taiwan (*5*).

In just 5 years, the number of people in low- and middle-income countries receiving ART grew 10-fold, from 400,000 at the end of 2003 to 4 million at the end of 2008, while new HIV infections decreased 17%

[1]Open Society Institute Public Health Program, New York, NY 10019, USA. [2]Médecins Sans Frontières, Cape Town, 2017, South Africa. [3]Division of AIDS, University of British Columbia, Vancouver, BC, V6Z 1Y6, Canada; President, International AIDS Society. [4]Director, Fundacion Huesped, C1202ABB, Buenos Aires, Argentina; Immediate Past President, International AIDS Society. [5]Department of Research, Makerere Medical School, Kampala, Uganda; President-Elect, International AIDS Society.

*Author for correspondence. E-mail: fgirard@sorosny.org

worldwide from 2001 to the end of 2008—and by higher margins in the global epicenter of sub-Saharan Africa (*6*). Country-driven, performance-based programs supported by the Global Fund to Fight AIDS, Tuberculosis, and Malaria (GFATM) have brought HIV treatment to 2.5 million people and have saved ~4.9 million lives (*7*, *8*). From 2004 to 2007, the U.S. President's Emergency Plan for AIDS Relief (PEPFAR) averted an estimated 1.2 million deaths in its 15 focus countries (*9*) and helped ensure that 340,000 babies were born HIV-free. The GFATM catalyzed the introduction of needle exchange and/or methadone programs to prevent HIV infection in people who inject drugs in countries such as Azerbaijan, China, Georgia, Moldova, Russia, Tajikistan, and Ukraine and has adopted forward-looking strategies to address the pandemic as it affects women and girls and sexual minorities.

Progress toward universal access has directly advanced efforts to achieve several of the U.N. Millennium Development Goals (MDGs), especially those that relate to reducing child mortality and improving maternal health. ART is lifesaving for the woman, prevents vertical HIV transmission, and allows for safe breast-feeding of infants, which prevents severe diarrheal diseases (*10*). A clear correlation between access to ART and reduction in all-cause mortality, and especially maternal and child mortality, has been demonstrated in several countries in sub-Saharan Africa (*10*, *11*). ART scale-up has been associated with significant declines in tuberculosis (TB) among both HIV-infected and uninfected populations (*12*). Despite these gains, HIV is still the leading killer of women of reproductive age worldwide and remains one of the leading causes of adult and child deaths in low- and middle-income countries (*13*). A recent *Lancet* study shows that HIV accounts for one in five pregnancy-related deaths worldwide (*14*).

HIV exacerbates other health and development problems, from economic development to food security and lack of access to educational opportunity. It will be impossible to improve maternal or child health outcomes, to reduce poverty, or to achieve other MDGs without aggressively combating AIDS.

Programs funded by the GFATM have promoted prevention, treatment, and care for marginalized and vulnerable groups, such as men who have sex with men, drug users, and sex workers (*15*). Despite substantial investments (*16*, *17*), HIV prevention has shown limited results, notably because those populations most at risk continue to experience human rights abuses that compromise their health and their access to health services and because of the persistence of harmful gender norms and inequity. Populations most at risk need to be able to access tools for HIV prevention—such as condoms, clean needles and syringes, and methadone—without fear of police harassment or of abuse at the hands of judgmental health personnel. Outreach services need to be in place to overcome these very legitimate fears, as do legal aid and police training. In too many places, HIV services and services to advance sexual and reproductive rights and health are not integrated, and vital opportunities to reach women and young people are missed.

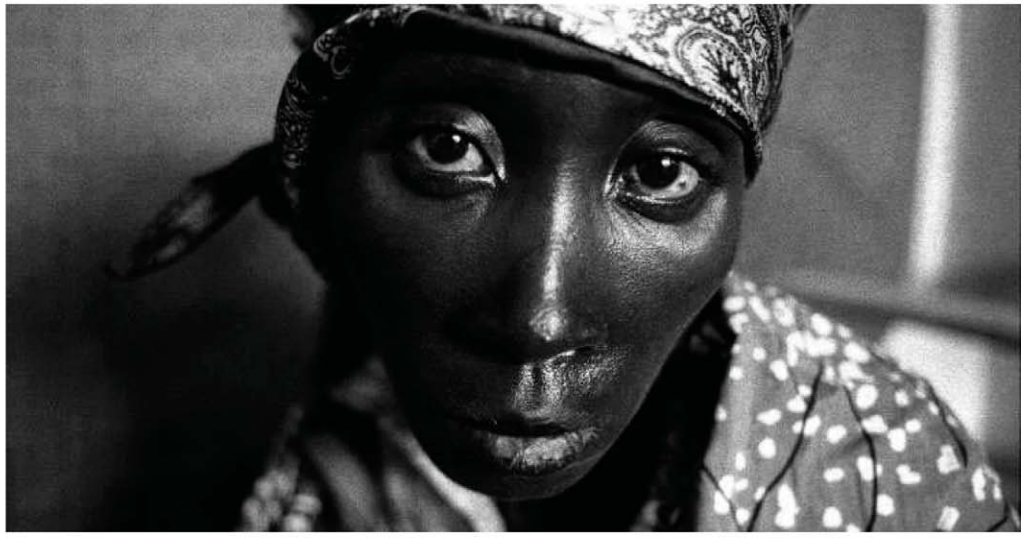

We need better care for people with HIV both in quality and quantity.

CREDIT: ANTONIN KRATOCHVIL/VII/AP PHOTO

Recently, HIV-specific programs have been challenged by claims that disease-specific programs distort, weaken, or cause duplication in national health systems (*18*, *19*). However, evidence shows that HIV funding can benefit health systems and non-HIV services. For example, HIV-specific resources used to improve laboratory capacity and training of health workers have improved nontargeted health services in Rwanda (*20*). In Haiti, HIV services have had a positive impact on immunization, family planning, and TB detection and cure, because the programs were designed in an integrated manner from the outset (*20*). Early negative effects on health systems of parallel coordinating bodies and processes appear to be lessening, as HIV-specific programs (and particularly the GFATM) have learned to align efforts with national plans and priorities (*15*) and are beginning to fund national strategies. The GFATM and PEPFAR currently devote 35% (*17*) and 32% (*21*) of their respective funding to health systems strengthening and health workforce support activities (*20*). More progress is still needed, however, in donor harmonization and in allowing countries to implement coordinated financial-management and human-resource strategies.

A more relevant criticism would be the need to do a much better job in terms of the quality and quantity of care for people with HIV. Even as treatment numbers have soared, patients in the developing world continue to be treated with stavudine-based, first-line ART regimens, which the World Health Organization (WHO) stopped recommending in 2006 (a decision it confirmed in the recently updated 2010 guidelines) and which are no longer prescribed in developed countries given their toxicity. Improved first-line treatment regimens, using tenofovir, although more costly initially, would ensure patients fare better and stay on first-line treatment longer before they need to be moved to more expensive second-line regimens (*22*). Many patients in the developing world still access treatment only when they are already presenting significant clinical symptoms, with the majority experiencing severe immune suppression (CD4 count below 100 cells/mm^3). Initiating them on ART earlier (when CD4 count falls below 350 cells/mm^3), as WHO is now recommending, would boost their immunity, reduce mortality and hospitalizations, and reduce transmission. Overall, this approach will also lower health-care costs, as treating healthier people can be undertaken with simpler, primary health-care models and less frequent monitoring; according to one recent modeling study, earlier initiation yields an incremental cost-effectiveness ratio of U.S.$1200 per year of life saved (*23*). The investment choices that countries are making today, in addition to being inequitable and

contravening internationally agreed-upon guidelines, will result in higher costs tomorrow for the very health systems for which so much concern is expressed.

Others have argued that the HIV response is over-resourced (*24*). In fact, it is global health overall and the Millennium Development Goals (MDGs) that are underresourced. According to a recent report of the Organization for Economic Cooperation and Development (OECD), wealthy nations are falling billions short in fulfilling their commitments to the MDGs (*25*, *26*). Certainly, compared with the hundreds of billions of dollars delivered almost overnight to rescue Wall Street and Greece, funding for the HIV response ($5.5 billion by the GFATM and $26 billion by PEPFAR since 2003, for example) remains modest. In 2009, UNAIDS estimated that $25 billion will be required in 2010 for the AIDS response in low- and middle-income countries—$11.3 billion more than is available today (*27*). The cost-effectiveness of ART is less than some commonly accepted public health priorities (such as malaria bed nets), but equivalent to others (such as oral rehydration therapy for diarrhea or directly observed short-course chemotherapy for TB where endemic) (*24*). We should not be pitting critical health priorities against each other, but instead calling for an urgent increase in overall health funding.

We should not be pitting critical health priorities against each other, but instead calling for an urgent increase in overall health funding.

As we come close to the end of the universal access target year, the impact of budget cuts is becoming evident. PEPFAR is directing recipient countries to accept new patients on treatment only as persons currently being treated die or default (*28*, *29*). Swaziland, Botswana, and Tanzania have already reduced their ART coverage goals owing to budget constraints. When stocks of antiretroviral drugs run out, as recently happened in Free State Province, South Africa, the result is treatment interruptions for those already on ART, endangering their health and increasing the risk of HIV drug resistance, which, if transmitted, could cause a major setback to efforts to control the epidemic. A moratorium on new enrollees in the program has already caused an estimated 3000 deaths (*30*).

In 2009, PEPFAR announced it would place greater emphasis on funding HIV prevention. Whereas prevention activities must be expanded and better supported, it was acknowledged almost a decade ago that prevention cannot be done at the expense of treatment (*31*). In the absence of treatment availability, people have little incentive to know their HIV status, which undermines prevention efforts. It is clear that both need to be adequately supported (*32*).

We believe the Group of Eight countries (G8) must increase their support for universal access and recommit to attaining universal access and the health-related MDGs. The larger and more diverse Group of 20 nations (G20) should place global health, and particularly responses to HIV, on their agenda.

Innovative financing mechanisms, such as the proposed Financial Transaction Tax, a small tax with the potential to raise tens of billions every year for global health (*33*), or the modest levy on airline tickets that funds the medicine and diagnostics purchasing efforts of the global nonprofit UNITAID, must be seriously considered by the G20, among others. These approaches could make universal access sustainable.

African states, which account for more than two-thirds of the global epidemic, must reach the largely unmet 2001 Abuja Declaration commitment to dedicate at least 15% of their national budgets to health. A corollary of asking poor countries to do more for themselves, however, means letting them use existing resources more efficiently; in particular, legal mechanisms to produce or purchase generic drugs without fear of trade retaliation by the United States and other wealthy countries. Also, human rights interventions need to be fully integrated into the AIDS response, so that sex workers, men who have sex with men, persons who use drugs, prisoners, young people, migrants, and others can access quality HIV prevention, treatment, and care without legal barriers and discrimination.

A retrenchment on AIDS today would seriously jeopardize the substantial progress made to date, at the cost of untold human sacrifice and billions of dollars in economic resources. Furthermore, the increasingly recognized benefit of ART in reducing HIV transmission dramatically enhances the value of the longstanding universal access pledge. As the deadline for universal access looms, greater investment in HIV is a necessary, evidence-based, economic, and moral choice.

References and Notes

1. United Nations, General Assembly, Political Declaration on HIV/AIDS, A/RES/60/262, 15 June 2006.
2. K. M. De Cock *et al*., *JAMA* **283**, 1175 (2000).
3. S. Attia, M. Egger, M. Müller, M. Zwahlen, N. Low, *AIDS* **23**, 1397 (2009).
4. D. Donnell *et al*.; Partners in Prevention HSV/HIV Transmission Study Team, *Lancet* **375**, 2092 (2010).
5. C. T. Fang *et al*.; Division of AIDS and STD, Center for Disease Control, Department of Health, Executive Yuan, *J. Infect. Dis.* **190**, 879 (2004).
6. WHO/UNAIDS/UNICEF, *Towards Universal Access: Scaling Up Priority Interventions in the Health Sector* (Progress Report 2009, WHO, Geneva, 2009), p. 26.
7. GFATM, *Resource Scenarios 2011–2013: Funding the Global Fight Against HIV/AIDS, Tuberculosis, and Malaria* (GFATM, Geneva, 2010).
8. GFATM, *The Global Fund 2010: Innovation and Impact* (GFATM, Geneva, 2010).
9. E. Bendavid, J. Bhattacharya, *Ann. Intern. Med.* **150**, 688 (2009).
10. J. Mermin *et al*., *Lancet* **371**, 752 (2008).
11. P. Braitstein *et al*., *Pediatr. Infect. Dis. J.* **28**, 626 (2009).
12. K. Middelkoop *et al*., "Widespread ART is associated with decline in TB prevalence" (WELBB105); Fifth International AIDS Society Conference on HIV Pathogenesis, Treatment, and Prevention, Cape Town, 19 to 22 July 2009.
13. WHO, "The Top Ten Causes of Death" [fact sheet] (WHO, Geneva, 2007); www.who.int/mediacentre/factsheets/fs310.pdf.
14. M. C. Hogan *et al*., *Lancet* **375**, 1609 (2010).
15. R. G. Biesma *et al*., *Health Policy Plan.* **24**, 239 (2009).
16. The GFATM reports spending 30% of its HIV funding on prevention between 2003 and 2008 (*17*).
17. GFATM, *Scaling up for Impact: Results Report* (GFATM, Geneva, 2009); www.theglobalfund.org/documents/publications/progressreports/ProgressReport2008_en.pdf.
18. R. England, *BMJ* **335**, 565 (2007).
19. Independent Evaluation Group of the World Bank, *Improving Effectiveness and Outcomes for the Poor in Health Nutrition and Population* (World Bank, Washington DC, 2009).
20. B. Samb *et al*.; World Health Organization Maximizing Positive Synergies Collaborative Group, *Lancet* **373**, 2137 (2009).
21. P. Piot, M. Kazatchkine, M. Dybul, J. Lob-Levyt, *Lancet* **374**, 260 (2009).
22. M. A. Bender *et al*., *Clin. Infect. Dis.* **50**, 416 (2010).
23. R. P. Walensky *et al*., *Ann. Intern. Med.* **151**, 157 (2009).
24. D. T. Jamison *et al*., *Disease Control Priorities in Developing Countries* (Oxford Univ. Press, Oxford, 2006).
25. Of the U.S.$21 billion shortfall, $4 billion is due to shrinking Gross Domestic Product; the additional $17 billion is due to donors not fulfilling their commitments (*27*).
26. V. Buffery, Reuters, 17 February 2010; www.reuters.com/article/idUSLDE61G1F120100217.
27. UNAIDS, *What Countries Need: Investments Needed for 2010 Targets* (UNAIDS, Geneva, 2009); http://data.unaids.org/pub/Report/2009/jc1681_what_countries_need_en.pdf.
28. F. Stockman, *Boston Globe*, 11 April 2010, p. A1; www.boston.com/news/nation/washington/articles/2010/04/11/us_seeks_to_rein_in_aids_program/?page=full.
29. D. G. McNeill Jr., *New York Times*, 10 May 2010, page A10.
30. Médecins Sans Frontières (MSF), *Punishing Success: Early Signs of a Retreat from Commitment to HIV/AIDS Care and Treatment* (MSF, Geneva, 2009); www.msf.org/source/countries/africa/southafrica/2009/aidsreport/punishing_success.pdf.
31. E. Goemaere, N. Ford, S. R. Benatar, *Lancet* **360**, 86 (2002).
32. V. D. Lima, R. S. Hogg, J. S. Montaner, P. Kissinger, *PLoS ONE* **5**, e10991 (2010).
33. D. McCoy, N. Brikci, *Bull. World Health Organ.* **88**, 478 (2010).

10.1126/science.1193294

TRANSCRIPTION

Repressive Transcription

Chromatin repression is ironically controlled by the initiation of transcription at specific sites in the genome.

Matthew G. Guenther and Richard A. Young

How are active and repressed portions of the genome established and maintained during development? In vertebrates, about 2 m of DNA is packaged into chromatin in a manner that allows for active transcription of some loci and repression of others. Most chromatin regulators do not recognize specific DNA sequences, so how are they recruited to specific sites throughout the genome? For actively transcribed genes, transcription factors or the transcription initiation apparatus recruit regulators associated with active chromatin (*1*). For genes that are repressed, recent studies suggest a counterintuitive model: Transcription initiates the formation of repressive chromatin (*2*–*9*).

The idea that transcription is involved in establishing repressed chromatin is not new. In many eukaryotes, transcription of pericentromeric regions and repetitive elements leads to recruitment of repressive chromatin regulators to these loci (*10*, *11*). But the mechanisms by which specific protein-coding genes are silenced by chromatin regulators have been less clear. This issue is important because genes encoding lineage-specific transcription factors must be repressed during early development. Although Polycomb regulators have been implicated in this repression, the means by which they are recruited and maintained at specific genes in vertebrates is not well understood (*12*).

Genetic and biochemical evidence suggests a competitive balance between the repressive and activating functions of Polycomb group (PcG) and Trithorax group (TrxG) chromatin regulators (*13*, *14*). The PcG protein complexes include Polycomb repressive complexes 1 and 2 (PRC1 and PRC2). PRC2 catalyzes the trimethylation of a lysine residue on the chromatin-associated protein histone H3 (H3K27me3). PRC1 and PRC2 can bind to one another and to nucleosomes (the basic packaging unit of DNA and histones) with histone H3K27me3, which provides a mechanism for spreading of these repressive complexes across chromatin domains. In the model fly *Drosophila melanogaster*, transcription factors are thought to recruit PcG complexes to specific sites, but in vertebrates, such recruiting transcription factors have yet to be identified. TrxG protein complexes are recruited to transcriptionally active promoters, most likely by the transcription initiation apparatus, where they catalyze a histone trimethylation modification (H3K4me3) and promote transcription.

How are PcG complexes recruited to specific sites in vertebrate genomes? Recent studies indicate that RNA molecules recruit them to the locus of transcription or to sites located elsewhere in the genome. During mammalian X chromosome inactivation, a noncoding RNA (ncRNA) transcribed from a portion of the *Xist* gene locus forms hairpin structures that recruit the PRC2 complex to the X-inactivation center X(ic) (*4*). Transcription of full-length *Xist* RNA, which forms the same hairpin structures, leads to further PRC2 recruitment and the spread of PcG-mediated repression across the inactive X chromosome. A ncRNA transcribed from a region adjacent to the *kcnq1* gene recruits PRC2, which represses genes in the *kcnq1* domain (*3*). Similarly, a ncRNA transcribed from the *INK4b*/*ARF*/*INK4a* locus mediates repression of that locus by binding PcG complexes (*8*). The *HOTAIR* ncRNA, which is transcribed from the *HOX C* locus, can target PRC2 and other chromatin regulators to the *HOX D* locus and potentially many other genomic loci (*2*, *6*, *9*). Short ncRNAs are frequently produced by RNA polymerase II in DNA regions that are rich in C and G nucleotides (CpG islands) that are proximal to gene promoters (*7*); many of these short ncRNAs can form CG-rich hairpin structures that are similar to those formed by *RepA* and *Xist*

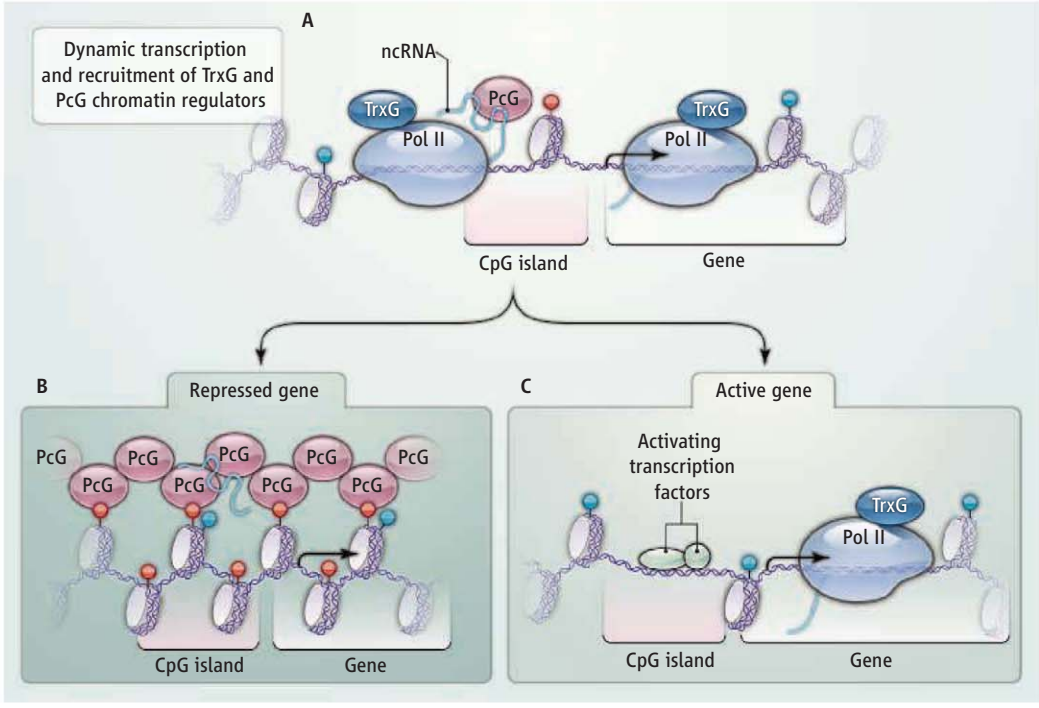

Transcription and chromatin dynamics. (A) Transcription initiation, recruitment of TrxG complexes, which catalyze H3K4me3 (blue dot), and production of CG-rich RNAs occur in the promoter regions of most genes. The CG-rich RNAs often form structures that recruit PcG complexes, which catalyze H3K27me3 (red dot). **(B)** PcG complexes can spread beyond the nucleation site to establish repression. **(C)** At genes where the transcription apparatus is continuously recruited by activating transcription factors, activities associated with TrxG proteins predominate, reducing PcG complexes and their associated histone modifications. Pol II, polymerase II.

CREDIT: Y. GREENMAN/*SCIENCE*

Whitehead Institute for Biomedical Research and Department of Biology, Massachusetts Institute of Technology, Cambridge, MA 02142, USA. E-mail: young@wi.mit.edu

RNAs, and some bind to PRC2. Together, these studies suggest that ncRNA molecules contribute to the recruitment of PcG complexes to promoter regions throughout the genome.

Most (70 to 80%) vertebrate promoter regions are transcriptionally active, and many produce short transcripts in sense (coding) and antisense directions (*15*, *16*). CpG islands occur in the immediate vicinity of most promoters, and it is within these domains that PcG- and TrxG-catalyzed histone modifications take place. The recent evidence that certain RNA structures can contribute to PRC2 recruitment and that transcripts from promoter regions frequently contain these structures (*2*–*9*) suggests a general model for establishing PcG domains (see the figure). An active transcription initiation apparatus can recruit TrxG proteins, whereas transcripts from CpG islands form structures that recruit PcG complexes. PcG complexes can spread across these domains, leading to chromatin repression. At promoters where activating transcription factors continuously recruit the transcription initiation apparatus, demethylation of H3K27me3 can occur (*17*), and PcG binding is lost. Thus, dynamic competition between PcG and TrxG complexes at promoters is resolved into the steady-state views, produced by genomic analysis, of H3K27me3 and H3K4me3 chromatin domains (*1*). This model can account for functional antagonism between PcG and TrxG proteins, for the presence of PcG- and TrxG-catalyzed modifications at CpG islands, and for the observation that H3K27me3 and H3K4me3 modifications can occur simultaneously in these promoter-proximal regions.

This model for transcription-linked establishment of PcG/TrxG domains raises many interesting questions. Transcription initiation occurs at most promoters, but what fraction of transcripts recruit PcG complexes and thus, how general is this transcript-mediated process? RNA molecules and transcriptional regulators have been implicated in PcG recruitment, but what exactly are their roles in the dynamics of establishing and maintaining PcG/TrxG domains in vertebrates? Is the conservation of CpG islands a consequence of RNA-mediated PcG recruitment in promoter regions? Answers to these questions should further improve our understanding of the establishment and maintenance of silent and active chromatin during development.

References and Notes

1. B. Li, M. Carey, J. L. Workman, *Cell* **128**, 707 (2007).
2. J. L. Rinn *et al.*, *Cell* **129**, 1311 (2007).
3. R. R. Pandey *et al.*, *Mol. Cell* **32**, 232 (2008).
4. J. Zhao *et al.*, *Science* **322**, 750 (2008).
5. A. M. Khalil *et al.*, *Proc. Natl. Acad. Sci. U.S.A.* **106**, 11667 (2009).
6. R. A. Gupta *et al.*, *Nature* **464**, 1071 (2010).
7. A. Kanhere *et al.*, *Mol. Cell* **38**, 675 (2010).
8. K. L. Yap *et al.*, *Mol. Cell* **38**, 662 (2010).
9. M. -C. Tsai *et al.*, *Science*, 8 July 2010 (10.1126/science.1192002).
10. M. Bühler, D. Moazed, *Nat. Struct. Mol. Biol.* **14**, 1041 (2007).
11. S. I. Grewal, S. C. Elgin, *Nature* **447**, 399 (2007).
12. R. Jaenisch, R. Young, *Cell* **132**, 567 (2008).
13. L. Ringrose, R. Paro, *Ann. Rev. Genet.* **38**, 413 (2004).
14. B. Schuettengruber, D. Chourrout, M. Vervoort, B. Leblanc, G. Cavalli, *Cell* **128**, 735 (2007).
15. M. G. Guenther, S. S. Levine, L. A. Boyer, R. Jaenisch, R. A. Young, *Cell* **130**, 77 (2007).
16. S. Buratowski, *Science* **322**, 1804 (2008).
17. P. A. Cloos, J. Christensen, K. Agger, K. Helin, *Genes Dev.* **22**, 1115 (2008).

18. We thank K. Helin, J. Lee, M. van Lohuizen, R. Paro, V. Pirrotta, J. Workman, and K. Zaret for helpful comments.

10.1126/science.1193995

BIOCHEMISTRY

Old Gate Gets a New Look

A proposed structure for a protein that enables potassium ions to move in and out of cells raises new questions about how its "gate" works.

Simone Weyand[1,2] and So Iwata[1,2,3]

Cells are constantly exchanging water-soluble molecules like nutrients and inorganic ions with their environment. The movement of these molecules across the cell's plasma membrane is mediated by various transport proteins that create pores through the membrane's lipid bilayer. One type of transport protein, an ion channel, is responsible for transporting certain ions, such as potassium, calcium, or sodium. Ion channels have filters that make the channel permeable only to a specific kind of ion and gates that regulate the flow of ions through the channel. Gates can be controlled by chemical and/or electrical signals, including those created by differences in the voltage inside and outside the cell (membrane potential), and the concentrations of binding molecules (ligands). On page 182, Yuan *et al*. offer new insights into the structure of an important potassium ion channel and the cues that cause its gate to open and close (*1*).

Potassium (K^+) channels are the best understood of the ion channels, and their selectivity filter is well characterized thanks to the Nobel prize-winning work of Roderick MacKinnon and his colleagues and the efforts of many other researchers (*2*, *3*). The

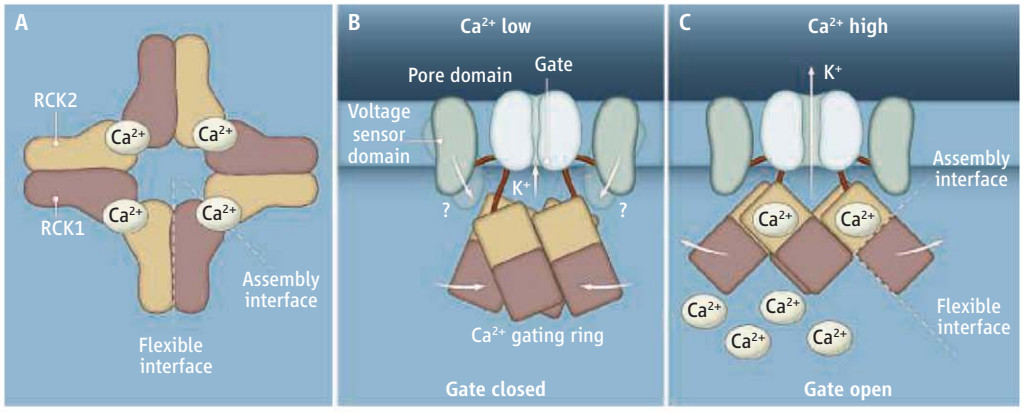

Open sesame. A proposed structure for the BK channel includes gating ring [(**A**) view from intracellular side], which is made of two regulator of K^+ conductance domains (RCK1 and RCK2). The structure offers insight into how changes in intracellular concentration of calcium ions (Ca^{2+}) can trigger the gate to close and open [(**B** and **C**) views parallel to membrane panel].

[1]Division of Molecular Biosciences, Membrane Protein Crystallography Group, Imperial College, London SW7 2AZ, UK. [2]Membrane Protein Laboratory, Diamond Light Source, Harwell Science and Innovation Campus, Chilton, Didcot, Oxfordshire OX11 0DE, UK. [3]Department of Cell Biology, Graduate School of Medicine, Kyoto University, Yoshida-Konoe-cho, Sakyo-Ku, Kyoto 606-8501, Japan. E-mail: s.iwata@imperial.ac.uk

molecular basis of the K^+ channel's gating mechanism, however, remains less clear.

Yuan *et al*. studied high conductance voltage- and calcium-activated K^+ channels known as BK or Slo1 channels, which are involved in numerous physiological processes, including neuronal excitability, smooth muscle contractility, and "tuning" of hair cells in the ear. The most unusual feature of the BK channel is its dual regulation by membrane voltage and intracellular concentration of calcium ions (Ca^{2+}). The channel has three domains: a pore and a voltage sensor that are embedded within the membrane and a gating ring (see the figure). To assemble a model of the structure of the whole BK channel, Yuan *et al*. drew on studies of homologous proteins found in human, chicken, bacteria, and rat cells (*4*, *5*). The new model suggests that the BK channel has a Ca^{2+} gating mechanism that is, not surprisingly, similar to one found in bacteria (specifically, the bacterial channel, MthK). There are, however, a couple of interesting twists.

The first surprise is the location of the Ca^{2+} binding site. As expected from the protein sequence, a Ca^{2+} ion was located at a region containing seven aspartate residues. This physical location—in the assembly interface of the gating ring—differs from that observed in the bacterial channels. The MthK channel has two Ca^{2+} ions in the flexible interface, which is another interface in the gating ring (*4*). By comparing the gating ring structures of Ca^{2+}-bound and –free channels (*6*), Jiang *et al*. concluded that Ca^{2+} ions, bound at the flexible interface, modulate the Ca^{2+} gating ring to increase its diameter, which triggers the gate opening in the pore domain via a linking structure (*4*). They proposed that the assembly interface is fixed during this transition. In light of the findings of Yuan *et al*., the mechanism proposed by Jiang *et al*. needs to be reinvestigated. A search for an additional Ca^{2+} binding site, or sites, is also essential because the BK channel can be activated by Ca^{2+} when the Ca^{2+} bowl is completely deleted.

Another interesting finding is a close association between the Ca^{2+} gating ring in the pore domain and the voltage sensor. It has been thought that the gate is controlled directly either by the ring or by the sensor. The new model and studies of mutations that can occur within the Ca^{2+} gating ring, however, raise the possibility of cooperation between the ring and the sensor. Direct interaction between the two domains would enable the stimulation of one to modulate the other.

This new work certainly answers some important questions concerning K^+ channel gating. At the same time, however, it raises a set of new questions. How many Ca^{2+} binding sites does the BK channel have and where are they located? How does the Ca^{2+} gating ring change its conformation upon Ca^{2+} binding? Is there any conformational cooperation between the Ca^{2+} gating ring and the voltage sensor?

To answer these questions, it will be essential to obtain the whole BK channel structure in both open and closed conformations, even at low resolution. The BK channel is an ideal platform from which to perform these experiments because researchers can easily control its gate state by manipulating Ca^{2+} ion concentrations. This is not the case for simple voltage-gated channels. Moreover, if the suggested interaction between the gating ring and the voltage sensor is true, the open and closed structures may also provide valuable information about the voltage sensor's gating mechanism.

References

1. P. Yuan *et al*., *Science* **329**, 182 (2010); published online 27 May (10.1126/science.1190414).
2. D. A. Doyle *et al*., *Science* **280**, 69 (1998).
3. Y. Zhou, J. H. Morais-Cabral, A. Kaufman, R. MacKinnon, *Nature* **414**, 43 (2001).
4. Y. Jiang *et al*., *Nature* **417**, 515 (2002).
5. S. B. Long, X. Tao, E. B. Campbell, R. MacKinnon, *Nature* **450**, 376 (2007).
6. Y. Jiang, A. Pico, M. Cadene, B. T. Chait, R. MacKinnon, *Neuron* **29**, 593 (2001).

10.1126/science.1192680

GEOPHYSICS

Finding Fault in Fault Zones

The seismogenic behavior of subduction faults depends on the structural evolution of the fault zone.

Kelin Wang

What controls the location and size of seismic rupture along the 43,500 km of the world's subduction faults? Two reports in this issue, based on seismological observations, emphasize the key role of the structural evolution of faults. On page 207, Dean *et al*. (*1*) propose that a structural flaw of the sedimentary formation brought into the Sumatra subduction zone may facilitate rupture propagation. On page 210, Kimura *et al*. (*2*) propose that fracturing of the downward-going plate beneath the Kanto area in central Japan causes the subduction interface to be diverted to a deeper position and change its seismogenic behavior.

An earthquake results from the unstable slip of a fault. If the fault becomes weaker with faster slip, the slip can become unstable and rapidly evolve into a seismic rupture (*3*). The opposite behavior tends to stabilize slip and provides resistance to seismic rupture. Whether a fault weakens during slip depends on the frictional properties of its fault-zone material. However, whatever the frictional properties, seismic slip also requires some geometrical conditions. The slip zone must be smooth and thin (a few millimeters) (*4*). To produce a large earthquake, the rupture has to span a large area—typically a few thousand square kilometers for a moment magnitude (M_w) = 8 earthquake.

The study area of Dean *et al*. covers the boundary between the rupture zones of two subduction earthquakes. The M_w = 9.2 Sumatra earthquake in December 2004 generated a huge tsunami that killed over 240,000 people, but the M_w = 8.8 Sumatra earthquake in March 2005 generated a smaller tsunami. The 2004 rupture propagated farther seaward than the 2005 event (*5*). Contrasting earthquake histories on both sides of the boundary (*6*) also suggest a major difference in seismogenic behavior. In the 2004 area, Dean *et al*. found a pronounced seismic reflector, indicative of a weak plane, starting seaward of the trench and extending well into the subduction zone. They propose that such a weak plane can accommodate seismic rupture farther seaward. The absence of a similar horizon in the 2005 area concluded by the same study is then consistent with the 2005 rupture stopping far short of the trench.

The focus of Kimura *et al*. is the deep end of the rupture zone of the M_w = 7.6 subduction earthquake, the largest aftershock of the great Kanto earthquake of 1923 that caused over 142,800 deaths. Seismic surveys indicate that the subduction interface takes a gradual step

Pacific Geoscience Centre, Geological Survey of Canada, Sidney, BC V8L 4B2 Canada, and School of Earth and Ocean Sciences, University of Victoria, Victoria, BC V8W 3P6 Canada. E-mail: kwang@nrcan.gc.ca

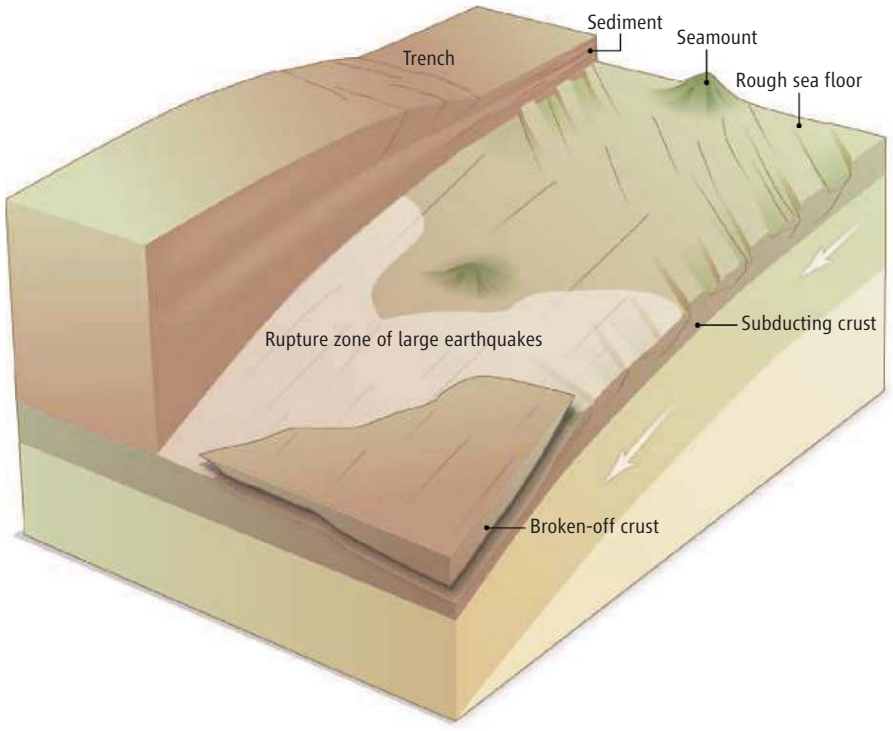

Battered fault zone. The internal structure of a subduction fault zone evolves during plate subduction. The uneven surface of the incoming plate and off-fault fracturing during subduction generate roughness. Subduction of sediment and wear of geometrical irregularities promote smoothness. Large earthquakes are due to unstable slip of large and smooth patches of the fault. Dean *et al*. and Kimura *et al*. provide examples of how structural evolution affects the seismogenic behavior of the fault.

down at depth, such that a chunk of the subducting crust is broken off and accreted to the upper plate (see the figure). They propose that the evolution of the fault-zone structure with increasing depth causes progressive changes in seismogenic behavior. The rupture zone of the M_w = 7.6 earthquake seems to be limited to be shallower than the step-down, but a band of small repeating earthquakes, also along the fault, occur deeper than the step-down. Between the two zones there is episodic aseismic slip.

Subduction faults are difficult to access—their surface trace is under several kilometers of seawater, and their seismogenic portion is typically 5 to 50 km deep. Our knowledge of how their internal structure affects their seismogenic behavior is based on interpretations of geophysical and geodetic data and extrapolation from laboratory experiments and shallow boreholes (*7*, *8*). Valuable information has also come from fault-zone rocks of ancient subduction zones (*9*, *10*).

Much has been learned from accessible faults on land, especially large strike-slip faults, which slip in the horizontal direction. Clearly, large faults are not planes of frictional contact but zones of structural complexity (*11*), typically featuring a core of localized shear, which may include thin zones of seismic slip, and a broad damage zone of fractured, sheared, and rotated wall rock. Off-fault damage can be due to the shattering effect of rupture propagation (*12*) or to the generation and wear of geometrical irregularities (*11*). The damage-zone concept can help explain the subduction channel (*9*, *13*), a zone several hundred meters thick along the shallow subduction interface widely seen on seismic survey sections (*8*). However, subduction faults are by no means strike-slip faults turned sideways. Their structural evolution follows a different path.

Whereas strike-slip faults become smoother and more prone to large rupture with increasing displacement (*14*), the roughness of subduction faults is frequently renewed by newly subducted uneven sea floor (see the figure). Various types of roughness influence the seismogenic behavior on different scales. For example, subducting seamounts concentrate stress to cause failure but distort fault geometry to resist rupture propagation, such that they generate mediocre earthquakes (*15*) but hinder large earthquakes (*16*).

Sediment brought into the subduction zone affects not only the frictional properties but also the structure of the fault zone. The sediment may help smooth the fault zone and thus facilitate rupture propagation (*17*). The large subduction earthquakes of 2004 Sumatra (M_w = 9.2), 1964 Alaska (M_w = 9.2), 1960 Chile (M_w = 9.5), and 1700 Cascadia (M_w ~ 9) all occurred in subduction zones with an ample supply of sediment. The structure of the incoming sedimentary formation may also play a part (*1*).

As the subducting plate dives into increasingly higher temperature and pressure, it undergoes a range of metamorphic changes that transform rock minerals into denser forms while removing water from them (*18*). The densification causes mechanical damage to the subducting plate itself (*19*), and the dehydration fluids further weaken it. The process discussed by Kimura *et al*. is likely facilitated by these effects.

The results of Dean *et al*. and Kimura *et al*. remind us that in the hierarchy of factors that control the seismogenic behavior of faults, structural evolution ranks high. A better understanding of the characteristics of such evolution will require a combination of geophysical imaging, geological ground-truthing, and comparison with observed spatial and temporal patterns of earthquake rupture.

References and Notes

1. S. M. Dean *et al*., *Science* **329**, 207 (2010).
2. H. Kimura, T. Tetsuya, K. Obara, K. Kasahara, *Science* **329**, 210 (2010).
3. At relatively low slip rates (<1 mm/s), the frictional behavior can be described with rate- and state-dependent friction laws. At seismic slip rates, more complex weakening mechanisms may come into play, usually associated with frictional heating.
4. R. H. Sibson, *Bull. Seismol. Soc. Am.* **93**, 1169 (2003).
5. F. J. Tilmann *et al*., *Geophys. J. Int.* **181**, 1261 (2010).
6. A. Meltzner *et al*., AGU *Fall Meet. Suppl*., abst. T11D-07 (2009).
7. T. H. Dixon, J. C. Moore, Eds., *The Seismogenic Zone of Subduction Thrust Faults* (Columbia Univ. Press, New York, 2007).
8. R. von Huene, C. R. Ranero, D. W. Scholl, in *Subduction Zone Geodynamics*, S. Lallemand, F. Funiciello, Eds. (Springer, Berlin, 2009), pp. 137–157.
9. P. Vannucchi, F. Remitti, G. Bettelli, *Nature* **451**, 699 (2008).
10. F. Meneghini *et al*., *Geol. Soc. Am. Bull.* **122**, 1280 (2010).
11. C. A. J. Wibberley, G. Yielding, G. Di Toro, in *The Internal Structure of Fault Zones: Implications for Mechanical and Fluid-Flow Properties*, Geol. Soc. Lond. Spec. Pub. 299, C. A. J. Wibberley, W. Kurz, J. Imber, R. E. Holdsworth, C. Collettini, Eds. (Geological Society of London, 2008), pp. 5–33.
12. E. L. Templeton, J. R. Rice, *J. Geophys. Res.* **113**, B09306 (2008).
13. K. Wang, Y. Hu, R. von Huene, N. Kukowski, *Geology* **38**, 431 (2010).
14. S. G. Wesnousky, *Nature* **444**, 358 (2006).
15. S. L. Bilek, S. Y. Schwartz, H. R. Deshon, *Geology* **31**, 455 (2003).
16. S. Kodaira, N. Takahashi, A. Nakanishi, S. Miura, Y. Kaneda, *Science* **289**, 104 (2000).
17. L. J. Ruff, *Pure Appl. Geophys. Res.* **129**, 263 (1989).
18. B. R. Hacker *et al*., *J. Geophys. Res.* **108**, 2030 (2003).
19. K. Wang, J. Cassidy, I. Wada, A. J. Smith, *Geophys. Res. Lett.* **31**, L01605 (2004).

10.1126/science.1192223

MEDICINE

Clearing Conformational Disease

Toxicity caused by aggregates of a misfolded protein is abolished with a drug that boosts cellular protein degradation mechanisms.

Richard N. Sifers

Research focused on defining the underlying characteristics of a disease can often lead to new treatment strategies. This is certainly the case for a rapidly expanding group of inherited diseases characterized by the toxic accumulation of a misfolded protein (*1*). Identifying, and then targeting, the cellular machinery responsible for orchestrating the degradation of these aberrant molecules, rather than correcting the mutations that cause them, represents a paradigm shift from the conventional wisdom associated with gene therapy. On page 229 of this issue, Hidvegi *et al*. (*2*) describe how a compound that stimulates autophagy—the process by which a cell destroys its own organelles through lysosomal compartments—can successfully eliminate the toxic effects of misfolded α_1-antitrypsin protein in a preclinical mouse model of the associated liver disease (*3*).

Department of Pathology and Immunology, Baylor College of Medicine, Houston, TX 77030, USA. E-mail: rsifers@bcm.edu

α_1-Antitrypsin, which is primarily synthesized in the liver (hepatocytes), is inserted into the endoplasmic reticulum (ER), where only the correctly folded monomer is allowed to travel as a soluble itinerant protein through an intracellular secretory pathway, for eventual release at the cell surface. A surveillance system initially assists the molecule's folding. Correct folding of α_1-antitrypsin involves modification of sugar moieties attached to specific asparagine residues (*4*, *5*). Thereafter, ER-associated degradation (ERAD) processes proteolyze and eliminate those molecules unable to achieve the correct structure (*6*). Misfolded monomers are extracted into the cytoplasm for elimination by 26*S* proteasomes (*7*). By retaining misfolded proteins and targeting them for destruction, the circulating concentration of α_1-antitrypsin is consequently low. This decrease in secreted α_1-antitrypsin, a member of the serine proteinase inhibitor superfamily, may underlie the development of chronic obstructive pulmonary emphysema as a central loss-of-function phenotype (*8*).

Despite this knowledge, the development of a strategy for reversing a gain-of-toxicity phenotype associated with the intracellular retention of α_1-antitrypsin has awaited a detailed understanding of how cells respond to a rogue form of the newly synthesized molecule. A mutation within the genetic variant α_1-antitrypsin Z (ATZ) promotes the spontaneous polymerization (*9*) of an early folding intermediate (*10*), the accumulation of which is toxic to cells and can lead to chronic liver injury. Unlike the monomer, insoluble polymers are not extracted into the cytoplasm,

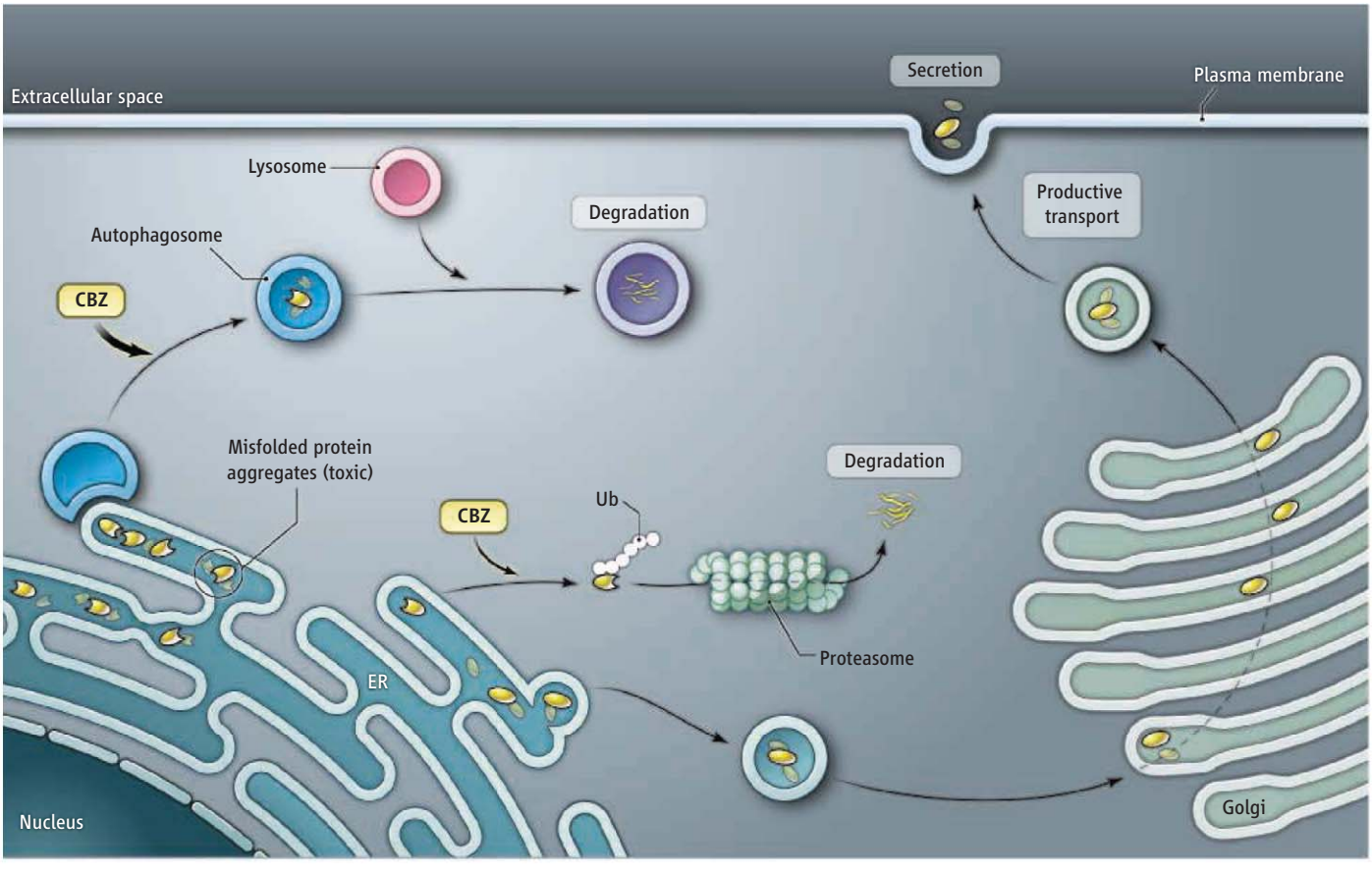

CREDIT: Y. GREENMAN/*SCIENCE*

Sites of therapeutic intervention. The productive folding and transport of human α_1-antitrypsin is shown, as well as two pathways for the proteolytic elimination of misfolded forms. The sites at which carbamazepine (CBZ) stimulates proteolysis are shown. Ub, ubiquitin.

but rather, undergo spatial separation into domains of the ER that are selectively eliminated by autophagy (*11*) (see the figure).

Hidvegi *et al*. used the drug carbamazepine to boost the capacity of the autophagic pathway beyond the degree to which it is activated by ATZ polymers (*11*). Stimulating the autophagic pathway, rather than proteasomes, that eliminate misfolded monomers, represents a safer therapeutic approach because excessive augmention of the latter system can prematurely eliminate a substantial fraction of normally folded protein intermediates (*12*). This unwanted elimination of normal proteins is not expected to be a by-product of stimulating autophagy.

Hidvegi *et al*. first established the success of carbamazepine in transfected human cells expressing ATZ. Treatment with the drug accelerated ATZ degradation, but did not alter the fate of wild-type α_1-antitrypsin. The authors repeated the approach with a transgenic mouse line (*3*) that has served as a preclinical model for the liver disease in humans, because the injury in these mice resembles the pathological features observed in many human patients with the corresponding liver condition. Furthermore, in addition to decreasing the amount of intracellular human ATZ in these mice, the reversal of liver fibrosis validated the therapeutic strategy in mitigating multiple aspects of the underlying pathophysiology. However, despite this promising result, carbamazepine also mildly enhanced the degradation of soluble ATZ by proteasomes. It is therefore still unknown whether the observed therapeutic efficacy is due solely to stimulation of autophagy by the drug, or whether augmentation of multiple proteolytic pathways is required as well. Hence, the data fall short of establishing the identity of the toxic species, although the insoluble polymers have been strongly implicated (*11*).

An important outcome of the study by Hidvegi *et al*. has been its support of the relationship between research and medicine. Conclusions that involve data generated from any preclinical study should be treated with cautious skepticism. However, the favorable outcome goes a long way toward supporting the conceptual framework associated with the use of postgenomic strategies, rather than gene therapy, as a way to correct genetic diseases caused by protein misfolding in humans.

References

1. P. Choudhury, Y. Liu, R. N. Sifers, *News Physiol. Sci.* **12**, 162 (1997).
2. T. Hidvegi *et al*., *Science* **329**, 229 (2010); published online 3 June 2010 (10.1126/science.1190354).
3. J. A. Carlson *et al*., *J. Clin. Invest.* **83**, 1183 (1989).
4. C. M. Cabral, Y. Liu, R. N. Sifers, *Trends Biochem. Sci.* **26**, 619 (2001).
5. B. Nyfeler *et al*., *J. Cell Biol.* **180**, 705 (2008).
6. R. K. Plemper, D. H. Wolf, *Mol. Biol. Rep.* **26**, 125 (1999).
7. D. Qu, J. H. Teckman, S. Omura, D. H. Perlmutter, *J. Biol. Chem.* **271**, 2791 (1966).
8. D. H. Perlmutter, J. A. Pierce, *Am. J. Physiol.* **257**, L147 (1989).
9. D. A. Lomas, D. Ll.- Evans, J. T. Finch, R. W. Carrell, *Nature* **357**, 605 (1992).
10. M. H. Yu, K. N. Lee, J. Kim, *Nat. Struct. Biol.* **2**, 363 (1995).
11. J. H. Teckman, D. H. Perlmutter, *Am. J. Physiol. Gastrointest. Liver Physiol.* **279**, G961 (2000).
12. E. T. Powers, R. I. Morimoto, A. Dillin, J. W. Kelly, W. E. Balch, *Annu. Rev. Biochem.* **78**, 959 (2009).

10.1126/science.1192681

APPLIED PHYSICS

Closing In on Models of Wall Turbulence

Properties of turbulent flow near a wall, which creates drag resistance, can be predicted from the velocities in the nearby flow region.

Ronald J. Adrian

Turbulence created when fluids flow past surfaces, called wall turbulence, affects the flux of water vapor and CO_2 from the ocean's surface, causes drag on airplanes and ships, and influences how atmospheric pollutants are transported near Earth's surface. Wall turbulence presents a particularly difficult computational problem, because very small motions that occur in a thin inner layer near the wall must be modeled accurately (see the figure). This inner layer is critical because it contains the region where the effects of molecular transport mechanisms, such as viscosity, resist the transport of momentum, heat, and/or mass between the wall and the fluid. These motions cannot be described in sufficient detail with direct computation; the number of grid points within the layer where numerical calculations would need to be performed would lead to an impractically large task.

School for Engineering of Matter, Transport and Energy, Arizona State University, Tempe, AZ 85287, USA. E-mail: rjadrian@asu.edu

A goal in modeling the inner layer is to find an empirical yet universal equation whose input parameters come from the more easily measured large-scale behavior of the overlying layer. It has been difficult to find such an equation because the average properties of the inner layer—how motions are correlated and how energy is distributed—cannot be entirely separated from those of the larger scale, nonuniversal outer part of the boundary layer (*1*). On page 193 of this issue, Marusic *et al*. (*2*) show that fluctuating turbulent motions within the inner layer respond to the larger-scale outer motions in two ways, thus connecting their average behaviors. The large outer motions add to the small-scale inner motions, and they also modulate the amplitude of the inner motions. The additive effect is not entirely unexpected, but the amplitude modulation effect is a nonlinear coupling that had not been anticipated. Using this model, Marusic *et al*. could remove the nonuniversal contributions of the outer flow from the inner flow, leaving a more universal inner layer that is amenable to empirical representation.

These findings relate to one of the grand challenges in the science and engineering of fluid dynamics: the development of governing equations that can be solved by numerical methods so as to reliably predict turbulent flow. More than a half century of turbulence modeling research has led to a solution in the form of model partial differential equations for the larger-scale motions of turbulent flow, which transport most of the energy of the flow and where viscosity plays a minimal role. These "large-eddy" equations can be computed on numerical grids of affordable size (~10^9 grid points), but to be complete, they require a statistical model to deal with motion that occurs on a scale finer than the grid size, including the very fine scales at which viscous dissipation occurs. They also require a model for the thin inner region, where the large-eddy equations cannot resolve the flow because all scales are small. In effect, the inner-region model is needed to provide a boundary condition for the large-eddy equations.

Marusic *et al*.'s model considers only the component of velocity parallel to the surface,

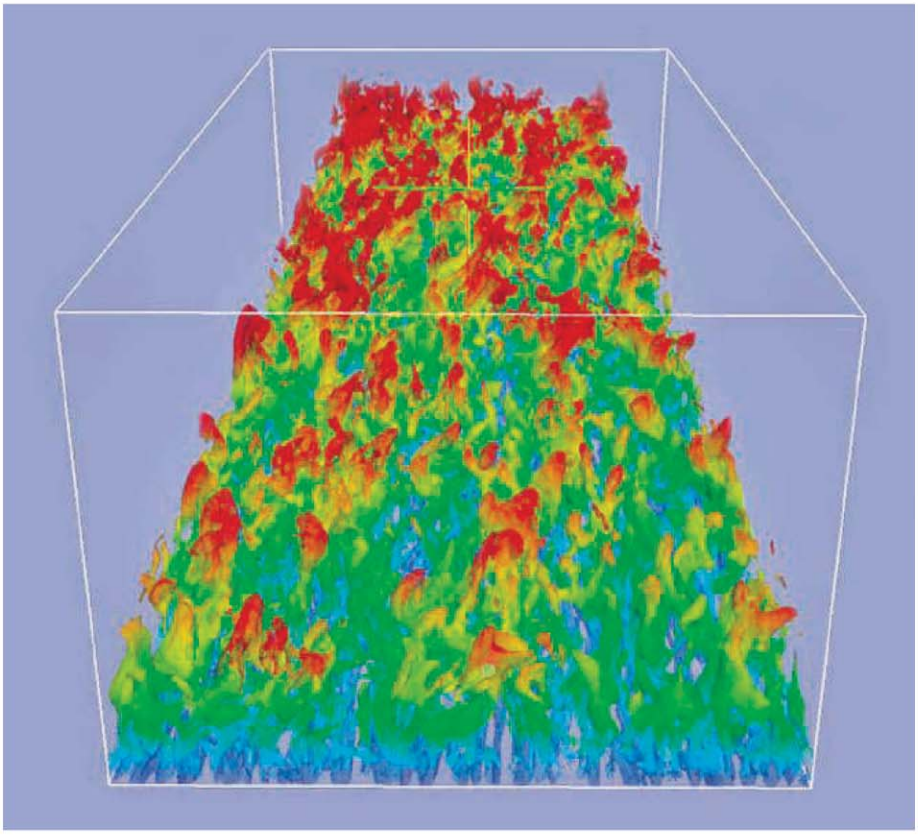

Chaos near a wall. Modeling shows how eddies develop in a turbulent boundary layer over a smooth wall. The flow is from bottom to top. The red-yellow-green colors identify the outer region, and the underlying inner region is colored blue. Near the wall, the eddies are long streaks in the flow direction, whereas in the outer region, they are inclined to the wall and often form loops. Note that the small eddies of the outer region tend to group together in long streaks. These larger-scale patterns are the large-scale outer flow discussed in the report by Marusic *et al*. Their model predicts the inner-scale motions using data from the large, outer-scale motions. This visualization follows the method of Ferrante and Elghobashi (*5*) and is based on direct numerical simulation data from the Database of the Computational Fluid Dynamics Laboratory, University of Washington (*6*).

$u(z, t)$, as a function of the distance from the surface z and time t. By removing the effects of outer motions from experimental time series, a signal $u^*(z, t)$ can be extracted from $u(z, t)$ that contains only the effects of the small scales created near the wall and is a more likely candidate for a universal empirical characterization. In terms of the variables u^+, z^+, and t^+ that have been made dimensionless (dividing them by scales appropriate to the inner layer), the universal signal is given by

$$u^*\left(z^+,t^+\right)=\frac{u^+\left(z^+,t^+\right)-\alpha\left(z^+\right)u^+_{\mathrm{OL}}\left(z^+_{\mathrm{O}},t^+\right)}{1+\beta\left(z^+\right)u^+_{\mathrm{OL}}\left(z^+_{\mathrm{O}},t^+\right)} \quad (1)$$

where u^+_{OL} is the large-scale component of the outer velocity measured at a representative point z^+_{O} in the middle of the logarithmic layer, and α and β are empirically chosen to maximize the correlation between the inner and outer velocity.

Marusic *et al*. explored the following simplification: If the additive velocity and the amplitude modulation are the only ways in which the outer flow affects the inner flow, then u^* should be characteristic only of the fluid dynamics in the inner region and universally independent of the outer flow. For example, it should be the same in different outer geometries (i.e., boundary layers, pipe flows, and channel flows) and at all values of the outer velocity and length scale. Then, one could combine measured time series $u^*(z, t)$ with knowledge of the outer velocity time series u^+_{OL} in any wall flow to create a "predictive" signal that characterizes the statistics of the total inner-layer velocity in that flow:

$$u^+_{\mathrm{P}}\left(z^+,t^+\right)=\left(1+\beta u^+_{\mathrm{OL}}\right)u^*\left(z^+,t^+\right)+\alpha u^+_{\mathrm{OL}} \quad (2)$$

Equation 2 is not just a rearrangement of Eq. 1, because the outer velocity in Eq. 2 pertains to the predicted flow, which may have outer motions quite different from those of the flow used to determine u^*. Although $u^+_{\mathrm{P}}(z^+, t^+)$ does not predict the random velocity $u^+(z^+, t^+)$ in the new flow, it can be used to generate the statistics of the new flow.

The test cases the authors have so far explored indicate that the process described above is remarkably successful in modeling the power spectra and correlations of u in the inner layer of boundary-layer flows over a large range of Reynolds numbers that are used to describe flow conditions (low Reynolds numbers usually correspond to laminar flow dominated by viscous forces, and high Reynolds numbers correspond to turbulent flow dominated by inertial forces). Further work will be needed to evaluate the predictive capability of this model for other velocity components and for flow geometries different from the flat plate that has been studied up to this point.

The form of Eq. 2 is similar in several respects to that of a closed-form mathematical solution for laminar flow over a flat wall, called (in modern terms) a composite-matched asymptotic expansion of the laminar boundary layer (*3*). The conceptual basis for this type of solution was developed by Prandtl (*4*), who showed that viscous effects cannot be ignored in a very thin region close to the wall that he called the boundary layer, even when the rest of the flow can be treated as an inviscid fluid—one with no viscosity. Any real fluid must have zero velocity parallel to the wall because of viscosity, but an ideal inviscid fluid still slips at the wall. The laminar boundary layer is a region in which viscosity, no matter how small, forces the velocity to diminish to zero at the wall. This theory resolved the 150-year-old paradox of d'Alembert, who observed that in theory, bodies moving through an inviscid fluid would experience no drag, contrary to experience. The modern analog of Prandtl's seminal development could be the time-dependent, three-dimensional large-eddy simulation equations (which are inviscid) for turbulence in the outer region plus a viscous boundary layer type of equation for the inner layer that takes the slip velocity of the outer flow as its upper boundary condition. The form of Eq. 2 derived by Marusic *et al*. encourages efforts along these lines.

References

1. I. Marusic, G. J. Kunkel, *Phys. Fluids* **15**, 2461 (2003).
2. I. Marusic *et al.*, *Science* **329**, 193 (2010).
3. M. Van Dyke, *Perturbation Methods in Fluid Mechanics* (Parabolic Press, Stanford, CA, 1975).
4. L. Prandtl, *Verhandlungen des dritten internationalen Mathematiker-Kongresses in Heidelberg 1904*, A. Krazer, Ed. (Teubner, Heidelberg, 1905), pp. 484–491.
5. S. Ferrante, S. Elghobashi, *J. Fluid Mech.* **503**, 345 (2004).
6. S. Ferrante, http://cfmdatabase.aa.washington.edu.

10.1126/science.1192013

RETROSPECTIVE

Martin Gardner (1914–2010)

An author of science, philosophy, and games delighted readers with explanations of how math is connected to the larger world

Dana Richards

On 22 May, American author Martin Gardner died at the age of 95. Until his last days, he was active and writing for an eager audience. He is well known for his writing on mathematics, science, philosophy of science, theology, and magic. However, few of his admirers knew the full breadth of his intellectual activities, as most were drawn only to some aspect by their own interest. In contrast to our increasingly specialized world, he was involved in many intellectual spheres.

Gardner would be quick to remind us that he was a "journalist." After getting a B.A. in philosophy at the University of Chicago in 1936, he attended seminary to continue his studies. After a year, he realized that he was training for an academic position, but that his real calling was to be an author. It was a decade before his writing allowed him to earn a decent living. A career in fiction gave way to articles on science, philosophy, and games.

A pivotal article was "The Hermit Scientist" (*Antioch Review*, 1950) in which Gardner critiqued three examples of pseudoscience that were very much in the news: the wild theories of writer Immanuel Velikovsky proposing Earth's near collision with other planets; the public craze with unidentified flying objects; and the idea of a metaphysical mind-body relationship touted by the science fiction author L. Ron Hubbard. Gardner's opinions on these topics led to his book *In the Name of Science* (1952; retitled *Fads and Fallacies in the Name of Science* in 1957), and its impact increased until the 1970s.

Gardner, magician James Randi, and psychologist Ray Hyman decided that a group was needed to address what was then called the "occult explosion," an alarming escalation of irrationalism in the popular press. Soon they were joined by sociologist Marcello Truzzi and philosopher Paul Kurtz, and the Committee for the Scientific Investigation of Claims of the Paranormal was formed. Gardner contributed to their publications regularly for decades, critically examining fringe science and paranormal claims, among other issues.

Gardner is often called the founder of the modern skeptical movement. His clearly written articles drew people in, convinced them that there was a problem worth caring about, and showed how simple argumentation could effectively combat unreason. His writing gave a common voice to those who were reluctant to speak out alone.

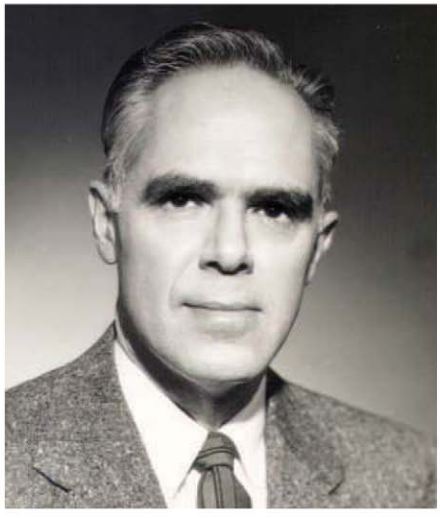

CREDIT: THE FAMILY OF MARTIN GARDNER

Department of Computer Science, George Mason University, 4400 University Drive, Fairfax, VA 22030, USA. E-mail: richards@cs.gmu.edu

Unlike most authors of nonfiction, Gardner had "fans," the most ardent ones for his 25 years at *Scientific American*. His "Mathematical Games" column, started in 1956, became so identified with the magazine that many readers said it was the first thing they turned to in each issue. Judging by public pronouncements, book dedications, and thousands of letters written to Gardner, his influence on the study and enjoyment of mathematics may well be unmatched.

Gardner often claimed in interviews that he was unprepared to write a monthly math column, but in fact, he had a lifelong interest in recreational mathematics. Admittedly, his mathematical training was weak, but he said that having to struggle with concepts helped him to write clear explanations. Moreover, he had developed a habit of finding connections between mathematics and the larger world—literature, art, science, philosophy, and magic. This was the secret of the column. He did not make mathematics interesting; he showed that it was interesting.

Gardner's first and last publications were in magic journals, from 1930 to 2010. Although never a performer, he was a constant and respected source of ideas for close-up magic, usually impromptu tricks. He contributed articles on tricks, puzzles, illusions, and science to *Physics Teacher* magazine for 12 years. He also annotated, or introduced, various editions of the works of his favorite authors. *The Annotated Alice* (1960) on Lewis Carroll's *Alice's Adventures in Wonderland* and *Through the Looking Glass* was his best-selling book, in which he explained associations with mathematics, clever wordplay, and Victorian history, among other fascinating insights.

Gardner's success was due to an extraordinary network of correspondents and his legendary files of information. He was the generous conduit through which ideas flowed, in the magic, math, and pseudoscience communities. His files started in shoe boxes while at college and grew to mammoth proportions. A description of using them, written in 1957, sounds remarkably like a modern description of surfing the Internet.

What motivated Martin Gardner? After a decade of soul-searching, in a 1940 interview he articulated a principle he held for the rest of his life (as expressed by writer Lord Dunsany): "Man is a small thing, and the night is large and full of wonder." After World War II, he studied with philosopher Rudolf Carnap, which led to his essay "Order and Surprise" (1950). It describes the deep sense of wonder that the natural world impresses upon philosophers and scientists. Over the next 60 years, he would return to this theme. He described himself as a "mysterian" because he believed that even though science will continue to resolve problems, behind every mystery there is another vexing mystery. This spurred most of his best writing. He wrote an entire book (*The Ambidextrous Universe*) about the paradoxical discovery of fundamental asymmetries in particle physics. The mathematical essays concentrated on surprises, unexpected connections, and paradoxes. His main goal was to remind us that we are surrounded by wonderful things.

His antipathy for pseudoscientists was not just because they were cranks, crackpots, or charlatans. He was furious about those who practiced medical hocus-pocus. But, in my opinion, his motivation was almost aesthetic. He was deeply offended by people offering "ugly" false phenomena and miracles when the natural world was so wonderful. We can honor Martin Gardner by pursuing the mysteries that surround us.

10.1126/science.1194002

AAAS is here – connecting government to the scientific community.

As a part of its efforts to introduce fully open government, the White House is reaching out to the scientific community for a conversation around America's national scientific and technological priorities.

To enable the White House's dialogue with scientists, AAAS launched Expert Labs, under the direction of blogger and tech guru Anil Dash. Expert Labs is building online tools that allow government agencies to ask questions of the scientific community and then sort and rank the answers they receive.

On April 12, 2010, AAAS asked scientists everywhere to submit their ideas to the Obama administration and at the same time launched the first of Expert Labs tools, Think Tank, to help policy makers collect the subsequent responses. The result was thousands of responses to the White House's request, many of which are already under consideration by the Office of Science and Technology Policy.

As a AAAS member, your dues support our efforts to help government base policy on direct feedback from the scientific community. If you are not already a member, join us. Together we can make a difference.

To learn more, visit **aaas.org/plusyou/expertlabs**

AAAS + U = Δ

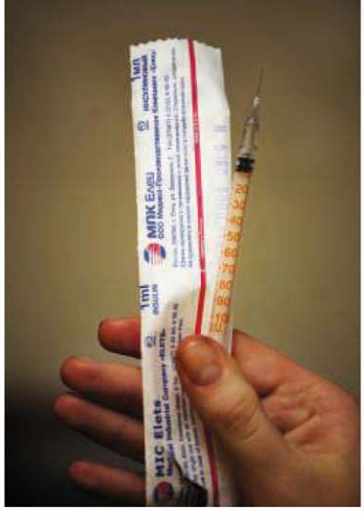

INTRODUCTION

HIV/AIDS: Eastern Europe

"WHY IS AIDS ALMOST NONEXISTENT IN THE SOVIET UNION?" ASKED A 1991 news story in *Science*, headlined the "Russian AIDS Puzzle." The story (13 September 1991, p. 1214) offered no good explanation for why the epidemic, then a decade old, had spared Eastern Europe and Central Asia but speculated that the dissolution of the Soviet Union might pave the way for HIV. It did. Today, the region is home to an estimated 1.5 million HIV-infected people, and the rate of spread remains dauntingly high.

From 18 to 23 July 2010, more than 20,000 HIV/AIDS researchers will gather in Vienna, Austria—the "gateway" to Eastern Europe—for the 18th International AIDS Conference to try to bridge the gap between scientists and policymakers in East and West. In this issue, *Science* looks closely at the factors that in the mid-1990s led to the rapid spread of HIV in Russia and Ukraine, which account for more than 90% of the infections in the region.

With a travel grant from the Open Society Institute's Public Health Program, correspondent Jon Cohen and photographer Malcolm Linton visited researchers, clinicians, advocates, and affected communities in both countries. The package of stories that begins on p. 160 examines how public health officials, health-care workers, researchers, and members of civil society in different regions have responded to the epidemic, as well as the criticisms that the governments have done too little to slow the spread of the virus. The central dilemma is that HIV in the region has been mainly transmitted by injecting drug users sharing needles, and the "harm reduction" strategies successfully used in Western Europe and elsewhere, such as needle exchange or opiate-substitution treatment, have not taken root in the more conservative climate of the East. Critics charge that stigma and discrimination against drug users by government officials, law enforcement, and the medical community have fueled the problem. A slideshow published online further captures some of the challenges in the region and how they are being addressed. Building a strong response to HIV/AIDS takes several years in almost every country. But Russia, Ukraine, and their neighbors have an advantage: They can learn from the many other countries that began confronting the virus more than a decade before it hit Eastern Europe.

The News package is followed by Policy Forums and original research about the field's most pressing topics, which will take center stage at the upcoming conference. Girard and colleagues (p. 147) advocate for the importance of a renewed commitment to universal access to prevention, treatment, and care. Jewkes (p. 145) discusses the continuing contribution of gender inequities to the prevalence of HIV/AIDS in women, especially in South Africa. A Review by Trono *et al*. (p. 174) focuses on the latent viral reservoir that persists in HIV-infected people, describing the underlying biology and potential interventions that may lead to a cure. A report by Wu *et al*. (*Science* Express) describes a trio of new broadly neutralizing antibodies isolated from an HIV-infected person that attach to the CD4 binding site of the virus and can potently neutralize a broad range of viral strains.

– BARBARA JASNY, KRISTEN MUELLER, LESLIE ROBERTS

CREDIT: MALCOLM LINTON

HIV/AIDS

CONTENTS

See also Editorial p. 120, Policy Forums pp. 145 and 147, and Science *Express Research Article by T. Zhou* et al. *and* Science *Express Report by X. Wu* et al., Science *Careers, and* Science Translational Medicine *at www.sciencemag.org/special/aids2010/.*

Science

NEWS

Late for the Epidemic: HIV/AIDS in Eastern Europe

The virus spared the region until the mid-1990s; treatment is becoming widely available, but prevention programs raise political antagonism

WHEN THE IRON CURTAIN FELL IN 1991, Eastern Europe and Central Asia were barely touched by HIV. According to the most authoritative estimates of HIV's prevalence, it was the least affected region in the world. Russia, the largest country, had fewer than 1000 reported cases, and hundreds of those were children who had been accidentally infected in hospitals. Many public health officials in the region believed the AIDS epidemic raging elsewhere would make few inroads in their societies. This was a disease spread by gay sex, drug injections, promiscuous heterosexual partnering, and prostitution—behaviors, they thought, their cultures rejected so thoroughly that HIV didn't stand a chance. Today, the Russian Federation and Ukraine alone have twice as many HIV-infected people as all of Western and Central Europe combined. And in an increasing number of countries in the former Soviet Union, *ВИЧ*, Russian for HIV, is no longer a foreigner's problem.

At the end of 2008, according to a December 2009 report from the Joint United Nations Programme on HIV/AIDS (UNAIDS), the number of infected people in the region totaled 1.5 million—a jump of 66% from 2001. "Eastern Europe and Central Asia is the only region where HIV prevalence clearly remains on the rise," the agency concluded.

The first signs that the epidemic was poised to explode came in 1995. But despite subsequent warnings from UNAIDS and others, few governments in Eastern Europe and Central Asia have made concerted efforts to slow the spread of the virus, and some have defiantly rejected methods that have worked elsewhere. "In all of the regions of the world, it was possible with awareness and prevention to stop the growth, and yet the epidemic is still growing here," says Dennis Broun, the UNAIDS regional director based in Moscow. Although the driving force is injecting drug users (IDUs) sharing needles, the Russian government in particular has refused to embrace "harm reduction" strategies, such as distributing methadone, a substitution treatment for heroin and other opiates, and exchanging needles and syringes, that have stymied the virus elsewhere. "It's a pity," Broun says.

Today, Russia and Ukraine account for more than 90% of the infections in the region. This spring, *Science* traveled to both countries and met with public health officials, researchers, clinicians, nongovernmental organizations (NGOs), vulnerable groups, and infected people. The countries have responded to the epidemic differently in some key ways—Ukraine, for example, in December 2007 legalized methadone importation (see p. 165)—reflecting their different resources, political climates, and cultures. But ultimately, they face many of the same challenges in both treatment and prevention, as they wrestle with antiquated health care systems from the Soviet era, patchy epidemiology, the increasing spread from IDUs to their sex partners, rampant tuberculosis, staggering infection rates in drug-using street youth (see p. 170), corruption, police brutality (see p. 169), isolation from the West, and weak and fractious research communities (see p. 173).

Many on the frontlines of combating the epidemic in both countries stress that great strides have been made in preventing mother-to-child transmission and providing anti-HIV drugs for treatment. But they have become

Continued on page 162

Online
sciencemag.org
Special photo gallery with more images and stories.

Desperation. Sasha has been waiting for months to join an opiate-substitution program in Ukraine.

CREDIT: MALCOLM LINTON

Explosive concoction? Some blame the manufacture and distribution of *chernaya* for sparking the epidemic.

Tracing the Regional Rise of HIV

ODESSA, UKRAINE—Abundant epidemiologic evidence shows that the HIV epidemic that has startled Eastern Europe traces back to this charming Black Sea city in the early 1990s, right on the heels of the fall of the Soviet Union and the resultant economic, cultural, and political upheaval. Without question, injecting drug users (IDUs) drove it. And detailed molecular analyses later revealed that HIV strains isolated in Belarus, Russia, Kazakhstan, and other countries in the former Soviet Union evolved from the southern Ukrainian strains (see graphic). But the factors behind the explosion of HIV in this region remain elusive.

Part of the confusion revolves around the drugs that people inject, their networks, and the way drugs are prepared and shared. HIV typically piggybacks on heroin, which has played a major role in the Russian epidemic. But here in southern Ukraine, heroin was not popular 15 years ago.

In Ukraine, Russia, and other Eastern European countries, people have long injected liquid poppy straw, or *chernaya*, a homemade opiate cooked from the cheap remains of plants harvested for their seeds, which are used in food or pressed for oil. According to several IDUs interviewed here, people started to sell syringes prefilled with *chernaya* in the early '90s, which were convenient but introduced new opportunities for HIV to spread. One commonly voiced thesis is that the Roma, a "gypsy" community in Odessa that prepares and sells the prefilled syringes, picked up used syringes off the street.

Social psychologist Robert Booth of the University of Colorado, Denver, has interviewed IDUs and dealers in Ukraine since 1998, and he doesn't believe that Romas kick-started the epidemic. "I'm sure there are some cases where people got used syringes, but it's more dangerous if they go to a dealer," says Booth.

Many dealers are users themselves. Booth contends that the way they prepare *chernaya* and a widely used ephedrine-based drug called *vindt* may indeed have spread HIV. In a 2003 study, Booth and his colleagues reported that dealers typically cook poppy straw with chemicals to make a solution of drug, draw it into their own syringes, and then squirt it into a buyer's syringe, or directly fill the user's syringe from the batch. "You have numerous syringes going into a common container and pulling out the solution," says Booth. "If anyone has HIV or hepatitis C, you're passing the virus through the solution."

HEROIN AND HIV'S SPREAD

Hitchhiker's guide. HIV subtype A followed heroin trading routes (arrows) into Eastern Europe; subtype B predominates in the west.

Interview-based research does not provide hard evidence of routes of transmission, however. Epidemiologist Robert Heimer of Yale University School of Public Health has gone to considerable lengths to assess whether these *chernaya* practices spread HIV. Working with Andrei Kozlov's team at the Biomedical Center in St. Petersburg, Russia, and Jean-Paul Grund at the Center for Addiction Research in Utrecht, the Netherlands, Heimer manufactured *chernaya* in his lab (with permission from the U.S. Drug Enforcement Administration). The researchers then spiked the *chernaya* with HIV-infected blood to simulate the contamination of the solution by a dirty syringe or by directly adding blood (a method used to remove impurities). In another test, they drew HIV-infected blood into syringes, discarded most of it, and then filled the syringes with *chernaya* or a saline control.

As the researchers reported in the May 2006 issue of *Addiction*, if HIV-infected blood contaminated the *chernaya* solution, heat and chemicals killed the virus. In the HIV-contaminated syringes, those rinsed with saline had viable HIV, whereas only 43% of those with *chernaya* did. So the drug reduced the risk of HIV being transmitted through a dirty needle. "It's completely impossible for contaminated *chernaya* to have been the root of the epidemic," says Heimer.

Sharing of syringes filled with *chernaya* may initially have spread HIV in southern Ukraine, but Heimer and co-author Grund say the epidemic fully blossomed in Russia with the increased supply of plentiful and potent heroin from Afghanistan. "It's the free-market system acting in the most open way in a completely unregulated market," says Heimer. Heroin and opium seizures in Russia charted by the United Nations Office on Drugs and Crime indeed show a steep increase that begins in 1994.

Heimer says the novelty of heroin in Russia contributed to HIV's spread there in the '90s, and its popularity is now on the wane, with his research showing a steadily increasing age of the average user. But he warns that IDUs are still being infected with HIV at a high rate and adds that this is no time to be complacent. "All of these epidemics of drugs follow the same cyclical patterns," says Heimer. "The question is, What will happen if the pattern recreates itself?"

–J.C.

CREDITS (TOP TO BOTTOM): MALCOLM LINTON; SOURCES: UN; BIOMEDICAL CENTER

HIV/AIDS in Eastern Europe

Double trouble. Ukraine and the Russian Federation account for more than 90% of the cases in the region.

Continued from page 160

deeply frustrated by many other aspects of the response to their epidemics—particularly the limited help available for IDUs, who often are reviled. "It's kind of a hopeless situation," says Anya Sarang, a sociologist in Moscow who heads the Andrey Rylkov Foundation for Health and Social Justice and studies IDUs and HIV. "But that's our reality."

Sarang will be one of the plenary speakers next week at the 18th International AIDS Conference, which the International AIDS Society decided to hold in Vienna—"the gateway" to Eastern Europe—to help change that fatalistic perspective. For the first time, the society will translate all conference material and presentations into Russian, says Robin Gorna, the society's executive director. And she hopes that removing the language barrier, and the meeting's proximity to Russia and Ukraine—as well as to smaller countries in the region with burgeoning epidemics such as Uzbekistan, Kazakhstan, Estonia, Belarus, Moldova, and Latvia—will create a momentum for change that she and others believe is desperately needed.

Improved responses, however, will require government leadership and accountability coupled with science. To that end, the society has made a great effort to attract government officials from Eastern European and Central Asian countries to the meeting. As of June, a few countries had shown some interest but not, notably, the largest and most influential one, Russia. "Sadly, at the moment we haven't had any of our invitations accepted," said Gorna. *Science*'s requests for interviews with several Russian government health officials similarly went unanswered.

Registered complaints

Theories outnumber facts in attempts to explain why the epidemic in the region took off in the mid-1990s among Ukrainian IDUs (see p. 161). Although mass screening began in the late 1980s, Ukraine had not detected more than 80 cases in a year. But in March and April of 1995, more than 1000 IDUs tested positive in two Ukrainian cities, Odessa and Nikolayev. Some 12,000 diagnoses were reported the next year, and the cases more than doubled by 1997. The majority were IDUs.

Russia in 1995 had only 1062 total reported cases, and a mere seven were IDUs. But the next year alone, Russia detected more than 1500 infections, and three times that number in 1997—60% IDUs.

As the number of HIV cases in both countries steadily grew, the limitations of their epidemiology became increasingly apparent, and today, vast differences separate government figures from those put out by UNAIDS. Russia and Ukraine count only "registered" HIV infections, which means people who come into the health care system and high-risk groups such as prisoners and identified drug users. No effort is made to assess the prevalence in men who have sex with men, a large high-risk group that is heavily ostracized and virtually ignored throughout the region by official HIV/AIDS efforts. UNAIDS and most countries outside the former Soviet Union combine officially reported cases with extrapolations from studies of high-risk groups and household surveys. "We don't have epidemiology here," complains molecular biologist Andrei Kozlov, who heads the Biomedical Center in St. Petersburg, the region's largest HIV/AIDS research lab.

UNAIDS's Broun says the Russian case count, or prevalence, clearly understates the true figure because many IDUs fear being registered in databases as drug users and avoid health care facilities because of stigma and discrimination. People also often do not seek care until they have been infected for years and suffered substantial immune destruction.

At the end of 2007, the latest available UNAIDS estimate, 940,000 people in the Russian Federation—1.1% of the adult population—were infected with HIV. Russia's Federal Research and Methodological Center for AIDS Prevention and Control reported at the end of October 2009, nearly 2 years later, just 516,167 registered cases.

Alexey Mazus, head of the well-appointed Moscow AIDS Center that provides care and treatment for city residents, staunchly defends his government's official figures, insisting that they capture almost every infected person. "I have no belief in UNAIDS," Mazus says.

The official Ukrainian numbers, 161,119 at the end of 2009, similarly differ dramatically from the UNAIDS estimate of 440,000 in 2007. According to UNAIDS, Ukraine has an adult prevalence of 1.6%, the highest in all of Europe.

The registration system in Ukraine has

SOURCE: UNAIDS

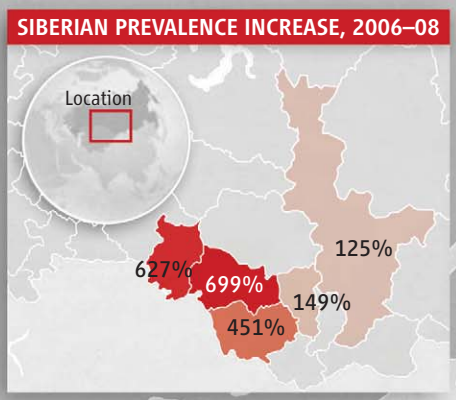

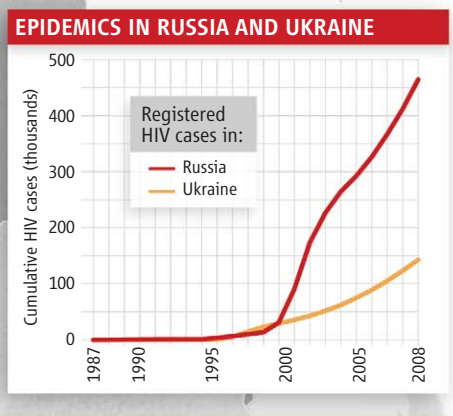

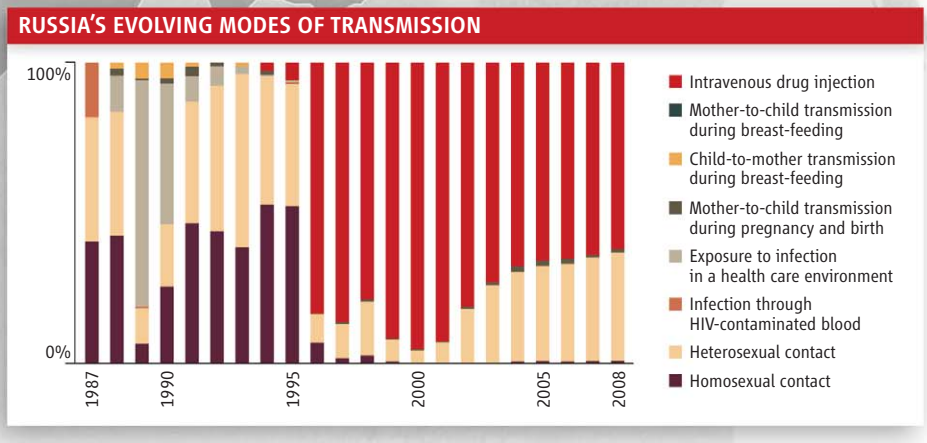

In flux. As transmission shifts from injecting drugs to sex, Russia's and Ukraine's epidemics have slowed, but Siberian cases recently spiked. Note official numbers of "registered" cases differ from UNAIDS's estimates.

SOURCES: CHARLES VITEK, U.S. CDC (LEFT); UKRAINE AIDS CENTER (RIGHT); RUSSIA'S FEDERAL RESEARCH AND METHODOLOGICAL CENTER FOR AIDS PREVENTION AND CONTROL (BOTTOM)

the same shortcoming as the one in Russia, but it has an additional problem, says Yuri Kobyscha, an epidemiologist in Kyiv who works with the World Health Organization (WHO). In Ukraine, individual states must pay for HIV tests, and many are cash strapped. "States often only test blood donors and pregnant women," he says. "So people in the most at-risk populations then don't have access."

Outside Russia and Ukraine, no country in the region topped 16,000 infections by 2007, but tiny Estonia and Latvia had higher prevalence rates—1.3% and 0.8%, respectively—than any country in Western Europe.

Coming up next

Confusion over the number of infected people pales next to the unknowns about the rate at which new infections are occurring—the incidence—which ultimately determines the epidemic's direction and how prevalence will change. Although a few rigorous studies have followed cohorts of uninfected IDUs to track new infection rates, researchers mostly look at fluctuations in the number of newly registered cases as a crude indicator. Some evidence suggests that the Russian and Ukrainian epidemics have stabilized and will not grow as large as once feared, yet a dearth of hard data mixed with increased spread in new locales make most prognosticators extremely cautious.

Past predictions about Russia's epidemic in particular have proved wide of the mark. The U.S. National Intelligence Council in 2002 projected that Russia today would have up to 8 million infections—and an adult prevalence rate of 11%. Alexey Bobrik, a director of the Open Health Institute in Moscow, says, "We should be quite realistic that we will not be decimated by HIV. We'll have more people die from car accidents and alcohol each year than from HIV for the foreseeable future. It's a public health problem, but not a public health priority."

Bobrik doubts that Russia will transition from a "concentrated" epidemic that is largely IDU driven to "generalized" spread, which is defined by prevalence above 2%. He notes that new registered cases peaked in 2001 at just under 88,000, and although there has been an uptick in official cases since 2006, the growth has been relatively stable, at about 10% per year. Epidemiologist Charles Vitek, who runs the U.S. Centers for Disease Control and Prevention office in Moscow, agrees. "I still don't see much in the way of evidence of a sustained, expanding epidemic in the general population," he says. "The number of new infections here is modest."

Yet Vitek and Bobrik stress that most of the new infections could have been averted with better harm-reduction programs. Vitek further cautions that Siberia recently has seen steep jumps in prevalence rates (see map).

Epidemiologist Robert Heimer of the Yale School of Public Health is far from convinced that the worst is over. "Since so little prevention is being done and few of the efforts are directed at stopping the source of the epidemic, there's the potential to see the transition from a concentrated epidemic in drug users to one in the generalized population," says Heimer, who has conducted several incidence studies in Russian IDUs. "That's never been seen on the planet." Working with the Biomedical Center, Heimer has used different methods to assess incidence in IDUs and found that between 2005 and 2008, annual new infection rates ranged from 14.1% to 20.4%. "That's not a stable epidemic," he says.

Ukraine has no incidence data, says WHO's Kobyscha, although the increase in registered cases has slowed. Kobyscha notes that prevalence in IDUs between 20 and 24 years old has plummeted from a high of nearly 30% to just over 8% in 2008, and sexual transmission eclipsed drug injection for the first time, suggesting that the country had reached the "saturation point" at which HIV has already infected the drug users who take the most risks. "We expect that in 2 or 3 years we'll reach a plateau stage," Kobyscha says.

Drug-drug interactions

On a chilly March night in St. Petersburg, social worker and psychiatrist Natasha Shuter asks the driver of her van to pull off a wide highway on the outskirts of the city and stop in front of a pay parking lot. Save for a man inside the guard tower at its entrance, the dimly lit lot looks eerie and lifeless, but Shuter, who works with the locally based NGO Stellit, knows better. She makes a call on her mobile phone, and minutes later, a 28-year-old woman emerges from one of the parked cars, resplendently dressed in a fur coat and knee-high black leather boots.

The woman, Tatyana, warmly greets Shuter, who for several years has helped the few dozen women who sell sex in this lot, educating them about HIV, providing condoms, and arranging doctor visits. Tatyana takes a seat in the van and catches Shuter up on her life. Tatyana started using heroin at 17 and learned

that she was infected with HIV 5 years ago. Although she has been arrested repeatedly and worries for her safety, she can't imagine leaving the business unless she quits the drug. "It's heroin that decides," Tatyana says. But Shuter can do little to help Tatyana kick her habit, short of referring her to a narcologist, a practitioner of a Soviet-era brand of psychiatry that has little success. So she tries to encourage Tatyana to receive proper care for her HIV infection, but that, too, is a challenge.

No plateau. UNAIDS's Denis Broun says Eastern Europe is the only region in the world with a growing HIV/AIDS epidemic.

As Tatyana explains, she does not know whether she has suffered enough immune damage to be eligible for treatment because she has not had her blood tested to see how much the virus has depleted her CD4 white blood cells. "It's very difficult to find time to get tested because of my working schedule," she says. "And until there's a great problem, there's no great reason to do this. Until the cork pops out, you don't do anything."

Shuter sends Tatyana off with a big bag of condoms to distribute to friends. "It's very difficult to break the cycle of the lifestyle," Shuter says. "They work, sleep, wake up, go to the dealer, go to work."

Russian AIDS centers have modern monitoring equipment, and access to anti-HIV drugs has steadily improved, with an estimated 66,000 people on treatment in December 2009. Still, IDUs in need often slip through the cracks. The same holds true in Ukraine, which has about 16,000 people on treatment. According to UNAIDS, Eastern Europe and Central Asia had reached just 22% of the people most in need of antiretroviral drugs (ARVs) by December 2008—half the coverage achieved in sub-Saharan Africa. "It's not difficult to get ARVs," says molecular epidemiologist Elena Dukhovlinova of the Biomedical Center. "It's difficult to get patients to them."

Psychologist Alla Shaboltas, who works with Dukhovlinova, surveyed people outside the AIDS center in St. Petersburg and found that only 30% were IDUs. "They should be the biggest portion of the population at the stage of AIDS," says Shaboltas. She says barriers to treatment exist within both the IDU and medical communities. Many IDUs, like Tatyana, don't perceive that they urgently need monitoring and care, or they believe that ARVs are dangerous. Physicians, she says, often worry that IDUs won't adhere to their treatment schedule and tell the patients they can't start ARVs until they stop using drugs. "They lie to them," Shaboltas says. Many IDUs also wind up in prison, where all health care is patchy.

On top of these obstacles, Russia and Ukraine have user-unfriendly health care systems: HIV, TB, and drug dependency are each treated in their own centers. There have been improvements since the Iron Curtain fell, says Shaboltas, "but you are in the Soviet system."

Both countries have attempted to integrate care, and Ukraine even distributes methadone at a few clinics that also treat HIV and TB. But Ukraine estimates that only 5000 IDUs were receiving opiate substitutes as of January 2010, a fraction of those in need. "It's not a problem," says Konstantin Lezhentsev, a clinician and harm-reduction advocate in Kyiv. "It's a tragedy."

A private matter. Natasha Shuter and the NGO Stellit—not the Russian government—do outreach with a heroin-dependent, HIV-infected sex worker.

CREDITS: MALCOLM LINTON

Their own clock

Despite the many frustrations faced by people combating the spread of HIV in Russia and Ukraine, ARVs have extended many lives. As Lezhentsev visits the Kyiv City HIV/AIDS Prevention and Control Center, he stops outside the morgue. "Nine of my best friends and 15 of my patients ended up there," he says. For the first time since it started tracking HIV, Ukraine recorded a drop in AIDS deaths last year. Russia similarly has seen a drop in AIDS deaths since 2007.

Olena Kravchenko, who heads outpatient treatment at the Kyiv AIDS center, points to what she calls her old "computer" that she had when they opened their doors 10 years ago: a three-ring binder. Kravchenko had little she could offer patients then other than an HIV test, and she had scant information about the disease in a language she understood. Today, thanks to money from the Global Fund to Fight AIDS, Tuberculosis and Malaria, her clinic treats 1300 adults and 120 children and monitors their CD4 counts and HIV levels in their blood. There are computers everywhere. The clinic also does TB diagnosis and has an IDU community center where they can exchange needles.

Yes, Kravchenko has a long wish list, and she disparages her government for relying on outside funding to address the country's HIV/AIDS problem. But she is resigned to the fact that progress has to be measured by its own clock here, and they often lag far behind their Western European neighbors. "The more we're developing, the more we want to work on international standards," she shrugs. "There's nothing perfect in this world."

–JON COHEN

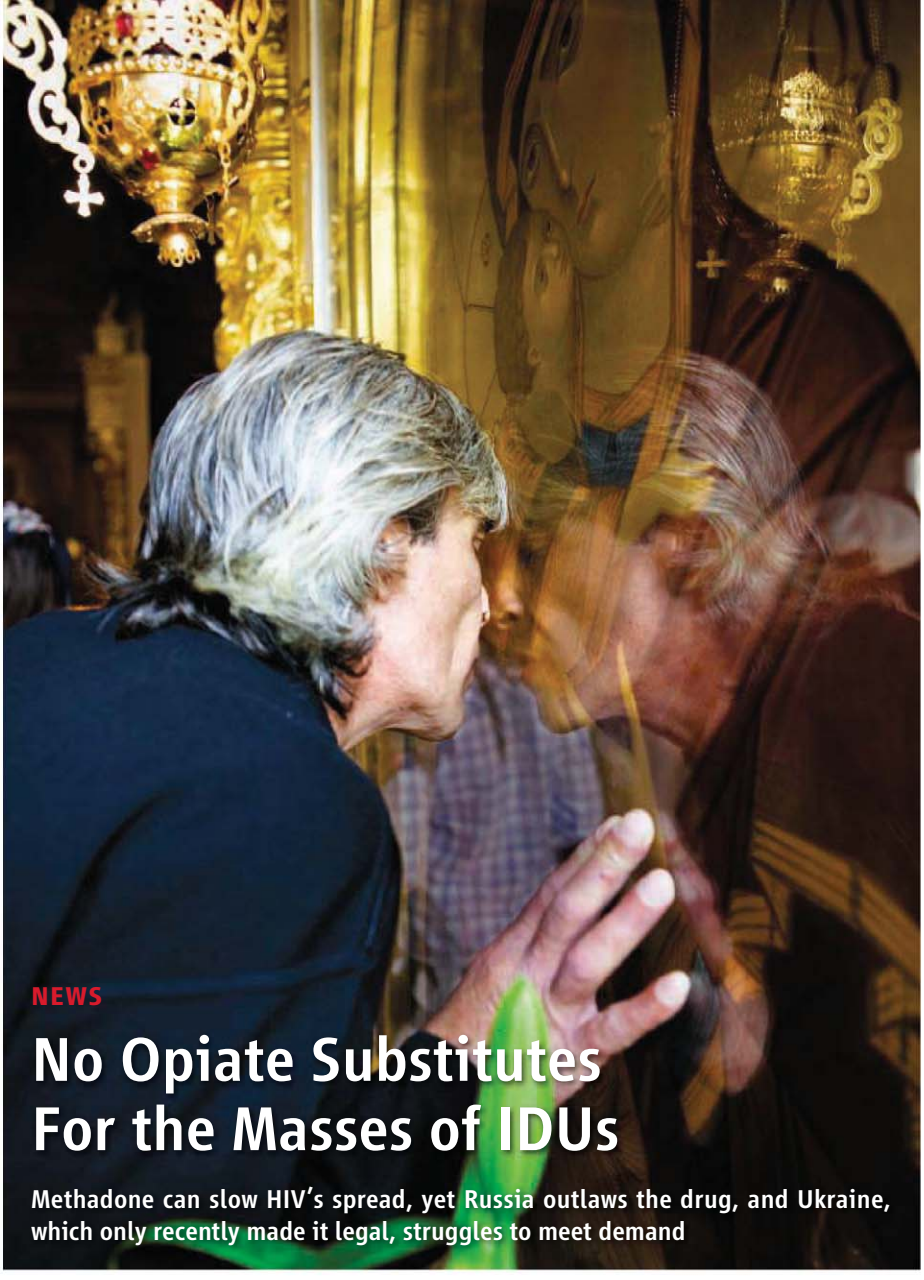

Giving thanks. Methadone has freed Sergey Nenov from opiates and put him on a road to health.

CREDIT: MALCOLM LINTON

NEWS

No Opiate Substitutes For the Masses of IDUs

Methadone can slow HIV's spread, yet Russia outlaws the drug, and Ukraine, which only recently made it legal, struggles to meet demand

KYIV, ODESSA, AND DNIPROPETROVSK, UKRAINE; MOSCOW AND ST. PETERSBURG, RUSSIA—On Easter Sunday, Sergey Nenov, along with hordes of other people in Odessa, took a basket filled with sprinkle-covered frosted cake, cookies, and other offerings to a gold-domed Orthodox church and lit candles in prayer. But when Nenov came to a gilded painting of the Madonna and Child, he separated himself from the crowd by pressing his lips to glass that protected the Christian icon. Nenov had reason to be grateful this year. He is one of 4300 opiate addicts in the country to receive methadone, a substitution treatment that has freed him from his dependency, allowing him to stop having run-ins with the law and, at long last, begin to tackle his dual infections with HIV and tuberculosis (TB).

Nenov, who lives at a TB hospital in the city that dispenses his daily dose of methadol—a pill form of methadone—started injecting *chernaya*, an opiate made from liquid poppy straw (see p. 161), in 1988. He is astonished that he survived long enough to see the substitute opiate come to Ukraine; importing it was illegal until December 2007. "Before, we would watch TV reports about these Dutch substitution treatment programs and say, 'It will never happen in our country,' " says Nenov.

Opiate substitutes are one component of harm reduction, an international movement that promotes treatment rather than arrest and incarceration of injecting drug users (IDUs). The harm-reduction "package," which aims to protect IDUs from infections and other health risks, also includes clean needles, counseling, HIV testing, and education. In a 2005 position paper, the Joint United Nations Programme on HIV/AIDS (UNAIDS), the World Health Organization, and the United Nations Office on Drugs and Crime explicitly backed opiate substitutes to prevent HIV's spread. An expert committee convened by the U.S. Institute of Medicine in 2007 cited "strong evidence" that methadone and another popular substitute, buprenorphine—now used by only 800 others in Ukraine—reduced illicit drug use and HIV-risk behaviors such as sharing injecting equipment. It recommended that they "be made widely available, where feasible."

Although Ukraine, Russia, and other countries in the former Soviet Union have IDU-driven HIV/AIDS epidemics that are increasingly spreading into the broader population through sex, harm reduction remains spotty throughout the region. Even the Ukrainian government has not fully embraced harm reduction, which is largely delivered by nongovernmental organizations (NGOs) that receive support from the Global Fund to Fight AIDS, Tuberculosis and Malaria. Ukraine's 2010 HIV/AIDS progress report to the United Nations, endorsed by the minister of health, acknowledges the shortcomings: "The scope, scale, quality and intensity of HIV prevention activities among the most vulnerable population groups remain insufficient to stop HIV spreading in these groups and limit the potential spread of HIV among the general population."

Russian roulette

In comparison, the Russian Federation seems outright hostile toward harm reduction, to the outrage of researchers, public-health specialists, and activists. The banning of opiate-substitution treatment (OST) has evoked the sharpest criticism. "OST does not exist in Russia, and it's the place where it's most needed," says UNAIDS's Denis Broun, the Moscow-based regional director for Europe and Central Asia. The government does offer treatment at "narcologic" clinics, but one recent study found a 90% relapse within a year among nearly 1000 users who sought help.

Unlike in Ukraine, the Russian government pays no heed to civil society's input, charges Anya Sarang, who specializes in drug policy and runs the Andrey Rylkov Foundation for Health and Social Justice in Moscow. "The government on every level—federal, city, oblast—they're never interested in listening to the community," Sarang says. "All the decisions here are totally

political and unsupported by evidence. They don't make any effort to find out what's going on in the world."

Adding to the lack of knowledge about the benefits of harm reduction, there's a "huge stigma" toward drug users, notes psychologist Alla Shaboltas, who studies IDUs at the Biomedical Center in St. Petersburg. "They've never been considered normal people who deserve treatment," says Shaboltas. "They're considered criminals who should die."

Prickly issue. A Kyiv NGO provides free needles and collects used ones, but Moscow says *nyet*.

Several Russian public-health officials and politicians did not reply to *Science*'s request for interviews over several months, but Alexey Mazus, head of the city-sponsored Moscow Centre for HIV/AIDS Prevention and Treatment, articulates the government position—which he shares—and makes it clear that he strongly objects to other countries criticizing his country's stance toward harm reduction. "It's not their business what's going on in the Russian Federation," says Mazus.

In his view, the evidence that OST and other harm-reduction interventions worked in some countries has no bearing on Russia. "Take into consideration whether people are the same in terms of culture and psychology," Mazus says, stressing that injection drugs like heroin are new to his conservative country. Giving a heroin user methadone, he says, is "like a doctor who tries to treat an alcoholic and gives the patient alcohol."

Similarly, he thinks that needle exchange—which is not allowed in Moscow—would "energize drug using. What is more, it will show that our government tolerates using drugs—and they're firmly against it, just like the whole society."

Russia has allowed a consortium of NGOs known as GLOBUS to run harm-reduction projects, which include needle exchange in many locales, with money from the Global Fund, but the government recently reneged on a promise to bankroll those efforts itself (see p. 168). "The Russian government says it's doing this because of lack of effectiveness," says Charles Vitek, head of the Global AIDS Program in Moscow for the U.S. Centers for Disease Control and Prevention (CDC). "It's hard to say what type of evidence would be sufficient to change the government's stance."

Alexey Bobrik of the Open Health Institute in Moscow, who heads GLOBUS, says harm reduction, and in particular OST, is essentially an ideological issue. "In Russian culture, science almost doesn't matter," says Bobrik. "It's similar to the Soviet Union and questioning the superiority of socialism. Regardless of whether you could support your argument with data, you'd be labeled as insane, an unnecessary person. The same with OST now." But if someone in a high enough position decides to back OST, the opinions of drug-control specialists and HIV experts won't matter. "If Putin says we should try OST," says Bobrik, "it will be done."

> ***Giving a heroin user methadone is "like a doctor who tries to treat an alcoholic [with] alcohol."***
>
> **—ALEXEY MAZUS, MOSCOW CENTRE FOR HIV/AIDS PREVENTION AND TREATMENT**

Ukraine's gains and pains

In the industrial city of Dnipropetrovsk, the City Clinical Hospital No. 21, built in 1908, looks its age. The sprawling institution sits on a steep hill and houses clinics in several low-slung buildings with corrugated tin roofs and heavy steel doors that are shielded by ornate awnings, some buckled with rust. Windows are boarded in places, and gates tilt on their hinges. It seems an unlikely place for one of the country's most modern and ambitious programs for HIV-infected IDUs, offering them OST, TB treatment, and antiretroviral drugs (ARVs) all at the same facility.

Each morning, the 48 IDUs in the program, which started in July 2008, gather at the OST clinic for their daily dose of methadol. They hang out on the front steps and smoke cigarettes while they wait their turn, and though some grumble about the drug killing their sex drive and the hassle of making daily visits to the clinic, there's wide agreement that the methadol is helping them lead what several refer to as "normal" lives. "The program is great," says Vlad, 45, on a drizzly and drab April morning. "I don't have to steal or hide from the police. Everything is cool."

Vlad and his wife, Natasha, 49, walk into the clinic and enter a small, tidy room at the front. After they sign in and a nurse checks their names off her own list, Alonya Lesnichaya, the doctor who runs the program, places their individual doses of methadol pills into plastic cups and pestles them into tiny chunks. One after the other, they toss the medicine into their mouths, chase it down with a sip of soda, and then open wide to show Lesnichaya that they have swallowed everything. The elaborate ritual has less to do with making sure that they received the methadol than the concern that they might hide it in their gums and later spit it out and sell it on the black market.

The potential "diversion" of substitute opiates is one of several reasons that

CREDITS: MALCOLM LINTON

Hard to swallow. Alonya Lesnichaya (*lower right*) says hospital staff at first resisted an integrated HIV/TB/methadone program for IDUs, but it's working well.

CREDITS: MALCOLM LINTON

Lesnichaya says many doctors on the staff did not initially support the idea of opening the OST clinic here, which is supported by the Clinton Health Access Initiative and a Global Fund grant monitored by the International HIV/AIDS Alliance in Ukraine. "Mainly, they were afraid it would turn out to be a drug-dealing place," says Liudmila Timoffeva, the director of the hospital. Lesnichaya adds that they also had to confront unease from other patients. "We didn't want to frighten people, and we worried that our society was not ready." But "we made it work," she adds, establishing "a very close, integrated link between the different specialists."

The clinic currently helps just a tiny number of people in Dnipropetrovsk, one of the cities hardest hit by HIV in the country, and there is only one other OST program operating here. And progressive as this program may be, it accepts only HIV-infected IDUs. Lesnischaya says they were put first in line because when they're using or preoccupied with trying to score and avoid withdrawal, they have great difficultly remembering to take their ARVs on time or even where they put them. But that shuts out IDUs like Sasha, who badly wants into the program.

A 35-year-old carpenter who lives with his mother in a nine-story tenement on the outskirts of the city, Sasha began using when he was 17. Now estranged from his wife and 1-year-old child, he works with an NGO, Way to Life, that also provides counselors to the program at City Clinical Hospital No. 21. Representatives from Way to Life come to visit him to drop off bags filled with clean needles, which he will then distribute to other users. He becomes sullen and angry when the Way to Life outreach workers explain that the OST program cannot take him because he is not infected with HIV.

Sasha carries the bags of needles into his bedroom and places them on a vanity next to a copy of the Bible. On the mirror, he has taped up a little prayer that reads, in part, "My God, I don't want to be dependent." He takes a long look at the floor. "I pray, and it doesn't help," he says.

Future prescriptions

The IDUs in Ukraine and their advocates have begun pushing to expand OST—which the Global Fund estimates now reaches only about 10% of the IDUs in need—and improve it. "Substitution treatment has a huge number of problems," says Iryna Borushek, a leader of the All-Ukrainian Network of People Living with HIV who sits on the country's coordinating mechanism that prepares and oversees Global Fund grants for the country. Borushek, a buprenorphine recipient herself, says at the top of the agenda is doing away with the requirement to make daily trips to an OST clinic. "People are chained to the site," she says. In all of Ukraine, only six people have prescriptions for OST that allow them to take the drugs without being observed.

Psychologist Olga Belyaeva, who runs an NGO in Dnipropetrovsk that helps IDUs, is one of the six Ukrainians who has a buprenorphine prescription. She and other community activists are lobbying for national regulations that will establish standards of care for substitution treatment, federal funding for it, and more flexible use of different substitution drugs. "We need political will from the new government to change the drug policy more to public health," says Belyaeva.

Some fear, however, that Ukraine's new president, Viktor Yanukovych—who was elected in February and has closer ties to Moscow than his predecessor did—will not be receptive to expanding OST. "The legalization of methadone in Ukraine was a hard-fought battle, and like many things, it may be vulnerable because of political changes there," says CDC's Vitek, who is relocating to Kyiv in August. "If groups could seize on any evidence of a lack of effectiveness, methadone overdose deaths, or diversion, there's a continued political risk."

For Belyaeva and other activists, any rollback of Ukraine's hard-won policies toward those of Russia would be disastrous. "When I was in Moscow in November," says Belyaeva, "I came back home and was kissing the ground."

–JON COHEN

NEWS

Praised Russian Prevention Program Faces Loss of Funds

In 2006, then-President Putin pledged increased support for HIV/AIDS programs, but the government recently declined to fund some key efforts

ON 21 APRIL 2006, VLADIMIR PUTIN, THEN president of the Russian Federation, unexpectedly called for increased spending and urgent new measures to combat HIV/AIDS. "We need more than words; we need action, and the whole of Russian society must get involved," Putin declared.

Putin's critics long had accused him of turning a blind eye to the country's epidemic; a 2004 report from Human Rights Watch complained that "the Russian government has for too long been acting as though HIV/AIDS is little worse than hemorrhoids." In particular, Putin and his underlings did not support harm-reduction efforts that aimed to slow the spread of HIV among injecting drug users (IDUs), who account for most infections in the country. Nor did the government target prevention efforts to other vulnerable groups like sex workers and men who have sex with men. Nongovernmental organizations (NGOs) picked up the slack and launched their own projects, receiving substantial financing from the Global Fund to Fight AIDS, Tuberculosis and Malaria.

Skeptics linked Putin's sudden concern for HIV/AIDS to Russia's first hosting of the annual Group of Eight (G8) summit, which would take place in St. Petersburg in July 2006. "He wanted to show we are normal people and care about HIV," says Alexey Bobrik, a clinician and director at the Open Health Institute, an NGO in Moscow. "It was much less sensitive than nuclear proliferation or other problems."

The Russian government did for a time take dramatic action. At the G8 summit, Russia announced that it would shift from being a Global Fund recipient to a donor. In another generous move, it pledged to reimburse the fund for the $217 million that Russian grantees—mainly NGOs—were slated to receive between 2007 and 2010 and also offered $40 million to help Africa. The 2007 federal Russian HIV/AIDS budget grew to $445 million—a 57-fold increase from 2005. And the government indicated that it would finance efforts aimed at high-risk groups.

The Russian NGOs working on HIV/AIDS were elated, if wary. They had organized themselves into a consortium, Global Efforts Against HIV/AIDS in Russia (GLOBUS), led by Bobrik and operating in 10 different regions. Nearing the end of a 5-year Global Fund grant of nearly $90 million, GLOBUS in May 2008 took heart when Russia's minister of health and social welfare, Tatyana Golikova, assured delegates at the 2nd annual Eastern Europe and Central Asia AIDS Conference (EECAAC), held in Moscow, that GLOBUS's work was appreciated. According to a press release from her office, "all projects and programs that were initiated by nonprofit organizations must be continued."

Climate change. Vladimir Putin's (*above*) bold HIV/AIDS stance has weakened, leaving the Global Fund to rescue Alexey Bobrik's (*below*) NGO consortium.

Yet in July 2009, a month before the end of the GLOBUS grant, Bobrik received word that the government would not bankroll the consortium after all. Several other NGOs had to lay off employees or close up shop. One is LaSky, a prevention project for men who have sex with men in St. Petersburg. "Our clients have no place to go," says Ilya Kurmaev, who runs the effort. A recent study by Stellit—another NGO in the city—found a prevalence in that population approaching 12%.

Evgeniy Petunin, who is based in Moscow and heads the Russian Harm Reduction Network—an NGO that has depended on Global Fund money—says the government has no specialists who work with IDUs. "Harm reduction in Russia is dying," says Petunin. "The government doesn't pay attention to the problem."

Nicolas Cantau, the portfolio manager for the Global Fund in charge of the GLOBUS grant, says a battle between government agencies led to the sudden change of heart about supporting GLOBUS: The health ministry argued that it made more sense to promote "healthy lifestyles" to prevent HIV infection than to back ineffective harm-reduction programs. "There's been an ideologically based approach as opposed to following scientific evidence," says Cantau. "GLOBUS is one of the most successful programs worldwide since the beginning of the Global Fund."

Complaints about the government's decision to abandon GLOBUS took center stage in October 2009 at the 3rd EECAAC, again held in Moscow. Attendees included Michel Kazatchkine, the head of the Global Fund, but no one came from the Russian health ministry. The next month, the Global Fund's board, on "an extraordinary basis" that recognized "an emergency situation," awarded GLOBUS $24 million to keep the consortium alive through 2011. "There's a lot of concern about the future," says Cantau. "It's just for 2 years, and 2 years is going to pass very quickly."

Bobrik has mixed feelings about the emergency grant; he's grateful to the Global Fund but says the new money lets the government off the hook for two more years. Maia Rusakova, a sociologist who runs Stellit, similarly contends that Russia must support these efforts at the local and federal level. "Our politicians know how to look quite nice and they say a lot of things, but they don't do it," says Rusakova. "The situation is very, very serious, and I'm concerned that it looks like a ticking bomb."

–JON COHEN

CREDITS (TOP TO BOTTOM): G8 RUSSIA (WWW.EN.G8.RUSSIA.RU); MALCOLM LINTON

Open-and-shut case. Oleg Vaschenko is one of many clients of this clinic who say a police raid was harassment.

CREDITS: MALCOLM LINTON

NEWS

Law Enforcement and Drug Treatment: A Culture Clash

A raid on an opiate-substitution treatment center in Ukraine highlights tense relationship between police, IDUs, and harm-reduction advocates

ODESSA, UKRAINE—On 11 March, Tatyana Afanasiadi went to the Odessa Oblast Narcological Dispensary for her dose of buprenorphine, an opiate-substitution drug distributed there each day along with methadone. Afanasiadi, 31, is not just one of the clinic's more than 200 drug-dependent clients, about half of whom are infected with HIV: She is a lawyer and head of the Union Together for Life, a nongovernmental organization that catalyzed the opening of this pioneering opiate-substitution treatment (OST) program, and she helps run the office. This role thrust her into the middle of a high-profile showdown with police that loudly broadcast the sharp tension throughout Eastern Europe between law enforcement and harm-reduction efforts like OST that are designed to slow HIV's spread.

According to Afanasiadi, as she was leaving the clinic that Thursday morning, three men dressed in civilian clothes approached, greeted her by name, slapped handcuffs on her wrists, and took her to an unmarked car with tinted windows. "At first I thought it was a scheme where police grab drug users and then ask them to identify another user they're already looking for," she says. Afanasiadi then worried that they were going to plant drugs on her and demand a bribe, so she stressed that she didn't have any money. When that had no impact, she tried another tack. "I told them I'm ill and tried to frighten them with my HIV infection, but they were knowledgeable, and it didn't work."

The men, who she says refused to show identification, took Afanasiadi to their police station. Unbeknownst to her, the clinic was being raided because of allegations that it did not have the authority to distribute substitute opiates and suspicions that staff members, including Afanasiadi, were selling the drugs on the side. At the station, with two female observers present, Afanasiadi had to remove her clothes, which were carefully inspected for stashed drugs. "They were extremely disappointed," she says. They next sent her to a gynecologist for a vaginal exam. "It was quite a disgusting procedure," she says of the ordeal. When that turned up nothing, they searched her home, which she shares with her husband and 6-year-old son, and her car. That evening, with no evidence against her, they locked her up. The clinic's doctor, Ilya Podolyan, was also detained, as was a nurse.

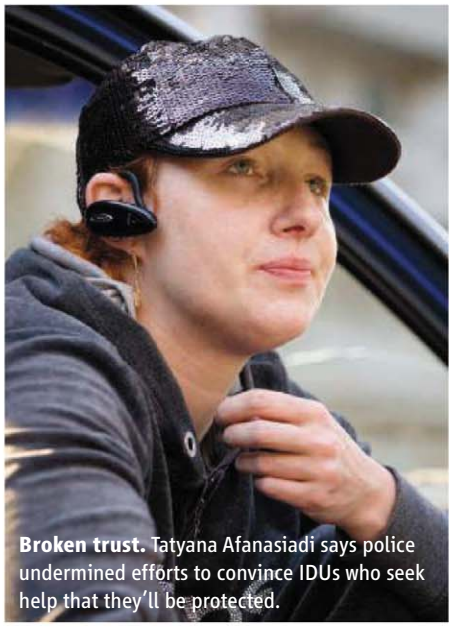

Broken trust. Tatyana Afanasiadi says police undermined efforts to convince IDUs who seek help that they'll be protected.

After a high-powered attorney intervened, the police freed Afanasiadi the next day without charging her. But Podolyan remained in jail for 4 days. The police also confiscated files from the clinic. Without the staff and the records, the clinic remained shuttered, leading to a massive protest by clients that Saturday that attracted much media attention and sent waves of concern that have rippled far and wide. "This is a very dangerous signal," says Yuri Kobyscha, an HIV/AIDS epidemiologist who works with the World Health Organization in Kyiv. This site, like most OST projects in Ukraine, is supported by the Global Fund to Fight AIDS, Tuberculosis and Malaria.

The fund's Ukraine portfolio manager, Andreas Tamberg, has strongly condemned the raid and arrests as "a violation of human rights" and "epidemiologically foolhardy."

Afanasiadi says the raid on the clinic undermines a broader agenda to encourage injecting drug users (IDUs) to seek help and, if they're still injecting, take advantage of other harm-reduction programs such as needle exchange or treatment and counseling for their HIV infection. "IDUs are really hard to connect with any services," says Afanasiadi. "We invite people into substitution treatment and guarantee anonymity and protection in some ways, and at the end of the day, we can't guarantee them anything."

Since the raid, events have taken a turn for the worse. On 28 May, the Ministry of Internal Affairs in Odessa indicted and rearrested Podolyan, charging him with 42 counts of illegally distributing buprenorphine. The International HIV/AIDS Alliance in Ukraine, which administers the Global Fund grant to the clinic, held a protest press conference on 3 June, documenting that this case is one of several in which police have interfered with OST programs and appealing to the country's general prosecutor to intervene in what it branded the "systematic unlawful criminal prosecution of narcology doctors."

–JON COHEN

NEWS

HIV Moves In on Homeless Youth

Studies have discovered shockingly high HIV prevalence rates in kids who live in the streets of Russia and Ukraine; NGOs are trying to give them new leases on life

ST. PETERSBURG, RUSSIA, AND ODESSA, UKRAINE—Russians frequently boast that St. Petersburg is the most beautiful city in the country, and Ukrainians say the same about Odessa. Both feature well-preserved architecture in Italian and French styles that date back to the 18th century, stunning monuments, and lots of water, be it the canals that wind through St. Petersburg pouring into the Neva River or the majestic Black Sea that laps Odessa's shores. Yet both cities have a dark underbelly that has caught the attention of HIV/AIDS researchers: Large numbers of youths living on the street who, as a group, are at as high a risk of becoming infected by the virus as any vulnerable population ever studied. "They're hard to reach and invisible for HIV statistics and often for HIV prevention programs," says Dmitry Kissin, an obstetrician/gynecologist who works for the U.S. Centers for Disease Control and Prevention (CDC) in Atlanta. "No one knows how many street youth there are because no one's counting them. And when you don't know about something, you don't pay attention."

Kissin, who is originally from St. Petersburg, has worked for the past 4 years with colleagues in both countries to bring attention to this underappreciated high-risk group. Estimates suggest that up to 3 million youths are living on the streets in Russia and 150,000 in Ukraine. They live in city shadows, sleeping in basements of apartment buildings and abandoned buildings, taking odd jobs and panhandling, and constantly dodging police. "You don't see them unless you look for them," he says.

Kissin has been trying to do just that. Along with CDC's Susan Hillis and co-workers from HealthRight International—a nongovernmental organization (NGO) formerly known as Doctors of the World-USA and founded by pioneering AIDS researcher Jonathan Mann—he launched a study in St. Petersburg in 2006. The researchers identified 41 different train stations, metro stops, street markets, and other sites where groups of teens gathered. They picked half of the sites at random and started enrolling youths in the study. In the end, they signed up 313 teenagers between the ages of 15 and 19, two-thirds of them male, who lived at least part-time on the street, were not cared for by their families, and did not regularly attend school. They questioned the participants in detail about their lifestyles and tested each one for HIV. When they first saw the results, says Konstantin Zakharov, the project coordinator for HealthRight, "it was a shock." A staggering 37.4% were infected.

Highs and lows

Shortly before dark one March night, three young men hanging out together on a canal near the center of St. Petersburg approach a mobile van operated by HealthRight and greet Zakharov. In the wake of their first study, which was published in the 12 November 2007 issue of *AIDS*, HealthRight started to send the van out on the streets twice each week to do HIV testing and counseling of street youth. The group also opened an overnight shelter, organized a drop-in center for counseling with psychologists, and helped connect youths in need of medical care with the appropriate doctors. The oldest of the three young men, Stas Fedorov, 23, has received vocational training and leads informal, HIV-prevention workshops with others in his situation. His two friends are drinking vodka from a soda bottle, but he seems sober, the wise elder of the group. "My dream is to live like a normal person," he says. "Start working and restore my documentation, which somebody stole."

Mean streets. Stas Fedorov (*center*) and his friends have risky lifestyles that HIV easily exploits.

Fedorov is infected with HIV—"My girlfriend gave me that present," he says—but he is relatively healthy, which is remarkable given his history. He says he started smoking cigarettes at 6. His friends took him to the big city, St. Petersburg, at 7, and he was dazzled by the bright lights and stayed, sleeping in basements or in abandoned buildings. Like many of the youths, Fedorov was an orphan and got into inhalants and injecting drugs, but he says he is clean now. "I've seen people do anything for the dose," he says.

Kissin, Zakharov, and their colleagues have attempted to tease out the risk factors that lead to such high infection rates among street youth—information that is key to tailoring prevention programs to each vulnerable population. Some behaviors are well known

CREDIT: MALCOLM LINTON

Shelter from the storm. Inna Nikiforova (*above*) and The Way Home offer street youths a nourishing environment, including a chance to rebuild self-esteem playing sports and winning medals.

to fuel HIV's spread: an astounding 78% of the youths who injected drugs tested positive, as did 70% who had another sexually transmitted infection (an indicator that they did not use condoms). But they also linked HIV infection to social forces particular to street youth. The death of both parents more than tripled the risk of becoming infected, and having no place to live raised it 2.4-fold.

Although many studies have found that people who learn they are infected take precautions not to infect others, in this group, teens who came into the study knowing they were HIV positive were *more* likely to share needles and inconsistently use condoms. "Maybe there's just a sense of hopelessness among them," says Kissin. "HIV may not be your first priority when you need to negotiate survival on the street and find food, drugs, alcohol, and some place to sleep."

Odessan odyssey

"Dima! Dima! Dima!"

Inna Nikiforova is crouching down and yelling through an iron grate that covers an opening to the dirt-floored basement of a downscale apartment building not far from Odessa's swank downtown. Nikiforova, a former injecting drug user (IDU) herself who lost an arm after a suicide attempt as a teen, is an outreach worker with The Way Home, an NGO that helps street youth, and Dima is one of the teens she has become closest to over the years. This Saturday afternoon, she has brought him a plastic crate filled with food, but he is not in his usual haunt, which is strewn with filthy mattresses, trash, cigarette butts, and burnt-out candles.

Nikiforova soon finds Dima at a nearby busy intersection approaching cars, hat in hand. He has clubbed feet, the result of nerve damage from injecting an ephedrine-based drug called *baltushka*, and he hobbles over and gives her a long hug, closing his eyes. He has few teeth left. He is 18 but looks much younger. Dima also is HIV infected, as are 27% of the street youth here, according to a study conducted in 2008 by HealthRight and the U.S. CDC. And like many teens who live on the street, he is difficult to help—and is in dire need of assistance. "We found his father in Moldova and said, 'Here's your kid, he wants to come home,' " says Nikiforova. "The father had a new wife and family and said, 'He's not my son until he stops using drugs.' "

> *"We … said, 'Here's your kid, he wants to come home.' The father … said, 'He's not my son until he stops using drugs.' "*
>
> —INNA NIKIFOROVA, THE WAY HOME

The Way Home runs a shelter that houses two dozen street youth, and Nikiforova, who lives with them in the well-kept dorms, brought Dima in. He lasted only 3 days. But he moved into a drug-rehab clinic and went clean for a time, joining a soccer team and winning a medal that Nikiforova hangs from a mirror in her bedroom. To return to his father, all he needed was proper documentation—like many street youths, he had none—and The Way Home tried to help him obtain them. Then Dima relapsed. "He just got drunk and left, and since then …" says Nikiforova.

Attempts to help the street youth are even more complicated when it comes to HIV prevention and care. As Sergey Kostin, the head of The Way Home, explains, they are not allowed to distribute clean needles to the youths. "It's against the norms," says Kostin, a geologist and former IDU himself. "It's hypocritical." Nataliya Kitsenko, a clinician who directs the HIV/AIDS program for the charity, says they have had many difficulties accessing anti-HIV drugs for the youths, too. "It's very hard because they don't have parents to give consent," says Kitsenko. "It's a big problem, and we don't know how to solve it."

Although NGOs such as The Way Home and HealthRight have joined with international groups to address the often-ignored epidemic of HIV/AIDS in street youth, Kitsenko doesn't expect her own economically challenged government to step up its efforts anytime soon. "The government doesn't do much of anything for the so-called normal people, and at such times, how can they think of programs for the marginalized?" she asks.

–JON COHEN

CREDITS: MALCOLM LINTON

Helping hand. Evgeny Voronin's work with HIV-infected children and pregnant women has drawn international attention.

CREDIT: MALCOLM LINTON

NEWS

Reducing HIV Infection and Abandonment of Babies

Injecting drug users often seek medical help late in pregnancy and then relinquish their babies to the state. Surprisingly, their drug use is not the major factor

ST. PETERSBURG, RUSSIA—In the late 1980s, when Russia had detected only a smattering of HIV cases, 270 children became infected in several hospitals through the reuse of contaminated needles. "The country was in shock," says Evgeny Voronin, who then ran an infectious-disease hospital in Ust-Izhora, on the outskirts of St. Petersburg. The Ministry of Health asked for his help, and he opened a pediatric AIDS center to care for the children. "It was very difficult for us," Voronin says. "The mothers called us murderers. It didn't matter that the children were infected very far from us. They thought all people in white coats were responsible for what had happened."

That early effort evolved into the Centre for Prevention and Treatment of HIV Infection in Pregnant Women and Children, which Voronin still runs. Now, rather than caring for accidentally infected children and their grieving mothers, the center focuses on helping infected mothers prevent transmission to their babies and raising HIV-infected children who have been orphaned or abandoned.

In March, the center's orphanage had only 33 HIV-infected children. "It's not the biggest group we help, but it's the most vulnerable," says Voronin. His work with HIV-infected children has made him something of a celebrity—visitors have included former U.S. first lady Laura Bush and Western movie stars—and also drawn attention to prevention of mother-to-child transmission (PMTCT) efforts and the country's staggering, post-Soviet explosion of orphaned and abandoned children. In 2002, the Russian government put the number of such children at 700,000.

More than 50,000 children have been born to HIV-infected women in Russia (half during the past 3 years). Although women increasingly are becoming infected through sex, many are injecting drug users (IDUs), and several studies have attempted to untangle how drug use influences both abandonment and the limited success of PMTCT.

Susan Hillis, a reproductive health specialist at the U.S. Centers for Disease Control and Prevention—who incidentally has adopted eight Russian children—collaborated with Voronin and other Russian colleagues in analyzing the factors that lead HIV-infected mothers in St. Petersburg to abandon their babies. The study followed 43 HIV-infected women, two-thirds IDUs, who learned their status during labor and delivery. Half of them abandoned their babies, a process that involves relinquishing the child to the state. "Everyone, including all of our Russian colleagues—people we respect and trust—really believed abandonment to be related to injecting drugs," says Hillis.

But the data said otherwise: The only significant risk factor was an unintended pregnancy. (Women typically abandon babies before they know the baby's HIV status, so that's not a factor.) "Women who aren't motivated to take care of babies and themselves before delivery are less likely to take care of them afterward," she says. Hillis, who published these results in the February 2007 *International Journal of STD & AIDS*, is now working with ob-gyn Anna Samarina at Botkin Hospital here to advocate that more of these women have easy access to contraceptives.

Hillis and co-workers next examined PMTCT in 1500 HIV-infected mothers in St. Petersburg who gave birth between 2004 and 2007. More than half had a history of injecting drugs—with one-third using while they were pregnant. (Only 11.4% abandoned their babies, which Hillis believes reflects the situation today better than the earlier study did.) They all received anti-HIV treatment to prevent transmission, but many began late in pregnancy, when it is less effective, or used substandard regimens. The study, published online on 3 February in the *Journal of Acquired Immune Deficiency Syndromes*, found that 6.3% of mothers passed HIV to their babies—about three times the rate seen in Western Europe. Women who injected drugs during pregnancy started treatment later, on average. But factors such as access to prenatal care, rather than drug use per se, were more critical in determining the risk of transmitting the virus. "The most important thing is not whether you're using drugs," says Hillis. "If we could figure out a way to get them early and give them proper prophylaxis, we could do a tremendous amount to reduce transmission."

These efforts with orphans and PMTCT have come full circle for Voronin: Twelve of the girls he cared for when they were infected by hospital procedures came to his center when they were pregnant. None infected their babies. "People ask me why do you do so much for orphans?" he says. "We took in these girls with AIDS, but they're healthy now after 20 years, they have normal lives, and they have their own families."

–JON COHEN

All together now. Andrei Kozlov's center works with U.S. investigators on a wide range of studies.

NEWS

HIV/AIDS Investigators Few and Far Between

The Biomedical Center conducts top-notch studies with foreign collaborators, a surprising rarity in Russia to this day

ST. PETERSBURG, RUSSIA—When it comes to HIV/AIDS research, insiders and outsiders agree that this country, nicknamed the bear, has not lived up to its big and strong moniker. "In the last decade of AIDS research, Russia has not contributed anywhere near her capacity or potential," says molecular epidemiologist Chris Beyrer of the Johns Hopkins Bloomberg School of Public Health in Baltimore, Maryland. In addition to language barriers and other difficulties in accessing information, Beyrer says the country is still reeling from a brain drain that happened when the Soviet Union fell. "It's been very difficult to get the universities back up and running," says Beyrer, who conducts collaborative HIV/AIDS studies in Russia and trains Russian graduate students. But there are islands of talented investigators. One of them is the Biomedical Center, a privately run and modest institution here. "AIDS science is neglected [in Russia], no question," says molecular biologist Andrei Kozlov, who runs the center. "This is a shame."

Set in a drab, gray-brick building with bars over the windows, the two-story center conducts studies on epidemiology, behavior, molecular characterizations of the virus, and basic vaccine questions. The two dozen investigators have helped clarify the rate of spread of HIV among injecting drug users and documented the transmission from IDUs into the broader population through heterosexual sex. It is the only Russian institution to have joined the U.S. National Institutes of Health's HIV Prevention Trials Network, establishing an IDU cohort for future studies. And several center investigators have trained at Yale University and other top U.S. institutions. "It's a big thing for us to have faith in our collaborators, and the people we're doing virology and social science with there we like enormously," says Myron Cohen, who directs the Institute for Global Health and Infectious Diseases at the University of North Carolina, Chapel Hill.

Kozlov, who did a fellowship in Robert Gallo's lab at the U.S. National Cancer Institute before AIDS surfaced, says Russia's difficulties in developing a robust HIV research community stem in part from a long-standing disconnect between medical schools and research institutions. There has also been a leadership vacuum and sharp enmities between different groups. Kozlov, no shrinking violet himself, has had his challenges collaborating, too.

Difficulties aside, the collaborations have delivered repeatedly. A recently published finding from a study with Cohen has put the group in the midst of a hot debate in HIV vaccine research. An infected person over time develops many viral variants, as HIV constantly mutates. Does a vaccine need to trigger an immune response to stop a swarm of variants, a decidedly tough job? To find out, researchers have hunted for HIVs in newly infected people as close to the moment of transmission as possible and then analyzed genetic variants. It's a tricky business that requires repeatedly taking blood samples from HIV-negative people who are at high risk of becoming infected, but the center and others have managed to do it.

Studies over the past 2 years have shown convincingly that there is a "bottleneck" with sexual transmission: In about 80% of heterosexuals and 60% of men who have sex with men, only one "founder" virus, for unknown reasons, makes it through the mucosal barriers and establishes an infection. Yet a vaccine that prevents sexual transmission might face steeper challenges if HIV enters by a dirty needle. That's just what a group led by George Shaw at the University of Alabama, Birmingham, found.

In the June 2010 *Journal of Virology*, Shaw's team reports that six of 10 IDUs had more than one variant at transmission; one man had 16. Yet the same month, the Biomedical Center team and Cohen published starkly contradictory findings in the *Journal of Infectious Disease*: In 13 IDUs, nine had a single variant at transmission—roughly the same as heterosexuals. Both studies involve small numbers, and Shaw's group focused on cocaine users who may have injected and shared needles more frequently than did the heroin users in St. Petersburg.

Whatever the answer, Russian scientists are illuminating a vexing HIV/AIDS issue that has implications far beyond the country's borders. And that, in itself, is something of a roar from what has been a relatively quiet research community. **–JON COHEN**

HIV TRANSMISSION BOTTLENECK IN IDUs

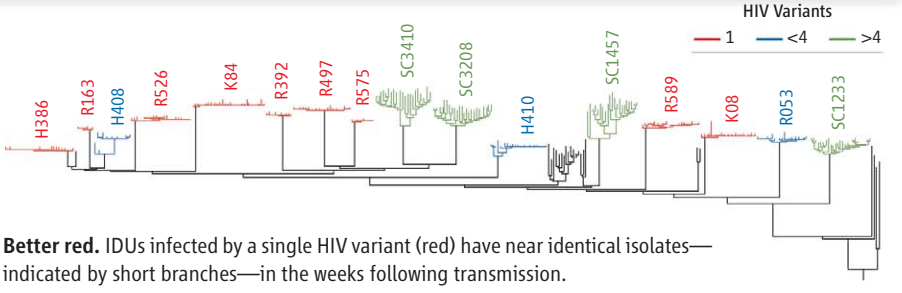

Better red. IDUs infected by a single HIV variant (red) have near identical isolates—indicated by short branches—in the weeks following transmission.

CREDITS (TOP TO BOTTOM): MALCOLM LINTON; ADAPTED FROM ALEXEY E. MASHARSKY *ET AL.*, *THE JOURNAL OF INFECTIOUS DISEASES* 201 (JUNE 2010)

REVIEW

HIV Persistence and the Prospect of Long-Term Drug-Free Remissions for HIV-Infected Individuals

Didier Trono,[1]* Carine Van Lint,[2] Christine Rouzioux,[3] Eric Verdin,[4] Françoise Barré-Sinoussi,[5] Tae-Wook Chun,[6]† Nicolas Chomont[7]†

HIV infection can persist in spite of efficacious antiretroviral therapies. Although incomplete inhibition of viral replication may contribute to this phenomenon, this is largely due to the early establishment of a stable reservoir of latently infected cells. Thus, life-long antiviral therapy may be needed to control HIV. Such therapy is prone to drug resistance and cumulative side effects and is an unbearable financial burden for regions of the world hit hardest by the epidemic. This review discusses our current understanding of HIV persistence and the limitations of potential approaches to eradicate the virus and accordingly pleads for a joint multidisciplinary effort toward two highly related goals: the development of an HIV prophylactic vaccine and the achievement of long-term drug-free remissions in HIV-infected individuals.

Less than 15 years after HIV (human immunodeficiency virus) was discovered as the causative agent of AIDS (acquired immunodeficiency syndrome), several classes of antiviral drugs had been developed that could curb viral replication to nearly undetectable amounts and, if used in proper combinations, could prevent the occurrence of AIDS-related symptoms in infected individuals. Twelve years later, it is obvious that these highly active antiretroviral therapies (HAARTs) do not eradicate the virus, the spread of which rapidly resumes upon their cessation in all but exceptional cases. Thus, HAART can control but does not cure HIV infection. This is sobering, considering the long-term adverse effects of current therapies and their prohibitive financial burden on regions of the world where the epidemics are worst (*1*). Can HIV infection be cured, or at least is long-term drug-free remission possible? The present Review tackles this question by comparing HIV with other persistent human viral infections, by summarizing our understanding of the underlying physiopathology from both virological and immunological standpoints, by examining the potential benefits but also risks of therapies currently envisioned to eliminate the virus, and lastly, by highlighting alternative approaches aimed at inducing prolonged drug-free remissions.

How Does HIV-Induced Disease Compare with Other Chronic Human Viral Infections?

In immunocompetent hosts, most human respiratory and enteric viruses cause acute infections: The pathogen multiplies mainly at and around its portal of entry; induces transmission-promoting symptoms such as sneezes, coughs, or diarrhea; kills its target cells; is countered by innate immune responses; and is cleared by adaptive immune responses that protect against reinfection with the same viral strain. In contrast, other human viral pathogens, often less transmissible, induce persistent rather than acute infections. These include all herpes virus family members, the hepatotropic hepatitis B and C viruses (HBV and HCV, respectively), the tumorigenic papilloma and polyoma viruses, and the retroviruses HIV and human T cell leukemia virus (HTLV). Although diverse in nature and in replicative properties, these viruses can persist in the host because they all share a dual ability: limiting their cytopathic potential and escaping adaptive immune responses. How they achieve this, however, varies greatly (*2*). For example, herpes simplex virus (HSV) escapes clearance by establishing latency within cells of the central nervous system, an immunologically protected sanctuary, and undergoes sporadic reactivation bouts effectively controlled by virus-specific immune responses (*3*). In contrast, HCV does not become dormant but rather shields from and antagonizes both innate and adaptive responses, thus inducing chronic disease in close to 80% of cases (*4*). With HBV, age at the time of infection is determinant: infants typically develop chronic infections because their immature immune system is overly tolerant to the virus, whereas infection later in life, for instance through sexual contact, is spontaneously cleared in more than 95% of individuals (*4*).

HIV always induces a persistent infection, irrespective of the immune status of the host; it becomes latent in a fraction of infected cells, yet never stops replicating in others; it is highly cytopathic to $CD4^+$ T cells but exhibits modest toxicity in macrophages; lastly, it has evolved multiple mechanisms to evade immune responses, including the direct infection and killing of the very cells that should normally be key to its clearance, the $CD4^+$ helper T lymphocytes. Together, these features allow for viral persistence despite antiviral therapies capable of keeping viremia undetectable for years (*5*).

What Is at the HAART of HIV Persistence?

Newly produced HIV virions have a circulating half-life of only a few hours, thus viremia reflects the size of the pool of virus-producing cells in an infected individual. After acute infection, virus-specific T cell responses lead to a drop in viremia to a relatively stable level termed the set point, predictive of the speed at which clinically manifest immunodeficiency will occur if the patient is left untreated (*6*, *7*). After initiation of HAART, the plasma viral load undergoes a multiphasic decay, with an initial rapid decline ($t_{1/2}$ ~ days) stemming from the elimination of short-lived infected cells (mostly activated $CD4^+$ lymphocytes) by virus- and immune-mediated mechanisms (*8*). This is followed by a second phase of slower decline ($t_{1/2}$ ~ weeks) thought to reflect the loss of infected macrophages, which are more resistant to virus-induced cytopathic effects, and possibly the attrition of other viral sanctuaries (*8*). Viremia then stabilizes often below the detection limit of current tests (<50 copies of viral RNA per ml of plasma). Occasional viral blips under therapy and the rapid return of high-level viremia whenever HAART is interrupted, however, demonstrate that the virus is not eradicated (*8*). Although incomplete inhibition of viral replication is likely to contribute to this phenomenon in a subset of individuals, the heart of the problem lays in the early establishment of a stable reservoir of latently infected cells that is not sensitive to current treatments.

Low amounts of viral replication seem to contribute to HIV persistence particularly in individuals displaying immune activation in organs such as the gastrointestinal tract (*5*, *9*). Although more potent or penetrating antiviral drugs might succeed in suppressing residual viral replication in this and other anatomical sites such as the central nervous system and the genital tract, they will not affect individual latently infected cells. It is estimated that an HIV-infected individual with no detectable viremia can harbor up to 10^7 latently

[1]School of Life Sciences and Frontiers-in-Genetics Program, École Polytechnique Fédérale de Lausanne (EPFL), 1015 Lausanne, Switzerland. [2]Institut de Biologie et de Médecine Moléculaires (IBMM), Université Libre de Bruxelles (ULB), 6041 Gosselies, Belgium. [3]CHU Necker, Université Paris Descartes, 75743 Paris, France. [4]Gladstone Institute of Virology and Immunology, San Francisco, CA 94158, USA. [5]Department of Virology, Unit of Regulation of Retroviral Infections, Institut Pasteur, 75015 Paris, France. [6]Laboratory of Immunoregulation, National Institute of Allergy and Infectious Diseases, National Institutes of Health, Bethesda, MD 20892, USA. [7]Vaccine and Gene Therapy Institute Florida, Port St. Lucie, FL 34987, USA.

*To whom correspondence should be addressed. E-mail: Didier.trono@epfl.ch

†These authors contributed equally to this work.

infected cells, mostly CD4$^+$ memory T lymphocytes (*10*). This reservoir is established from the earliest times of infection and is maintained in part by homeostatic proliferation (*11*–*13*). Although its size may be reduced when HAART is initiated very early, mathematical models predict that viral eradication could take up to several decades under conditions of complete viral suppression (*14*). This has led to the proposal of combining HAART with "purging regimens," that is, therapeutic approaches aimed at forcing viral expression by latently infected cells to induce their destruction by virus- or immune-mediated mechanisms. A good comprehension of the molecular mechanisms of HIV latency is necessary to understand the rationale and evaluate the prospects of such therapeutic interventions.

What Are the Molecular Mechanisms of HIV Latency?

When HIV infects resting CD4$^+$ T cells in vitro, it stalls before integrating. This preintegration latency probably occurs in vivo, but is unlikely to represent a functionally significant reservoir given the short half-life of episomal viral DNA (<10 days) (*15*). In contrast, integrated viral genomes (proviruses) can be durably yet reversibly repressed by a combination of mechanisms (*16*). First, the provirus can be subjected to repression via neighboring cis-acting sequences. The HIV preintegration complex is normally tethered to expressed genes by the transcription factor LEDGF/p75, presumably to foster viral expres-

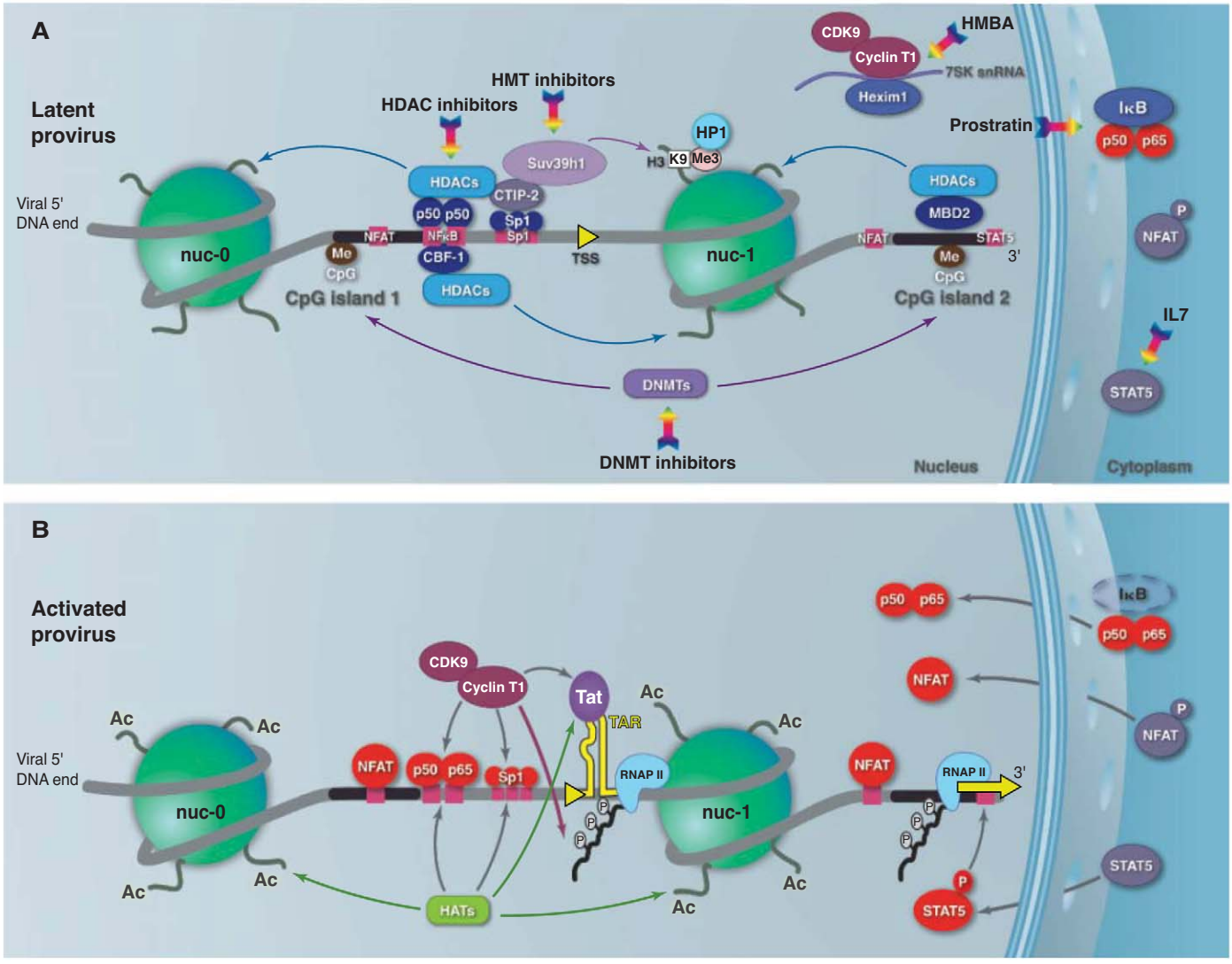

Fig. 1. The yin and yang of HIV transcription in CD4$^+$ T cells. The viral DNA 5′ end is depicted as a light gray ribbon wrapped around nucleosomes Nuc 0 and Nuc 1, with CpG islands in dark gray; sequences binding transcription factors NFAT, NFκB, Sp1, and STAT5 as pink boxes; transcriptional start site (TSS) as a yellow triangle. Gray arrows depict protein movements; color-coded arrows link enzymes and their targets; rainbow arrows indicate potential pharmacological interventions leading to HIV transcriptional activation. (**A**) In resting T cells, HDACs and HMTs (such as Suv93h1) are recruited to the HIV promoter via p50 homodimers and CBF-1 bound to the NFκB sites and via the Sp1-binding CTIP-2 and the methylated DNA-binding MBD2 proteins. Deacetylation and indicated histone methylation on Nuc 0 and Nuc 1 induce a state of heterochromatin. Methylation of two CpG islands by DNA methyltransferases (DNMTs) can further repress transcription. Moreover, the cyclin T1/CDK9-containing pTEFb is sequestered by the Hexim1/7SK RNA complex, whereas the active form of NFκB (p50-p65 heterodimers) is kept by IκB in the cytoplasm, where the phosphorylated and unphosphorylated forms of NFAT and STAT5, respectively, are also retained. (**B**) In activated T cells, HATs and the cyclin T1/CDK9 complex are recruited to the viral promoter by NFκB p50-p65 and Sp1 bound to their cognate sites, and by Tat bound to the TAR (Tat responsive) sequence of nascent RNA transcripts. Histone acetylation of nearby nucleosomes and phosphorylation of the RNAPII C-terminal domain ensue, leading to more accessible chromatin conformation and increased transcriptional elongation, respectively. HIV gene expression is further stimulated by the binding of NFAT and phosphorylated STAT5 to their cognate sites.

sion (*17*). However, integration can occasionally occur within less favorable chromatin environments, leading to latency. Second, the transcriptional status of HIV is tightly coupled to the activation state of its host cell (Fig. 1A). In resting T cells, nucleosomes adjacent to the HIV promoter, notably one situated at the transcriptional start site (Nuc 1), bear markers of silent heterochromatin, such as lysine 9 trimethylated histone 3 (H3K9me3), heterochromatin protein 1 (HP1), and low levels of histone acetylation (*18*). The 5′ long terminal repeat (LTR) of HIV harbors sequences that, in resting T cells, can bind negative regulators. For instance, two adjacent nuclear factor κB (NFκB) sites recruit either p50 homodimers or the C-promoter binding factor-1 (CBF-1), both of which bring in histone deacetylases (HDACs) that act on Nuc 1. Sp1 binding to the basal promoter similarly tethers the corepressor CTIP-2, which recruits HDACs and the histone methyltransferase Suv39h1 (*19*), leading to histone deacetylation and H3K9 trimethylation at Nuc 1 with secondary recruitment of HP1 and promoter repression. Silencing is reinforced by methylation of two CpG islands, possibly through stochastic influences exerted by neighboring cis-acting sequences (*20*, *21*). Methyl-CpG binding domain protein 2 (MDB2) and HDAC-2 bind to the most distal of these methylated CpG islands, a process that negatively correlates with HIV transcription. Lastly, latency can be strengthened by posttranscriptional mechanisms, such as impaired HIV mRNA nuclear export, be-

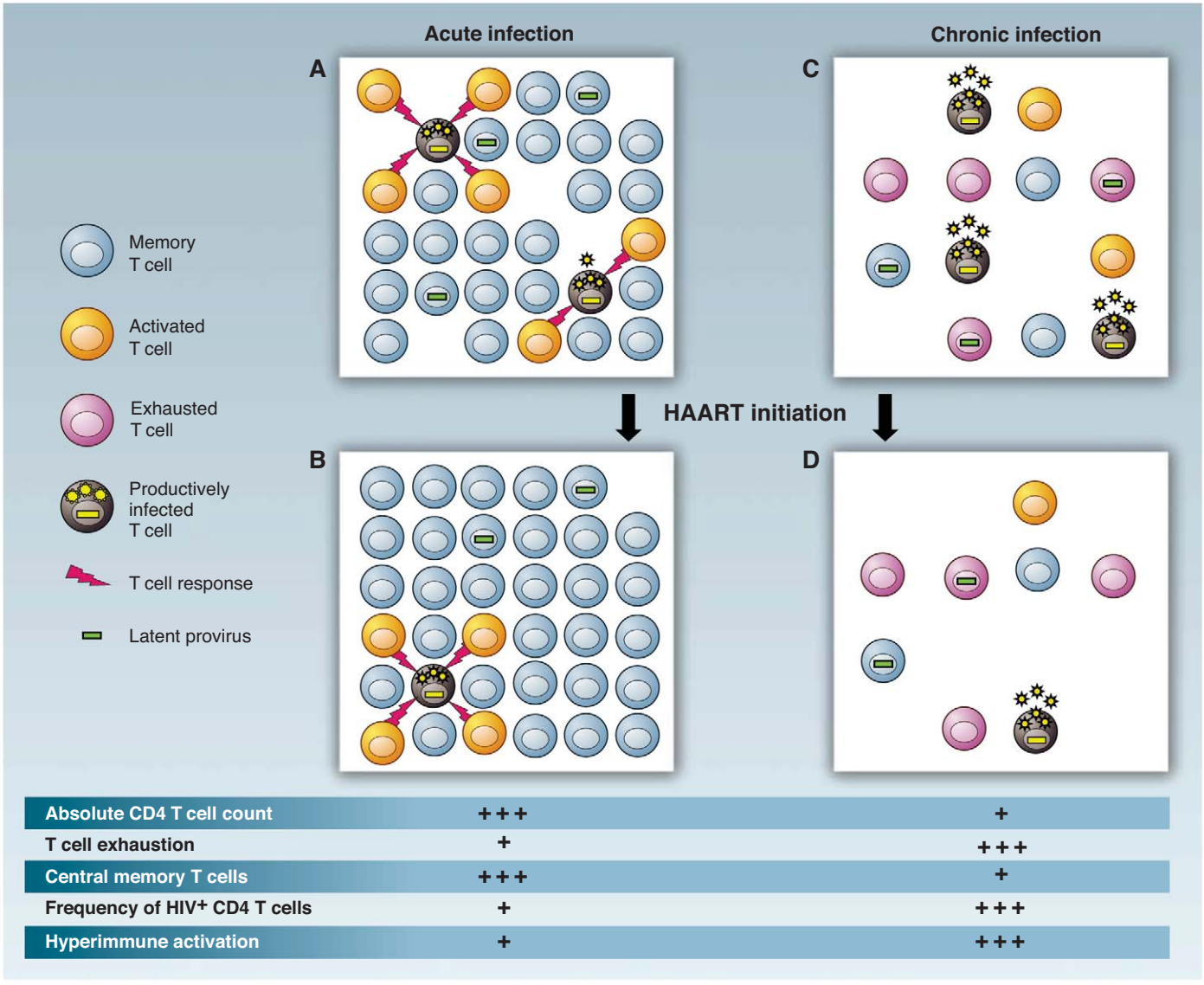

Fig. 2. HIV–T cells dynamics, on and off HAART. (**A**) During acute infection, HIV replication is partially controlled by T cell responses, and depletion of the $CD4^+$ T cell compartment is limited. Because of viral cytopathic effects or immune mediated killing, productively infected activated T cells do not generally survive for long enough to revert to a memory state. A small pool of latently infected memory $CD4^+$ T cells harboring integrated HIV DNA, however, is established. (**B**) HAART initiation during the acute phase generally results in the normalization of $CD4^+$ T cell counts and the preservation of memory T cell responses, which can subsequently contribute to the control of viral replication upon reactivation from stable reservoirs. (**C**) Chronic infection is accompanied by depletion of the $CD4^+$ compartment and exhaustion of HIV-specific T cells, leading to uncontrolled viral production. (**D**) HAART initiation during the chronic phase of the disease generally abrogates viral replication, but $CD4^+$ T cell reconstitution is limited. This is associated with hyperimmune activation of T cells of diverse specificities even in the absence of their cognate antigen. The profound depletion of memory $CD4^+$ T cells along with the exhaustion of HIV-specific $CD8^+$ T cells result in the incapacity of the immune system to control sporadic reactivation events. Although viral dissemination is limited by HAART, de novo infection can occur and may contribute to HIV persistence.

cause of low amounts of polypyrimidine tract-binding protein (PTB) (*22*) and expression of host or viral micro-RNAs (miRNAs) [reviewed in (*23*)].

Upon T cell activation, a series of events inverts this flow of repressive inputs (Fig. 1B). Degradation of IκB (inhibitor of NFκB) allows the nuclear migration and HIV promoter binding of p50-p65 heterodimer, the active form of NFκB, which stimulates HIV expression, notably through the recruitment of histone acetyltransferases (HATs) that remodel Nuc 1. Similarly, intracellular calcium fluxes activate the enzyme calcineurin, which dephosphorylates and thus induces the nuclear localization of NFAT (nuclear factor of activated T cells), another positive regulator of HIV transcription. HIV expression is also dependent on the viral Tat protein, which recruits the cellular positive transcription elongation factor b (P-TEFb) complex onto the nascent viral transcript. P-TEFb comprises cyclin T1 and cyclin-dependent kinase 9 (CDK9), which stimulates transcriptional elongation by phosphorylating the C-terminal domain (CTD) of RNA polymerase II (RNAPII). In quiescent T cells, P-TEFb is sequestered by the HEXIM-1 [hexamethylene bisacetamid (HMBA)–induced protein 1]/7SK snRNA (7SK small nuclear RNA) complex. Upon activation, P-TEFb is liberated and tethered to the HIV 5′ LTR, first by p65/NFkB and Sp1 and second by Tat bound to the 5′ end of the nascent RNA transcripts (*24*). Lastly, whereas T cells constitute the most quantitatively important HIV reservoir in HAART-treated individuals, other targets may contribute to viral persistence—for instance, brain microglial or hematopoietic stem cells, in which molecular mechanisms of viral latency are yet to be deciphered (*25*).

What Are the Shortcomings of the Immune Response?

After acute infection, the development of HIV-specific T cell responses leads to suppression of HIV replication and to a decrease in viral load, although the latter is modest, indicating that productive viral replication goes on in spite of the immune response. This sharply contrasts with the situation observed with herpes viruses, where only latently infected cells are preserved in the immediate aftermath of the acute infection. With HIV, a pool of productively infected cells is constantly replenished, and the continuous exposure to viral antigens during the chronic phase of infection leads to T and B cell exhaustion and ultimately to a broad and severe dysfunction of antigen-specific immune responses (*26*–*30*). The viral and immunological mechanisms underlying the lack of control of HIV replication are numerous and probably synergistic, including (i) the extraordinary capacity of HIV to escape immune pressure through mutations and virus-mediated down-regulation of key molecules such as major histocompatability complex class I (MHC-I) from the surface of infected cells (*26*, *27*), (ii) the depletion of $CD4^+$ T cells through direct and indirect cytopathic effects and the subsequent loss of T helper activity (*31*), (iii) defects in the priming and function of HIV-specific effector T cells, and (iv) the skewed development and maintenance of HIV-specific memory T cells (*32*). Together, these mechanisms result in an immune system unable to control HIV replication in a context of continuous and sustained hyperimmune activation attributed to high levels of viral replication and to the translocation of microbial products from the gut, an apparent consequence of the early immunological damage inflicted on this organ (*33*).

Intervention	Impact on the HIV reservoir	Impact on immune functions
HAART initiation during acute HIV infection	Limits the frequency of latently infected cells	Preserves HIV-specific T cell responses
HAART intensification	May decrease ongoing viral replication in anatomical reservoirs (but is unlikely to affect the pool of latently infected cells)	May reduce immune activation and increase absolute CD4 T cell counts in a subset of individuals
IL-7 therapy	May induce viral reactivation but also homeostatic proliferation of latently infected cells	Increases both CD4 and CD8 absolute T cell counts and improves HIV-specific responses
HDAC inhibitors and other chromatin modifiers	May reactivate HIV production thereby decreasing the pool of latently infected cells	Unknown
Therapeutic vaccination	May achieve natural control of HIV reactivation after HAART cessation	Should induce potent and long-lasting HIV-specific T cell responses

Impact has been clearly demonstrated in several studies; Limited number of observations, needs further investigation; Hypothetical impact, not yet tested/achieved

Fig. 3. Possible strategies for the long-term control of HIV infection.

The introduction of HAART had raised hope for viral eradication or at least for a natural, long-term control of HIV replication. The reproducible observation of viral rebounds during structured treatment interruptions (STI) trials, however, indicates that the immune system, even after a long "antigen-free" period, is unable to control HIV resurgence (*34*). By comparison, reactivation bouts of herpes virus infections are swiftly put to rest, probably often before they even become detectable, except in immunocompromised individuals. Immune hyperactivation and suboptimal priming of T cells during the viremic period might preclude the establishment of long-lasting memory T cells, explaining why viral rebounds during STI cannot be tamed (*32*, *35*, *36*). There could also be depletion of HIV-specific $CD4^+$ T cells early in the disease and creation of an immunological "hole," as viral antigen-mediated stimulation of these cells renders them highly susceptible to infection (*31*). Supporting both of these models, initiation of HAART shortly after the primary infection, before immune activation and exhaustion reach their maximal level, increases the breadth and the magnitude of HIV-specific memory $CD4^+$ T cells in virally suppressed participants, suggesting that early treatment could be a prerequisite to the natural control of HIV replication (*37*, *38*) (Fig. 2).

Recent observations in both humans and non-human primates indicate that long-lasting central memory $CD4^+$ T cells (T_{CM}) might play a particularly important role in the control of HIV replication. Through their expression of the chemokine receptor CCR7 and the selectin CD62L, T_{CM} preferentially home to secondary lymphoid organs and readily proliferate and differentiate into effector cells in response to antigenic stimulation (*39*). Furthermore, they are long-lived, ensuring long-term immunological memory (*40*). HIV infection is characterized by defects in the generation and maintenance of T_{CM} cells (*32*, *35*, *41*). $CD8^+$ T_{CM} have a shorter half-life and are less abundant in HIV-infected individuals than in controls (*42*). Also, the frequency of detection of both $CD4^+$ and $CD8^+$ HIV-specific T cells decreases rapidly after HAART initiation (*43*, *44*). Nevertheless, early treatment of simian immunodeficiency virus (SIV) infection is associated with a restoration of $CD4^+$ T_{CM} cells in the gut, suggesting that a fraction of T_{CM} cells generated during an acute infection could be preserved so as to constitute a functional pool when viral replication is suppressed by HAART (*45*).

Increased frequency and survival capacity of high interleukin (IL)-2–producing $CD4^+$ and $CD8^+$ T_{CM} cells were measured in elite controllers (ECs), a rare population of HIV-infected individuals who control viral replication in the absence of therapy (*46*, *47*). ECs most likely represent a

heterogeneous group, with contributions of identified host factors (e.g., HLA alleles B27 and B57) in some but not all. ECs' $CD4^+$ T_{CM} cells appear protected from viral infection, as do those from SIV-infected sooty mangabeys, a model of natural resistance to disease progression (*48*, *49*). All together, these observations indicate that both $CD4^+$ and $CD8^+$ T_{CM} cells contribute to the natural control of HIV and suggest that a drug-free control of HIV replication may be achieved by preventing the elimination of these cells through early treatment interventions and specific vaccination strategies.

Is Long-Term Drug-Free Remission Possible?

The latent reservoir is established from the earliest times of infection. Rare patients, when placed on HAART at this time, exhibit prolonged viral control after treatment interruption (*50*). This suggests that early treatment may help to preserve immune responses. Furthermore, HAART with STIs in acutely infected macaques increases SIV-specific responses, and the capacity of the immune response to temporarily control viral rebounds (*51*). Whether such an outcome is restricted to particular genetic backgrounds in humans remains to be determined (*52*).

A recent longitudinal study of the rebounding virus in patients subjected to multiple 2-week STIs revealed that its clonal origin differed between episodes. Furthermore, assembled phylogenies indicated no temporal structure between the rebounding viruses and their pretreatment counterparts, sequences obtained during different STIs clustering with different pretreatment clones (*53*). In another group of patients, the sequences of rebounding viruses were distinct from those of proviral DNAs detected in the circulating latent reservoir before HAART interruption (*54*). Most likely, only a fraction of the total pool of HIV-infected clones is represented in the blood, and T cells residing, for instance, in the gut are more susceptible to undergo antigen-induced immune activation and reignite the infectious process (*55*). HIV thus appears to reemerge from the stochastic activation of long-lived clones rather than from the expansion of viral populations replicating at low levels during treatment. Correspondingly, treatment intensification trials with new and potent antiretroviral drugs have failed to eliminate residual HIV viremia. In several instances where ultrasensitive assays capable of detecting as low as one copy of HIV per ml of plasma were used, no clear benefit of HAART intensification could be demonstrated in patients who had previously achieved undetectable (<50 copies per ml) viremia (*56*–*59*). Recently, addition of a potent integrase inhibitor to a cocktail of antiretrovirals induced a transient increase in episomal viral DNA in 30% of HAART-treated participants, a sign that this drug was curtailing some ongoing replication, yet it did not lead to any measurable change in their viral loads (*60*).

Recent efforts have therefore focused on the possibility that latent viruses could be "purged" by pharmacological manipulations. For this, whether in vitro or, for selected agents, in the setting of controlled clinical trials, HAART has been combined with interventions aimed at forcing viral expression from the latent reservoir. It was reasoned that HIV induction would expose latently infected cells to virus- and immune-mediated killing, whereas HAART would block any further viral spread. Owing to the molecular mechanisms at play in the establishment and maintenance of HIV latency, three categories of agents have been tested: T cell activators, inhibitors of histone-modifying enzymes, and inhibitors of DNA methylation (Fig. 1). Early clinical studies assessing the potential benefit of combining T cell activating agents, such as IL-2 or antibodies specific to the T cell receptor CD3 subunit (OKT3), with antiviral drugs demonstrated a transient drop in the apparent size of the viral reservoir, but patients experienced rapid plasma viral rebound upon HAART cessation (*61*). IL-7, an important controller of T cell homeostasis, can reactivate latent HIV in vitro through the induction of the Janus kinase–signal transducer and activator of transcription (JAK-STAT) signaling pathway (*62*). But IL-7 also promotes the homeostatic proliferation of HIV latently infected cells, which questions its usefulness for purging viral reservoirs (*13*). An initial report that valproic acid (VPA), an antiepileptic agent with weak histone deacetylase inhibitory activity, may decrease the size of the pool of latently infected resting $CD4^+$ T cells was not subsequently confirmed (*63*, *64*). In vitro and ex vivo analyses have further demonstrated that the transcriptional activity of latent HIV proviruses can be induced by combining various types of activators, including the NFκB-inducer prostratin, with HDAC inhibitors such as VPA or suberoylanilide hydroxamic acid, and inhibitors of DNA methylation such as 5-aza-2′-deoxycytidine (*20*, *21*, *65*).

Although these data indicate that latent HIV proviruses can be forced out of transcriptional silence, evidence that latently infected, resting $CD4^+$ T cells are destroyed upon exposure to purging agents is still lacking both in vitro and in vivo (*66*). Furthermore, many of the mechanisms involved in the establishment and maintenance of HIV latency are also responsible for keeping endogenous retroelements at bay. More than 40% of the human genome is derived from such ge-

Table 1. Some of what we want to know and should dare to ask.

1. What are the relative contributions to HIV persistence under HAART of:
   - Long-lived latently infected $CD4^+$ T cells?
   - Other latently infected cells (microglia, hematopoietic stem cells)?
   - Ongoing/residual viral replication, including in anatomical territories less accessible to antiviral drugs (e.g., the brain)?
2. Can HAART intensification completely suppress residual viral replication?
3. Is there a functionally important decay of the latent reservoir under intensified HAART?
4. Are rebounding viruses in STI:
   - Immunological escape mutants?
   - Viruses for which specific memory immune cells were previously lost?
   - Virologically and immunologically different depending on the time of HAART initiation?
5. Is early HAART initiation capable of:
   - Limiting the pool of latently infected cells?
   - Preserving immune functions?
   - Reducing damage to the GALT (gut-associated lymphoid tissue) and hence subsequent inflammation triggered by systemic leakage of microbial products?
6. Can chronic gut inflammation be curtailed in HIV-infected individuals, and does this affect viral control?
7. Are the gut microbiome and virome altered in chronic HIV infection, and can they be manipulated to minimize antigenic stimulation by intestinal microbial products?
8. Can therapeutic strategies aimed at reactivating latently infected $CD4^+$ T cells lead to a decreased HIV burden in infected individuals receiving HAART without prohibitive adverse effects (e.g., mobilization of endogenous retroelements)?
9. Is pathogenic SIV infection a reliable model to evaluate therapeutic strategies aimed at interfering with HIV persistence? What is the effect of HAART on virological and immunological parameters of (nonpathogenic) SIV infection in its natural hosts?
10. Can a combination of early HAART initiation and therapeutic vaccination lead to subsequent drug-free HIV control?

netic invaders, whether endogenous retroviruses or non-LTR retrotransposons such as LINEs (long interspersed nuclear elements) and SINEs (short interspersed nuclear elements, which include *Alu* repeats). Endogenous retroelements are formidable motors of evolution, yet their uncontrolled spread could have deleterious consequences, as demonstrated by their occasional involvement in both hereditary and acquired human diseases, including various forms of cancer. Accordingly, retroelements are tightly repressed by histone deacetylation, histone methylation, and DNA methylation. These epigenetic marks are established early in embryogenesis and are maintained throughout life (*67*). The combination of drugs aimed at purging latent HIV reservoirs will likely activate endogenous retroelements, the propagation of which will not be reliably suppressed by HAART. Thus, the potential benefit of purging latent HIV from patients otherwise stably maintained on HAART should be carefully weighed against the risk of retrotransposition-induced insertional mutagenesis.

What Can Be Done?

In sum, the prospect of achieving a sterilizing cure, where all functionally important HIV-positive cells are eliminated from an infected individual receiving HAART, is rather remote. Accordingly, we propose that an increased emphasis be placed on efforts aimed at achieving a functional cure (Fig. 3). Reaching this objective may be facilitated by the rapid initiation of potent antiretroviral drug regimens, which could minimize the size of the latent reservoir and the amount of damage inflicted on the immune system, particularly in the gut, during the early times of infection (*68*). Remarkably, natural SIV infections are characterized not by low viremia, but rather by levels of immune activation considerably reduced compared with those of pathogenic SIV and HIV infections, with preservation of mucosal immunity and absence of significant microbial translocation (*49*). Whether this parameter can be favorably manipulated in HIV-infected individuals should be assessed (Table 1). As well, we need to understand better why a viral clone that resurges from latently infected cells succeeds so reproducibly in reestablishing an infection that is within weeks uncontrollably propagated by broad viral quasi-species. What is the immunological nature of the initially rebounding virus? Is it an early viral clone, the virus-specific helper T cells of which were eliminated during the acute phase of the infection (*31*)? An escape mutant unrecognized by preexisting virus-specific antibodies and cytotoxic T cells (*69*)? Or is reemergence of latent viruses the result of exhausted HIV-specific B and T cell responses due to chronic antigenic exposure? Accordingly, does the lack of such exhaustion when HAART is instated early change the genetic, biological, and immunological profile of rebounding viruses upon subsequent treatment interruption?

Therapeutic HIV and SIV vaccination trials in humans and nonhuman primates, respectively, have so far given mixed results, with boosting of virus-specific immune responses in some cases but no clear prolonged reduction of viremia in any (*70*, *71*). However, much fewer efforts have focused on this goal than on the development of a prophylactic HIV vaccine. As the latter is now recognized as critically needing a more in-depth and scientifically sophisticated research investment (*72*), we propose that the two lines of investigation be pursued jointly. Both will benefit from an increased understanding of antiretroviral immunity, whether innate or adaptive, and will have to rely on similar experimental tools and models. Furthermore, the comparable degrees of clonality of transmitted/founder and rebounding viruses suggest that the immunological challenges posed in both situations bear some similarities, even though the founder virus is selected from a broad quasi-species present in the inoculum through the action of a naive yet intact immune system (*73*), whereas the rebounding virus faces immune responses that have been primed but also damaged by the preexisting infection. Moreover, owing to the integrative properties of HIV and its ability to enter latency, it is likely that a successful prophylactic vaccine will not be sterilizing but will rather minimize the systemic spread of the virus, the very goal of a therapeutic vaccine. Of note, testing the latter is logistically easier, because HAART interruption immediately provides the proper challenge in all enrolled individuals.

What leads could one follow for developing a therapeutic HIV vaccine? The study of ECs and nonhuman primates points to interesting avenues. Although it appears that neutralizing antibodies do not have a major role in ECs, the immunological profile of these individuals speaks for the critical influence of a strong polyfunctional $CD8^+$ T cell response to essential immunodominant epitopes, resulting in effective granzyme B-mediated killing of HIV-infected T cells (*74*). Moreover, the relative resistance of sooty mangabeys and ECs $CD4^+$ T_{CM} cells to viral infection suggests that a virus-free T_{CM} compartment may be a major correlate of protection during lentiviral infection, including for controlling reactivation from latent reservoirs. Understanding how this compartment is established and how its expansion can be stimulated may lead to the development of approaches for the long-term, drug-free control of HIV infection. Experience acquired while trying to develop an HIV vaccine, however, indicates that this will require wandering off the beaten paths (*72*). More provocatively, innate and adaptive responses do not significantly control SIV in its natural hosts, yet these animals rarely develop disease (*49*). Whether the accompanying and probably explanatory limited immune activation and preserved mucosal immunity can be obtained only at the price of a long and costly evolutionary adaptation, or whether it can be induced by external interventions, warrants investigation.

When the first signs of the AIDS disaster became apparent and a human retrovirus was discovered as its cause, few would have predicted that barely 20 years later one would be discussing how to keep HIV-infected individuals healthy without medication. The very topic of the present Review is thus a tribute to the extraordinary achievements of the past two decades. Still, the challenge ahead is tremendous and reflects the depth of our remaining ignorance on many fundamental aspects of the interactions between HIV and the human body, and as a consequence our current inability to devise rational approaches to tilt irreversibly the balance in favor of the infected host. Similar to developing an HIV vaccine, obtaining long-term drug-free remissions for HIV-infected individuals should be defined as a top strategic priority, and proper incentives and programs should be put in place to recruit the broad and multidisciplinary scientific research community that will be indispensable to succeed in this endeavor.

References and Notes

1. J. A. Esté, T. Cihlar, *Antiviral Res.* **85**, 25 (2010).
2. H. W. Virgin, E. J. Wherry, R. Ahmed, *Cell* **138**, 30 (2009).
3. S. Efstathiou, C. M. Preston, *Virus Res.* **111**, 108 (2005).
4. L. G. Guidotti, F. V. Chisari, *Annu. Rev. Pathol.* **1**, 23 (2006).
5. T. W. Chun *et al.*, *J. Clin. Investig.* **115**, 3250 (2005).
6. J. W. Mellors *et al.*, *Science* **272**, 1167 (1996).
7. E. Connick *et al.*, *J. Infect. Dis.* **184**, 1465 (2001).
8. A. S. Perelson *et al.*, *Nature* **387**, 188 (1997).
9. T. W. Chun *et al.*, *J. Infect. Dis.* **197**, 714 (2008).
10. T. W. Chun *et al.*, *Nature* **387**, 183 (1997).
11. T. W. Chun *et al.*, *Proc. Natl. Acad. Sci. U.S.A.* **95**, 8869 (1998).
12. D. Finzi *et al.*, *Science* **278**, 1295 (1997).
13. N. Chomont *et al.*, *Nat. Med.* **15**, 893 (2009).
14. L. Rong, A. S. Perelson, *J. Theor. Biol.* **260**, 308 (2009).
15. Y. Zhou, H. Zhang, J. D. Siliciano, R. F. Siliciano, *J. Virol.* **79**, 2199 (2005).
16. L. Colin, C. Van Lint, *Retrovirology* **6**, 111 (2009).
17. A. Ciuffi *et al.*, *Nat. Med.* **11**, 1287 (2005).
18. C. Van Lint, S. Emiliani, M. Ott, E. Verdin, *EMBO J.* **15**, 1112 (1996).
19. C. Marban *et al.*, *EMBO J.* **26**, 412 (2007).
20. J. Blazkova *et al.*, *PLoS Pathog.* **5**, e1000554 (2009).
21. S. E. Kauder, A. Bosque, A. Lindqvist, V. Planelles, E. Verdin, *PLoS Pathog.* **5**, e1000495 (2009).
22. K. G. Lassen, K. X. Ramyar, J. R. Bailey, Y. Zhou, R. F. Siliciano, *PLoS Pathog.* **2**, e68 (2006).
23. P. Corbeau, B. B. Finlay, *PLoS Pathog.* **4**, e1000162 (2008).
24. X. Contreras, M. Barboric, T. Lenasi, B. M. Peterlin, *PLoS Pathog.* **3**, 1459 (2007).
25. C. C. Carter *et al.*, *Nat. Med.* **16**, 446 (2010).
26. C. L. Day *et al.*, *Nature* **443**, 350 (2006).
27. L. Trautmann *et al.*, *Nat. Med.* **12**, 1198 (2006).
28. S. Moir *et al.*, *J. Exp. Med.* **205**, 1797 (2008).
29. G. Pantaleo *et al.*, *Proc. Natl. Acad. Sci. U.S.A.* **87**, 4818 (1990).
30. G. Pantaleo, S. Koenig, M. Baseler, H. C. Lane, A. S. Fauci, *J. Immunol.* **144**, 1696 (1990).
31. D. C. Douek *et al.*, *Nature* **417**, 95 (2002).
32. P. Champagne *et al.*, *Nature* **410**, 106 (2001).

33. J. M. Brenchley *et al.*, *Nat. Med.* **12**, 1365 (2006).
34. L. Zhang *et al.*, *J. Clin. Investig.* **106**, 839 (2000).
35. V. Appay *et al.*, *Nat. Med.* **8**, 379 (2002).
36. S. A. Younes *et al.*, *J. Exp. Med.* **198**, 1909 (2003).
37. T. W. Chun *et al.*, *Proc. Natl. Acad. Sci. U.S.A.* **98**, 253 (2001).
38. S. A. Younes *et al.*, *J. Immunol.* **178**, 788 (2007).
39. F. Sallusto, D. Lenig, R. Förster, M. Lipp, A. Lanzavecchia, *Nature* **401**, 708 (1999).
40. C. Riou *et al.*, *J. Exp. Med.* **204**, 79 (2007).
41. C. J. van Noesel *et al.*, *J. Clin. Investig.* **86**, 293 (1990).
42. K. Ladell *et al.*, *J. Immunol.* **180**, 7907 (2008).
43. S. A. Kalams *et al.*, *J. Virol.* **73**, 6721 (1999).
44. C. J. Pitcher *et al.*, *Nat. Med.* **5**, 518 (1999).
45. D. Verhoeven, S. Sankaran, M. Silvey, S. Dandekar, *J. Virol.* **82**, 4016 (2008).
46. F. Pereyra *et al.*, *J. Infect. Dis.* **197**, 563 (2008).
47. J. van Grevenynghe *et al.*, *Nat. Med.* **14**, 266 (2008).
48. M. Paiardini *et al.*, paper presented at 17th Conference on Retroviruses and Opportunistic Infections, San Francisco, 16 to 19 February 2010.
49. D. L. Sodora *et al.*, *Nat. Med.* **15**, 861 (2009).
50. L. Hocqueloux *et al.*, *AIDS* **24**, 1598 (2010).
51. F. Lori *et al.*, *Science* **290**, 1591 (2000).
52. C. Dalmasso *et al.*, *PLoS ONE* **3**, e3907 (2008).
53. B. Joos *et al.*, *Proc. Natl. Acad. Sci. U.S.A.* **105**, 16725 (2008).
54. T. W. Chun *et al.*, *Nat. Med.* **6**, 757 (2000).
55. A. A. Lackner, M. Mohan, R. S. Veazey, *Gastroenterology* **136**, 1965 (2009).
56. T. W. Chun *et al.*, *J. Infect. Dis.* **195**, 1762 (2007).
57. J. B. Dinoso *et al.*, *Proc. Natl. Acad. Sci. U.S.A.* **106**, 9403 (2009).
58. R. M. Gulick *et al.*, *AIDS* **21**, 813 (2007).
59. D. McMahon *et al.*, *Clin. Infect. Dis.* **50**, 912 (2010).
60. M. J. Buzón *et al.*, *Nat. Med.* **16**, 460 (2010).
61. L. Geeraert, G. Kraus, R. J. Pomerantz, *Annu. Rev. Med.* **59**, 487 (2008).
62. F. X. Wang *et al.*, *J. Clin. Investig.* **115**, 128 (2005).
63. G. Lehrman *et al.*, *Lancet* **366**, 549 (2005).
64. J. D. Siliciano *et al.*, *J. Infect. Dis.* **195**, 833 (2007).
65. S. Reuse *et al.*, *PLoS ONE* **4**, e6093 (2009).
66. N. M. Archin *et al.*, *PLoS ONE* **5**, e9390 (2010).
67. H. M. Rowe *et al.*, *Nature* **463**, 237 (2010).
68. A. T. Haase, *Nature* **464**, 217 (2010).
69. Y. Kawashima *et al.*, *Nature* **458**, 641 (2009).
70. A. J. McMichael, *Annu. Rev. Immunol.* **24**, 227 (2006).
71. E. S. Rosenberg *et al.*, *PLoS ONE* **5**, e10555 (2010).
72. H. W. Virgin, B. D. Walker, *Nature* **464**, 224 (2010).
73. J. F. Salazar-Gonzalez *et al.*, *J. Exp. Med.* **206**, 1273 (2009).
74. K. A. O'Connell, J. R. Bailey, J. N. Blankson, *Trends Pharmacol. Sci.* **30**, 631 (2009).

75. We thank Marie-Capucine Penicaud, from the International AIDS Society, for coordinating the launching of this review, and the Swiss National Science Foundation, the National Institutes of Health, the Belgian National Fund for Scientific Research, the Programme of Excellence "Cibles" of the Walloon Region, the Agence Nationale de Recherche sur le Syndrome d'Immuno-Deficience Acquis (SIDA), SIDACTION (Ensemble Contre le SIDA), AMfAR (the Foundation for AIDS Research), and other agencies and foundations supporting work in our laboratories.

10.1126/science.1191047

Firefly Synchrony: A Behavioral Strategy to Minimize Visual Clutter

Andrew Moiseff[1]* and Jonathan Copeland[2]

In synchronous flashing by fireflies (*1*, *2*), many males produce flashes simultaneously, rhythmically, and repeatedly (*3*, *4*). An entire forest can seem to flash at the same time. Hypotheses abound about possible behavioral roles and benefits that would favor the evolution of synchrony (*3*, *5*–*9*), yet no experiments have tested them.

We addressed the hypothesis that synchrony facilitates the female's ability to recognize her conspecific male's flash pattern (*5*). Female *Photinus carolinus* were placed in a virtual environment where they were presented with computer-synthesized flashes (*10*) that simulated the flash patterns of conspecific males (Fig. 1E). Eight light-emitting diodes (LEDs) represented eight separate conspecific males (i.e., virtual males). Each produced an identically patterned malelike species-specific flash pattern stimulus (Fig. 1, A to D). Unison synchrony was simulated by presenting the flash patterns with no phase delay between virtual males (Fig. 1A). Near-unison synchrony had phase delays ranging from 2 to 150 ms (Fig. 1B). The remaining stimuli were nonsynchronic, comprising phase delays from 4 to 4560 ms (Fig. 1C) and from 7 to 4900 ms (Fig. 1D).

At the beginning of each experiment, females responded to 82% (Fig. 1F) of unison synchrony stimuli (Fig. 1A), a result that did not differ significantly (Fig. 1F, paired *t* test, $P > 0.05$) from the number of responses to near-unison stimuli (Fig. 1B). Females responded to 10% and 3% (Fig. 1F) of nonsynchronous stimuli (Fig. 1, C and D). These results show that synchrony affected the responsiveness of females (Fig. 1F) and provide experimental evidence of a behavioral function for flash synchrony.

We speculate from these results about how females process temporal patterns of flashes, a physiological problem. If the female restricted her visual attention to a single virtual male, she would detect the species-specific pattern from that virtual male and respond accordingly. However, females' responses decreased when the virtual males were not well synchronized (Fig. 1F), suggesting that females were integrating flashes over a large spatial area and that the conspecific flash pattern was not recognized. An alternative could be that flashes were recognized as male *P. carolinus* but that asynchronous flashes were less attractive than synchronous flashes. Future experiments will be required to differentiate between these alternatives. However, behavioral considerations lead us to favor the pattern recognition interpretation.

Because a typical male flies as he flashes in search of a female (*11*, *12*), his flashes will appear in different locations. If a female processed only flashes from a restricted spatial area, she might miss some of the male's flashes as he changed location and fail to recognize his temporal pattern. By integrating visual information in a spatially independent manner, she would detect the conspecific temporal pattern even if the individual flashes came from different locations.

This strategy facilitates recognition of a single flying male but presents a potential problem when multiple flashing males are in a female's field of view. Under such visually cluttered conditions, a female's inability to isolate (i.e., selectively attend to) a limited field of view would make it difficult for her to recognize the pattern produced by any single male. Synchrony may be the behavioral solution to this problem by maintaining the overall fidelity of the males' species-specific patterns even when several males are flashing.

Thus, we propose that one function of synchronous flashing in *P. carolinus* is to preserve species and sexual recognition in a visually cluttered environment.

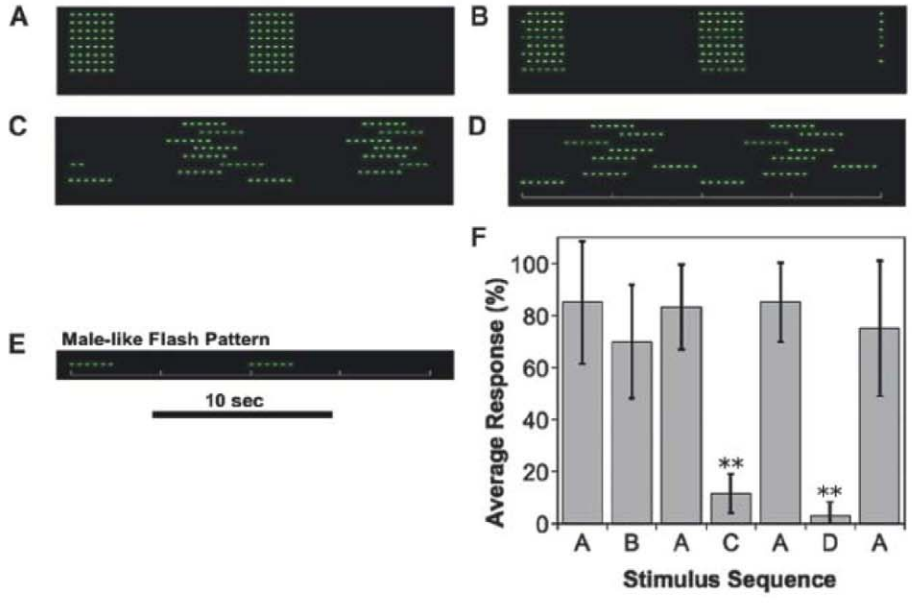

Fig. 1. Female responses to synchronous and asynchronous virtual males. (**A** to **D**) Flash patterns of eight LEDs for different stimuli. Green indicates that the LED is producing light. Each horizontal line corresponds to one LED. For all stimuli, each LED produced the same malelike pattern, but the relative phase delays between the LEDs differs. (A) Unison synchrony. No phase delays between any LEDs. (B) Near-unison synchrony. Short phase delays between LEDs. (C) Nonsynchronous stimuli with moderate variation of phase delays between the LEDs. (D) Nonsynchronous stimuli with large variation of phase delays between the LEDs. (**E**) Two phrases of the *P. carolinus* malelike flash pattern. The time calibration also applies to (A) and to (D). (**F**) Percent female response to 10 stimulus phrases for each stimulus sequence (mean ± SD; $^{**}P < 0.01$, paired *t* test, one tail). Unison synchrony was presented repeatedly as a control.

References and Notes

1. J. Buck, *Q. Rev. Biol.* **13**, 301 (1938).
2. S. Strogatz, *Sync: The Emerging Science of Spontaneous Order* (Hyperion, New York, 2003).
3. J. Buck, E. Buck, *Science* **159**, 1319 (1968).
4. J. Buck, E. Buck, J. F. Case, F. E. Hanson, *J. Comp. Physiol.* **144**, 287 (1981).
5. J. Buck, *Q. Rev. Biol.* **63**, 265 (1988).
6. M. D. Greenfield, *Annu. Rev. Ecol. Syst.* **25**, 97 (1994).
7. J. E. Lloyd, S. R. Wing, T. Hongtrakul, *Biotropica* **21**, 373 (1989).
8. E. S. Morse, *Science* **43**, 169 (1916).
9. D. Otte, *Am. Nat.* **116**, 587 (1980).
10. Materials and methods are available as supporting material on *Science* Online.
11. J. E. Lloyd, *Misc. Publ. Mus. Zool. Univ. Mich.* **130**, 1 (1966).
12. G. Adams, *Fla. Entomol.* **64**, 66 (1981).

13. Support for portions of this study were provided by the Georgia Southern University Department of Biology and the University of Connecticut Research Foundation. We thank L. Faust for assistance in the field, E. Lechowicz for technical support, and W. Chapple for commenting on the manuscript. K. Langdon and the Great Smoky Mountain National Park provided logistical support.

Supporting Online Material

www.sciencemag.org/cgi/content/full/329/5988/181/DC1
Materials and Methods

2 April 2010; accepted 19 May 2010
10.1126/science.1190421

[1]Department of Physiology and Neurobiology, University of Connecticut, Storrs, CT 06269, USA. [2]Department of Biology, Georgia Southern University, Statesboro, GA 30460, USA.

*To whom correspondence should be addressed. E-mail: Andrew.Moiseff@UConn.edu

Structure of the Human BK Channel Ca^{2+}-Activation Apparatus at 3.0 Å Resolution

Peng Yuan, Manuel D. Leonetti, Alexander R. Pico,* Yichun Hsiung, Roderick MacKinnon†

High-conductance voltage- and Ca^{2+}-activated K^+ (BK) channels encode negative feedback regulation of membrane voltage and Ca^{2+} signaling, playing a central role in numerous physiological processes. We determined the x-ray structure of the human BK Ca^{2+} gating apparatus at a resolution of 3.0 angstroms and deduced its tetrameric assembly by solving a 6 angstrom resolution structure of a Na^+-activated homolog. Two tandem C-terminal regulator of K^+ conductance (RCK) domains from each of four channel subunits form a 350-kilodalton gating ring at the intracellular membrane surface. A sequence of aspartic amino acids that is known as the Ca^{2+} bowl, and is located within the second of the tandem RCK domains, creates four Ca^{2+} binding sites on the outer perimeter of the gating ring at the "assembly interface" between RCK domains. Functionally important mutations cluster near the Ca^{2+} bowl, near the "flexible interface" between RCK domains, and on the surface of the gating ring that faces the voltage sensors. The structure suggests that the Ca^{2+} gating ring, in addition to regulating the pore directly, may also modulate the voltage sensor.

High-conductance voltage- and calcium-activated K^+ channels (BK or Slo1 channels) participate in numerous physiological processes, including neuronal excitability, smooth muscle contractility, and hair cell tuning (*1*–*6*). BK channels have an unusually high single-channel conductance, but their most important physiological property is dual regulation through membrane voltage and intracellular Ca^{2+} (*7*–*9*). Depolarization of the membrane voltage and increased intracellular Ca^{2+} levels both cause BK channels to open, which hyperpolarizes the membrane and closes voltage-dependent channels, including Ca^{2+} channels, reducing Ca^{2+} influx into the cell. Thus, BK channels are negative-feedback regulators of electrical excitation (membrane depolarization) as well as the numerous biochemical pathways that are stimulated through Ca^{2+} acting as a second messenger.

The complexity of BK channel function mirrors the complexity of its protein structure. The amino acid sequence includes the integral membrane pore shared by all K^+ channels, the integral membrane voltage sensor domains present in voltage-dependent channels, and also a cytoplasmic domain (CTD) consisting of approximately 800 amino acids per subunit, which accounts for the C-terminal two thirds of the entire channel. The CTD structure confers upon the BK channel its ability to respond to changes in intracellular Ca^{2+}. It is also the source of functional heterogeneity through alternate splicing, polymorphisms, phosphorylation, and protein interactions, which modulate BK channel activity (*10*–*12*).

The only information currently available on BK channel structure is either low resolution from cryogenic electron microscopy (cryo-EM) (*13*) or indirect through homology models. The pore and voltage sensors of the BK channel will undoubtedly resemble the corresponding regions of other voltage-dependent K^+ channels, but the CTD structure is less certain. The BK C terminus was proposed to contain two regulator of K^+ conductance (RCK) domains (*14*). RCK domains are found in certain prokaryotic K^+ channels and K^+ transport systems, but the sequence identity between BK RCK domains and prokaryotic RCK domains is so low (<20%) that homology models for the BK CTD contain a high degree of uncertainty.

Mutagenesis studies have identified the putative primary Ca^{2+} binding site within the BK CTD, which comprises a stretch of aspartic amino acids referred to as the "Ca^{2+} bowl" (*15*). Na^+-activated (Slo2) and H^+-dependent (Slo3) channels, which are homologous to the BK channel, contain a similar CTD but have different sequences of amino acids in the region corresponding to the Ca^{2+} bowl (*9*). Mutations within the Ca^{2+} bowl influence Ca^{2+} activation, whereas mutations outside, spread throughout the BK CTD primary sequence, also influence various aspects of gating. These mutational data promise rich mechanistic interpretation in the context of an atomic structure. Here, we present the structure of the human BK CTD and its quaternary organization on the cytoplasmic surface of the BK channel.

BK domain organization and structure determination. The BK channel contains four identical subunits, each comprising seven transmembrane segments and a large intracellular C terminus (Fig. 1A) (*16*). Transmembrane segments S1 to S4 form the voltage sensor; S5, S6, and the intervening amino acids form the pore and selectivity filter; and the C terminus forms the large CTD. The locations of disease-causing mutations, alternate splice sites, regulatory sites, and site-directed mutations that alter specific channel properties are highlighted (Fig. 1B). Blue and red secondary structure elements, on the basis of the x-ray structure presented here, indicate the locations of two RCK domains (RCK1 and RCK2). The Ca^{2+} bowl sequence is located within RCK2.

Residues 341 to 1056 were expressed in *Spodoptera frugiperda* (*sf* 9) insect cells and purified to homogeneity. The excluded 57 C-terminal amino acids are not essential to function (Δ58 in Fig. 2D) (*17*). Crystals belonging to space group $P6_322$ with one monomer per asymmetric unit were grown in the presence of 50 mM Ca^{2+} and diffracted x-rays to a resolution of 3.0 Å. Experimental phases to 3.3 Å were derived from a multi-wavelength anomalous diffraction experiment with a selenomethionine-containing crystal. Experimental electron density is shown (fig. S1A) alongside electron density ($2f_o$-f_c) calculated to a resolution of 3.0 Å by using the final model refined to R_{work}/R_{free} = 0.25/0.28 (fig. S1B), where R_{work} is the working R factor and R_{free} is the free R factor.

Structure of the BK CTD. The crystal structure defines two tandem RCK domains in the BK C terminus, shown in blue (RCK1) and red (RCK2) (Figs. 1B and 2A). Each RCK domain has a bi-lobed shape. The larger N-terminal lobe of each RCK domain forms a Rossmann fold, which is attached to a smaller C-terminal lobe via a helix-turn-helix connector. The tandem RCK1-RCK2 domains are folded tightly against each other, forming an interface that is reminiscent of the "flexible interface" created through the dimerization of two separate identical RCK domains in the prokaryotic MthK K^+ channel (fig. S2) (*18*). As in the MthK RCK dimer, the flexible interface is dominated by a clasping of the helix-turn-helix connectors that attach the two lobes of each RCK domain (Fig. 2, A and B). Although the overall architecture and signature features are conserved, the BK RCK domains vary in certain details from their prokaryotic counterparts; one result of the variations is a more extensive interface between RCK domains in the BK channel.

The RCK1-RCK2 interface buries 8500 $Å^2$ of solvent-accessible surface area and has a shape complementarity (SC) index of 0.68. The SC index is a geometric measure of a matched protein-protein interface (*19*). The value here is similar to that for a typical antibody-antigen interface (0.64 to 0.68) and supports the existence of a highly specific, strong interaction. This finding is compatible with experiments that show that functional channels result when two-channel fragments, separated between the RCK domains, are co-expressed in the same cell (*17*, *20*). The extensive interface between the RCK domains supports co-assembly of the individual components, which is analogous to the assembly of separate identical RCK domains in the MthK channel (*18*).

Laboratory of Molecular Neurobiology and Biophysics, Rockefeller University, Howard Hughes Medical Institute, 1230 York Avenue, New York, NY 10065, USA.

*Present address: Gladstone Institute of Cardiovascular Disease, San Francisco, CA 94158, USA.

†To whom correspondence should be addressed. E-mail: mackinn@rockefeller.edu

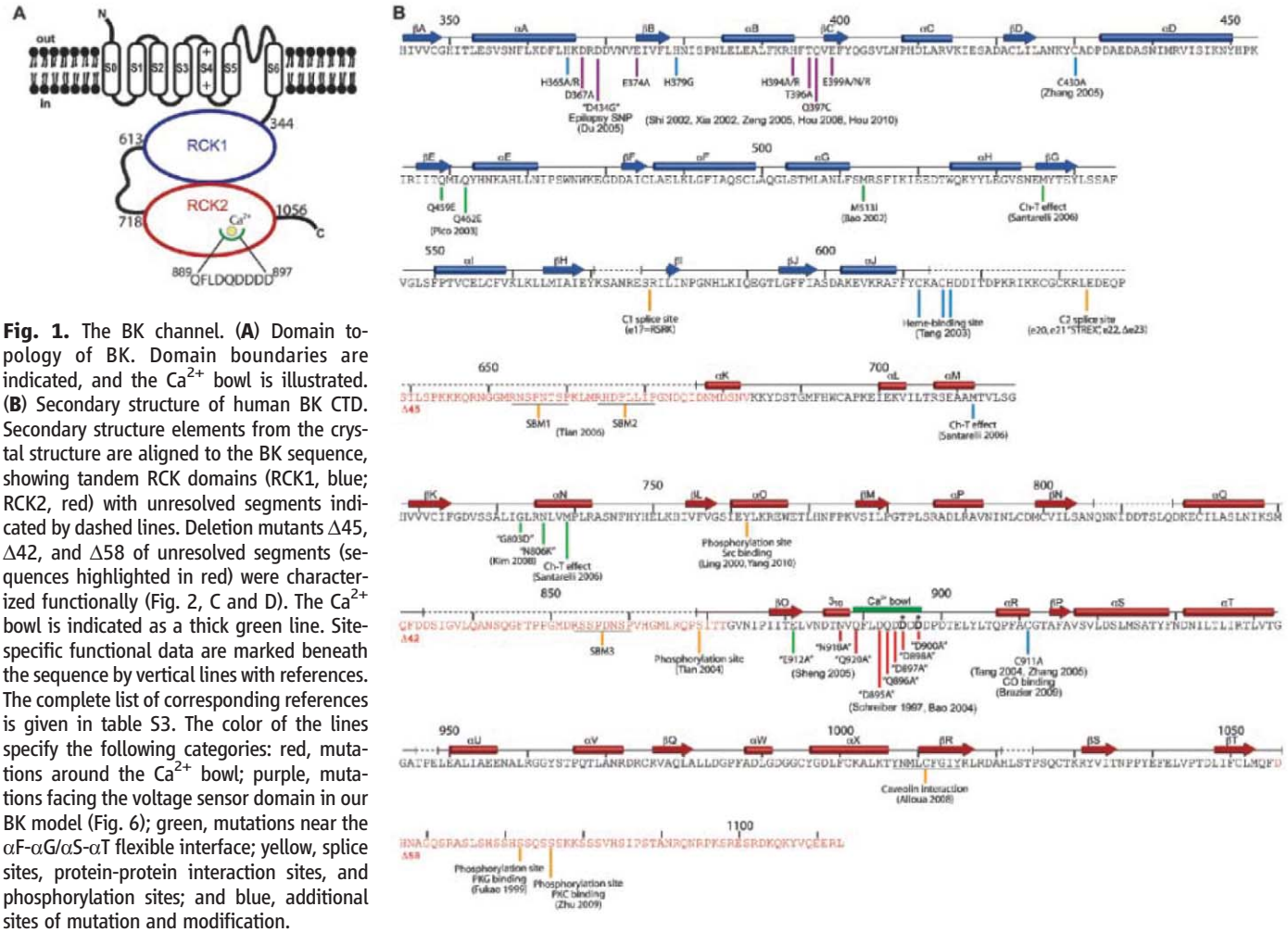

Fig. 1. The BK channel. (**A**) Domain topology of BK. Domain boundaries are indicated, and the Ca^{2+} bowl is illustrated. (**B**) Secondary structure of human BK CTD. Secondary structure elements from the crystal structure are aligned to the BK sequence, showing tandem RCK domains (RCK1, blue; RCK2, red) with unresolved segments indicated by dashed lines. Deletion mutants Δ45, Δ42, and Δ58 of unresolved segments (sequences highlighted in red) were characterized functionally (Fig. 2, C and D). The Ca^{2+} bowl is indicated as a thick green line. Site-specific functional data are marked beneath the sequence by vertical lines with references. The complete list of corresponding references is given in table S3. The color of the lines specify the following categories: red, mutations around the Ca^{2+} bowl; purple, mutations facing the voltage sensor domain in our BK model (Fig. 6); green, mutations near the αF-αG/αS-αT flexible interface; yellow, splice sites, protein-protein interaction sites, and phosphorylation sites; and blue, additional sites of mutation and modification.

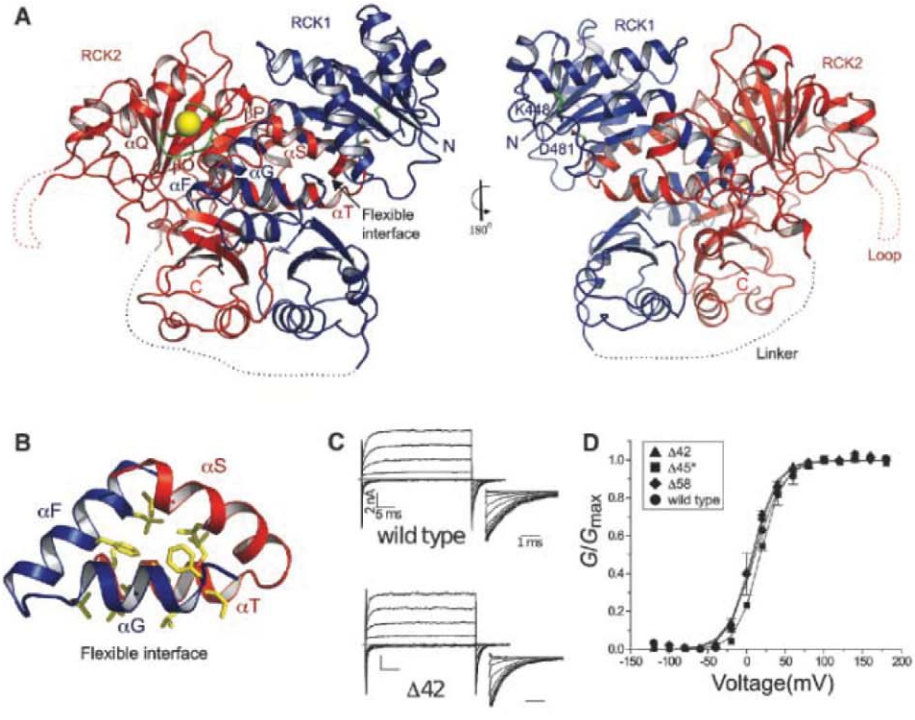

Fig. 2. Structure of the BK CTD. (**A**) Ribbon representations of front and back views of the BK CTD showing RCK1 in blue and RCK2 in red. The Ca^{2+} bowl is colored in green, and the Ca^{2+} ion is shown as a yellow sphere. Large disordered segments are indicated as dashed lines. (**B**) Close-up view of the αF-αG/αS-αT flexible interface. Side chains of hydrophobic residues in the interface are shown as sticks. (**C**) Channel activation. Currents from inside-out patches are shown for wild-type BK and Δ42 deletion mutant in the presence of 10 μM Ca^{2+}. Voltage pulses are −120 to +180 mV, $\Delta V = 20$ mV, and a holding potential of −60 mV. (**D**) Normalized *G-V* curves for wild type and deletion mutants in 10 μM Ca^{2+}. Δ45* was tested by means of co-expression of two separated channel segments instead of deletion from a single construct.

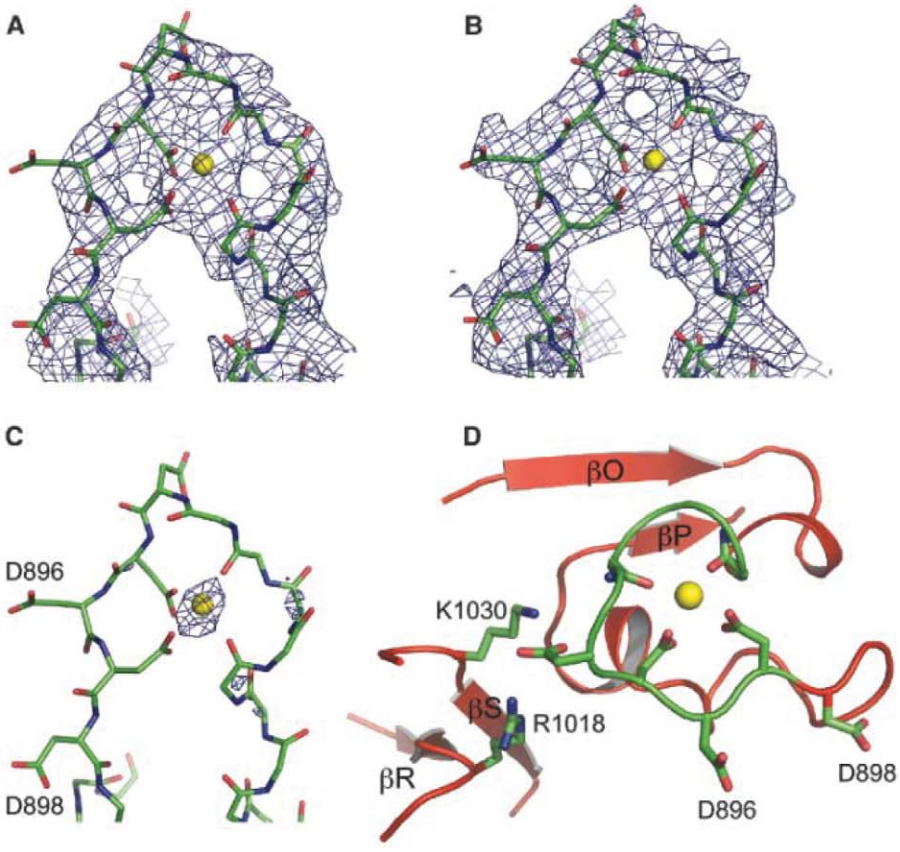

Fig. 3. The Ca^{2+} bowl. (**A**) Experimental electron density at 3.3 Å in the Ca^{2+} bowl region contoured at 1.0 σ above the mean density, where σ is the RMSD of the density. (**B** and **C**) Weighted $2f_o$-f_c electron density at 3.0 Å after refinement contoured at 1.0 σ and 4.0 σ, respectively. The final refined model is shown as sticks, with most side chains removed for clarity. (**D**) Structure of the Ca^{2+} bowl, showing key residues coordinating the Ca^{2+} ion (yellow sphere).

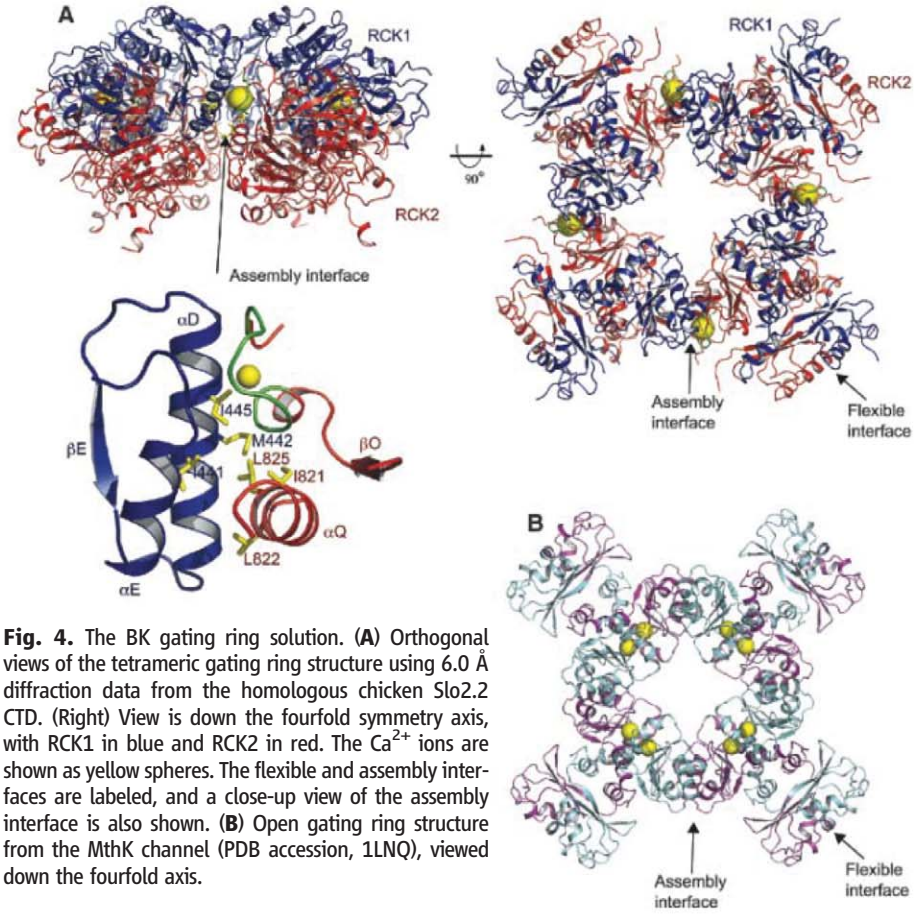

Fig. 4. The BK gating ring solution. (**A**) Orthogonal views of the tetrameric gating ring structure using 6.0 Å diffraction data from the homologous chicken Slo2.2 CTD. (Right) View is down the fourfold symmetry axis, with RCK1 in blue and RCK2 in red. The Ca^{2+} ions are shown as yellow spheres. The flexible and assembly interfaces are labeled, and a close-up view of the assembly interface is also shown. (**B**) Open gating ring structure from the MthK channel (PDB accession, 1LNQ), viewed down the fourfold axis.

Two amino acid segments are not visible in the crystal structure (Figs. 1B and 2A). The absence of electron density for the long linker connecting RCK1 to RCK2 is consistent with this region being unstructured and nonessential to function. Deletion of 45 amino acids from this loop in an experiment in which two channel fragments were co-expressed in the same cell resulted in channels with wild-type properties (Δ45* in Fig. 2D). Past studies showed that the specific amino acid sequence of this region is not important but that it has to reach at least a certain minimum length (*21*). The crystal structure explains the length requirement because the end of RCK1 is located a long distance away from the beginning of RCK2 (Fig. 2A, blue dotted linker). The second unstructured region connects αQ to βO in RCK2 (Figs. 1B and 2A). A 42 amino acid deletion of this loop yields normally functioning channels (Δ42 in Fig. 2, C and D). Although these two unstructured segments are not essential to basic channel function, they may play a role in higher-level channel regulation because both contain consensus sequences for binding SH3 domains (Fig. 1B) (*12*).

A pair of salt bridge–forming amino acids was identified in the structure of the *Escherichia coli* RCK domain (*14*). Double mutant cycle analysis of the corresponding amino acids predicted that this salt bridge is conserved in the BK channel, and this is confirmed in the structure: Amino acids K448 and D481, which are well defined in the electron density, show distances in the final model between Lys N-ζ and Asp O-δ1 and O-δ2 of 2.7 Å

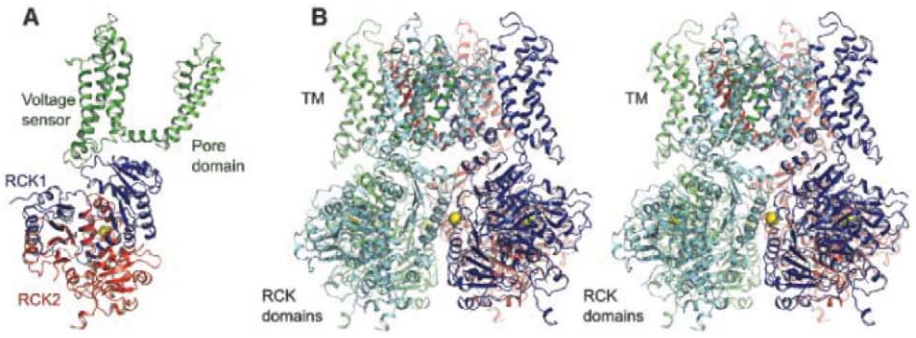

Fig. 5. A model of the BK channel. (**A**) Ribbon representation of a single subunit from the BK model generated by superimposing the BK gating ring and Kv paddle chimera (PDB accession, 2R9R) onto the MthK channel (PDB accession, 1LNQ). The transmembrane domain, RCK1, and RCK2 are colored in green, blue, and red, respectively. (**B**) Stereoview of the BK model from the side with the transmembrane domain above. Each subunit of the tetramer is colored differently.

Fig. 6. The gating ring and the voltage sensor modules. Sensitive functional mutations from the CTD (colored spheres) were mapped onto a single subunit from the BK model. Three distinct groups of mutations are distinguished by using the same colors as in Fig. 1B. The Ca^{2+} bowl mutations are colored in red. Mutations near the αF-αG/αS-αT flexible interface (backbone highlighted in red) are colored in green, and mutations in the RCK1 domain facing the voltage sensor domain are colored in purple. The voltage sensor domain is shown as a surface representation.

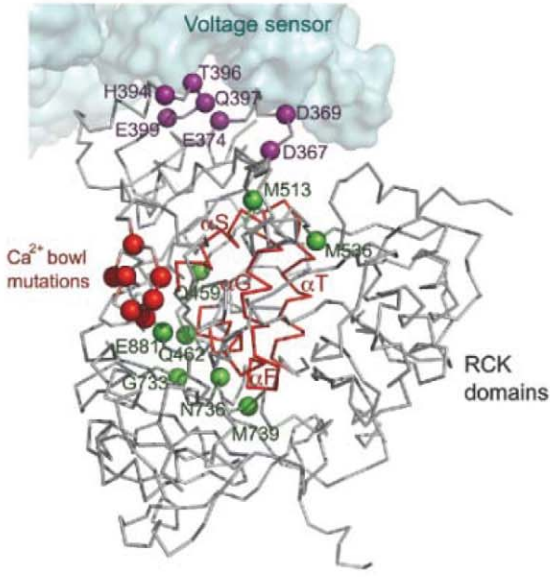

and 3.3 Å, respectively, which is compatible with a salt-bridge interaction (Fig. 2A) (*14*, *17*, *22*).

In the MthK channel, RCK dimers were proposed to undergo Ca^{2+}-induced conformational changes to open the pore (*18*, *23*). Two RCK subunits adopted distinct relative positions across the flexible interface in different crystal forms and as a function of whether or not ligand was bound (*18*, *23*, *24*). The flexible interface between two tandem RCK domains may play a similar role in Ca^{2+}-mediated gating of the BK channel.

The Ca^{2+} bowl. A major focus of research on the BK channel has been aimed at defining the region of Ca^{2+} binding (*8*). Deletions and point mutations within the Ca^{2+} bowl sequence, DQDDDDDPD, rendered the channel less sensitive to Ca^{2+} and caused a shift in the conductance-voltage (*G-V*) curve to more depolarized membrane voltages (*15*). The activation process exhibited high selectivity for Ca^{2+} over Cd^{2+}, even though the ionic radius of Cd^{2+} (0.97 Å) is only slightly smaller than that of Ca^{2+} (0.99 Å) (*15*). Other studies demonstrated a good correlation between Ca^{2+} binding to a C-terminal fragment of the channel using a radioactive Ca^{2+} assay and activation of the channel using an electrophysiological assay (*25*, *26*). Alanine-scanning mutagenesis of the Ca^{2+} bowl identified the most important amino acids for Ca^{2+} sensing to be those corresponding to D895 and D897 in the human BK channel (*26*). Because of the uncertainty and disagreement in sequence-based models of the BK channel CTD, there have been different proposals for the placement of the Ca^{2+} bowl sequence within the context of a model that is based on tandem RCK domains (*17*, *27*).

Experimental electron density for the Ca^{2+} bowl contained less detail than most of the experimental map, but the main chain was continuous, and certain side chain features emerged with cycles of model building and refinement (Fig. 3, A and B). The model was built on the basis of crystallographic data alone, independently of information from prior mutational studies. An atom that is more electron-dense than carbon, nitrogen, or oxygen accounted for the strongest electron density at the center of the structure formed by the Ca^{2+} bowl sequence (Fig. 3C). This was presumably a Ca^{2+} ion, given its presence at 50 mM concentration in the crystallization solution.

In the context of the entire CTD, the Ca^{2+} bowl is located between the last two β strands, βO and βP of the RCK2 Rossmann fold (Figs. 1B, 2A, and 3D). Thus, the Ca^{2+} bowl does not follow but rather is an integral structural element of RCK2. Atoms making direct contact with the Ca^{2+} ion include two main-chain carbonyl oxygen atoms from Q889 and D892 and oxygen atoms from the side-chain carboxylate groups of D895 and D897. In searching the protein database of known structures, we observed a similar geometry of Ca^{2+} binding in a high-resolution crystal structure of calpain, which is an intracellular cysteine protease whose activity is regulated by Ca^{2+} (fig. S3).

Because of the quality of electron density, there is some uncertainty in the conformation of the Ca^{2+} binding site in our model. However, the model is consistent with the scanning mutagenesis studies of Cox and colleagues (*26*). The two most critical residues for Ca^{2+} activation, D895 and D897, are both directly involved in the coordination of the Ca^{2+} ion in the x-ray structure (Fig. 3D). The third most effective mutation involved D894, which is not in direct contact with Ca^{2+} but forms salt bridges simultaneously with R1018 and K1030 in the C-terminal lobe of RCK2. D894 probably plays an important role in stabilizing the conformation of the Ca^{2+} bowl. The mutation D896A, on the other hand, had almost no effect on the channel's sensitivity to Ca^{2+} (*26*). In the x-ray structure, this side chain is directed out and away from the Ca^{2+} ion and does not make other protein contacts.

When the Ca^{2+} bowl is deleted, the BK channel is still activated by Ca^{2+} but with lower affinity (*15*, *28*, *29*). We have not identified a secondary Ca^{2+} binding site in this structure.

Quaternary structure formed by a CTD tetramer. The BK (Slo1) Ca^{2+}- (and voltage-) activated channel is related in sequence and structure to the Na^{+}-activated (Slo2) and H^{+}-dependent (Slo3) channels (fig. S4) (*9*). We expressed and purified the chicken Slo2.2 CTD, which included amino acids 347 to 1201. On size exclusion chromatography, the Slo2.2 CTD elutes as a tetramer, and even under the dispersive conditions of SDS–polyacrylamide gel electrophoresis (SDS-PAGE) the majority of protein migrates as a tetramer. Thus, the Slo2.2 CTD forms a very stable tetrameric complex. We crystallized this Na^{+}-activated CTD in the presence of 500 mM NaCl. The crystals diffracted x-rays to a resolution of 6 Å and were of space group I422, with one monomer (subunit) in the asymmetric unit (table S1). Using a polyalanine model of the BK CTD, we obtained a single outstanding solution in molecular replacement against the Slo2.2 diffraction data (table S2). This solution indicates that the human BK and chicken Slo2.2 CTDs must have very similar structures. By applying the crystallographic symmetry operators, we obtained the tetramer structure of the human BK CTD (Fig. 4A). This objective solution

reveals the quaternary organization of subunits but not its exact atomic details because the resolution is low and the data are from the Slo2.2 homolog.

Two main lines of evidence support the biological relevance of this tetrameric structure. First, it is immediately apparent that the ring of subunits generated by crystallographic symmetry corresponds very well to the "gating ring" observed in the MthK channel, in which RCK domains form a ring through the alternate packing of flexible and assembly interfaces (Fig. 4, A and B) (*18*). In MthK, both interfaces are formed between independent identical RCK domains (Fig. 4B). In the BK channel, the flexible interface is formed between the nonidentical tandem-linked RCK domains, whereas the assembly interface joins the tandem-linked pairs together (Figs. 2A and 4A). The second line of evidence supporting a biologically relevant structure comes from prior mutational studies on the BK channel (*17*, *30*). Pairs of amino acids were shown to interact in double mutant cycles (*30*). These amino acid pairs, including I441-L822, M442-L825, and I445-L825, are far away from each other in the monomer but are brought close together in space through creation of the assembly interface (Fig. 4A). Even though very low sequence identity exists between the MthK RCK domain and the C terminus of the eukaryotic Slo channels, the overall three-dimensional structure of the gating ring has been conserved across evolution. As is often the case, the protein originating from the "simpler" prokaryotic organism contains higher symmetry because it is constructed from a single repeated unit, in this case the RCK domain. Because the BK and Slo2.2 structures were determined in the absence of a transmembrane pore, we cannot conclude whether the conformations are "opened" or "closed." However, given that both proteins were crystallized in very high concentrations of the ions that activate them, we speculate that the gating ring shown in Fig. 4A approximates an open conformation.

A notable difference exists between the MthK and BK gating rings: The ligand Ca^{2+} is bound on the flexible interface in MthK (Fig. 4B) and on the assembly interface in BK (Fig. 4A). On the basis of the known ligand-binding properties of Rossmann folds, we should expect ligand to be bound on or near the flexible interface, where the C-terminal edges of the central β-sheets of adjacent RCK domains come close together (Fig. 2A and fig. S2, A and B). Evolution of tandem nonidentical RCK domains in the BK channel allowed the creation of a single Ca^{2+} binding site at the assembly interface. Helical elements αD and αE from RCK1 pack against αQ and the Ca^{2+} bowl from RCK2. The Ca^{2+} bowl probably evolved from a helix in RCK2 that corresponded to αE in RCK1. Thus, variation through evolution has brought about a fundamental difference between the MthK and BK gating rings. In BK, Ca^{2+} binds at the assembly interface at a site facing the outer perimeter of the gating ring (Fig. 4A).

A model for the BK channel. Guided by amino acid sequence alignments and structural components shared by the MthK channel (*18*), the paddle chimera voltage-dependent K^+ channel (*31*), and the BK gating ring, we have constructed a working structural model for the BK channel (Fig. 5 and figs. S4 and S5). The paddle chimera channel structure (residues 140 to 409) was superimposed on the MthK channel structure by aligning the main-chain atoms from the pore helix and selectivity filter (fig. S5). The pore in paddle chimera and MthK, which adopts an open conformation in both channels, superimposes with a root mean square deviation (RMSD) of 0.87 Å. The BK gating ring was then superimposed on the MthK channel by matching the secondary structural elements of the BK RCK1 domain and the MthK RCK domain. The resulting model for one subunit of the BK channel is shown with the transmembrane pore and voltage sensor in green and the gating ring in blue and red (Fig. 5A). A tetramer was generated from this model and is shown with each individual subunit in a single color (Fig. 5B). Overall, the gating ring appears to fit well against the surface of the Kv channel, with ridges from the gating ring fitting naturally into grooves that exist between the voltage sensors and the pore (Fig. 5B).

Mutations within the gating ring that affect BK channel function tend to occur in three distinct regions of the structure. One regional group surrounds the Ca^{2+} bowl (Fig. 6, red spheres) (*15*, *26*). These mutations reduce the channel's sensitivity to Ca^{2+} ions. A second group of mutations are scattered in the primary sequence but cluster together on the structure around the helix-turn-helix connector, which forms a large surface on the flexible interface (Fig. 6, green spheres) (*17*, *28*, *32*–*34*). These mutations probably affect conformational changes that occur in the gating ring associated with Ca^{2+}-induced gating. A third group of mutations cluster on the N terminus of RCK1 (Fig. 6, purple spheres) (*29*, *35*–*39*). These amino acids reside on the surface of the gating ring that faces the voltage sensor in the BK channel model.

This third group of mutations support an idea concerning dual regulation by Ca^{2+} and voltage. The pore is controlled directly by Ca^{2+} through the connection of S6 to the gating ring and directly by voltage through the S4–S5 linker and voltage sensors. But the structure and this third group of mutations raise the possibility of an additional interaction between the gating ring and the voltage sensor. One interesting experiment identified a putative Mg^{2+} binding site bridging amino acids on the gating ring to amino acids on the voltage sensor (*39*). Direct interaction between the Ca^{2+} and voltage sensory domains would enable one input stimulus to modulate the other in the dual stimulus control of BK channel gating.

References and Notes

1. R. Robitaille, M. L. Garcia, G. J. Kaczorowski, M. P. Charlton, *Neuron* **11**, 645 (1993).
2. R. Fettiplace, P. A. Fuchs, *Annu. Rev. Physiol.* **61**, 809 (1999).
3. M. T. Nelson *et al.*, *Science* **270**, 633 (1995).
4. R. Brenner *et al.*, *Nature* **407**, 870 (2000).
5. G. V. Petkov *et al.*, *J. Physiol.* **537**, 443 (2001).
6. G. J. Kaczorowski, H. G. Knaus, R. J. Leonard, O. B. McManus, M. L. Garcia, *J. Bioenerg. Biomembr.* **28**, 255 (1996).
7. K. L. Magleby, *J. Gen. Physiol.* **121**, 81 (2003).
8. R. Latorre, S. Brauchi, *Biol. Res.* **39**, 385 (2006).
9. L. Salkoff, A. Butler, G. Ferreira, C. Santi, A. Wei, *Nat. Rev. Neurosci.* **7**, 921 (2006).
10. M. J. Shipston, *Trends Cell Biol.* **11**, 353 (2001).
11. R. Schubert, M. T. Nelson, *Trends Pharmacol. Sci.* **22**, 505 (2001).
12. L. Tian *et al.*, *FASEB J.* **20**, 2588 (2006).
13. L. Wang, F. J. Sigworth, *Nature* **461**, 292 (2009).
14. Y. Jiang, A. Pico, M. Cadene, B. T. Chait, R. MacKinnon, *Neuron* **29**, 593 (2001).
15. M. Schreiber, L. Salkoff, *Biophys. J.* **73**, 1355 (1997).
16. P. Meera, M. Wallner, M. Song, L. Toro, *Proc. Natl. Acad. Sci. U.S.A.* **94**, 14066 (1997).
17. A. R. Pico, thesis, The Rockefeller University (2003).
18. Y. Jiang *et al.*, *Nature* **417**, 515 (2002).
19. M. C. Lawrence, P. M. Colman, *J. Mol. Biol.* **234**, 946 (1993).
20. A. Wei, C. Solaro, C. Lingle, L. Salkoff, *Neuron* **13**, 671 (1994).
21. J. H. Lee *et al.*, *Biophys. J.* **97**, 730 (2009).
22. In the mutants, other amino acids were substituted at certain locations; for example, R182Q indicates that arginine at position 182 was replaced by glutamine. Single-letter abbreviations for the amino acid residues are as follows: A, Ala; C, Cys; D, Asp; E, Glu; F, Phe; G, Gly; H, His; I, Ile; K, Lys; L, Leu; M, Met; N, Asn; P, Pro; Q, Gln; R, Arg; S, Ser; T, Thr; V, Val; W, Trp; and Y, Tyr.
23. S. Ye, Y. Li, L. Chen, Y. Jiang, *Cell* **126**, 1161 (2006).
24. J. Dong, N. Shi, I. Berke, L. Chen, Y. Jiang, *J. Biol. Chem.* **280**, 41716 (2005).
25. S. Bian, I. Favre, E. Moczydlowski, *Proc. Natl. Acad. Sci. U.S.A.* **98**, 4776 (2001).
26. L. Bao, C. Kaldany, E. C. Holmstrand, D. H. Cox, *J. Gen. Physiol.* **123**, 475 (2004).
27. T. Yusifov, N. Savalli, C. S. Gandhi, M. Ottolia, R. Olcese, *Proc. Natl. Acad. Sci. U.S.A.* **105**, 376 (2008).
28. L. Bao, A. M. Rapin, E. C. Holmstrand, D. H. Cox, *J. Gen. Physiol.* **120**, 173 (2002).
29. X. M. Xia, X. Zeng, C. J. Lingle, *Nature* **418**, 880 (2002).
30. H. J. Kim, H. H. Lim, S. H. Rho, S. H. Eom, C. S. Park, *J. Biol. Chem.* **281**, 38573 (2006).
31. S. B. Long, X. Tao, E. B. Campbell, R. MacKinnon, *Nature* **450**, 376 (2007).
32. L. C. Santarelli, R. Wassef, S. H. Heinemann, T. Hoshi, *J. Physiol.* **571**, 329 (2006).
33. H. J. Kim *et al.*, *Biophys. J.* **94**, 446 (2008).
34. J. Z. Sheng *et al.*, *Biophys. J.* **89**, 3079 (2005).
35. J. Shi *et al.*, *Nature* **418**, 876 (2002).
36. X. H. Zeng, X. M. Xia, C. J. Lingle, *J. Gen. Physiol.* **125**, 273 (2005).
37. W. Du *et al.*, *Nat. Genet.* **37**, 733 (2005).
38. S. Hou, R. Xu, S. H. Heinemann, T. Hoshi, *Nat. Struct. Mol. Biol.* **15**, 403 (2008).
39. H. Yang *et al.*, *Nat. Struct. Mol. Biol.* **15**, 1152 (2008).

40. We thank K. R. Rajashankar and K. Perry at beamline 24ID-C (Advanced Photon Source, Argonne National Laboratory) and the staff at beamline X29 (National Synchrotron Light Source, Brookhaven National Laboratory) for advice at the synchrotron; members of the MacKinnon laboratory for assistance; and L. Feng and M. Whorton for comments on the manuscript. R.M. is an Investigator in the Howard Hughes Medical Institute. The research is supported by the American Asthma Foundation grant 07-0127. The x-ray crystallographic coordinates and structure factors have been deposited in the Protein Data Bank (PDB) with accession code 3MT5.

Supporting Online Material

www.sciencemag.org/cgi/content/full/science.1190414/DC1
Materials and Methods
Figs. S1 to S5
Tables S1 to S3
References

2 April 2010; accepted 6 May 2010
Published online 27 May 2010;
10.1126/science.1190414
Include this information when citing this paper.

Capture of the Sun's Oort Cloud from Stars in Its Birth Cluster

Harold F. Levison,[1]* Martin J. Duncan,[2] Ramon Brasser,[3] David E. Kaufmann[1]

Oort cloud comets are currently believed to have formed in the Sun's protoplanetary disk and to have been ejected to large heliocentric orbits by the giant planets. Detailed models of this process fail to reproduce all of the available observational constraints, however. In particular, the Oort cloud appears to be substantially more populous than the models predict. Here we present numerical simulations that show that the Sun captured comets from other stars while it was in its birth cluster. Our results imply that a substantial fraction of the Oort cloud comets, perhaps exceeding 90%, are from the protoplanetary disks of other stars.

The solar system is surrounded by a huge cloud of comets, known as the Oort cloud, which extends nearly halfway to the nearest star, or ~10^5 astronomical units (AU). It is believed that objects currently in the Oort cloud either accreted among, or slightly beyond, the giant planets (*1*–*4*). According to these models, as the planets formed and evolved, some of the icy objects from which they were made were scattered outward, entering the so-called scattered disk. During this time, these objects had perihelia in the planetary region and semimajor axes that slowly diffused outward as a result of the gravitational effects of the planets (*1*). Most of these objects were eventually ejected to interstellar space. However, a few entered a region in which they were gravitationally affected by the solar system's interstellar environment (*5*) (at heliocentric distances of >~10,000 AU) while they were still bound to the Sun. These objects had their perihelia lifted from the planetary region by interstellar tides, thereby forming the Oort cloud.

Unfortunately, detailed modeling of this process fails to reproduce all of the available observational constraints. Of particular note is a problem concerning the relationship between the scattered disk and the Oort cloud. The Oort cloud currently contains at least ~4×10^{11} objects with radii (r) greater than 1 km (*6*). Models of Oort cloud and scattered disk formation predict that the ratio between the number of comets in the scattered disk and that in the Oort cloud should be ~0.1 (*2*). This implies a population of at least 4×10^{10} objects with $r > 1$ km in the scattered disk. However, the observations suggest that this number is ~6×10^8 [see supporting online material (SOM) text 1]—a discrepancy of roughly a factor of 70! Although there may be other solutions, we feel that the simplest interpretation of this result is that the Oort cloud has at least an order of magnitude more comets than existing theories would predict.

Although it is possible that future models and/or observations may solve this discrepancy, it has motivated us to explore a potential independent solution: that Oort cloud comets formed around other stars and were gravitationally captured by the Sun when it was still in its birth cluster. This idea was first suggested 20 years ago (*7*) but was abandoned because previous work (*7*, *8*) calculated a capture efficiency that was too low to be consistent with observations. However, the calculations in those papers were crude by modern standards, and their authors were forced to make several simplifying assumptions that probably affected their results. Thus, we revisited this idea.

Our simulations consisted of integrating the orbits of a large number of comets and stars embedded in a spherically symmetric distribution of gas (see SOM text 2 for more detail). The star cluster itself was constructed using the methods in (*9*). In particular, we distributed stars in a spherical volume of radius R_c, so that their number density scaled as r^{-1}. Most clusters had R_c's in the range of 0.3 to 1 pc, or 6×10^4 to 2×10^5 AU (*10*). Based on observations, (*9*) argues that $N \sim 300\left(\frac{R_c}{1\ \mathrm{pc}}\right)^2$, where N is the total number of stars in the cluster. We adopted this relationship here. Thus, $30 < N < 300$ (*11*). The gas was modeled as a gravitational potential that remained fixed for the first 3 million years (My) and then was quickly removed over a period of 10^4 years, causing the cluster to quickly dissolve. Initially, the total mass of gas within R_c was taken to be $[1/(\varepsilon)] - 1$ of the total mass of stars, where ε is the star formation efficiency. The value of ε ranged from ~0.1 to ~0.3 (*10*). Around each star, we constructed a scattered disk consisting of approximately 100 comets (*12*, *13*). Initially, the comets had perihelion distances (q) of 30 AU and semimajor axes (a) uniformly spread from 1000 to 5000 AU. The orientation of each disk was chosen at random.

We integrated each system until the median spacing between stars was 5×10^5 AU, or roughly 10 times the size of the Oort cloud and roughly the spacing of stars in the solar neighborhood. The integration time ranged from 10 to 50 My, depending on the cluster characteristics. However, in all of our simulations, the stars remained in a dense configuration for only 3 My, at which point we removed the gas. After that, the cluster quickly dispersed (movie S1). The extra time was required to allow the Oort clouds of singleton stars (*14*) to become well separated. In all, we performed 26 simulations (table S1).

We determined how many comets that formed in the protoplanetary disk of one star ended up in Oort cloud–like orbits [a < 50,000 AU (*15*)] around a different star, scaled by the amount of material in a typical protoplanetary disk (Fig. 1 (*13*) (see SOM text 4 for a discussion of the role of binary stars). Unsurprisingly, the fraction of the number of comets (f_c) per star, which we call one scattered disk (OSD), varied from cluster to cluster and from star to star within a cluster. Although typically a few tens of percent of singleton stars captured no new comets during our simulations, we found that the capture efficiency could be substantial. Indeed, the maximum value we saw was 0.26 OSD (red curve in Fig. 1A).

The comets were mainly captured through two mechanisms. The first, which we call random capture, relies on the fact that before the clusters dispersed, they had half-mass radii that ranged from 36,000 to 80,000 AU and thus were comparable to the size of the Oort cloud. As the stars orbited in these clusters, most of their comets were stripped away by close stellar encounters. These comets then orbited freely within the cluster (Fig. 2). Thus, when the cluster dispersed, most of the stars had a large population of comets that were sufficiently close to be potential Oort cloud members. In the example shown in Fig. 2, although at the end of the simulation the comets marked in blue are found in the Oort cloud of the star marked in red, these comets are spread throughout the cluster at the dispersal time. There are many other stars closer to these comets than the comets are to their future partner. They became captured because they, by chance, had velocities similar to that of the star. Thus, as the cluster expanded, these comets headed in the same direction as the star and became bound to it (*16*) (movie S2).

This process is aided by the cluster expansion itself (Fig. 3). After the gas was removed at 3 My, the cluster expanded (Fig. 3A and movie S2). However, because there was still a substantial amount of mass in the cluster due to the stars, the kinetic energy dropped in order to conserve energy. There is a monotonic drop in the curve in Fig. 3B between 3 and 3.5 My. (The large

[1]Southwest Research Institute, 1050 Walnut Street, Suite 300, Boulder, CO 80302, USA. [2]Department of Physics, Queen's University, Kingston, Ontario K7L 3N6, Canada. [3]Departement Cassiopé, University of Nice–Sophia Antipolis, CNRS, Observatoire de la Côte d'Azur, Nice, France.

*To whom correspondence should be addressed. E-mail: hal@boulder.swri.edu

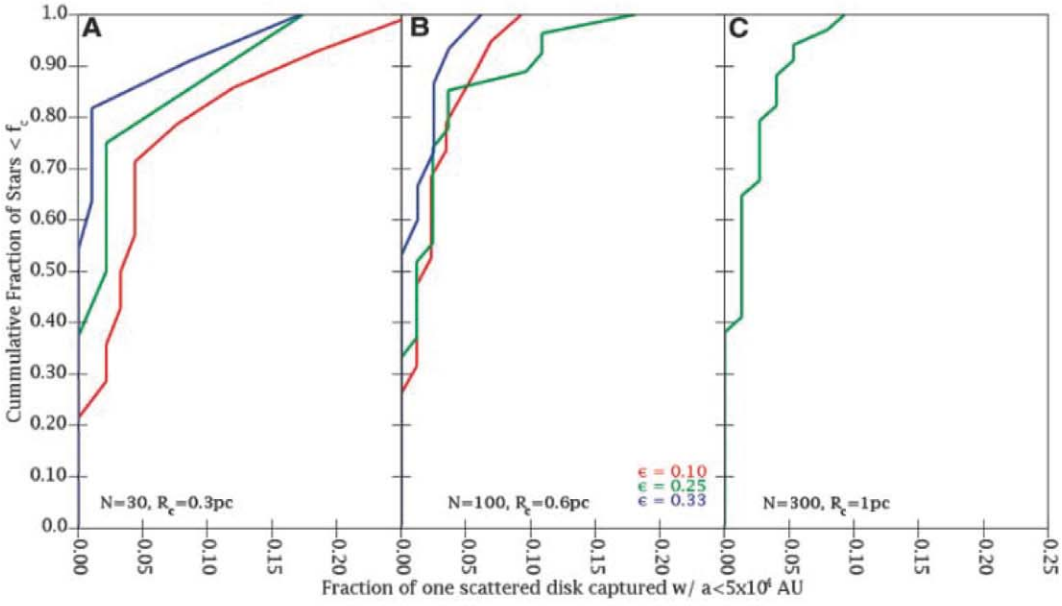

Fig. 1. (**A** to **C**) Cumulative distribution of capture efficiency, f_c, around Sun-like stars as a fraction of the original scattered disk. Each curve represents a different simulation or combination of simulations with the same cluster parameters: N, R_c, and ε. Color denotes different values of ε; different panels show runs with different N-R_c combinations. The orbital element distribution of the captured comets is shown in fig. S1. We plot this value only for stars that (i) have masses between 0.5 and 2 $M_\odot$ and (ii) were singleton stars at the end of the simulation. Each curve is for a different combination of cluster parameters. We combined the results of three separate simulations in each of the N = 30 and N = 100 cases in order to improve our statistics.

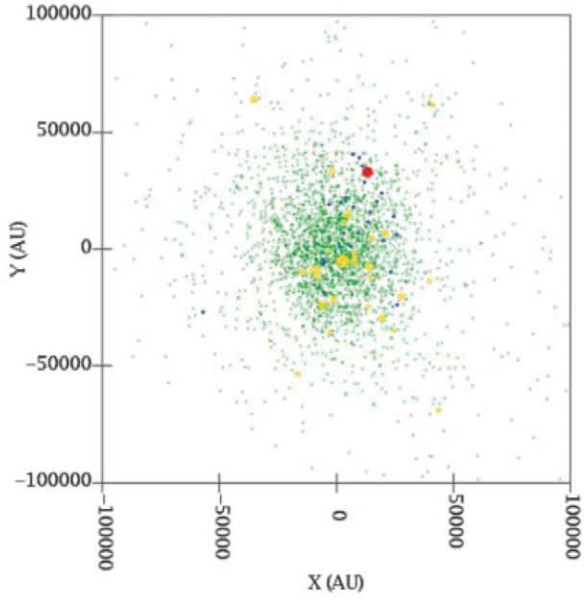

Fig. 2. A snapshot of the structure of a cluster with N = 30, R_c = 0.3 pc, and ε = 0.25 at 3 My just before it dispersed. The large yellow and red dots are the stars, and the smaller green and blue dots are the comets. The size of a star's symbol scales as the cube root of its mass.

variations before the gas was removed are due to close stellar encounters.) It is during this drop in kinetic energy, and therefore in relative velocities, that the Oort clouds formed (Fig. 3C). When the cluster started to expand, the relative velocities between the comets and their new host stars were too large for most comets to be bound. However, during expansion, the stars in the cluster had to climb out of their mutual gravitational potential, and thus the relative velocities between objects decreased. This led to comet capture and Oort cloud formation. For the cluster in Fig. 3, only 18% of the comets that eventually become Oort cloud members are bound at 3 My. Another 71% become bound between 3 and 3.5 My.

The direct exchange of comets between two stars involved in a close encounter is the second important process of Oort cloud formation that we observed in our simulations (*17*). In an example of such an encounter (Fig. 4), 19% of the comets that were initially in the scattered disk of a 0.32–solar mass ($M_\odot$) star were transferred to orbits about a 1-$M_\odot$ star with semimajor axes less than 50,000 AU. The smallest semimajor axis was 1100 AU. These comets remained in orbit around their new host until the end of the simulation. The closest approach distance between the two stars during the encounter was 1000 AU. There are only a few examples of direct exchange in our simulations. However, although rare, when it did occur the yield was substantial.

We now turn to the topic of whether our mechanism can solve the problem that the standard model has in explaining the large population of the Oort cloud. As discussed above, f_c can be as large as 0.26 OSD. The issue now becomes what value we should use for OSD. Because most of the captured comets spent time free-floating in the cluster environment, this value should include not only scattered disk objects but objects that were directly ejected from the protoplanetary disk to intracluster space by the giant planets during the first 3 My (*18*). This depends on three factors: (i) the mass of a typical protoplanetary disk, (ii) the masses and orbits of the giant planets in a typical planetary system, and (iii) the average mass of a planetesimal (a comet) in the giant planet regions of planetary systems. Unfortunately, these parameters are not well known.

Although far from ideal because we have no way of knowing whether it is a typical planetary system, we are forced to look at the solar system for guidance. Jupiter and Saturn are the only planets that could have delivered material to either the scattered disk or to intracluster space while the Sun was still in its birth cluster (*2*). Planet formation models require roughly 200 $M_\odot$ of solids in the Jupiter-Saturn zone in order to form the cores of the gas giants before the solar nebula dispersed (*19*). Assuming that roughly 50% of this material was incorporated into planets (*19*) and that the objects being scattered outward by Jupiter and Saturn had the same mass as a typical comet, 4×10^{16} g (*20*, *21*), we find that OSD would contain 2×10^{13} comets. If this is typical of other planetary systems as well, we might expect the Oort cloud to contain $2 \times 10^{13}\ f_c$ comets. As we described above, it is actually made up of $\sim 4 \times 10^{11}$ comets. Thus, we need $f_c \approx 0.03$ OSD to explain the Oort cloud with this mechanism. This value of f_c is clearly within reach of our models (Fig. 1). If we were naïvely to take the above numbers at face value and combine them with comets originally from the Saturn-Neptune zone that populated the Oort cloud after the cluster has dispersed, plus those comets retained by their parent stars in our

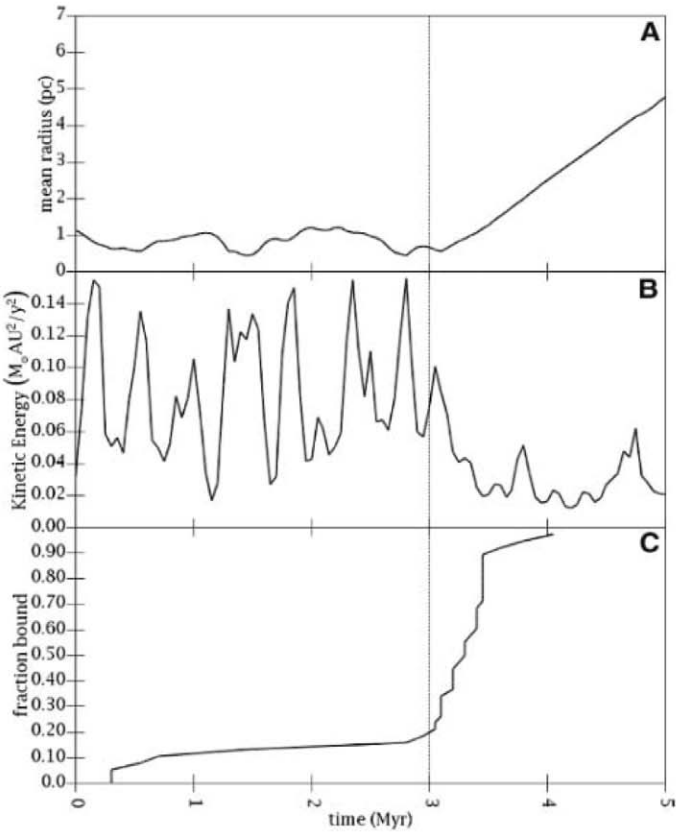

Fig. 3. (**A**) The mass-weighted mean radius of stars that eventually become singletons from the cluster shown in Fig. 2 as a function of time. This value oscillates near its original value until the gas is removed at 3 My (shown as a vertical dotted line). After this time, the cluster expands. (**B**) Sum of the kinetic energy of the stars that eventually become singletons. (**C**) A cumulative plot of the time at which comets become trapped in orbit about their new host stars. Only those comets that exchanged stars are included. In addition, we only considered new hosts that are singletons at the end of the simulation.

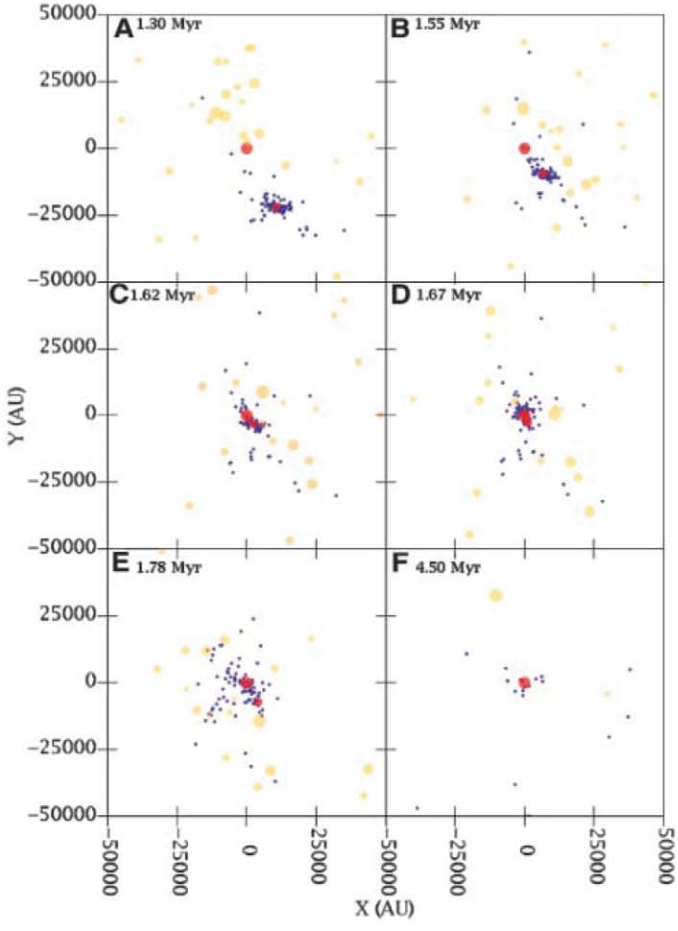

Fig. 4. (**A** to **F**) Snapshots of an encounter that leads to the direct transfer of comets from the scattered disk of one star (star A) to the Oort cloud of another (star B). These frames are centered on star B. The two stars involved in the encounter are shown in red, and background stars are yellow. The size of a star's symbol scales as the cube root of its mass. The blue dots show the location of all the comets that were initially in the scattered disk of star A (see movie S3).

simulations (*22*), we would find that between one-third and two-thirds of the Oort cloud had an extrasolar origin. Therefore, although we cannot make a solid conclusion because of the uncertainties described above, it seems likely that a substantial fraction of the Oort cloud is composed of objects that formed in the protoplanetary disks of other stars (*23*).

Given the difficulties in estimating OSD, we believe that it is more accurate to make use of the standard formation model's prediction of the ratio of the Oort cloud to the scattered disk (*2*), coupled with the observed population of the scattered disk (SOM text 1), to estimate the indigenous population of the Oort cloud. This calculation gives a population of ~6×10^9 comets. Observations suggest that the Oort cloud currently contains 4×10^{11} comets (*6*). Thus, because we know of no other mechanism that can compensate for this discrepancy, it is likely that over 90% of the observed Oort cloud comets have an extrasolar origin.

References and Notes

1. M. Duncan, T. Quinn, S. Tremaine, *Astron. J.* **94**, 1330 (1987).
2. L. Dones, P. R. Weissman, H. F. Levison, M. J. Duncan, in *Comets II*, M. C. Featou, K. U. Keller, H. A. Weaver, Eds. (Univ. of Arizona Press, Tucson, AZ, 2004), p. 153.
3. T. Paulech, M. Jakubík, L. Neslusan, P. A. Dybczyński, G. Leto, *Astron. Astrophys.* **509**, A260000 (2010).
4. This basic picture does not change if we invoke a model in which the planets migrate substantially (*24–26*).
5. The Sun was embedded in a star cluster for the first few million years of its existence. During this time, the gravitational potential of this cluster was the dominant perturber. After the Sun left the cluster, the Galaxy as a whole became the most important perturber.
6. The total number of objects in the Oort cloud, which is calculated by comparing the observed flux of new long-period comets to the rate at which Galactic tides feed Oort cloud comets into the inner solar system, has been estimated to lie between 2×10^{11} (*27*) and 2×10^{12} (*20*) comets. Historically, it was assumed that long-period comets came only from the region with $a >$ ~10,000 AU, called the outer Oort cloud. Oort cloud formation models predict that the total population of the Oort cloud is between ~2 (*2*) and ~5 (*1*) times larger than that in the outer cloud, which gives a total Oort cloud population of between 4×10^{11} and 5×10^{12}. However, (*28*) has recently shown that at least some of the long-period comets originate in the inner parts of the Oort cloud and puts an upper limit on the inner cloud of 10^{12} comets. In order to be conservative, we take the smallest of the above values: 4×10^{11}.
7. J.-Q. Zheng, M. J. Valtonen, L. Valtaoja, *Celest. Mech. Dyn. Astron.* **49**, 265 (1990).
8. S. Eggers, H. U. Keller, P. Kroupa, W. J. Markiewicz, *Planet. Space Sci.* **45**, 1099 (1997).
9. F. C. Adams, E. M. Proszkow, M. Fatuzzo, P. C. Myers, *Astrophys. J.* **641**, 504 (2006).
10. C. J. Lada, E. A. Lada, *Annu. Rev. Astron. Astrophys.* **41**, 57 (2003).
11. As suggested by figure 2 of (*9*).
12. This was varied from run to run in order to optimize processing time.
13. We have placed the same number of comets around each star, independent of its mass. We took this simple approach because too little is known about other planetary systems to make a more physically based assumption. See SOM text 3 for a discussion and for results where we have relaxed our assumption.
14. Here we define a singleton as a star that is not gravitationally bound to either another star or to the cluster as a whole. The Sun is a singleton.

15. The Oort cloud has been evolving and losing objects over the lifetime of the solar system. Thus, although the Oort cloud extends to $a > \sim 10^5$ AU, we only included comets with $a < 50{,}000$ AU in our analysis in order to avoid the need to account for this loss. We chose 50,000 AU because this is the largest semimajor axis for which survival for 4 billion years is likely (*2*).
16. As we were preparing this manuscript, we became aware of (*29*), who independently found that this mechanism can be responsible for the formation of wide binary star systems.
17. An encounter between the Sun and another star has been invoked before (*30*, *31*) to explain the origin of Sedna, which has an unusual orbit with a semimajor axis of 526 AU and a perihelion distance well beyond the orbits of the planets at 76 AU. See (*32*) for a detailed early study of this type of encounter.
18. In the real system, there are two dynamical mechanisms for stripping comets away from their original parent stars. The first involves close encounters between the stars. This effect is included in our calculations. The second is caused by close encounters between the comets and the planets in orbit around the parent stars. For computational reasons, this effect was not directly included in these calculations. However, because most comets are stripped by the first process in our simulations, the lack of the second is not significant from the dynamical point of view.
19. H. F. Levison, E. W. Thommes, M. J. Duncan, *Astron. J.* **139**, 1297 (2010).
20. P. R. Weissman, in *Completing the Inventory of the Solar System: A Symposium Held in Conjunction with the 106th Annual Meeting of the ASP*, T. Rettig, J. M. Hahn, Eds., vol. 107 of the Astronomical Society of the Pacific Conference Series (Astronomical Society of the Pacific, San Francisco, 1996), pp. 265–288.
21. The uncertainty in this value is over an order of magnitude. Here, we are simply using the classic value from (*20*).
22. This estimate assumes that the Saturn-Neptune region originally contained 35 $M_\odot$ (*26*) and that the average mass of a comet is 4×10^{16} g (*20*), which is very uncertain (*21*). Thus, it considers all possible sources for Oort cloud comets.
23. It is interesting to speculate whether we would expect to see substantial compositional differences between comets due to our results. These stars formed in the same cluster as the Sun, and thus all the comets formed basically from the same cloud of material. Thus, it is not obvious what to expect.
24. R. Malhotra, *Astron. J.* **110**, 420 (1995).
25. E. W. Thommes, M. J. Duncan, H. F. Levison, *Nature* **402**, 635 (1999).
26. K. Tsiganis, R. Gomes, A. Morbidelli, H. F. Levison, *Nature* **435**, 459 (2005).
27. P. J. Francis, *Astrophys. J.* **635**, 1348 (2005).
28. N. A. Kaib, T. Quinn, *Science* **325**, 1234 (2009).
29. M. B. N. Kouwenhoven *et al.*, *Mon. Not. R. Astron. Soc.* **404**, 1835 (2010).
30. A. Morbidelli, H. F. Levison, *Astron. J.* **128**, 2564 (2004).
31. S. J. Kenyon, B. C. Bromley, *Nature* **432**, 598 (2004).
32. C. J. Clarke, J. E. Pringle, *Mon. Not. R. Astron. Soc.* **261**, 190 (1993).
33. We thank A. Morbidelli and L. Dones for useful discussions. This work was supported by NASA's Astrobiology Institute through a grant to the Goddard Center for Astrobiology. H.F.L. is grateful to NASA for funding through its Operational Support Services and Outer Planets Research programs. M.J.D. is grateful for the hospitality and financial support of the Isaac Newton Institute at Cambridge University, where some of this work was performed. M.J.D. acknowledges the continuing financial support of the Natural Sciences and Engineering Research Council, Canada. R.B. thanks Germany's Helmholz Alliance for financial support.

Supporting Online Material

www.sciencemag.org/cgi/content/full/science.1187535/DC1
SOM Text
Figs. S1 to S3
Table S1
References
Movies S1 to S3

26 January 2010; accepted 24 May 2010
Published online 10 June 2010;
10.1126/science.1187535
Include this information when citing this paper.

Mesoscopic Percolating Resistance Network in a Strained Manganite Thin Film

Keji Lai,[1]* Masao Nakamura,[2]* Worasom Kundhikanjana,[1] Masashi Kawasaki,[2,3] Yoshinori Tokura,[2,4] Michael A. Kelly,[1] Zhi-Xun Shen[1]†

Many unusual behaviors in complex oxides are deeply associated with the spontaneous emergence of microscopic phase separation. Depending on the underlying mechanism, the competing phases can form ordered or random patterns at vastly different length scales. By using a microwave impedance microscope, we observed an orientation-ordered percolating network in strained $Nd_{1/2}Sr_{1/2}MnO_3$ thin films with a large period of 100 nanometers. The filamentary metallic domains align preferentially along certain crystal axes of the substrate, suggesting the anisotropic elastic strain as the key interaction in this system. The local impedance maps provide microscopic electrical information of the hysteretic behavior in strained thin film manganites, suggesting close connection between the glassy order and the colossal magnetoresistance effects at low temperatures.

Doped cuprate superconductors and colossal magnetoresistive (CMR) manganites, the two most studied complex oxides, exhibit rich phase diagrams as a result of the simultaneously active charge, spin, orbital, and lattice degrees of freedom (*1*, *2*). Recent work on these strongly correlated materials has shown that multiple states can coexist near certain phase boundaries, a scenario known as microscopic phase separation (*1*). The configurations of these spatially inhomogeneous phases reflect the underlying interactions. When the long-range Coulomb interaction prevails, the competing phases usually form nanometer-scale orders because of the electrostatic energy penalty for macroscopic phase separation (*3*–*6*). For self-organized patterns at larger length scales, weaker long-range interactions, such as the elastic strain arising from either the cooperative lattice distortions or lattice mismatch between substrates and epitaxial thin films, become the dominant factors (*7*–*9*). Lastly, the unavoidable quenched disorders in real materials always introduce short-range potential fluctuations, which usually smear out the orders or even result in micrometer-sized clusters with random shapes (*10*).

Many physical properties affected by the phase separation, such as the local density of states (*4*–*6*, *11*, *12*), the local magnetization (*13*–*15*), and the atomic displacement (*16*), can be spatially mapped out by established microscopy tools. For CMR manganites with drastic resistance changes at different temperatures (T) and magnetic fields (H), the local resistivity (ρ) has a large span that makes spatially resolved direct current (DC) measurements challenging. Imaging with high-frequency alternating current (AC)–coupled local probes is thus desirable. We carried out a microwave impedance microscopy (MIM) study (*17*, *18*) on manganite thin films. Unlike other GHz microscopes (*19*), the cantilever probe is well shielded to reduce the stray fields (*18*). In the microwave electronics, the high-Q resonator (*20*) susceptible to environmental conditions is eliminated so that the system can be implemented under variable temperatures (2 to 300 K) and high magnetic fields (9 T). Our cryogenic MIM (*21*) (fig. S1) is therefore a versatile tool to investigate various electronic phase transitions. Only the imaginary part of the tip-sample impedance (*21*) (fig. S2) is presented here because the local resistivity information is fully captured by the capacitive channel (MIM-C).

We studied $Nd_{1/2}Sr_{1/2}MnO_3$ (NSMO) thin films grown on (110) $SrTiO_3$ (STO) substrates by pulsed-laser deposition. In single-crystal NSMO, both resistivity and magnetization measurements show a paramagnetic (PM) to ferromagnetic (FM) transition at the Curie temperature $T_C \sim 250$ K and a charge/orbital-order (COO) transition at $T_{COO} \sim 160$ K (*22*). When a magnetic field is turned on at temperatures below T_{COO}, a dramatic first-order

[1]Geballe Laboratory for Advanced Materials, Department of Physics and Department of Applied Physics, Stanford University, CA 94305, USA. [2]Cross-Correlated Materials Group (CMRG) and Correlated Electron Research Group (CERG), RIKEN, Advanced Science Institute (ASI), Wako 351-0198, Japan. [3]WPI–Advanced Institute for Materials Research (AIMR), Tohoku University, Sendai 980-8577, Japan. [4]Department of Applied Physics, University of Tokyo, Tokyo 113-8586, Japan.

*These authors contributed equally to this work.
†To whom correspondence should be addressed. E-mail: zxshen@stanford.edu

phase transition from the antiferromagnetic COO insulating (COO-I) state to the FM metallic (FM-M) state is observed. We emphasize that two types of CMR, the *T*-driven PM-FM CMR and the low-*T* *H*-driven CMR, are widely discussed in the literature (*23*), and we only focus on the latter in this work. Recent effort in this model system has been devoted to epitaxial films (*24*, *25*). To date, bulklike behaviors are only seen for films grown

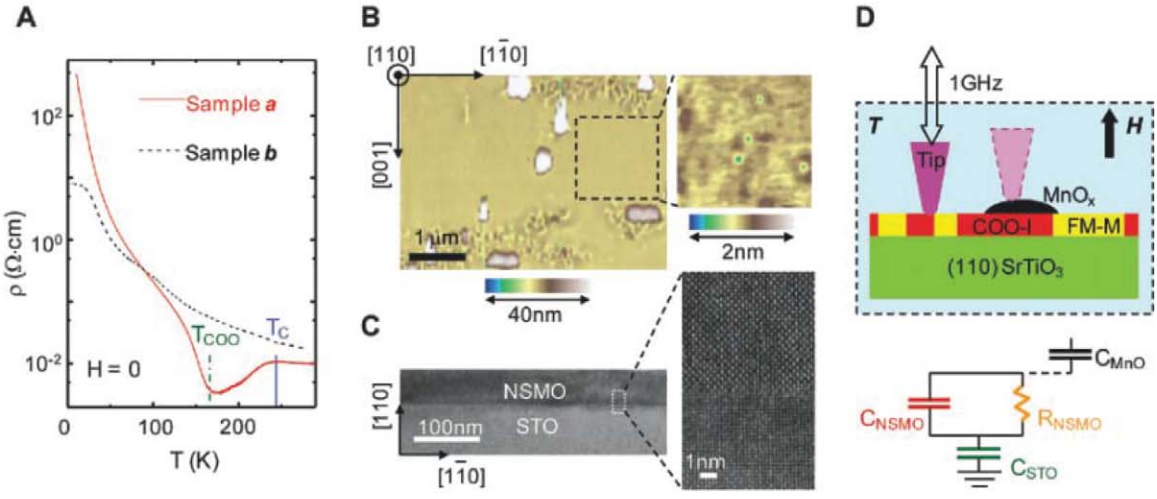

Fig. 1. (**A**) Zero-field $\rho(T)$ curves of two samples, a (30-nm NSMO/STO) and b (60-nm NSMO/STO). The metallic temperature region between the bulk T_C (blue) and T_{COO} (green) is present in sample a but missing in sample b. At low T, $\rho_a(T)$ diverges and $\rho_b(T)$ saturates. (**B**) The AFM surface topography contains MnO_x precipitates (~20 nm in height) and corrugations. Crystal axes of the STO substrate are indicated. (Inset) An atomically flat region 1 to 2 μm in size. Note the different false-color scales between the main image (40 nm) and the inset (2 nm). (**C**) Cross-sectional TEM image of the NSMO-STO interface of sample a. The good crystallinity and coherent epitaxy are confirmed by a high-resolution TEM picture (inset). (**D**) Schematics of the system setup (top) and the corresponding lumped-element circuit (bottom). When the tip scans over the FM-M domains (yellow), the small R_{NSMO} shunts the capacitor, C_{NSMO}, giving a larger signal than that of the COO-I background (red). The insulating particles (black), on the other hand, introduce a series capacitor (C_{MnO}), resulting in lower MIM-C signals.

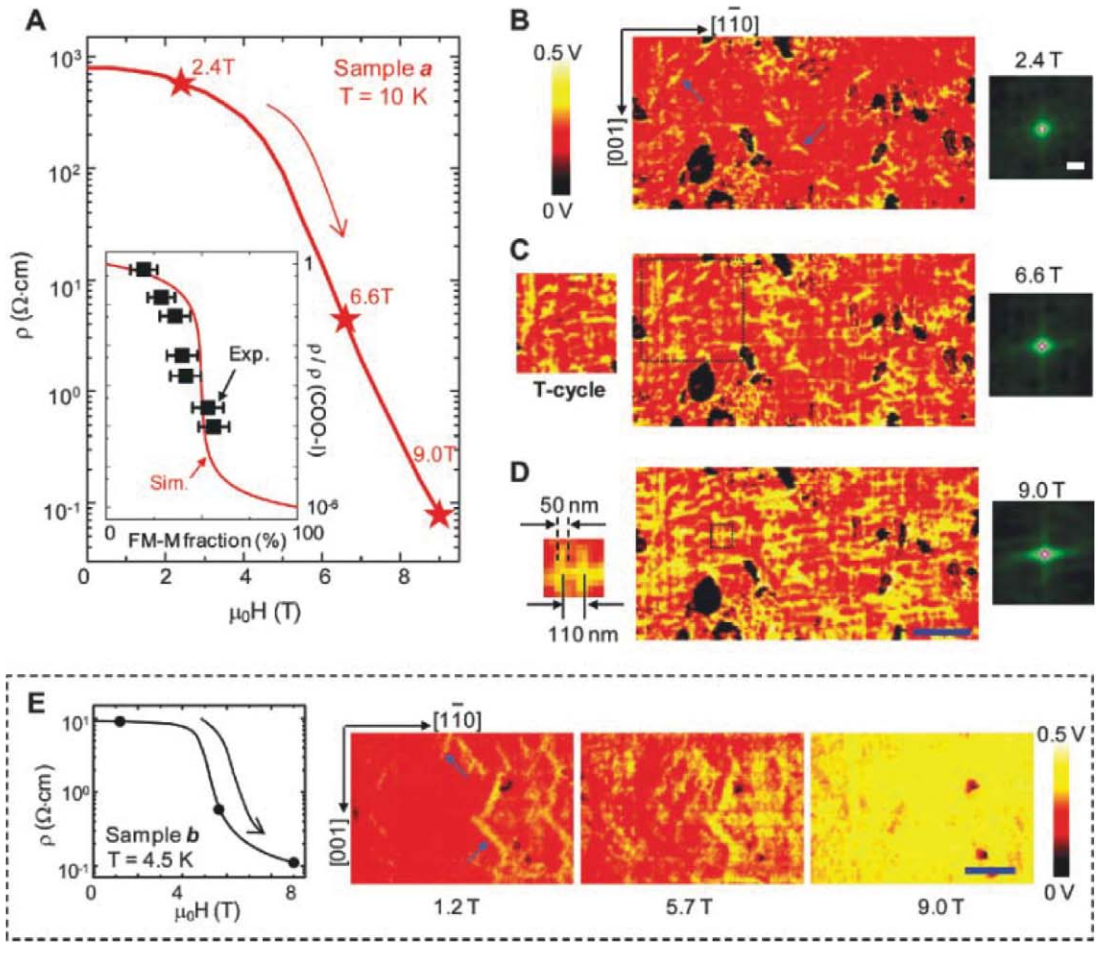

Fig. 2. (**A**) $\rho_a(H)$ during the field sweep at T = 10 K. The three fields at which MIM images in (B to D) were taken are labeled by the red stars. (Inset) Comparison between the two-dimensional (2D) square-lattice simulation ($\rho_{COO-I} \sim 10^3$ ohm·cm and $\rho_{FM-M} \sim 10^{-3}$ ohm·cm, see Fig. 3A) and the experimental data. The large error bars and deviations near the percolation transition may result from the surface defects, the finite resolution, and the fact that percolation in NSMO is 3D in nature. For method of estimating the FM-M areal fraction, see fig. S5. (**B** to **D**) (Center) Microwave images (6 μm by 3 μm, scale bar = 1 μm) taken at 10 K and under $\mu_0 H$ = 2.4 T, 6.6 T, and 9.0 T, respectively. MnO_x particles appear black in the images. At low fields, some isolated rodlike FM-M domains (yellow) are indicated by blue arrows. [(C) Left inset] Measurement taken at 15 K and 6.5 T after a thermal cycle. [(D) Left inset] Closeup of a small region in (D) (black square) shows the typical width and spacing of the filaments. [(B) to (D) Right images] The center portions of autocorrelation images (scale bar = 0.2 μm), with a notable center cross seen at 9.0 T. (**E**) Transport and three MIM images (4.5 μm by 3 μm, scale bar = 1 μm) of sample b taken at 4.5 K. The low-field FM-M "rods" are indicated by arrows.

on (110) STO substrates, presumably because of the strong dependence on the lattice strain. Even on the same substrate, sample degradation resulting from partial loss of crystalinity and epitaxial coherency (*21*) (fig. S3) is sometimes detected. We present data from two samples, sample a, in which signatures of T_C and T_{COO} are present (Fig. 1A), and for comparison a degraded sample b, which lacks metallic temperature regions. The samples (*21*) (fig. S4) were characterized by atomic force microscopy (AFM) (Fig. 1B) and cross-sectional transmission electron microscopy (TEM) (Fig. 1C). The surfaces contain micrometer-sized precipitates, most likely MnO_x (*26*), and some corrugations next to these particles. In between the defective regions, there exist atomically flat areas where pure electrical signals can be obtained. The contrast in MIM-C images is qualitatively understood by the lumped-element circuit in Fig. 1D.

Simultaneously taken transport data and low-*T* microwave images (*21*) (figs. S5 and S6) are shown in Fig. 2, A to D, for sample a and Fig. 2E for sample b. Both the DC voltage (<1 V) and microwave excitation (1 μW) were kept low to avoid any extrinsic perturbation. The insulating MnO_x particles behaved as field-independent markers. At low fields where ρ barely decreases, some rodlike FM-M domains (indicated by blue arrows) tilted with respect to the [001] direction were observed on the COO-I background in both samples. The presence of such low-field conducting domains implies that phase separation already occurs before the magnetic field is turned on. We note that sample b showed larger low-field FM-M areal fraction than sample a. As *H* was increased to about 6 to 7 T, metallic areas grew from the low-field nucleation sites; their positions and shapes indicate a certain memory effect (*27*). In a subsequent experiment, sample a was warmed up to 250 K and cooled back to 15 K at $H = 0$. A field of 6.5 T was turned on after this thermal cycle. Most FM-M domains, as shown in Fig. 2C, left inset, reappeared in the same locations compared with the corresponding area in Fig. 2C main (dotted box), indicative of pinning by an intrinsic long-range energy landscape and short-range disorder potentials. A distinction between the two samples at intermediate fields is that the *H*-induced FM-M filaments of sample a (Fig. 2C) show directional ordering and preferentially align along [001] and [1$\bar{1}$0] axes of the substrate, whereas no such feature is seen in sample b within our spatial resolution. At about 8 to 9 T, the prominent FM-M filaments in sample a form an interconnected percolating network. Although the smallest measured feature width (30 to 50 nm) may be set by our spatial resolution (*21*) (fig. S7), the typical spacing ~ 100 nm is resolved here. Because $\rho_a(H)$ does not show any sign of saturation at 9 T, the FM-M domains should further expand at higher fields. $\rho_b(H)$, on the other hand, levels off at 9 T, consistent with the nearly full coverage of FM-M regions.

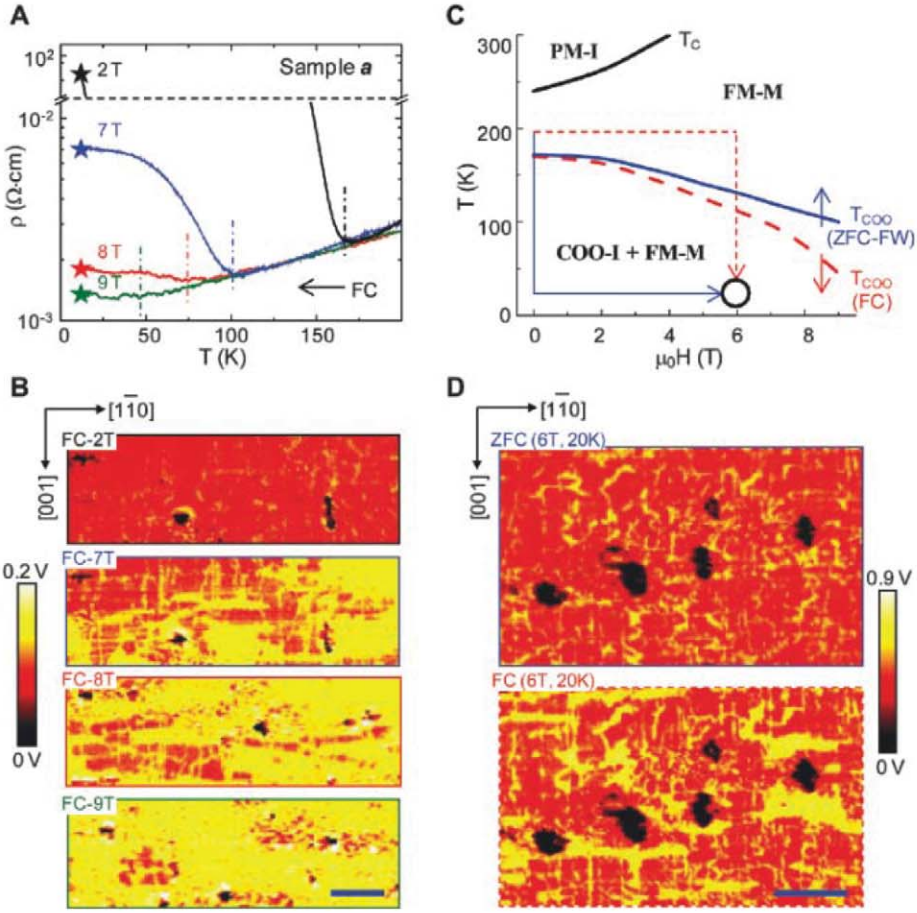

Fig. 3. (**A**) FC resistivity and (**B**) MIM images (6 μm by 2 μm, scale bar = 1 μm) at 2 T, 7 T, 8 T, and 9 T. T_{COO} values for the four magnitudes of the H-field are denoted in (A) by vertical dash-dot lines, color-coded to match the resistivity curves. (**C**) Phase diagram of sample a, showing the PM-I, FM-M, and phase coexistence (COO-I + FM-M) regions demarcated by transport signatures T_C or T_{COO} from ZFC-FW (field-warm, solid blue line) and FC (dashed red line) processes. Two paths from 200 K and 0 T to 20 K and 6 T are sketched in the plot. (**D**) MIM images (5 μm by 3 μm, scale bar = 1 μm) taken at the same $T = 20$ K and $\mu_0 H = 6$ T. The FC image (bottom) contains much bigger conducting domains than the ZFC one (top).

The salient liquid-crystal–like metallic network accompanying the low-*T* CMR effect in sample a is not seen by structural characterization and must be electronic in origin. We can obtain some insight by comparing this result with experiments on other manganites. Nanometer-sized domains with no preferred directions were observed in $La_{1-x}Ca_xMnO_3$ (*11*, *28*) due to Coulomb interaction. Large sub-micrometer clusters with no particular shapes were imaged in $(La,Pr)_{1-x}Ca_xMnO_3$ (*16*) owing to the strong disorders. In the NSMO films, the elastic strain must play a vital role because neither Coulomb interaction nor quenched disorders can generate such a mesoscopic ordered network (*1*–*3*). It is likely that the accommodation strain (*7*, *14*) between the pseudo-cubic FM-M and distorted orthorhombic COO-I phases is responsible for the low-field FM-M rods, which appear in both sample a and b. The more important epitaxial strain imposed by the (110) STO substrate (*23*, *24*), which is crucial for producing the bulklike behaviors, must account for the observed glassy orders in sample a. The lack of a universal form of phase separation in both the PM-FM (*11*, *28*) and the low-T CMR effects (*16*) (this work) points to the robustness of the phenomenon; the effect occurs because of energetically competing states, whereas the exact CMR magnitude depends on detailed microscopic configurations.

Taking the areal fraction of FM-M states as the probability of connected bonds, we can compare the experimental data to the square-lattice random resistor network simulation (*29*, *30*). Despite some deviations near the threshold (*21*) (fig. S5), the agreement between experiment and modeling in the Fig. 2A inset shows that the low-T CMR is indeed percolative in nature. Second, the autocorrelation analysis (*21*) (fig. S8) is performed for Fig. 2, B to D. The nearly circular autocorrelation peak at 2.4 T evolves into a clear center-cross at 9 T with a characteristic length ~ 0.5 μm. In analogy to the stripes or checkerboard patterns seen in cuprates (*4*–*6*), the 100-nm period may be set by the long-range

strain field, whereas the typical length of the filaments is determined by the strength of disorders. Interestingly, discernible anisotropy is seen in that the "nematic" domains along the [1$\bar{1}$0] direction are statistically more favorable than the [001] direction, in fair agreement with the transport anisotropy observed in control samples (*21*) (fig. S9). In the strained NSMO/(110)STO films, the in-plane lattice constant is locked to that of the substrate along the [001] direction while relaxed along the [1$\bar{1}$0] direction (*23*, *24*). At the same time, the charge-ordered planes are parallel to the (100) or (010) planes. Because the low-*T* CMR effect is accompanied by lattice deformation (*22*), the metallic domains may tend to expand along the more strain-free axis, resulting in the in-plane anisotropy. The nematic phase at this length scale provides a contrasting framework to understand the "stripe" phenomenon that also breaks in-plane C_2 symmetry at much shorter length scales (*31*).

The physical picture depicted above is further corroborated by results combining both *T* (*21*) (fig. S10) and *H*. In particular, by using a field-cool (FC) process, we can access states with much lower ρ than the zero-field-cool (ZFC) process discussed so far. Figure 3, A and B, shows the FC curves at four different fields and the corresponding microwave images taken at 12 K, which is below T_{COO} for all fields. The continuous COO-I phases at FC-2T break into isolated micrometer-sized domains at FC-7T, which continue to be percolated through by FM-M filaments at FC-8T and shrink down to small droplets at FC-9T. Taking the transport signatures T_C and T_{COO}, we construct the phase diagram of this NSMO/STO sample in Fig. 3C, where phase coexistence is denoted below T_{COO}. This phase diagram is reminiscent of the one for single-crystal NSMO (*22*) except that the reentrant behavior reported there is beyond our field range. By using MIM, we can directly study the microscopic origin of the hysteresis. In Fig. 3C, two paths arriving at the same external conditions are shown: the ZFC process from 200 K to 20 K followed by a field sweep to 6 T, or field sweep to 6 T at 200 K before FC to 20 K (*21*) (fig. S11). The two MIM images in Fig. 3D display remarkably different percolating networks. For the high-ρ (1.4 ohm·cm) ZFC state, glassy FM-M filaments are observed in the COO-I background. For the low-ρ (0.02 ohm·cm) FC state, on the other hand, the FM-M phases occupy a much larger portion and even form micrometer-sized puddles elongated in the [1$\bar{1}$0] direction. Although hysteresis during the low-T CMR effect is known in single-crystal NSMO from bulk measurements, tools like MIM enable real-space electrical imaging and demonstrate the strong dependence of phase separation on local disorders and strain fields near the multiphase boundary.

References and Notes

1. E. Dagotto, *Science* **309**, 257 (2005).
2. Y. Tokura, *Rep. Prog. Phys.* **69**, 797 (2006).
3. S. Yunoki *et al.*, *Phys. Rev. Lett.* **80**, 845 (1998).
4. M. Vershinin *et al.*, *Science* **303**, 1995 (2004); published online 12 February 2004 (10.1126/science.1093384).
5. T. Hanaguri *et al.*, *Nature* **430**, 1001 (2004).
6. C. Howald, H. Eisaki, N. Kaneko, M. Greven, A. Kapitulnik, *Phys. Rev. B* **67**, 014533 (2003).
7. N. D. Mathur, P. B. Littlewood, *Solid State Commun.* **119**, 271 (2001).
8. K. H. Ahn, T. Lookman, A. R. Bishop, *Nature* **428**, 401 (2004).
9. J. Burgy, A. Moreo, E. Dagotto, *Phys. Rev. Lett.* **92**, 097202 (2004).
10. A. Moreo, M. Mayr, A. Feiguin, S. Yunoki, E. Dagotto, *Phys. Rev. Lett.* **84**, 5568 (2000).
11. M. Fäth *et al.*, *Science* **285**, 1540 (1999).
12. Ch. Renner, G. Aeppli, B.-G. Kim, Y. A. Soh, S. W. Cheong, *Nature* **416**, 518 (2002).
13. L. Zhang, C. Israel, A. Biswas, R. L. Greene, A. de Lozanne, *Science* **298**, 805 (2002); published online 19 September 2002 (10.1126/science.1077346).
14. W. Wu *et al.*, *Nat. Mater.* **5**, 881 (2006).
15. J. C. Loudon, N. D. Mathur, P. A. Midgley, *Nature* **420**, 797 (2002).
16. M. Uehara, S. Mori, C. H. Chen, S.-W. Cheong, *Nature* **399**, 560 (1999).
17. K. Lai, W. Kundhikanjana, M. Kelly, Z. X. Shen, *Rev. Sci. Instrum.* **79**, 063703 (2008).
18. K. Lai, W. Kundhikanjana, M. Kelly, Z. X. Shen, *Phys. Lett.* **93**, 123105 (2008).
19. B. T. Rosner, D. W. van der Weide, *Rev. Sci. Instrum.* **73**, 2505 (2002).
20. Z. Wang *et al.*, *J. Appl. Phys.* **92**, 808 (2002).
21. Materials and methods are available as supporting material on *Science* Online.
22. H. Kuwahara, Y. Tomioka, A. Asamitsu, Y. Moritomo, Y. Tokura, *Science* **270**, 961 (1995).
23. H. Aliaga *et al.*, *Phys. Rev. B* **68**, 104405 (2003).
24. M. Nakamura, Y. Ogimoto, H. Tamaru, M. Izumi, K. Miyano, *Appl. Phys. Lett.* **86**, 182504 (2005).
25. Y. Wakabayashi *et al.*, *Phys. Rev. Lett.* **96**, 017202 (2006).
26. T. Higuchi *et al.*, *Appl. Phys. Lett.* **95**, 043112 (2009).
27. D. D. Sarma *et al.*, *Phys. Rev. Lett.* **93**, 097202 (2004).
28. J. Tao *et al.*, *Phys. Rev. Lett.* **103**, 097202 (2009).
29. S. Kirkpatrick, *Rev. Mod. Phys.* **45**, 574 (1973).
30. M. Mayr *et al.*, *Phys. Rev. Lett.* **86**, 135 (2001).
31. J. A. Robertson, S. A. Kivelson, E. Fradkin, A. C. Fang, A. Kapitulnik, *Phys. Rev. B* **74**, 134507 (2006).

32. We thank X.-L. Qi, Y. Chen, J. C. Davis, and S. A. Kivelson for valuable discussions. The work is supported by NSF (grants DMR-0906027 and Center of Probing the Nanoscale PHY-0425897), Department of Energy (DE-FG03-01ER45929-A001), Funding Program for World-Leading Innovative R and D on Science and Technology (FIRST) of Japan Society for the Promotion of Science (JSPS), and King Abdullah University of Science and Technology Fellowship (KUS-F1-033-02). Stanford University has filed a patent application with the U.S. Patent Office on the AFM compatible microwave imaging technique. This technology was modified for low-temperature measurement in this report.

Supporting Online Material

www.sciencemag.org/cgi/content/full/329/5988/190/DC1
Materials and Methods
Figs. S1 to S11

22 March 2010; accepted 3 June 2010
10.1126/science.1189925

Predictive Model for Wall-Bounded Turbulent Flow

I. Marusic,* R. Mathis, N. Hutchins

The behavior of turbulent fluid motion, particularly in the thin chaotic fluid layers immediately adjacent to solid boundaries, can be difficult to understand or predict. These layers account for up to 50% of the aerodynamic drag on modern airliners and occupy the first 100 meters or so of the atmosphere, thus governing wider meteorological phenomena. The physics of these layers is such that the most important processes occur very close to the solid boundary—the region where accurate measurements and simulations are most challenging. We propose a mathematical model to predict the near-wall turbulence given only large-scale information from the outer boundary layer region. This predictive capability may enable new strategies for the control of turbulence and may provide a basis for improved engineering and weather prediction simulations.

Flow over a solid surface or wall produces a region of strong shear due to the no-slip condition at the surface. This strong shear induces tangential stresses at the surface, which, from an engineering perspective, will lead to energy expenditure (drag for aerodynamic and hydrodynamic vehicles, increased pumping requirements for pipe networks, etc.). Under most practical conditions, this thin region of shear—known as a boundary layer—is turbulent; the fluid motion is no longer well ordered and instead succumbs to highly chaotic motions, leading to further increases in mechanical losses. Up to half of the fuel burned by a modern airliner during flight is used to overcome drag due to turbulent boundary layers (this proportion is higher still for a large oil tanker or submarine). In addition to energy expenditure, turbulent boundary layers also promote increased mixing, heat transfer, and exchange processes; thus, when they occur on an atmospheric scale, they have important meteorological and climatological implications.

A long-standing challenge has been to understand and predict the behavior of wall-bounded turbulence, especially because the ability to predict

Department of Mechanical Engineering, University of Melbourne, Victoria 3010, Australia.

*To whom correspondence should be addressed. E-mail: imarusic@unimelb.edu.au

such behavior often implies opportunities for control (*1*). Such aspirations were strengthened by the discovery during the 1950s and 1960s that turbulent boundary layers, despite their obvious disorder, possess certain recurrent features or coherent patterns, and recent studies have considerably expanded this view (*2*). Our current work uses recently acquired knowledge of large-scale recurrent features to build a predictive model for the complex small-scale motions that occur very close to the surface. Under typical practical conditions, this important near-wall region is often beyond the scrutiny of experimental measurement techniques and therefore remains largely undocumented. The current model provides a basis for predicting flows in the near-wall region, where data would otherwise be unavailable, using only information gathered farther away from the surface. In addition to offering valuable insight into the complex physics of wall-bounded turbulence, the model could also have ramifications for the simulation of these flows.

Computer simulations of wall-bounded turbulence are extremely challenging because the simulation must resolve the entire range of scales of turbulent motion (*3*). For a boundary layer that has developed over the length of a large aircraft fuselage, these motions could range from the meter scale down to just a few micrometers for the smallest dissipative motions. Atmospheric surface layers will have similar scale separation, with the largest scales on the order of 1 km and the smallest around 1 mm. In general, turbulent boundary layers are characterized by the dimensionless parameter known as the Reynolds number (*Re*), which is essentially the ratio of the largest inertial scale to the smallest dissipative scale in the flow. To date, even the largest supercomputers can solve such flows only at comparatively low *Re* values, which are several orders of magnitude below most practical applications. In overcoming this limitation, one approach has been large-eddy simulation (*4*), in which a sparse grid is used to resolve the large-scale motions, whereas the unresolved small-scale motions are modeled. For high-*Re* wall-bounded flows, this also requires a near-wall model to account for the relationship between the wall shear stress and the outer-layer flow (*5*). This current work aims to improve our understanding of this complex interaction, offering a simple mathematical model that can accurately predict near-wall turbulent statistics based only on large-scale outer-layer information.

For wall turbulence, the most relevant Reynolds number is $Re_\tau = \delta U_\tau/\nu$ (known as the friction Reynolds number or Karman number), which is a ratio of the inner and outer length scales. Here, the outer scale is δ, the boundary layer thickness, which corresponds to the normal distance from the wall (beyond which the velocity recovers to the free stream). The inner length scale is ν/U_τ, where ν is the kinematic viscosity and $U_\tau = (\tau_0/\rho)^{1/2}$ is the friction velocity, where τ_0 is the mean wall-shear stress and ρ is the fluid density.

The classical view is that the inner region is taken nominally to be $0 < z^+ < 0.15Re_\tau$, where z is the distance normal to the wall and the superscript + denotes normalization with inner variables (i.e., $z^+ = zU_\tau/\nu$, $U^+ = U/U_\tau$, etc). The outer region is nominally taken to be $30/Re_\tau < z/\delta < 1$, and the overlap of the inner and outer regions is referred to as the logarithmic layer, as here the mean streamwise (x-direction) velocity nominally follows a log-law formulation (*6*). These different regions, or layers, are illustrated schematically in the left panel of Fig. 1. The near-wall inner region (say, $0 < z^+ < 30$) in the classical description is taken to be independent of the outer region, and all the turbulence statistics U^+, $\overline{u^2}^+$, $\overline{u^3}^+$, etc., are universal functions of z^+. Here, U and u are the mean and fluctuating streamwise velocities, respectively, and overbars denote ensemble time-averaged quantities. A number of studies have challenged this classical description in recent years, showing evidence that the inner region has a dependence on *Re*, and thus on the outer length scale δ (*7*–*10*).

Recent studies conducted at higher values of *Re* have also noted the presence of very-large-scale motions (VLSMs, also referred to as "superstructures") in the logarithmic layer of turbulent boundary layers (*11*–*13*). Our understanding of these features is somewhat nascent, yet in general they can be categorized as very large elongated regions of negative velocity fluctuation (with instantaneous reported lengths of 15δ to 20δ), flanked on either side in the spanwise direction by regions of positive fluctuation. These regions are inclined slightly to the horizontal (such that the downstream end extends farther from the wall) and, in a mean sense, are accompanied by large-scale counterrotating roll modes. These elongated features meander, or appear sinuous, in the streamwise direction and in general seem to be ubiquitous for all high-*Re* wall-bounded turbulence. They have been noted in high-*Re* pipe, channel, and flat-plate turbulent boundary layers, as well as in the atmospheric surface layer (where they are on the kilometer scale) (*9*, *13*–*15*). The sketch in the upper left of Fig. 1 shows a conceptual view of these events (where red and blue represent positive and negative fluctuations of u, respectively). Although these events seem to be primarily centered (and most energetic) in the logarithmic region, they have an influence that extends to the wall, and a large-scale fluctuation (or footprint) is superimposed on the near-wall turbulence. This is as predicted by Townsend's attached-eddy hypothesis (*16*). However, in addition to this superimposition of energy, the superstructure events also modulate the magnitude of the small-scale fluctuations (*12*, *17*). Within a large-scale low-speed event (the blue region of Fig. 1), it is found that close to the wall the small-scale fluctuations are attenuated, while farther away from the wall the small-scale fluctuations are amplified above

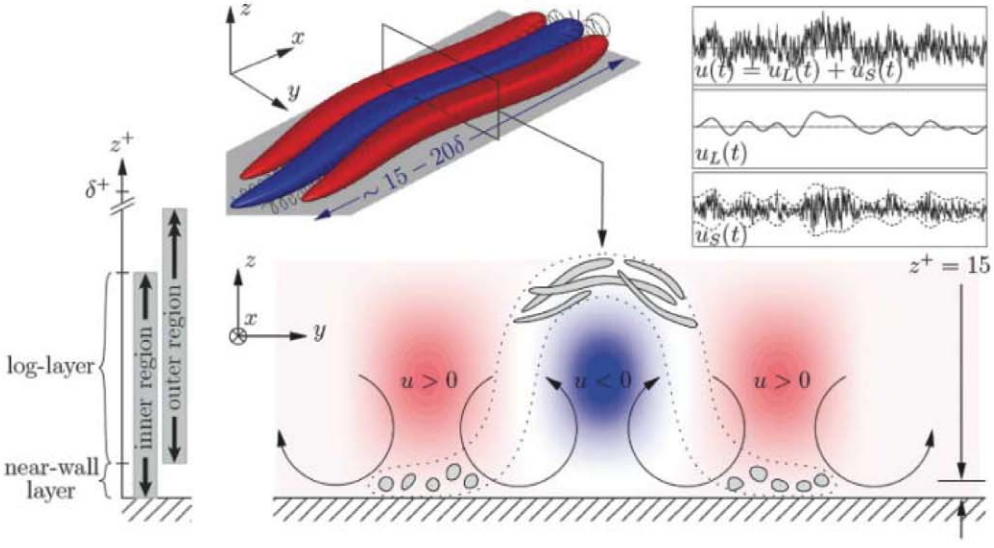

Fig. 1. Schematic of organized coherent flow motion known as a superstructure and its interaction across the turbulent boundary layer. These very-large-scale motions extend from the log region down toward the wall, both superimposing their signature and modulating the near-wall region. The sample u time series highlight the modulation effect of the large scales on the small scale at $z^+ = 15$; the near-wall location corresponds to the peak turbulence intensity. The features shown in gray indicate elongated filamentary vortex structures and their conjectured alignment with the superstructure.

background levels. The reverse scenario is noted in the red regions of Fig. 1 (in the large-scale regions of positive u). This observation is represented in the upper right plot of Fig. 1, where a sample instantaneous fluctuating time signal of streamwise velocity $u(t)$ is shown at a location near the wall (at $z^+ = 15$, close to the peak in turbulence production). The two lower plots show the signal spectrally decomposed into large-scale (u_L) and small-scale (u_S) components, where u_L contains only energy with $\lambda_x > \delta$ and u_S has energy with $\lambda_x < \delta$ (where λ_x is streamwise wavelength). It is apparent from the signal of u_S (bottom plot) that the small-scale fluctuations are modulated by an envelope that is well described by the large-scale signal (u_L) (*17*). Close to the wall, the small-scale fluctuations are attenuated within negative u_L and amplified within positive u_L. Recently (*17*) we showed that u_L is highly correlated with the large-scale velocity signal in the log region (u_{OL}), and thus the large-scale "superstructure" events modulate the near-wall scales in a manner akin to amplitude modulation. Farther from the wall, the sign of the correlation between u_L and the envelope of u_S reverses, such that for $z^+ \geq 3.9(Re_\tau)^{1/2}$ the small-scale fluctuations are increased within negative large-scale events (and reduced within positive large-scale events). The crossover position $3.9(Re_\tau)^{1/2}$ was empirically determined, but such a scaling is consistent with the geometric center of the log layer (*17*). The bottom plot of Fig. 1 shows an overview of this modulation scenario. The blue and red regions show a cross section through the elongated low- and high-speed superstructure events, with associated counterrotating roll modes also shown. The modulation is represented by the gray contours highlighting the increased small-scale vortical activity close to the wall beneath the high-speed (red) regions, and also farther away from the wall within the low-speed (blue) regions.

If one accepts the amplitude modulation effect as the mechanism linking the large-scale superstructures to the behavior of the near-wall region, then this leads to the possibility that a simple mathematical model may be devised that captures this interaction. This is very desirable, as it would allow prediction of the fluctuating velocity statistics in the near-wall region given only information about the large-scale signal in the log region. Such a model can be expressed as

$$u_P^+ = u^*(1 + \beta u_{OL}^+) + \alpha u_{OL}^+ \qquad (1)$$

where u_P^+ is the predicted u signal at z^+, u_{OL} is the fluctuating large-scale signal from the log region, u^* is the statistically "universal" signal at z^+ (normalized in wall units), and α and β are, respectively, the superimposition and modulation coefficients. Note that the model consists of two parts; the first part, $u^*(1 + \beta u_{OL}^+)$, models the amplitude modulation at z^+ by the large-scale motions, and the second part, αu_{OL}^+, models the superimposition of the large-scale motions felt at z^+.

The large-scale signal, u_{OL}, is the only user input required for Eq. 1 and is obtained from the u signal in the log region (at a given z/δ value) involving two steps. First, the u signal is low-pass filtered to retain only large scales (here, streamwise wavelengths of $\lambda_x^+ > 7000$ are retained), and second, because we are equating a log-region signal (from z_O^+) to a specified position z^+, the measured u signal phase information is retained and the signal is shifted to account for the structure inclination angle, θ_{LS}, between these two wall-normal positions, which previous studies have shown to be effectively invariant with Re (*18*, *19*). Figure 2 shows a sample of a measured u_{OL}^+ signal together with the corresponding simultaneously measured u signal at $z^+ = 15$. Note the high degree of correlation of u_{OL}^+ with the low-frequency content of u^+ (z^+).

The procedure for finding u^*, α, β, and θ_{LS} is as follows: An experiment was conducted at $Re_\tau = 7300$ that involved simultaneously sampling u signals from two hot wires mounted at z_O^+ and z^+ (*20*). z_O^+ was fixed nominally in the center of the classical log region, which corresponds to $z_O^+ = 3.9(Re_\tau)^{1/2}$ (*17*), whereas z^+ could be traversed within the range $0 < z^+ < z_O^+$. The modulation coefficient β was found by using Eq. 1 and optimizing the value of β that returned a u^* signal with no amplitude modulation. Thus, the value of β that returns an unmodulated u^* signal was determined to be the universal value with the corresponding u^* as the universal signal. The structure inclination angle, θ_{LS}, corresponds to the time delay that locates the maximum in a cross-correlation between the large-scale u signals at z_O^+ and z^+, and α corresponds to the value of the maximum cross-correlation coefficient between these signals. These are taken as invariants, and therefore α, β, and θ_{LS} are functions only of z^+, and u^* is a universal function of t^+ at a given z^+ level. Time-series data files of u^* together with its large-scale phase information are available from the authors, as are corresponding tabulated values of α, β, and θ_{LS}. The $u^*(z^+, t^+)$ signals are records over a nondimensional time of $T^+ = 4.55 \times 10^6$, which means that they are sufficiently long to ensure a statistically representative realization (*21*). With u^*, α, and β known and fixed for a given wall-normal position, prediction of u_P^+ can now be made using Eq. 1 where the only input is the large-scale u signal at z_O^+.

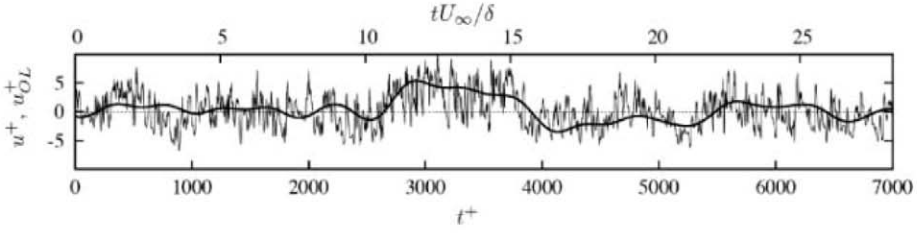

Fig. 2. Example of fluctuating signal u^+ at $z^+ = 15$ and large-scale fluctuating component u_{OL}^+ in the outer layer (thick blank line) at $z^+ = 330$ measured in a turbulent boundary layer at $Re_\tau = 7300$.

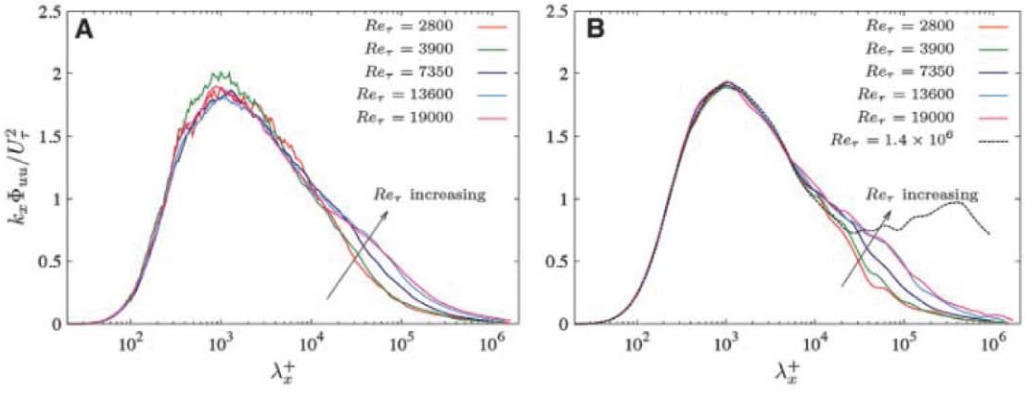

Fig. 3. (**A** and **B**) Reynolds number evolution of the premultiplied energy spectra of streamwise velocity at the inner-peak location ($z^+ = 15$) for the true measurements (A) and the prediction based on the filtered u signal measured in the log region (B).

The experimental data were obtained in the Melbourne High Reynolds Number Boundary Layer Facility, a wind tunnel that obtains high values of *Re* with very low free-stream turbulence levels (<0.05%) over a flat plate of 27 m length (*22*, *23*). The boundary layer thickness at x = 21 m is in excess of 300 mm, allowing for excellent spatial and temporal resolution (*21*). The velocity signatures are obtained by hot-wire anemometry; full details of the experimental setup are given in (*17*). Single hot-wire measurements were also carried out at five values of Re_τ (2800, 3900, 7300, 13,600, and 19,000), and these provide the profiles against which predictions can be validated. For the predictions of these experiments, only the large-scale filtered velocity signal measured at $z_O^+ = 3.9(Re_\tau)^{1/2}$ is used to provide the u_{OL} input to Eq. 1, from which predicted velocity signals can be calculated at any wall-normal position [in the range $0 < z^+ < 3.9(Re_\tau)^{1/2}$]. Thus, all near-wall fluctuating signals are recreated on the basis of a single log-region measurement. Comparison is also made here to data at $Re_\tau = 1.4 \times 10^6$ from experiments by the authors in the atmospheric surface layer on the salt flats of the Utah Western Desert using a wall-normal array of sonic anemometers (*13*, *15*).

Figures 3 and 4 show some indicative results of the prediction scheme. Figure 3B shows predictions of premultiplied spectra at $z^+ = 15$ compared to the measured results shown in Fig. 3A. Excellent agreement is seen for the available data. (Note that no comparison exists for the Utah case at this very–near-wall position.) The area under the curves in Fig. 3 corresponds to $\overline{u^2}^+$, and the measurements and predictions indicate a clear increase in the area with increasing values of *Re* resulting from the extra energy at long wavelengths. This explains the findings of previous studies (*7*–*10*, *21*) that have also noted this increase in the peak value of $\overline{u^2}^+$ with increasing *Re*. Although this result is contrary to the classical wall-scaling theories used in many commercial simulation schemes, it is consistent with the Townsend attached-eddy hypothesis (*10*). Figure 4 compares measurements and predictions for the various wall-normal positions of $\overline{u^2}^+$, together with higher-order moments. For brevity, here only the sixth-order moment is shown along with the skewness profiles. Again, excellent agreement is found for all moments up to the sixth-order moment. While the experimental uncertainty increases with the higher-order moments, the trends predicted by the model follow the experimental results well. The predictions are able to capture the change in sign of skewness in the viscous buffer region (at $z^+ \approx 30$) as *Re* increases. Previously this trend had been puzzling (*7*), but here we are able to confirm that this behavior is likely due to the modulation effect of the superstructure events in the near-wall region.

These promising results lend support to the superimposition and modulation coupling mechanism between the inner and outer regions of wall turbulence. At this stage, the model presented is for zero-pressure-gradient boundary layer flows only, but it can be extended to other flows if the corresponding two-point experiments required for u^* are carried out in those flows at any value of *Re*. Caution is indicated concerning the trends predicted by the Utah data, which are subject to larger experimental uncertainties (*24*). These data have been used to illustrate an application of the model at very high *Re*, but whether the predicted trend in Fig. 4 holds—with an outer peak in $\overline{u^2}^+$ exceeding the level of the inner peak at $z^+ \approx 15$—remains an open question.

The simple algebraic form of Eq. 1 is an ideal basis for a near-wall model for high-*Re* large-eddy simulations. These simulations rely on near-wall inputs based only on large-scale information of the velocity field in the logarithmic region (where the first grid point is typically located) (*25*–*27*). This is exactly the information that Eq. 1 provides, and future studies in this direction are continuing. Our predictive model can also be used to provide the missing information from leading high-*Re* facilities [such as in the Princeton superpipe (*28*)], where the near-wall region is largely inaccessible to measurement because of the extremely small viscous scales associated with such facilities.

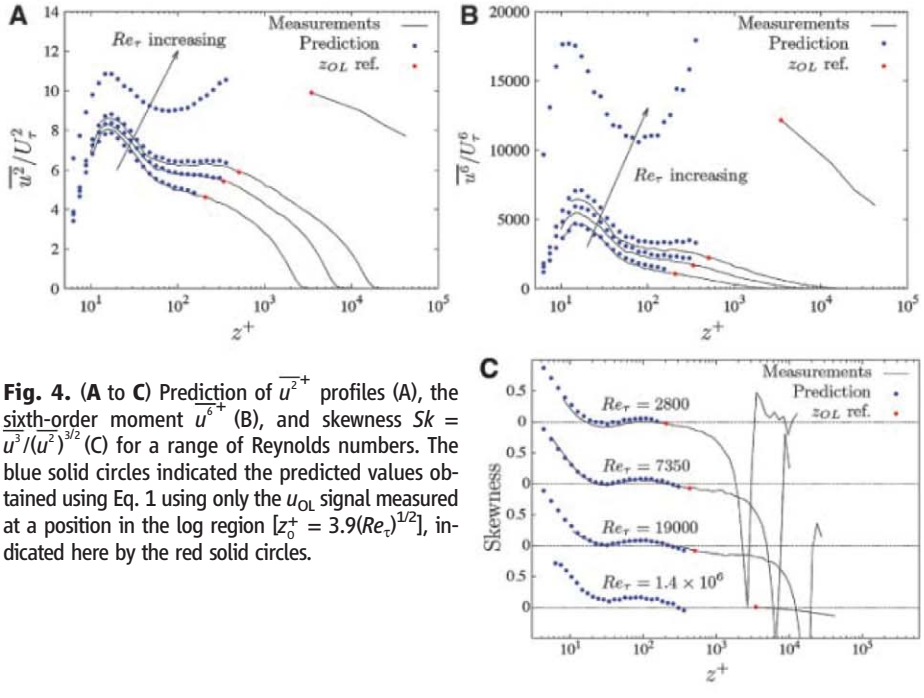

Fig. 4. (**A** to **C**) Prediction of $\overline{u^2}^+$ profiles (A), the sixth-order moment $\overline{u^6}^+$ (B), and skewness $Sk = \overline{u^3}/(\overline{u^2})^{3/2}$ (C) for a range of Reynolds numbers. The blue solid circles indicated the predicted values obtained using Eq. 1 using only the u_{OL} signal measured at a position in the log region [$z_o^+ = 3.9(Re_\tau)^{1/2}$], indicated here by the red solid circles.

References and Notes

1. B. Hof, A. de Lozar, M. Avila, X. Tu, T. M. Schneider, *Science* **327**, 1491 (2010).
2. R. J. Adrian, *Phys. Fluids* **19**, 041301 (2007).
3. P. Moin, K. Mahesh, *Annu. Rev. Fluid Mech.* **30**, 539 (1998).
4. C. Meneveau, J. Katz, *Annu. Rev. Fluid Mech.* **32**, 1 (2000).
5. U. Piomelli, *Prog. Aerosp. Sci.* **35**, 335 (1999).
6. S. B. Pope, *Turbulent Flows* (Cambridge Univ. Press, Cambridge, 2000).
7. M. M. Metzger, J. C. Klewicki, *Phys. Fluids* **13**, 692 (2001).
8. D. B. De Graaff, J. K. Eaton, *J. Fluid Mech.* **422**, 319 (2000).
9. S. Hoyas, J. Jiménez, *Phys. Fluids* **18**, 011702 (2006).
10. I. Marusic, G. J. Kunkel, *Phys. Fluids* **15**, 2461 (2003).
11. K. C. Kim, R. J. Adrian, *Phys. Fluids* **11**, 417 (1999).
12. N. Hutchins, I. Marusic, *Philos. Trans. R. Soc. London Ser. A* **365**, 647 (2007).
13. N. Hutchins, I. Marusic, *J. Fluid Mech.* **579**, 1 (2007).
14. J. Monty, J. Stewart, R. Williams, M. Chong, *J. Fluid Mech.* **589**, 147 (2007).
15. I. Marusic, N. Hutchins, *Flow Turbul. Combus.* **81**, 115 (2008).
16. A. A. Townsend, *The Structure of Turbulent Shear Flow, Vol. 2* (Cambridge Univ. Press, Cambridge, 1976).
17. R. Mathis, N. Hutchins, I. Marusic, *J. Fluid Mech.* **628**, 311 (2009).
18. I. Marusic, W. D. Heuer, *Phys. Rev. Lett.* **99**, 114504 (2007).
19. G. R. Brown, A. S. W. Thomas, *Phys. Fluids* **20**, S243 (1977).
20. Note that this experiment is conducted at an arbitrary value of *Re*.
21. N. Hutchins, T. B. Nickels, I. Marusic, M. S. Chong, *J. Fluid Mech.* **635**, 103 (2009).
22. T. B. Nickels, I. Marusic, S. M. Hafez, M. S. Chong, *Phys. Rev. Lett.* **95**, 074501 (2005).
23. T. B. Nickels, I. Marusic, S. M. Hafez, N. Hutchins, M. S. Chong, *Philos. Trans. R. Soc. London Ser. A* **365**, 807 (2007).
24. G. J. Kunkel, I. Marusic, *J. Fluid Mech.* **548**, 375 (2006).
25. I. Marusic, G. J. Kunkel, F. Porté-Agel, *J. Fluid Mech.* **446**, 309 (2001).
26. U. Piomelli, E. Balaras, *Annu. Rev. Fluid Mech.* **34**, 349 (2002).
27. D. Chung, D. I. Pullin, *J. Fluid Mech.* **631**, 281 (2009).
28. M. V. Zagarola, A. J. Smits, *J. Fluid Mech.* **373**, 33 (1998).

29. Supported by Australian Research Council grants FF0668703, DP0984577, and DP1092585.

24 February 2010; accepted 13 May 2010
10.1126/science.1188765

Step-Growth Polymerization of Inorganic Nanoparticles

Kun Liu,[1] Zhihong Nie,[1]* Nana Zhao,[1] Wei Li,[1] Michael Rubinstein,[2]† Eugenia Kumacheva[1,3,4]†

Self-organization of nanoparticles is an efficient strategy for producing nanostructures with complex, hierarchical architectures. The past decade has witnessed great progress in nanoparticle self-assembly, yet the quantitative prediction of the architecture of nanoparticle ensembles and of the kinetics of their formation remains a challenge. We report on the marked similarity between the self-assembly of metal nanoparticles and reaction-controlled step-growth polymerization. The nanoparticles act as multifunctional monomer units, which form reversible, noncovalent bonds at specific bond angles and organize themselves into a colloidal polymer. We show that the kinetics and statistics of step-growth polymerization enable a quantitative prediction of the architecture of linear, branched, and cyclic self-assembled nanostructures; their aggregation numbers and size distribution; and the formation of structural isomers.

The focus of nanoscience is gradually shifting from the synthesis of individual nanoparticles (NPs) to the organization of larger nanostructures. Ensembles of NPs show optical, electronic, and magnetic properties that are determined by collective interactions of individual NPs (*1*). To fully understand and exploit these cooperative properties, it is important to achieve control of the structural characteristics of NP ensembles. Self-assembly has emerged as a promising, cost-efficient methodology for generating different types of nanostructures (*2*–*10*). In particular, one-dimensional (1D) NP arrays have potential applications in optoelectronics (*11*–*15*) and sensing (*16*, *17*). Currently, the lack of models describing the kinetics and statistics of the self-assembly of 1D arrays does not allow the quantitative prediction of their structural features (for instance, the length of NP chains; the degree of branching; or the coexistence of rings, linear chains, and branched structures). Phase diagrams provide useful information on the equilibrium architectures of the linear NP assemblies (*18*); however, they do not currently describe their detailed structural characteristics and do not characterize the kinetics of NP organization.

Recently, several research groups reported on the assembly of colloidal particles in 1D polymerlike structures. Binding of particles into chains was achieved by chemical cross-linking or physical attraction of ligands (*4*, *10*, *19*, *20*), external field-induced attraction between colloids (*9*, *21*), and oriented attachment and fusion of nanocrystals (*22*, *23*). No quantitative approach has been successfully applied to the prediction of chain topology and the kinetics of chain growth. For example, in contrast to step-growth polymerization, the rate of growth of nanowires by oriented attachment of NPs could not be characterized by a characteristic rate constant (*22*), whereas in chemically mediated assembly, the description of the

[1]Department of Chemistry, University of Toronto, 80 Saint George Street, Toronto, Ontario M5S 3H6, Canada. [2]Department of Chemistry, University of North Carolina, Chapel Hill, NC 27599–3290, USA. [3]Institute of Biomaterials and Biomedical Engineering, University of Toronto, 4 Taddle Creek Road, Toronto, Ontario M5S 3G9, Canada. [4]Department of Chemical Engineering and Applied Chemistry, University of Toronto, 200 College Street, Toronto, Ontario M5S 3E5, Canada.

*Present address: Department of Chemistry and Chemical Biology, Harvard University, 12 Oxford Street, Cambridge, MA 02138, USA.

†To whom correspondence should be addressed. E-mail: mr@unc.edu (M.R.); ekumache@chem.utoronto.ca (E.K.)

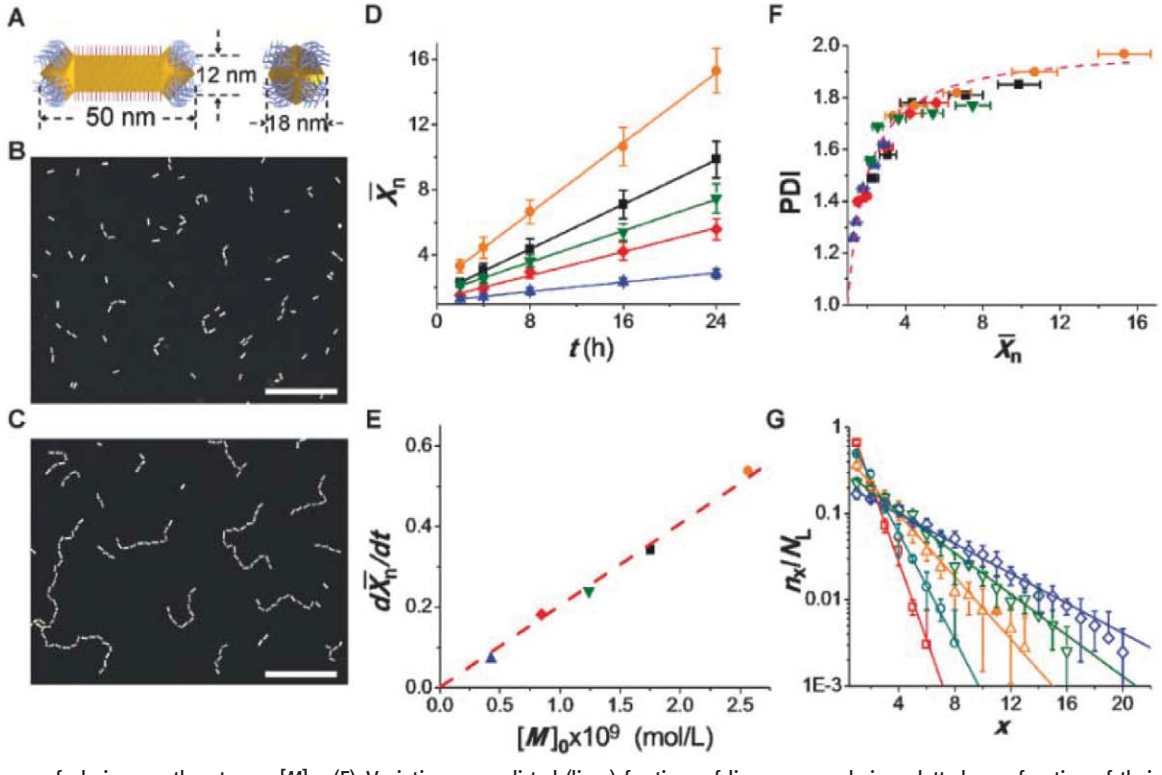

Fig. 1. Growth of colloidal polymer chains. (**A**) Schematics of the side view of the long face (left) and the edge (right) of the NR carrying CTAB on the long side and thiol-terminated PS molecules on the ends. (**B** and **C**) Dark-field TEM images of the NR chains after 2 (B) and 24 (C) hours assembly. $[M]_0 = 0.84 \times 10^{-9}$ (mol/L). Scale bar, 100 nm (both panels). (**D** to **F**) Polymerization of NRs at $[M]_0$ of 0.42×10^{-9} (solid blue triangles), 0.84×10^{-9} (solid red diamonds), 1.24×10^{-9} (solid green inverted triangles), 1.76×10^{-9} (solid black squares), and 2.56×10^{-9} (solid orange circles) (mol/L). (D) Variation in the number average degree of polymerization, $\bar{X}_n$, with time *t*. h, hours. (E) Dependence of chain growth rate on $[M]_0$. (F) Variation in the PDI of the chains with $\bar{X}_n$. The dashed line shows the relation $PDI = (2 - 1/\bar{X}_n)$. For each data point in (D) and (F), the total number of NRs used in the analysis was 5000. (**G**) The experimental (symbols) and theoretically predicted (lines) fractions of linear *x*-mer chains, plotted as a function of their degree of polymerization, *x*, for the time of 2 (open red squares), 4 (open teal circles), 8 (open orange triangles), 16 (open green inverted triangles), and 24 (open blue diamonds) hours. $[M]_0 = 0.84 \times 10^{-9}$ (mol/L). Error bars indicate SD.

kinetics of polymerization was complicated by the ligand-exchange step (*4*).

We report an approach to the quantitative prediction of the structural characteristics of linear, branched, and cyclic ensembles of NPs, as well as their structural isomers. We hypothesized that NPs act as multifunctional monomer units that, in a process analogous to step-growth polymerization, organize themselves into macromolecule-like assemblies. Polymerization occurred because of the formation of reversible (controlled by solvent quality), noncovalent bonds at specific bond angles, and it yielded a colloidal polymer. The growth of NP chains was described by the kinetics and statistics of step-growth polymerization (*24*–*26*), which, for a particular time, allowed the prediction of the aggregation number and the size distribution of NP ensembles, similar to the degree of polymerization and polydispersity index (PDI) of polymers, respectively.

Figure 1A shows the architecture of the individual asymmetric NP. A gold nanorod (NR) was coated with a bilayer of cetyl trimethyl ammonium bromide (CTAB) along its sides, and the two arrowhead edges were coated with thiol-terminated polystyrene (PS) molecules (*10*, *27*). Arrowhead gold NRs with a mean length and width of 50 and 12 nm, respectively, were prepared by seed-mediated synthesis of cylindrical NRs (*28*), followed by the synthesis of two arrowhead ends, each with four {111} facets (figs. S1 and S2) (*29*). Preferential binding of CTAB to the {100} facets of the longitudinal side of the NRs left the {111} facets of the arrowheads deprived of CTAB and allowed for the attachment of thiol-terminated PS molecules to the facets of the arrowheads (*10*). After ligand exchange, the NRs were dispersed in dimethyl formamide, a good solvent for both CTAB and PS.

The self-assembly of the NRs was mediated by reducing the solubility of the PS tethers after adding 15 weight percent of water to the solution of NRs in dimethyl formamide (*10*). To minimize the surface energy of the system in a poor solvent, the hydrophobic PS molecules formed a physical bond between the arrowheads of the neighboring NRs, thereby organizing them into chains (Fig. 1, B and C). The use of PS with an intermediate molecular weight of 12,000 g/mol ensured that the polymer-coated facets of the arrowheads acted as distinct functional groups. In the chains, the length of the bond—defined as the average distance between the facets of the arrowheads of adjacent NRs—was 7.5 ± 0.5 nm. The self-assembly of the NRs was monitored by ultraviolet (UV)–visible spectroscopy (fig. S3) and by the analysis of transmission electron microscopy (TEM) and scanning electron microscopy images of the NR chains on various substrates.

With increasing time *t*, the number of NRs in the chains gradually increased (Fig. 1, B and C) (*30*). Inspection of the TEM images of the chains revealed that most of the NRs reacted as bifunctional monomers and formed one bond per arrowhead: After 24 hours, even at the highest initial NR concentration, the fraction of arrowheads forming two bonds per arrowhead was only 1.4% versus 91% of monoreacted arrowheads (~7.6% of arrowheads did not react). A reduced reactivity of the three remaining facets of the arrowheads after the formation of the first bond was presumably caused by steric hindrance.

We used an analogy to polymer molecules to characterize the evolution of the NR chains by the change in their number-average degree of polymerization ($\overline{X}_n$), weight-average degree of polymerization ($\overline{X}_w$), and PDI as in (*25*)

$$\overline{X}_n = \frac{\sum n_x x}{\sum n_x} \quad \overline{X}_w = \frac{\sum n_x x^2}{\sum n_x x} \quad \text{PDI} = \frac{\overline{X}_w}{\overline{X}_n} \qquad (1)$$

where x is the number of NRs in the chain and n_x is the number of chains containing x NRs. The individual NRs were included in the calculations, and the increasing values of $\overline{X}_n$ or $\overline{X}_w$ reflected conversion of the polymerization reaction.

We initially focused on the linear chains. The initial concentration of active functional groups of the NRs was found as $[M]_0 \approx 2[C_{NR}]_0$, where $[C_{NR}]_0$ is the initial mole concentration of the NRs. The value of $[C_{NR}]_0$ was determined by measuring the intensity of extinction of the NRs at the wavelength corresponding to their longitudinal plasmon-band maximum (table S1) (*31*). In the concentration range of $0.42 \times 10^{-9} \leq [M]_0 \leq 2.56 \times 10^{-9}$ mol/liter, the value of $\overline{X}_n$ increased linearly with time (Fig. 1D). The relation $\overline{X}_n \sim t$ was characteristic of reaction-controlled step-growth polymerization, in which the reactivity of functional groups of the monomers is independent of the chain length [the Flory's assumption (*24*)].

The assembly of the chains occurred at a low rate: At $[M]_0 = 2.56 \times 10^{-9}$ mol/L, the increase of $\overline{X}_n$ by one unit took 6.7×10^3 s (Fig. 1D). The long time of bond formation was caused by the small reactive volume of the arrowheads, the excluded volume repulsion between CTAB-coated sides of the NRs, and the requirement for a particular NR orientation to bond the facets of the arrowhead (*32*).

In the range of initial concentrations of functional groups studied, the variation in the average-number degree of polymerization

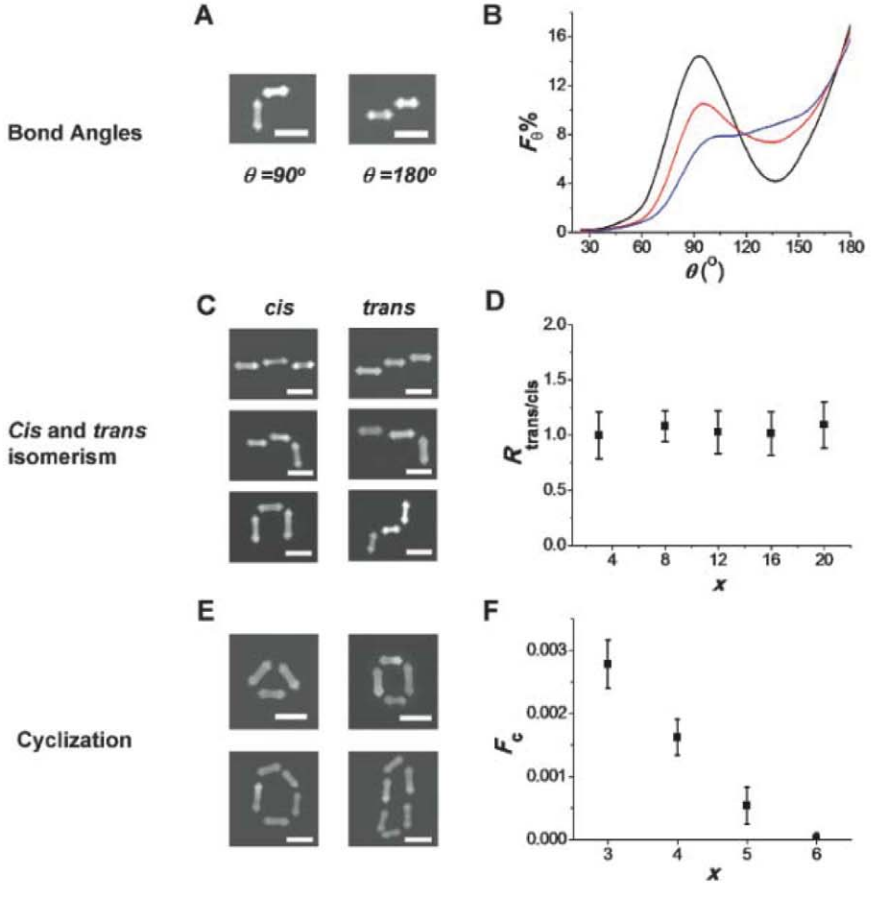

Fig. 2. Structural isomerism of the self-assembled polymer chains. (**A**) TEM images of the NRs linked at a bond angle of θ = 90° (left) and θ = 180° (right). (**B**) Variation in the distribution of bond angles for dimers (black), tetramers (red), and octamers (blue). (**C**) TEM images of the chains with cis-isomers (left) and trans-isomers (right). (**D**) Variation in the ratio of the number of trans-to-cis isomers ($R_{trans/cis}$), plotted as a function of the number of NRs in the chain. (**E**) TEM images of cyclic molecules assembled at $[M]_0 = 0.84 \times 10^{-9}$ (mol/L) and $t = 6$ hours. (**F**) Variation in the fraction of cyclic isomers (F_c), as in (E), plotted for chains with different degrees of polymerization. Scale bars in (A), (C), and (E), 50 nm. Error bars indicate SD.

$\overline{X}_n = 2\,[M]_0 kt + 1$, where k is the rate constant (Fig. 1D), was characteristic of the kinetics of externally catalyzed polymerization of bifunctional monomers with identical functional end groups (*24*). The rate of chain growth, $d\overline{X}_n/dt$, was linearly proportional to the initial concentration of functional groups (Fig. 1E), which yielded a rate constant for the self-assembly process of $k = 2.9 \times 10^4$ $M^{-1}s^{-1}$. For all values of $[M]_0$, the PDI of the growing chains changed as $\mathrm{PDI} = 2 - 1/\overline{X}_n$, approaching the value of two for the nearly complete reaction (Fig. 1F), also characteristic of step-growth polymerization.

For different self-assembly times, we determined the distribution of degrees of polymerization of the chains (equivalent to the distribution of chain lengths). Figure 1G shows the variation in the fraction of x-mers among linear chains (n_x/N_L), where n_x is the number of chains with degree of polymerization x, and N_L is the total number of linear chains in the system at time t. The value of n_x/N_L for linear step-growth polymerization was theoretically determined as in (*33*)

$$n_x/N_L = (1-p)p^{x-1} \qquad (2)$$

where p is the fraction of arrowheads of the NR forming a single bond. (We note that p is the extent of polymerization reaction, equal to the probability of an arrowhead of a NR to form a single bond with another NR at time t.) The value of p as a function of time was determined by analyzing TEM images. A good agreement between the experimental and theoretical values of n_x/N_L (Fig. 1G) implied that the statistics of step-growth polymerization predicted the distribution of chain lengths at different reaction times.

The self-assembly of the NRs generated several types of structural isomers. First, in chains with a low degree of polymerization ($x \leq 4$) most of the NRs were aligned with their long axes either parallel or perpendicular to each other (that is, with a bond angle $\theta = 90°$ or 180°, respectively) (Fig. 2, A and B). The distribution of bond angles resulted in two energy minima and the formation of structures resembling trans-gauche isomers. With increasing x, the fraction of bond angles of $\theta = 90°$ diminished because of the stronger stretching of the longer chains on the surface, caused by the surface tension–driven flow. Second, due to the existence of facets on the arrowheads, the preceding and subsequent NRs attached to the two opposite arrowheads of a particular NR were in a cis- or a trans-position with respect to each other (Fig. 2C). Cis- and trans-isomers randomly alternated along the chain, and for $x \leq 20$, the relative ratio ($R_{cis/trans}$) of cis-to-trans isomers was close to a unit (Fig. 2D). Third, we also observed a small (below 0.5%) number of cyclic polymers forming triangles, squares, pentagons, or hexagons (Fig. 2E). With an increasing degree of polymerization of the chains, the fraction of cycles reduced (Fig. 2F). A low fraction of cycles stemmed from the low probability of the assembly of all the NRs in the cycle at specific bond angles. For example, the probability of the formation of the tetramer cycle was estimated as $P_{c\text{-}tetra} = P_{90}{}^3 \times P_f^2$, where P_{90} is the average probability of attaching an ith and the $(i-1)$th NRs at a bond angle $\theta = 90°$, and P_f is the average probability of linking an ith NR to a particular facet of the arrowhead of the $(i-1)$th NR, so that the ith NR was located in the plane determined by the $(i-1)$th and $(i-2)$th NRs. The value $P_{90} = 0.26$ was found by integrating the area below the angle distribution curve for tetramer chains at $75° \leq \theta \leq 105°$ (Fig. 2B), and the value of $P_f = 1/4$ was used for four equally reactive facets on each arrowhead of the NR for $i > 2$. The value of $P_{c\text{-}tetra}$ was estimated to be 1.2×10^{-3}, in agreement with the experimentally determined fraction of tetramer rings of 1.4×10^{-3} among chains with $x = 4$.

The value of the bond angle of 90° led to reduced strain in small cycles, in comparison with carbon-based polymers. In addition, mismatch of the bond angles with respect to the optimal angles between the arrowhead facets could result in a larger surface energy of PS molecules in a poor solvent. Linkage of the NRs with PS molecules exposed to the solvent allowed for the adjustment of the bond angles between the facets to minimize the energy of the system.

We analyzed the structure of branched NR chains formed at $t = 24$ hours and $[M]_0 = 2.56 \times 10^{-9}$ mol/L. Approximately 30% of the chains formed three-arm stars [~5% of the chains had two branches, similar to H-polymers (*33*)] (Fig. 3A). For star chains, the PDI of 1.25 ± 0.14 was lower than the PDI of the linear chains with an identical degree of polymerization, and it was close to the expected value of 1.33 (*33*). To characterize the architecture of star assemblies, we denoted the degrees of polymerization of the long, medium, and short arms of the chains as X_L, X_M, and X_S, respectively (Fig. 3A, top). The number average degrees of polymerization of the arms were 16, 8, and 3, in very good agreement with the theoretical predictions of 17, 8, and 4, respectively, as determined in (*33*)

$$\overline{X}_L = \frac{1 + 2p + 3p^2 + 3p^3 + 2p^4}{(1-p^2)(1+p+p^2)} \qquad (3)$$

where $p = 0.9$ (for $\overline{X}_M$ and $\overline{X}_S$, see eqs. S8 and S10). In addition, we characterized the distribution of arm lengths by determining the fraction of each arm as a function of its degree of polymerization (Fig. 3B). The fractions of the long, medium, and short arms (P_L, P_M, and P_S, respectively) were theoretically predicted using the statistics of polymerization of branched poly-

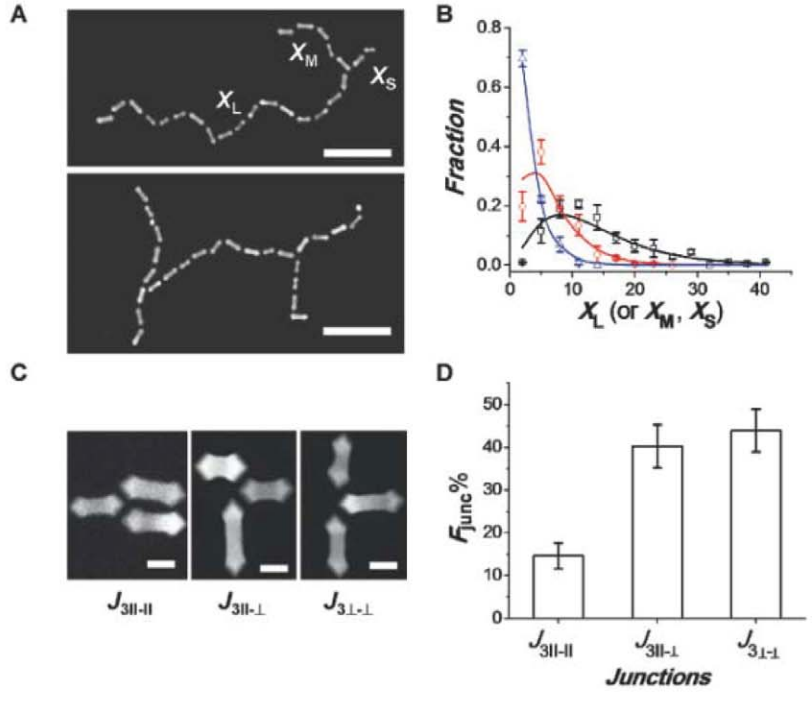

Fig. 3. Structure of branched NR chains. (**A**) TEM images of three-arm star polymer (top) and H-shaped polymer (bottom). The corresponding degrees of polymerization of the long, medium, and short arms of the star polymers are denoted as X_L, X_M, and X_S, respectively. Scale bars, 200 nm. (**B**) Experimentally determined fractions of long (black squares), medium (red circles), and short (blue triangles) arms of star polymers, plotted as a function of the corresponding degrees of polymerization. Solid lines show the corresponding theoretically estimated fractions of the long (Eq. 4), medium, and short arms (eqs. S7 and S9). (**C**) TEM images of the junctions at branching points in NR chains. The subscripts in the notations define the number of NRs in the junction and the orientation of NRs with respect to each other. Scale bars, 20 nm. (**D**) Distribution of the fractions of junctions with different orientations of NRs for $t = 24$ hours and $[M]_0 = 2.56 \times 10^{-9}$ mol/L. Error bars indicate SD.

mers (Eq. 4 and eqs. S7 and S9, respectively). For example, the fraction of the long arm with degree of polymerization X_L was determined as in (*33*)

$$P_L(X_L) = \frac{p^{X_L}\sum_{X_M=1}^{X_L} p^{X_M}\sum_{X_S=1}^{X_M} p^{X_S}}{\sum_{X_L=1}^{\infty} p^{X_L}\sum_{X_M=1}^{X_L} p^{X_M}\sum_{X_S=1}^{X_M} p^{X_S}} = (1-p^3)(p^{X_L-1}-p^{2X_L-1}-p^{2X_L}+p^{3X_L}) \quad (4)$$

The experimental and theoretical distributions of the arm length in star molecules were in good agreement (Fig. 3B).

In the branching points, we observed three types of mutual orientation of the NRs (Fig. 3C). We labeled the junctions as $J_{3||-||}$, $J_{3\perp-\perp}$, and $J_{3||-\perp}$ where the number 3 in the subscripts denotes the number of NRs in the junction, and the symbols ||-||, ⊥-⊥, and ||-⊥ reflect two parallel, two perpendicular, and one parallel/one perpendicular NR alignments, respectively. The histogram of the fractions of each type of junction in the chains showed a lower fraction of $J_{3||-||}$ junctions in comparison with $J_{3\perp-\perp}$ and $J_{3||-\perp}$ junctions (Fig. 3D), due to the steric constraints in attaching the second NR in the parallel orientation to the reacted arrowhead.

The polymerization model was applicable to the self-assembly of arrowhead and cylindrical gold NRs (*28*), with a length in the range from 30 to 50 nm, which were end-tethered with PS molecules with a molecular weight ranging from 5000 to 20000 g/mol. We anticipate that the approach can be applied to the organization of other types of NPs, as long as their self-assembly follows a reaction-limited process.

This work bridges the gap between polymerization reactions taking place at a molecular level and NP self-assembly occurring at the length scale two orders of magnitude larger. It shows that the theory of step-growth polymerization is valid for the assembly of NPs linked by physical bonds. The polymerization approach enables pre-programming the dimensions of 1D nanostructures by assembling NP chains with a predetermined length. It can facilitate the design of new, complex nanostructures by mimicking a large library of polymers produced by step-growth polymerization, e.g., hyperbranched (dendritic) polymers, polymer networks, and copolymerization of different NPs (e.g., metal and semiconductor NPs) with a high degree of control over the structure of alternating, block and graft-copolymers. Owing to the progress in NP synthesis, the self-assembly of NPs with asymmetric functional groups can be explored and modeled using the theory developed for polymerization of more complex monomers. On the other hand, the capability to visualize the polymerization process by imaging emerging nanostructures provides the unique ability to test theoretical models developed for step-growth polymerization.

References and Notes

1. Z. Nie, A. Petukhova, E. Kumacheva, *Nat. Nanotechnol.* **5**, 15 (2010).
2. S. C. Glotzer *et al.*, *Curr. Opin. Colloid Interface Sci.* **10**, 287 (2005).
3. S. C. Glotzer, M. J. Solomon, *Nat. Mater.* **6**, 557 (2007).
4. G. A. DeVries *et al.*, *Science* **315**, 358 (2007).
5. W. U. Huynh, J. J. Dittmer, A. P. Alivisatos, *Science* **295**, 2425 (2002).
6. M. Rycenga, J. M. McLellan, Y. Xia, *Adv. Mater.* **20**, 2416 (2008).
7. Z. Tang, N. A. Kotov, M. Giersig, *Science* **297**, 237 (2002).
8. A. Courty, A. Mermet, P. A. Albouy, E. Duval, M. P. Pileni, *Nat. Mater.* **4**, 395 (2005).
9. D. Zerrouki, J. Baudry, D. Pine, P. Chaikin, J. Bibette, *Nature* **455**, 380 (2008).
10. Z. Nie *et al.*, *Nat. Mater.* **6**, 609 (2007).
11. S. A. Maier *et al.*, *Nat. Mater.* **2**, 229 (2003).
12. S. A. Maier *et al.*, *Adv. Mater.* **13**, 1501 (2001).
13. W. Nomura, M. Ohtsu, T. Yatsui, *Appl. Phys. Lett.* **86**, 181108 (2005).
14. C.-J. Wang, L. Huang, B. A. Parviz, L. Y. Lin, *Nano Lett.* **6**, 2549 (2006).
15. T. Yatsui *et al.*, *Appl. Phys. Lett.* **96**, 133106 (2010).
16. J. N. Anker *et al.*, *Nat. Mater.* **7**, 442 (2008).
17. G. Kawamura, Y. Yang, M. Nogami, *Appl. Phys. Lett.* **90**, 261908 (2007).
18. Z. Nie, D. Fava, M. Rubinstein, E. Kumacheva, *J. Am. Chem. Soc.* **130**, 3683 (2008).
19. M. E. Leunissen *et al.*, *Nat. Mater.* **8**, 590 (2009).
20. K. K. Caswell, J. N. Wilson, U. H. F. Bunz, C. J. Murphy, *J. Am. Chem. Soc.* **125**, 13914 (2003).
21. K. D. Hermanson, S. O. Lumsdon, J. P. Williams, E. W. Kaler, O. D. Velev, *Science* **294**, 1082 (2001).
22. C. Ribeiro, E. J. H. Lee, E. Longo, E. R. Leite, *ChemPhysChem* **7**, 664 (2006).
23. S. Shanbhag, Z. Tang, N. A. Kotov, *ACS Nano* **1**, 126 (2007).
24. P. J. Flory, *Principles of Polymer Chemistry* (Cornell Univ. Press, New York, 1953).
25. G. Odian, *Principles of Polymerization* (Wiley, New York, ed. 4, 2004).
26. S. Kuchanov, H. Slot, A. Stroeks, *Prog. Polym. Sci.* **29**, 563 (2004).
27. Materials and methods are available as supporting material on *Science* Online.
28. B. Nikoobakht, M. A. El-Sayed, *Chem. Mater.* **15**, 1957 (2003).
29. Y. Xiang *et al.*, *J. Phys. Chem. C* **112**, 3203 (2008).
30. Evidence that chain formation occurred in solution, as opposed to being caused by solvent evaporation, was obtained in light-scattering and UV-visible spectroscopy experiments, as well as in the control experiments conducted at different solvent evaporation rates and on different substrates.
31. C. J. Orendorff, C. J. Murphy, *J. Phys. Chem. B* **110**, 3990 (2006).
32. In the control experiments, the time of bond formation was markedly reduced for the self-assembly of cylindrical Au nanorods end-terminated with thiolated PS, which did not require specific orientation of the NR during bond formation.
33. M. Rubinstein, R. H. Colby, *Polymer Physics* (Oxford Univ. Press, Oxford, 2003).

34. We thank the National Science and Engineering Research Council of Canada (under Discovery program and Canada Research Chair program) for financial support. M.R. acknowledges financial support from the NSF under grants CHE-0911588, DMR-0907515, and CBET-0609087 and the NIH under grant 1-R01-HL077546-03A2. The authors are grateful to Y. Chen and G. Wu for their contribution in image analysis.

Supporting Online Material

www.sciencemag.org/cgi/content/full/329/5988/197/DC1
Materials and Methods
SOM Text
Figs. S1 to S3
Tables S1
References

11 March 2010; accepted 2 June 2010
10.1126/science.1189457

Deepwater Formation in the North Pacific During the Last Glacial Termination

Y. Okazaki,[1] A. Timmermann,[2]* L. Menviel,[2] N. Harada,[1] A. Abe-Ouchi,[1,3] M. O. Chikamoto,[1] A. Mouchet,[4] H. Asahi[3]

Between ~17,500 and 15,000 years ago, the Atlantic meridional overturning circulation weakened substantially in response to meltwater discharges from disintegrating Northern Hemispheric glacial ice sheets. The global effects of this reorganization of poleward heat flow in the North Atlantic extended to Antarctica and the North Pacific. Here we present evidence from North Pacific paleo surface proxy data, a compilation of marine radiocarbon age ventilation records, and global climate model simulations to suggest that during the early stages of the Last Glacial Termination, deep water extending to a depth of ~2500 to 3000 meters was formed in the North Pacific. A switch of deepwater formation between the North Atlantic and the North Pacific played a key role in regulating poleward oceanic heat transport during the Last Glacial Termination.

Massive meltwater discharges during the Last Glacial Termination [~19 to 10 thousand years ago (ka)], such as Heinrich event 1 (H1: ~17.5 to 15 ka) and the Younger Dryas event (YD: ~13 to 11.5 ka), reduced North Atlantic surface density conditions and interrupted the steady flow of the Atlantic meridional overturning circulation (AMOC) (*1*). Through atmospheric and oceanic teleconnections, climate conditions changed substantially in the North Pacific, as documented by numerical climate modeling studies (*2*–*4*) and paleo-proxy data (*5*, *6*).

Recent studies (*7*–*11*) using data obtained from single-sediment cores in the North Pacific reported local evidence for major reorganizations of the North Pacific Ocean circulation during H1, the Bølling-Allerød (BA: ~14.5 to 13 ka) warm period, and the YD. The interpretation of radiocarbon data in these cores reveals that during H1,

very old water masses seeped into intermediate layers of the eastern tropical Pacific, whereas the western North Pacific sites near Japan show relatively young radiocarbon ventilation ages at intermediate depths (1000 to 2000 m). Understanding the mechanisms by which old carbon-rich water from the deep North Pacific was vented to the surface and replaced by younger water masses may also hold important clues toward resolving the puzzle of the carbon sources that caused the rise of atmospheric CO_2 during the last deglaciation.

The goal of this study is to provide a more comprehensive view of what triggered ventilation changes in the North Pacific during the early deglaciation and to reconstruct spatial patterns and pathways of intermediate-deepwater circulation. For these purposes, we compiled a comprehensive data set of published radiocarbon sediment core data from the North Pacific with temporal coverage large enough to resolve the H1/BA transition (*12*). Together with a climate model simulation that mimics H1, we used these data to determine the effects of AMOC changes on the large-scale conveyor-belt circulation, with an emphasis on the North Pacific.

To better understand the driving mechanisms of North Pacific circulation changes, we provide an overview of North Pacific climate conditions during the Last Glacial Termination (Fig. 1). During H1, a time of weak AMOC (Fig. 1A) (*1*), the eastern subarctic Pacific was warm and relatively saline, as documented by dinocyst assemblages in core PAR87A-10 [54.36°N, 148.47°W, 3664-m water depth (*13*)] (Fig. 1, B and C). Planktonic foraminiferal Mg/Ca and $\delta^{18}O$ analyses in core GH02-1030 [42.23°N, 144.21°E, 1212-m water depth (*14*)] in the western North Pacific reveal the presence of cold and saline surface waters during the early deglaciation (Fig. 1, D and E).

As documented by these analyses, salinity dropped in the eastern and western North Pacific after ~16 thousand years, attaining minimum values during BA. By accounting for dating uncertainties among the different cores, we found that the drop of surface salinity during the H1/BA transition coincided with an increase in near-bottom phosphate contents inferred from benthic foraminiferal $\delta^{13}C$ values in cores MR01K03-PC4 from the western North Pacific [41.12°N, 142.40°E, 1366-m water depth (*15*)] and BOW9A from the Bering Sea (54.04°N, 178.68°E, 2391-m water depth) (Fig. 1F). This change in the western North Pacific indicates a transition from nutrient-depleted and well-ventilated intermediate-deep waters during H1 to nutrient-enriched less-ventilated waters during BA.

The reduced abundance of dysaerobic benthic foraminiferal taxa in the Bering Sea core BOW9A during H1 compared with that in the BA period (*16*) is also consistent with the notion of enhanced deepwater ventilation extending to a depth of ~2500 m (Fig. 1G). Oxygen-rich intermediate-deep waters during H1 were also reconstructed

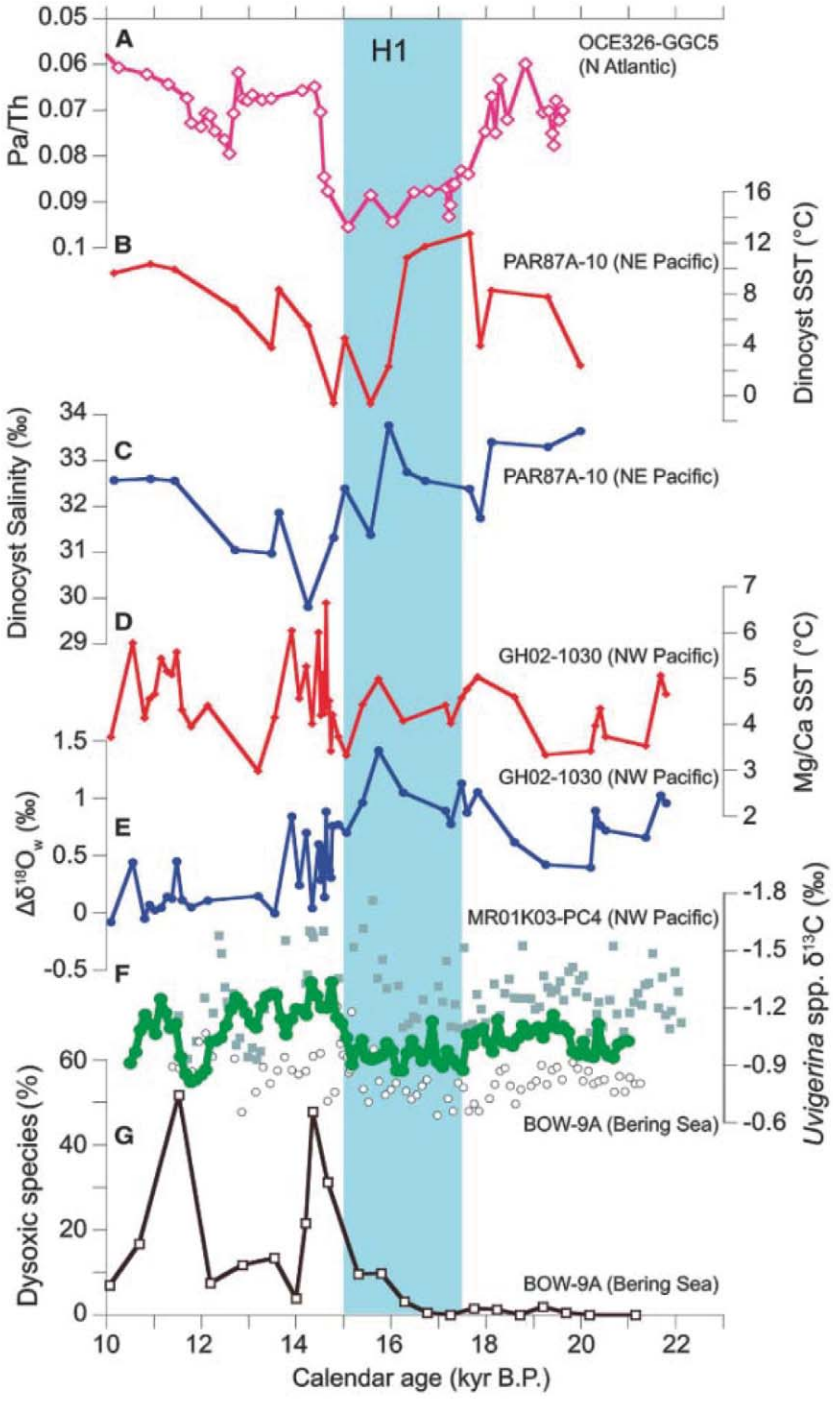

Fig. 1. Sediment proxy records in the North Pacific from 23 to 10 ka on their re-established time scales (table S2) with (**A**) Pa/Th ratio as a proxy for the AMOC strength in the North Atlantic (*1*); sea-surface temperature and salinity changes in (**B** and **C**) the eastern North Pacific based on dinocyst assemblages (*13*) and in (**D** and **E**) the western North Pacific based on planktonic foraminiferal Mg/Ca and $\delta^{18}O$ (*14*); (**F**) raw benthic foraminiferal $\delta^{13}C$ data in the western North Pacific (*15*) (1366 m, gray squares), the Bering Sea (2391 m, open circles), and spline-interpolated and averaged benthic $\delta^{13}C$ values (green circles); and (**G**) percentage of dysaerobic benthic foraminifera species in the Bering Sea (2391 m) (*16*).

[1]Japan Agency for Marine-Earth Science and Technology, 2-15 Natsushima-cho, Yokosuka 237-0061, Japan. [2]International Pacific Research Center, School of Ocean and Earth Science and Technology, University of Hawaii, 2525 Correa Road, Honolulu, HI 96822, USA. [3]Atmosphere and Ocean Research Institute, University of Tokyo, 5-1-5 Kashiwanoha, Kashiwa 277-8568, Japan. [4]Université de Liège, Laboratoire de physique atmosphérique et planétaire, Allée du Six-Août 17, BAT B5C, 4000 Liège, Belgium.

*To whom correspondence should be addressed. E-mail: axel@hawaii.edu

from benthic foraminiferal assemblages (*17*) and redox-sensitive metals (*18*) in records from the western North Pacific. Because the millennial-scale variations in oxygen concentrations found in these cores are out of phase with those obtained from deeper sites in the North Pacific (ODP882 at 3200 m, and ODP887 at 3600 m) (*9*), we estimate the maximum vertical extent of North Pacific intermediate to deep water spreading during H1 to be ~3000 m. When this value is compared with present-day values of about 800 m (*19*), it becomes evident that such changes would have required a major reorganization of the entire North Pacific ocean circulation.

To develop a better understanding of the nature of ocean circulation changes during the deglaciation, we compiled published radiocarbon data from 29 intermediate-deepwater cores in the North Pacific (table S1). ^{14}C ages were converted to calendar ages on planktonic foraminifera samples from these cores using the Calib 6.0 routine with the Marine09 calibration data set (*20*). Ventilation ages estimated from ^{14}C age differences between coexisting benthic and planktonic foraminifera shells (BF–PF age), projection ages (*21*) (table S3), and reconstructed bottom water Δ^{14}C activities (*9*) (table S4) were then calculated for all cores.

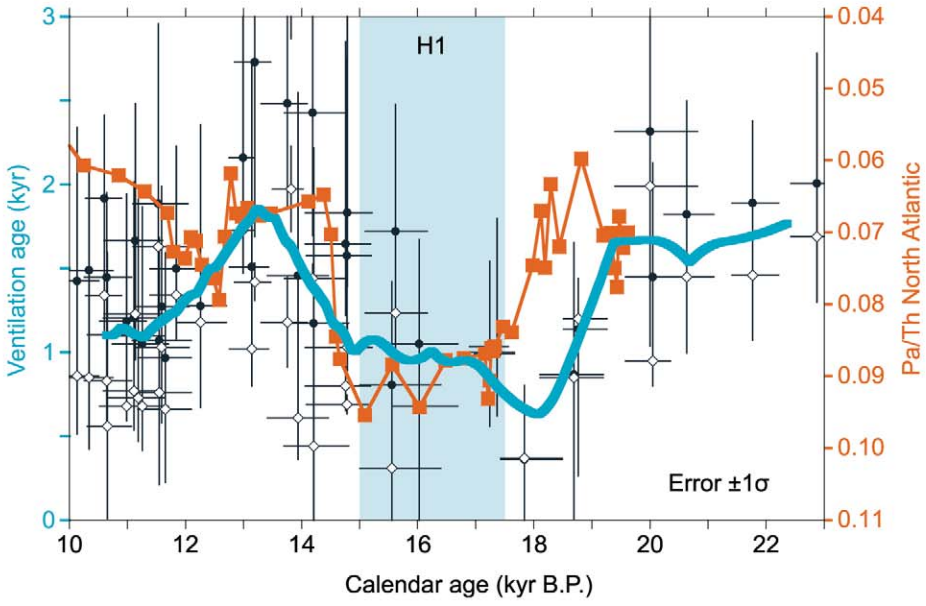

Fig. 2. Compilation of ventilation age changes based on published radiocarbon data in the western North Pacific (*8*, *14*, *30*–*32*). BF–PF ages (open diamonds), projection ages (gray circles), and smoothed spline interpolation of averaged BF–PF and projection ages (blue line). Uncertainty of calendar age and ventilation age is 1σ; Pa/Th ratio (orange squares) as a proxy for the AMOC strength in the North Atlantic (*1*).

The compilation of western North Pacific radiocarbon ages (Fig. 2, for depth range 900 to 2800 m) reveals notable changes in deepwater ventilation during the last deglaciation. By averaging radiocarbon age estimates derived from the projection method and the BF–PF method, we obtained ventilation age estimates for the Last Glacial Maximum (LGM: ~23 to 19 ka), H1 (~17.5 to 15 ka), and BA (14.5 to 13 ka) periods of ~1500 years, ~950 years, and ~1550 years, respectively. The ~600-year drop in ventilation age between the LGM and H1 is significantly larger than the typical one-sided uncertainties in the projection method during this time (385 years), which supports the notion of a major reorganization of North Pacific intermediate-deepwater flow during H1.

No coherent averaged projection and BF–PF age ventilation changes were observed between the LGM (~1540 years), H1 (~1450 years), and BA (~1600 years) in the eastern North Pacific (900 to 2800 m) (table S5 and fig. S6). These findings for the western and eastern North Pacific are consistent with reconstructed bottom water Δ^{14}C activities (table S5). The presence of a well-ventilated water mass above 2000 m, the so-called glacial North Pacific intermediate water (GNPIW), has been suggested previously for LGM conditions (*22*, *23*), with the Bering Sea being the source of this water mass (*24*). Our reconstructed ventilation changes during H1 show a much more pronounced reorganization of deep western North Pacific flow.

To explore how this reorganization of deep North Pacific flow in response to changes of the AMOC came about, freshwater perturbation experiments were conducted with the Earth system model of intermediate complexity LOVECLIM (version 1.1) (*25*, *26*) under both preindustrial and LGM background conditions. These experiments enabled us to compare simulated changes in radiocarbon with those reconstructed by the sediment core compilation (table S3). The freshwater perturbation experiments simulate the climate response to an idealized glacial meltwater pulse that mimics H1. By linearly increasing the freshwater forcing to 2 Sv in the northern North Atlantic for 100 years, the water becomes less dense, leading to a reduction of deep convection in the North Atlantic and a subsequent collapse of the AMOC. An associated reduction of poleward heat transport leads to large-scale cooling in the Northern Hemisphere, as in other climate models (*2*–*4*). Air-sea interactions in the North Atlantic and emanating atmospheric teleconnections are vital for cooling the western North Pacific (*4*). Furthermore, in response to the AMOC weakening and the associated North Atlantic cooling, the Atlantic-Pacific moisture transport weakens (*25*) and the Pacific Intertropical Convergence Zone shifts south, leading to a persistent reduction of precipitation and hence an overall increase of surface salinity in the North Pacific. Once the Pacific meridional overturning cell (PMOC) establishes, the anomalous poleward surface currents (fig. S3) transport more saline subtropical waters into the North Pacific, thereby providing a positive-salinity feedback. A closed Bering Strait facilitates the build-up of such North Pacific salinity anomalies (*27*). The resulting changes in surface density trigger deep oceanic convection in the subarctic Pacific. The three-dimensional adjustment to the resulting North Pacific density anomalies in the preindustrial and LGM LOVECLIM1.1 freshwater perturbation experiment leads to the establishment of a deep PMOC (Fig. 3B and fig. S2), which distributes young and oxygen-rich deep water throughout the entire western North Pacific down to ~2500 m (Fig. 3B), in accordance with reconstructions of oxygen conditions in BOW9A (Fig. 1G).

Both model results (Fig. 3C) and paleo reconstructions (Fig. 1, B and D) suggest the existence of an east-west sea surface temperature gradient in the North Pacific during H1. The simulated cooling in the western North Pacific can be partly explained in terms of an intensification of the Aleutian Low (*4*) and cold-air advection. Simulated warming in the eastern North Pacific results from an enhanced poleward advection of heat, which is associated with the northeastward-flowing surface branch of the PMOC (Fig. 3C). Moreover, a very pronounced east-west gradient in intermediate-deepwater ventilation (Fig. 3D) is found, both in the paleoproxy reconstructions and the modeling experiments. The main simulated pathway of deepwater circulation is along the western margin of the North Pacific, in a deep western boundary current that is analogous to the one currently in the North Atlantic. The model results demonstrate that the western boundary flow is the principal factor in establishing the east-west gradient of intermediate-deep Pacific ventilation, which is also evident in the compilation of radiocarbon-based ventilation data (Fig. 3, A and D).

However, simulated radiocarbon age anomalies associated with the onset of the PMOC are too weak to explain the data from recent eastern Pacific intermediate-depth sediment cores (*10*, *11*) that reveal the presence of extremely old

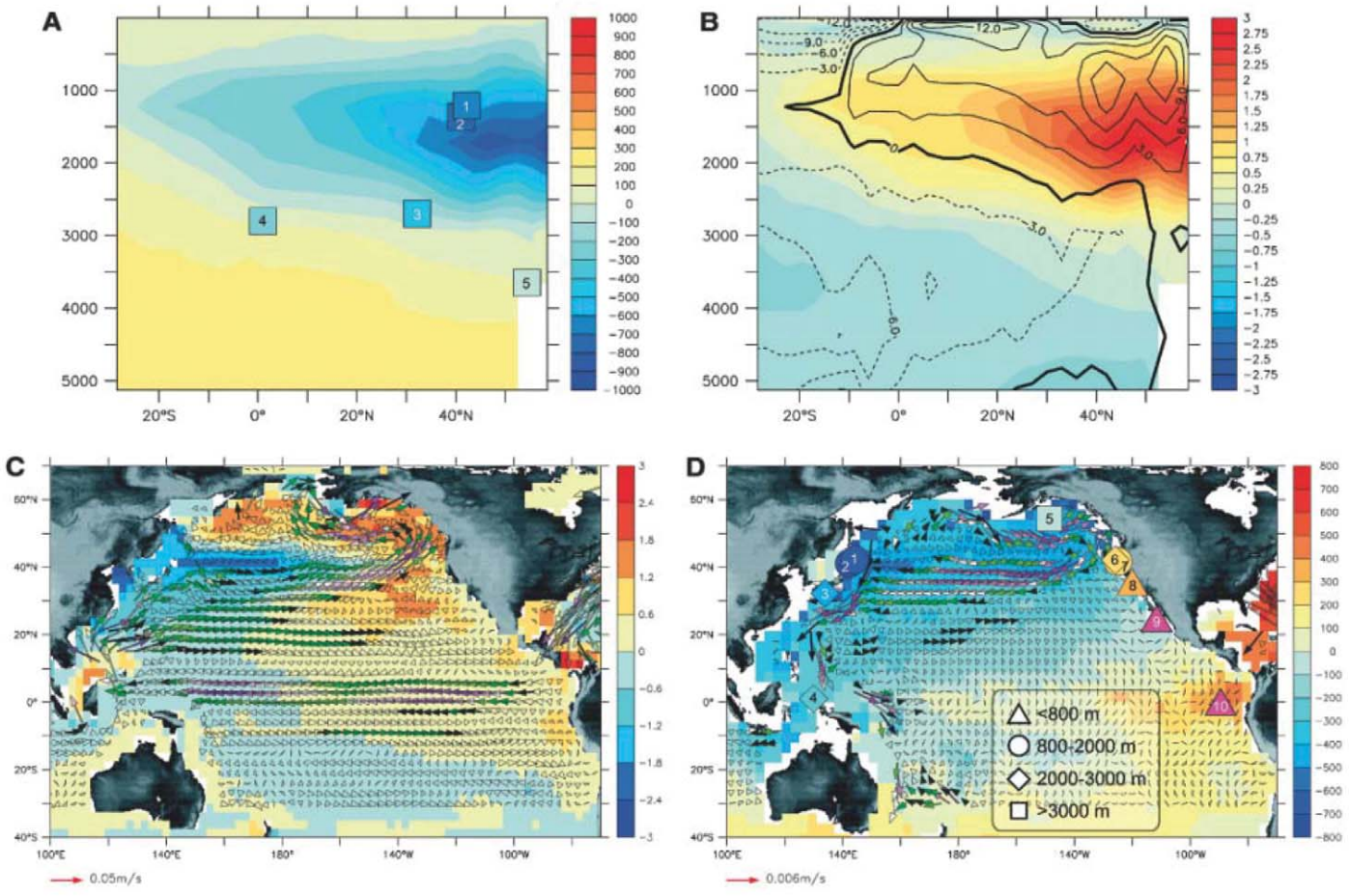

Fig. 3. (**A**) The shading indicates the sections of zonally averaged simulated radiocarbon age anomalies (in years) in the North Pacific between a collapsed AMOC state (years 400 to 500 of the freshwater experiment) and the control simulation using preindustrial background conditions. The squares indicate the reconstructed projection age anomaly (in years) (colored shading) of western North Pacific cores (*8*, *9*, *14*, *31*, *33*) (numbers of cores refer to table S1). (**B**) Shading indicates simulated zonally averaged Pacific oxygen anomalies (in ml oxygen per l of water) between a collapsed AMOC state (years 400 to 500 of the freshwater experiment) and the preindustrial control simulation. The contours indicate the simulated Pacific mean meridional stream function (10^6 m^3/s) (years 400 to 500 of the freshwater experiment). (**C**) Simulated upper ocean (0 to 65 m) temperature (shading) (°C) and velocity (vectors) (m/s) anomalies between collapsed AMOC state (years 400 to 500 of the freshwater perturbation experiment) and control simulation, using preindustrial background conditions. (**D**) Colored symbols indicate the projection age anomalies (in years) between H1 and the LGM (*8*–*11*, *14*, *31*, *33*–*35*) of radiocarbon data used in this analysis (numbers in symbols refer to table S1). The shading indicates simulated deep (1225 to 2963 m) minus near-surface (0 to 20 m) radiocarbon age anomalies (in years) between collapsed AMOC state (years 400 to 500 of the freshwater perturbation experiment) and control simulation. The arrows indicate the anomalous deep ocean currents averaged between 1225 and 2963 m.

intermediate water. To explain the very old eastern tropical Pacific intermediate waters during H1, a process unrelated to the onset of a PMOC has to be invoked (*11*).

The match between the simulated ventilation age anomalies in the western North Pacific and those reconstructed from a compilation of radiocarbon records (Fig. 3, A and D) makes a compelling case for the existence of a deep PMOC during H1 and an associated see-saw in deepwater formation between the North Atlantic and Pacific.

In our preindustrial and LGM freshwater perturbation experiments, the PMOC is maintained by the poleward advection of salinity from the subtropical regions (fig. S3) (*3*, *28*), a southward shifted Intertropical Convergence Zone, and reduced atmospheric export of fresh water from the Atlantic to the Pacific (*25*). As a result of the reorganization of the global conveyor belt circulation, the simulated Indonesian Throughflow weakens by 30 to 50% (*25*), which leads to a strengthening of the Kuroshio and the intrusion of North Pacific Intermediate Water into the tropical Pacific intermediate layers (*29*).

The shutdown of the AMOC in our model reduces the Atlantic heat transport at 40°N by ~0.6 PW (1 PW = 10^{15} W). At the same time, and in response to the establishment of a PMOC, poleward heat transport in the Pacific at 40°N increases by 0.4 PW. The PMOC hence played an important role in buffering the decrease in the poleward global oceanic heat transport caused by the shutdown of the AMOC. The evidence presented here demonstrates that the North Pacific was a very active region of thermohaline flow during the deglaciation and operated out of phase with the North Atlantic (Fig. 2). Viewing the North Pacific as participating in the ventilation of the global oceans could also help to explain the release of old carbon during the Last Glacial Termination.

References and Notes

1. J. F. McManus, R. Francois, J. M. Gherardi, L. D. Keigwin, S. Brown-Leger, *Nature* **428**, 834 (2004).
2. U. Mikolajewicz, T. J. Crowley, A. Schiller, R. Voss, *Nature* **387**, 384 (1997).
3. O. A. Saenko, A. Schmittner, A. J. Weaver, *J. Clim.* **17**, 2033 (2004).
4. Y. M. Okumura, C. Deser, A. Hu, A. Timmermann, S. P. Xie, *J. Clim.* **22**, 1424 (2009).
5. T. Kiefer, M. Kienast, *Quat. Sci. Rev.* **24**, 1063 (2005).
6. E. A. Boyle, L. Keigwin, *Nature* **330**, 35 (1987).
7. M. Sarnthein, P. M. Grootes, J. P. Kennett, M.-J. Nadeau, in *Ocean Circulation: Mechanisms and Impacts*, A. Schmittner, J. C. H. Chiang, S. R. Hemming, Eds. (American Geophysical Union, Washington, DC, 2007), pp. 175–197.
8. N. Ahagon, K. Ohkushi, M. Uchida, T. Mishima, *Geophys. Res. Lett.* **30**, 2097 (2003).
9. E. D. Galbraith *et al.*, *Nature* **449**, 890 (2007).

10. T. M. Marchitto, S. J. Lehman, J. D. Ortiz, J. Flückiger, A. van Geen, *Science* **316**, 1456 (2007).
11. L. Stott, J. Southon, A. Timmermann, A. Koutavas, *Paleoceanography* **24**, PA2223 (2009).
12. Materials and methods are available as supporting material on *Science* Online.
13. A. de Vernal, T. F. Pedersen, *Paleoceanography* **12**, 821 (1997).
14. T. Sagawa, K. Ikehara, *Geophys. Res. Lett.* **35**, L24702 (2008).
15. M. Hoshiba *et al*., *Mar. Micropaleontol.* **61**, 196 (2006).
16. Y. Okazaki *et al*., *Deep Sea Res. Part II Top. Stud. Oceanogr.* **52**, 2150 (2005).
17. A. Shibahara, K. Ohkushi, J. P. Kennett, K. Ikehara, *Paleoceanography* **22**, PA3213 (2007).
18. J. Crusius, T. F. Pedersen, S. Kienast, L. Keigwin, L. Labeyrie, *Geology* **32**, 633 (2004).
19. L. D. Talley, *J. Phys. Oceanogr.* **23**, 517 (1993).
20. P. J. Reimer *et al*., *Radiocarbon* **51**, 1111 (2009).
21. J. F. Adkins, E. A. Boyle, *Paleoceanography* **12**, 337 (1997).
22. L. D. Keigwin, *Paleoceanography* **13**, 323 (1998).
23. K. Matsumoto, T. Oba, J. Lynch-Stieglitz, H. Yamamoto, *Quat. Sci. Rev.* **21**, 1693 (2002).
24. K. Horikawa, Y. Asahara, K. Yamamoto, Y. Okazaki, *Geology* **38**, 435 (2010).
25. U. Krebs, A. Timmermann, *J. Clim.* **20**, 4940 (2007).
26. L. Menviel, A. Timmermann, A. Mouchet, O. Timm, *Paleoceanography* **23**, PA1203 (2008).
27. A. Hu, G. A. Meehl, W. Han, *Geophys. Res. Lett.* **34**, L05704 (2007).
28. H. M. Stommel, *Tellus* **13**, 224 (1961).
29. J. P. McCreary Jr., P. Lu, *J. Phys. Oceanogr.* **31**, 932 (2001).
30. J. C. Duplessy *et al*., *Radiocarbon* **31**, 493 (1989).
31. M. Murayama, A. Taira, H. Iwakura, E. Matsumoto, T. Nakamura, *Summaries of Researches Using AMS at Nagoya University* (Nagoya University Center for Chronological Research, Nagoya, Japan, vol. 3, 1992), pp. 114–121.
32. K. Minoshima *et al.*, *Mater. Atoms* **259**, 448 (2007).
33. W. Broecker, E. Clark, S. Barker, *Earth Planet. Sci. Lett.* **274**, 322 (2008).
34. A. C. Mix *et al*., in *Mechanisms of Global Climate Change at Millennial Time Scales*, P. U. Clark, R. S. Webb, L. D. Keigwin, Eds. (American Geophysical Union, Washington, DC, 1999), pp. 127–148.
35. J. P. Kennett, B. L. Ingram, *Nature* **377**, 510 (1995).
36. This research was supported by NSF grant number ATM-0712690. Additional support was provided by the Japan Agency for Marine-Earth Science and Technology (JAMSTEC), by NASA through grant number NNX07AG53G, and by the National Oceanic and Atmospheric Administration through grant number NA09OAR4320075, all of which sponsor research at the International Pacific Research Center. A.M. acknowledges funding from the Belgian Federal Science Policy (contract SD/CS/01).

Supporting Online Material

www.sciencemag.org/cgi/content/full/329/5988/200/DC1
Materials and Methods
Figs. S1 to S6
Tables S1 to S5
References

7 April 2010; accepted 1 June 2010
10.1126/science.1190612

Explaining the Structure of the Archean Mass-Independent Sulfur Isotope Record

Itay Halevy,* David T. Johnston, Daniel P. Schrag

Sulfur isotopes in ancient sediments provide a record of past environmental conditions. The long–time-scale variability and apparent asymmetry in the magnitude of minor sulfur isotope fractionation in Archean sediments remain unexplained. Using an integrated biogeochemical model of the Archean sulfur cycle, we find that the preservation of mass-independent sulfur is influenced by a variety of extra-atmospheric mechanisms, including biological activity and continental crust formation. Preservation of atmospherically produced mass-independent sulfur implies limited metabolic sulfur cycling before ~2500 million years ago; the asymmetry in the record indicates that bacterial sulfate reduction was geochemically unimportant at this time. Our results suggest that the large-scale structure of the record reflects variability in the oxidation state of volcanic sulfur volatiles.

Most natural processes fractionate sulfur in proportion to the mass difference between the isotopes (*1*). Ultraviolet (UV) photolysis of atmospheric SO_2, however, produces a mass-independent fractionation (MIF) that is delivered to the surface only if atmospheric O_2 levels are very low (*2*–*7*). The presence of MIF in sedimentary sulfides and sulfates older than 2450 million years (My) and its absence from later sediments has led to the accepted view that atmospheric O_2 levels crossed a threshold value near the Archean-Proterozoic boundary (*2*–*6*). Beyond simply recording MIF, the Archean sulfur isotope record appears to carry a discernable temporal structure: moderate [<4 per mil (‰)] early Archean $\Delta^{33}S$ (*2*) anomalies, followed by a mid-Archean minimum (<2‰) and a late Archean explosion in the magnitude of MIF (<12‰ in $\Delta^{33}S$). Previous studies attribute this variability to changes in the composition and oxidation state of the atmosphere and the associated evolution of photochemical pathways (*7*–*9*). In addition, an asymmetry in the record, with strongly positive but only weakly negative isotopic anomalies, remains without a quantitative explanation.

Here we explore the effect of a variety of extra-atmospheric processes on the characteristics and preservation of MIF. We present an integrated model of the full surface-sulfur cycle, accounting for the production and translation of atmospherically derived MIF through a marine reservoir and its preservation in the geologic record (*10*). We use recent measurements and theoretical calculations of $^{3x}SO_2$ (x = 2, 3, 4, 6) UV absorption cross sections to constrain atmospheric MIF production (*10*–*12*). By solving mass-balance equations for the steady-state reservoir sizes and isotopic compositions of four different oxidation states of sulfur [S^{6+} (sulfate), S^{4+} (sulfite, SO_2), S^0 (elemental sulfur), and S^{2-} (sulfide, H_2S)], we track MIF from production to lithification.

Rates of volcanic supply, photolytic destruction, gas-phase reactions, and net deposition to the surface govern the atmospheric lifetime of SO_2. Any process that destroys atmospheric SO_2 at the expense of photolysis reduces the production, by mass, of MIF [for example, atmospheric oxidation (Fig. 1A)], but as long as photolysis rates are non-negligible relative to the other atmospheric SO_2 sinks, MIF is produced (though not necessarily preserved). In addition to nonphotolytic atmospheric sinks, which attenuate MIF by decreasing production, homogenization reduces MIF by remixing anomalous compositions back toward the original SO_2 value. Whereas atmospheric oxidation to sulfate has been discussed in this context (*6*), microbial processes, which can perform a similar function, have not been rigorously investigated (Fig. 1B). Given a quantitatively important flux of MIF from SO_2 photolysis, cycling between the sulfur reservoirs (e.g., microbial activity) or transformation to one oxidation state (e.g., quantitative reduction to sulfide) must be minor, as not to erase the anomaly. An immediate implication is that low atmospheric O_2 is necessary but insufficient for preservation of MIF in the geologic record.

Our model results illustrate the sensitivity of MIF to a few key properties of the ocean-atmosphere system, as well as its relative insensitivity to several other properties. Atmospheric deposition of SO_2 leads to its speciation in seawater [$SO_2(aq) \rightleftharpoons HSO_3^- + H^+ \rightleftharpoons SO_3^{2-} + H^+$], where subsequent oxidation by Fe^{3+} (*13*–*15*) leaves other aqueous oxidation pathways less important (for instance, Fe^{2+}-catalyzed oxidation by aqueous O_2 or by atmospherically produced H_2O_2). This leaves vanishingly little marine S^{4+} ($\sim 10^{-3}$ μM) and only modest sulfate concentrations ($\sim 10^2$ μM). Given these oxidation rates, the absolute magnitude of MIF is only moderately sensitive to the adopted rate of S^{4+} disproportionation (Fig. 1D) (*10*), although the symmetry of

Department of Earth and Planetary Sciences, Harvard University, Cambridge, MA 02138, USA.

*To whom correspondence should be addressed. E-mail: itay.halevy@gmail.com

the sulfate–elemental sulfur MIF is rate-sensitive. This is because the isotopic composition of SO_2 propagates to both sulfate and elemental sulfur when disproportionation is rapid, but only to sulfate when oxidation dominates. The negative-positive asymmetry of the MIF record suggests that oxidation, not disproportionation, was the dominant aqueous S^{4+} sink. Hydrated formaldehyde complexes S^{4+}, preventing its oxidation and disproportionation; however, this only affects MIF preservation at concentrations higher than those likely in an Archean ocean (Fig. 1E) (*16*).

The magnitude of MIF in pyrite, but not in sulfates, is very sensitive to the SO_2:H_2S ratio in volcanic volatiles (Fig. 1C). This is because the elemental sulfur that ends up in pyrite originates from both atmospheric SO_2 and H_2S, but H_2S photoreactions do not generate MIF. When the outgassing rate of SO_2 increases relative to that of H_2S, more of the elemental sulfur budget comes from SO_2 photolysis and, as a result, is anomalously fractionated. Sulfate, on the other hand, is produced almost entirely from oxidation and photolysis of SO_2, and so its isotopic composition is insensitive to changes in the relative abundance of SO_2 and H_2S. Changes in the total sulfur (SO_2 + H_2S) outgassing rate with constant SO_2:H_2S produce no change in MIF magnitudes (Fig. 1F), but this may be due to the simplified nature of our atmospheric model; S_8 production in more detailed atmospheric models is sensitive to the total sulfur outgassing rate (*7*, *17*). We note, however, that more rapid S_8 production does not necessarily translate into stronger MIF if the S_8 is derived from H_2S.

MIF depends critically on the partial pressure of CO_2 (P_{CO_2}); increased P_{CO_2} results in stronger scattering and UV absorption, decreasing SO_2 photolysis rates (Fig. 2A). In more detailed atmospheric models, the relative abundances of atmospheric CO_2 and CH_4 also influence SO_2 oxidation rates and the efficacy of MIF export

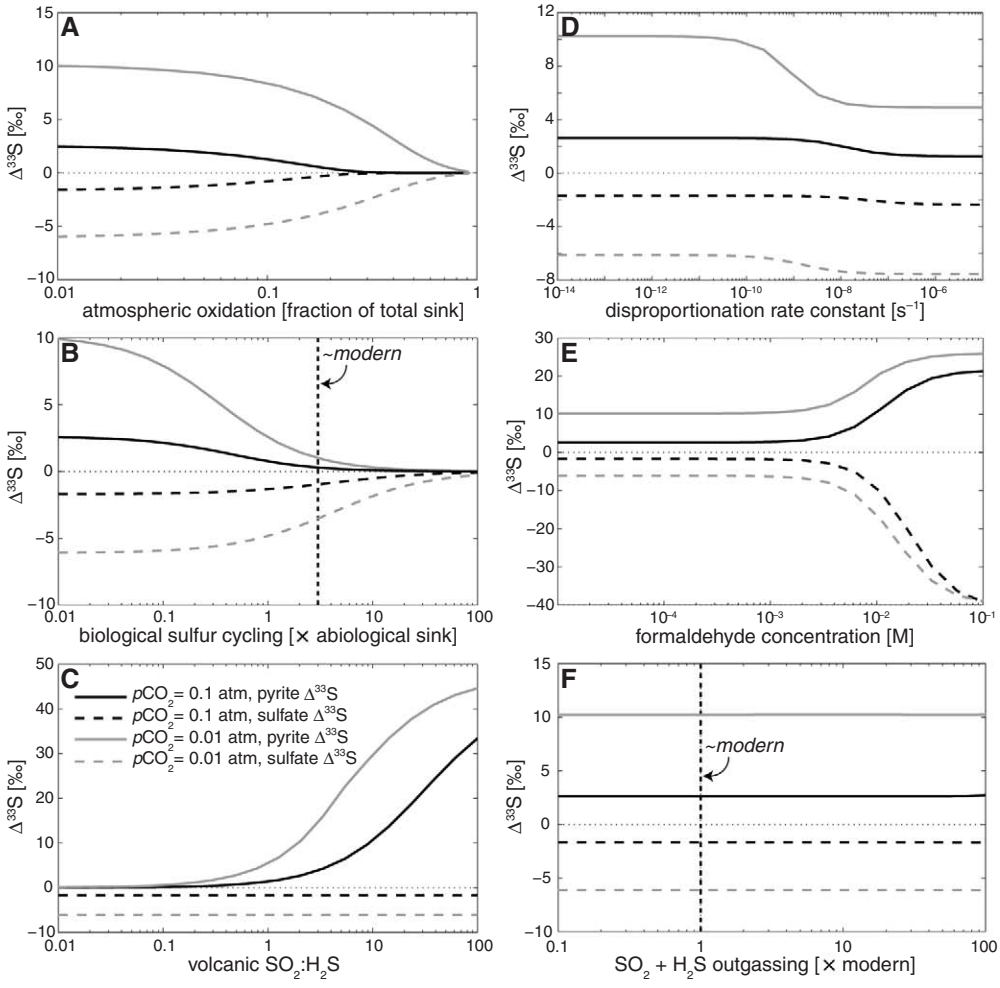

Fig. 1. The sensitivity of MIF in pyrite and sulfate, for P_{CO_2} of 0.01 and 0.1 atm, plotted as a function of (**A**) the fraction of outgassed SO_2 that is oxidized in the atmosphere, (**B**) microbial cycling, represented as a multiple of the sum of nonbiological sinks, (**C**) SO_2:H_2S in volcanic gases, (**D**) the disproportionation rate constant, (**E**) the hydrated formaldehyde concentration, and (**F**) the total sulfur (SO_2 + H_2S) outgassing rate. Metabolisms included in (C) are sulfate reduction, elemental sulfur oxidation, disproportionation and reduction, and sulfide oxidation. Estimates of modern biological sulfur cycling and volcanic outgassing are also shown.

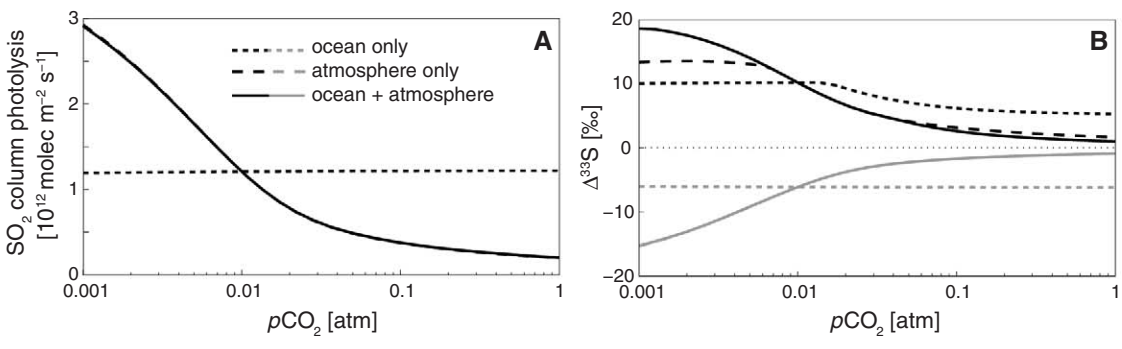

Fig. 2. The sensitivity of (**A**) the SO_2 column photolysis rate and (**B**) MIF in pyrite (black) and in sulfates (gray) to P_{CO_2}. Dashed lines represent the response of MIF to changes in atmospheric opacity due to increased molecular absorption and scattering by CO_2, with P_{CO_2} held constant at 0.01 atm in the ocean. Dotted lines represent the response to changes in the ocean (pH, Fe^{3+} concentration, etc.), with P_{CO_2} held constant at 0.01 atm in the atmosphere. Solid lines show the combined effect.

(*6*, *7*, *17*). Our model highlights that, with a more acidic ocean (at high P_{CO_2}), the degree of pyrite saturation decreases, and H_2S partitions more strongly into the atmosphere. As the importance of H_2S photolysis relative to pyrite precipitation increases, more S^0 is H_2S-derived. This does not affect the $\Delta^{33}S$ of sulfate ($\Delta^{33}S_{sulfate}$), but it decreases the $\Delta^{33}S$ of pyrite [$\Delta^{33}S_{pyr}$ (Fig. 2B, dotted lines)] and influences the symmetry of the $\Delta^{33}S$ signal.

Four properties emerge as important for the preserved magnitude and symmetry of Archean MIF: (i) atmospheric SO_2 oxidation rates, (ii) redox transformations (including microbial cycling rates), (iii) SO_2:H_2S in volcanic gases, and (iv) P_{CO_2}. The very presence of MIF in the rock record points to low oxidant availability, suggesting that atmospheric oxidation was not the dominant SO_2 sink (*6*, *7*). With constraints from the geologic record on the remaining three properties, we explore their potential to explain the structure in the Archean MIF record using two quantities: $\Delta^{33}S_{pyr}$ and R_{asym}, a measure of the asymmetry ($|\Delta^{33}S_{pyr}/\Delta^{33}S_{sulfate}|$). A successful explanation of the record must account for early Archean $\Delta^{33}S_{pyr} \approx 4‰$ and $R_{asym} \approx 2$, mid-Archean $\Delta^{33}S_{pyr} \approx 2‰$ and $R_{asym} \approx 1$, and latest Archean $\Delta^{33}S_{pyr} \approx 11‰$ and $R_{asym} > 5$.

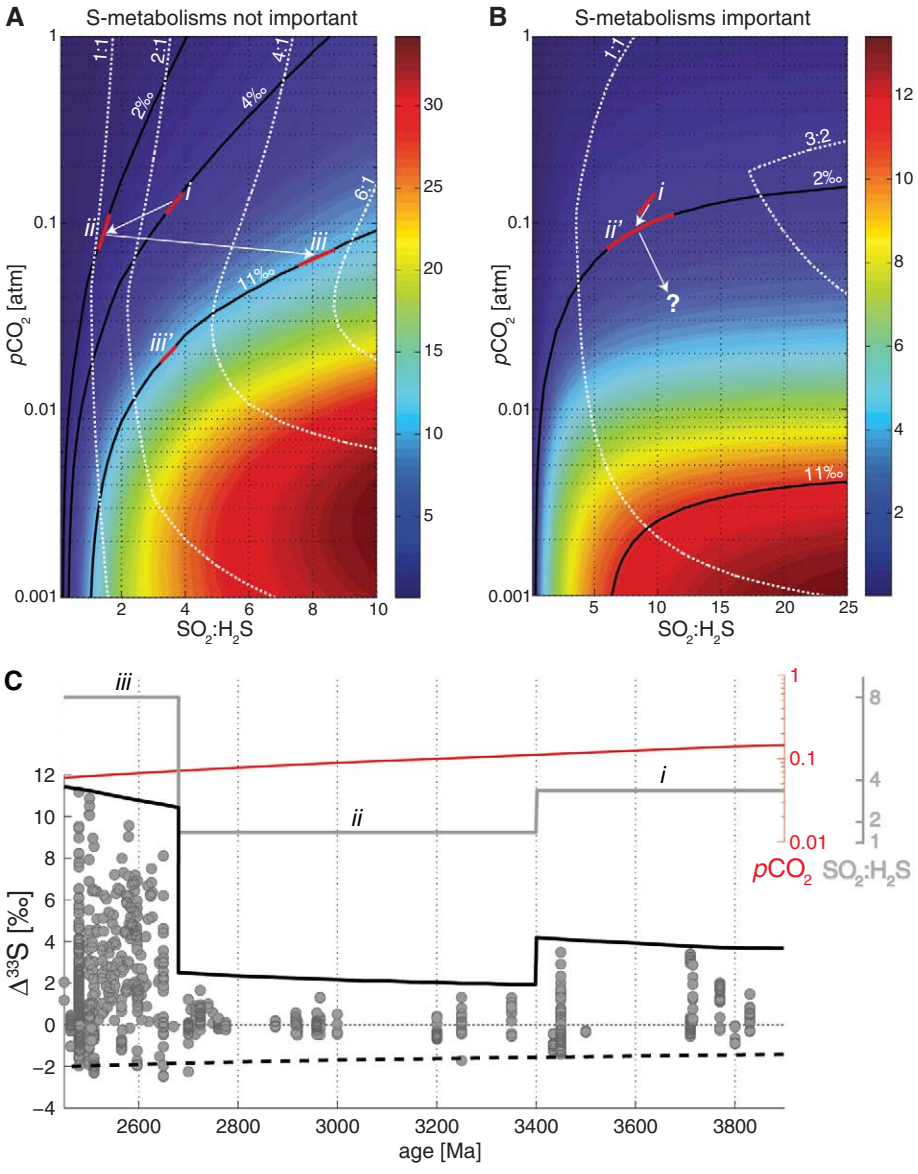

Fig. 3. The dependence of preserved MIF on P_{CO_2}, volcanic SO_2:H_2S, and biological activity. (**A**) Color contours of pyrite $\Delta^{33}S$ ($\Delta^{33}S_{pyr}$) with no biological sulfur cycling, highlighting values relevant to the early, middle, and late Archean (solid black lines). Also shown are contours of the absolute value of the ratio of pyrite to sulfate $\Delta^{33}S$ (R_{asym}, dotted white lines). (**B**) Same as in (A), but with biological cycling between sulfate, sulfur, and sulfide at ~10% modern values. (**C**) A section (*i* → *ii* → *iii*) through the phase space plotted in (A), with gradually evolving P_{CO_2} (red line) and the value of volcanic SO_2:H_2S required to reproduce the observed $\Delta^{33}S_{pyr}$ and R_{asym} (thick gray line). The modeled $\Delta^{33}S$ values of pyrite (thick solid black line) and sulfate minerals (thick dashed black line) are compared with the observed record (gray circles) in the lower half of (C). Regions *iii'* in (A) and *ii'* in (B) illustrate the effect of biological methanogenesis on P_{CO_2} and the effect of microbial sulfur cycling on $\Delta^{33}S_{pyr}$, respectively.

When imposed on a purely abiological early Archean sulfur cycle, metabolic cycling between the different sulfur pools can potentially explain portions of the Archean MIF record (Fig. 1B). Both microbial S^0 disproportionation and dissimilatory sulfate reduction may have existed since ~3500 million years ago (Ma) (*18*, *19*). Adopting for the moment a scenario in which biological sulfur cycling is not important before ~3500 Ma, an increase in the role of microorganisms equivalent to ~10% modern cycling rates could drive a change in $\Delta^{33}S_{pyr}$ and R_{asym} similar to that observed from the early to mid-Archean (Fig. 3B, *i* → *ii'*). Difficulty arises, however, when microorganisms persist into the late Archean. Given that sulfate reduction delivers $\Delta^{33}S < 0$ to sulfide, a greater degree of symmetry (and even reversed asymmetry, $R_{asym} < 1$) would be expected for the late Archean; this is in marked contrast to the observed R_{asym} of 5 to 6 and suggests that dissimilatory sulfate reduction only rises to geochemical importance between 2400 and 2500 Ma, when high MIF magnitudes and large asymmetry are no longer observed. A late Archean or early Paleoproterozoic onset of sulfate reduction is consistent with a reanalysis of traditional sulfur isotope ($\delta^{34}S$) records (*10*) and suggests an explanation for the persistence of nonzero and relatively symmetric MIF for 10 to 100 My postdating the major loss of MIF at ~2500 Ma in some locations (*5*), but not in others (*20*).

In the absence of biological sulfur cycling, we find that, with constant volcanic SO_2:H_2S, climatically reasonable changes in P_{CO_2} (*21*–*23*) cannot alone produce the observed MIF history (Fig. 3A). If we adopt instead an evolving value for Archean P_{CO_2}, calculated to offset changes in solar luminosity and to maintain liquid water [together with ~10 parts per million by volume atmospheric methane maintained by about twice modern sea-floor serpentinization rates (*21*–*24*)], changes in volcanic SO_2:H_2S well within observed values (*25*, *26*) easily account for the histories of both $\Delta^{33}S_{pyr}$ and R_{asym} (Fig. 3A, *i* → *ii* → *iii*). This result does not preclude further changes in P_{CO_2} affecting the MIF signal [for example, through the effect of methanogens on P_{CO_2} and P_{CH_4} (*21*, *23*)], though the asymmetry in the latest Archean almost by necessity indicates a substantial increase in volcanic SO_2:H_2S. Such an increase may be related to a major shift in the style of large igneous province eruption from submarine to subaerial in the late Archean (2700 to 2500 Ma), also suggested to have been the cause for the rise in atmospheric O_2 and the loss of MIF (*25*). Consistent with the sulfur isotope record, our results suggest that this loss would be preceded by a MIF spike due to the elevated volcanic SO_2:H_2S. A small clustering of plume events during the early Archean [3500

to 3300 Ma (*27*)] may suggest an attendant increase in SO_2:H_2S, explaining the earliest MIF record, though it is not clear that these events were subaerial. The eruption rate required to raise global volcanic SO_2:H_2S from ~1.5 to ~8 (as in Fig. 3A, *ii* → *iii*) is only about half to twice that of the Hawaiian plume (*28*), if the magma composition and SO_2:H_2S are comparable to those of Hawaii [1000 to 1500 parts per million sulfur, SO_2:H_2S of 50 to 100 (*26*)]. Given the plausibility of these changes, the structure of the $\Delta^{33}S$ record may speak to large-scale crustal processes, superimposed onto and participating with low-O_2 atmospheric chemistry.

Despite oceanic anoxia, rapid oxidation of SO_2 by Fe^{3+} in the surface ocean suggests that, like the present, deposition into the Archean ocean was a terminal sink for atmospheric SO_2 with a characteristic time scale of a few days. This implies that atmospheric SO_2 was not well mixed and that spatio-temporal variability in its concentration is expected. Considering the demonstrated sensitivity of MIF to the relative abundance of SO_2, this translates into the potential for large variability in pyrite $\Delta^{33}S$, with a much more muted signal in the $\Delta^{33}S$ of sulfate minerals (Fig. 3). Additional variability in pyrite $\Delta^{33}S$ is expected as a result of small-scale processes occurring in sediment pore water, given the possibility for sedimentary sulfides to adopt MIF from a variety of sources [dissolved sulfide, elemental sulfur, sulfite, or sulfate (*17*, *29*)]. An aqueous oxidation origin for most of the oceanic sulfate may also explain the lack of correlation between $\Delta^{17}O$ and $\Delta^{33}S$ in early Archean barite (*30*).

Changes in atmospheric composition and chemistry probably explain a fraction of the variability in the Archean MIF record. In addition, we highlight the importance of variability in volcanic SO_2:H_2S, which may have caused the spike in MIF magnitudes ~2700 Ma, immediately preceding the ultimate loss of MIF brought on by the rise of atmospheric O_2. In the absence of atmospheric O_2 and a complex biosphere, it may have been the interactions between the solid Earth (mantle-crust) and fluid Earth (ocean-atmosphere) that drove the sedimentary record of $\Delta^{33}S$.

References and Notes

1. J. R. Hulston, H. G. Thode, *J. Geophys. Res.* **70**, 3475 (1965).
2. MIF is expressed as the difference in per mil between measured isotopic compositions and those expected if the fractionations were mass-dependent: $\Delta^{33}S \equiv \delta^{33}S - 0.515 \times \delta^{34}S$, $\Delta^{36}S \equiv \delta^{36}S - 1.89 \times \delta^{34}S$.
3. J. Farquhar, J. Savarino, S. Airieau, M. H. Thiemens, *J. Geophys. Res. Planets* **106**, 32829 (2001).
4. J. Farquhar, H. Bao, M. Thiemens, *Science* **289**, 756 (2000).
5. J. Farquhar, B. A. Wing, *Earth Planet. Sci. Lett.* **213**, 1 (2003).
6. A. A. Pavlov, J. F. Kasting, *Astrobiology* **2**, 27 (2002).
7. K. Zahnle, M. Claire, D. Catling, *Geobiology* **4**, 271 (2006).
8. S. D. Domagal-Goldman, J. F. Kasting, D. T. Johnston, J. Farquhar, *Earth Planet. Sci. Lett.* **269**, 29 (2008).
9. J. Farquhar *et al.*, *Nature* **449**, 706 (2007).
10. Further details are available in the supporting material on *Science* Online.
11. S. O. Danielache, C. Eskebjerg, M. S. Johnson, Y. Ueno, N. Yoshida, *J. Geophys. Res. Atmos.* **113**, D17314 (2008).
12. H. Ran, D. Q. Xie, H. Guo, *Chem. Phys. Lett.* **439**, 280 (2007).
13. Photooxidation of Fe^{2+} (*14*), thought to have been abundant in the Archean ocean (*15*), exceeds SO_2 deposition under most circumstances (*10*).
14. P. S. Braterman, A. G. Cairns-Smith, R. W. Sloper, *Nature* **303**, 163 (1983).
15. H. D. Holland, in *Treatise on Geochemistry*, vol. 6, K. K. Turekian, H. D. Holland, Eds. (Elsevier-Pergamon, Oxford, 2004), pp. 583–625.
16. H. J. Cleaves II, *Precambrian Res.* **164**, 111 (2008).
17. S. Ono *et al.*, *Earth Planet. Sci. Lett.* **213**, 15 (2003).
18. P. Philippot *et al.*, *Science* **317**, 1534 (2007).
19. Y. A. Shen, R. Buick, D. E. Canfield, *Nature* **410**, 77 (2001).
20. Q. Guo *et al.*, *Geology* **37**, 399 (2009).
21. J. D. Haqq-Misra, S. D. Domagal-Goldman, P. J. Kasting, J. F. Kasting, *Astrobiology* **8**, 1127 (2008).
22. P. von Paris *et al.*, *Planet. Space Sci.* **56**, 1244 (2008).
23. A. A. Pavlov, J. F. Kasting, L. L. Brown, K. A. Rages, R. Freedman, *J. Geophys. Res. Planets* **105**, 11981 (2000).
24. S. Emmanuel, J. J. Ague, *Geophys. Res. Lett.* **34**, L15810 (2007).
25. L. R. Kump, M. E. Barley, *Nature* **448**, 1033 (2007).
26. M. M. Halmer, H.-U. Schmincke, H.-F. Graf, *J. Volcanol. Geotherm. Res.* **115**, 511 (2002).
27. A. E. Isley, D. H. Abbott, *J. Geophys. Res. Solid Earth* **104**, 15461 (1999).
28. E. Van Ark, J. Lin, *J. Geophys. Res. Solid Earth* **109**, B11401 (2004).
29. J. R. Lyons, *Chem. Geol.* **267**, 164 (2009).
30. H. M. Bao, D. Rumble III, D. R. Lowe, *Geochim. Cosmochim. Acta* **71**, 4868 (2007).

31. I.H. was supported by the Harvard University Origins of Life Initiative, and D.T.J. was supported by NASA Exobiology. D.P.S. thanks H. Breck and W. Breck for support. We also thank three anonymous reviewers.

Supporting Online Material

www.sciencemag.org/cgi/content/full/science.1190298/DC1
SOM Text
Figs. S1 to S3
Tables S1 and S2
References

31 March 2010; accepted 17 May 2010
Published online 27 May 2010;
10.1126/science.1190298
Include this information when citing this paper.

Contrasting Décollement and Prism Properties over the Sumatra 2004–2005 Earthquake Rupture Boundary

Simon M. Dean,[1]* Lisa C. McNeill,[1] Timothy J. Henstock,[1] Jonathan M. Bull,[1] Sean P. S. Gulick,[2] James A. Austin Jr.,[2] Nathan L. B. Bangs,[2] Yusuf S. Djajadihardja,[3] Haryadi Permana[4]

Styles of subduction zone deformation and earthquake rupture dynamics are strongly linked, jointly influencing hazard potential. Seismic reflection profiles across the trench west of Sumatra, Indonesia, show differences across the boundary between the major 2004 and 2005 plate interface earthquakes, which exhibited contrasting earthquake rupture and tsunami generation. In the southern part of the 2004 rupture, we interpret a negative-polarity sedimentary reflector ~500 meters above the subducting oceanic basement as the seaward extension of the plate interface. This predécollement reflector corresponds to unusual prism structure, morphology, and seismogenic behavior that are absent along the 2005 rupture zone. Although margins like the 2004 rupture zone are globally rare, our results suggest that sediment properties influence earthquake rupture, tsunami hazard, and prism development at subducting plate boundaries.

The 2004 moment magnitude (M_w) = 9.2 Sumatra earthquake initiated close to Simeulue Island and generated a regionally destructive tsunami (*1*, *2*). The 2005 M_w = 8.7 earthquake, immediately to the south across an apparently persistent rupture boundary, caused only a local tsunami (*3*). Both earthquakes initiated at similar depths (~30 to 40 km), but the 2004 rupture offshore North Sumatra propagated farther seaward than the 2005 rupture (*1*–*3*), with the latter more similar to other large subduction-zone earthquakes, including the 1960 Chile and 1964 Alaska earthquakes [e.g., (*4*–*6*)]. The different rupture patterns of the two Sumatra earthquakes are likely controlled by rheology (sediment properties), stress state, and fault properties and will generate different tsunami by affecting both magnitude and water depth of the associated seafloor deformation. Sediment properties, both before and after incorporation into the subduction zone, may also affect the morphology and deformation of the margin [e.g., (*4*, *7*)], which in turn are linked to the dynamics of the earthquake rupture (*8*). On some other subduction margins [e.g., Nankai (*9*) and Barbados (*10*)], accretionary prism faults

[1]National Oceanography Centre, Southampton, University of Southampton, Southampton SO14 3ZH, UK. [2]Institute for Geophysics, Jackson School of Geosciences, University of Texas at Austin, Austin, TX 78758–4445, USA. [3]Agency for the Assessment and Application of Technology (BPPT), Jakarta 10340, Indonesia. [4]Research Center for Geotechnology, Indonesia Institute for Sciences, Bandung 40135, Indonesia.

*To whom correspondence should be addressed. E-mail: smd9@noc.soton.ac.uk

merge at depth into a well-defined décollement (a low-angle detachment fault) identified as the plate boundary thrust. However, beneath the Sumatran margin, the exact mechanism of rupture propagation and transfer of fault slip to the sea floor is poorly understood.

We collected 2500 km of multichannel seismic reflection (MCS) profiles along the Sumatra margin from northwest of Simeulue Island to Nias Island (Fig. 1) (*11*). Trench sediment velocities above oceanic basement are high (~4 km/s) north of the 2004–2005 rupture boundary, in contrast to equivalent sediments south of the rupture boundary (~3 to 3.5 km/s) (*11*) (fig. S1). North of the rupture boundary, a distinctive and regionally continuous high-amplitude negative polarity (HA-NP) reflector lies near the base of this trench deep-ocean sediment section.

The reflector is identified in MCS profiles perpendicular (Fig. 2) and parallel (Fig. 3) to the trench axis, typically ~0.5 km above the top of the oceanic basement, within the ~4-km/s high-velocity layer (*11*), and has consistent character in all profiles. Its amplitude is higher than that of other sediment horizons more than 0.25 km beneath the seabed and is generally stronger than that of the top oceanic basement reflector. The reflector's wave form is similar to that of the seabed and of the seabed multiple (Fig. 2, inset) and shows a clear negative polarity. The reflector may represent either a discrete layer, thinner than the seismic wavelength (<<100 m), or a single interface between two units with contrasting seismic velocity and density. Mean reflection coefficients of at least −0.1 for the reflector versus 0.32 for the seabed (table S1) indicate a major impedance decrease. We clearly image the reflector in the trench to the seaward end of our profiles from 2°N to 4°N (Fig. 1), up to ~35 km from the deformation front. The reflector is less clearly imaged beneath the outer prism ~0.5 km above the top of oceanic basement (Fig. 2), up to ~20 km landward from the deformation front; the reflector has reduced amplitude and lateral continuity, possibly due to seismic imaging compromised by steep bathymetry and overlying prism fault structure, but retains negative polarity where observed.

The accretionary prism consists of fault-bounded blocks of relatively weakly deformed sediment. The vertical thickness of these blocks suggests that almost the entire incoming sediment section, to within ~500 m of the top of the incoming plate, is accreted. We do not image the precise contact between the reflector and major outer-prism thrust faults, but these faults extend with ~45° dip from the seabed to at least 2 km below the sea floor close to the reflector (Fig. 2), and we expect them to intersect the HA-NP reflector (Fig. 2, inset).

Offshore of Simeulue, the trench seabed deepens by ~0.1 km over ~50 km toward the southeast, whereas the oceanic basement shallows by 1.75 km (Fig. 3). The deep-ocean sediment layer thins and shallows over the rising basement with the basal ~0.75 km of sediments (including the reflector) terminating against basement. Southeast of ~1°30′N, at the latitude of the 2005 rupture zone, the oceanic basement deepens again (e.g., Fig. 4) and the subduction angle beneath the trench increases (*12*). The incoming sediment thickness is similar to that of the section just

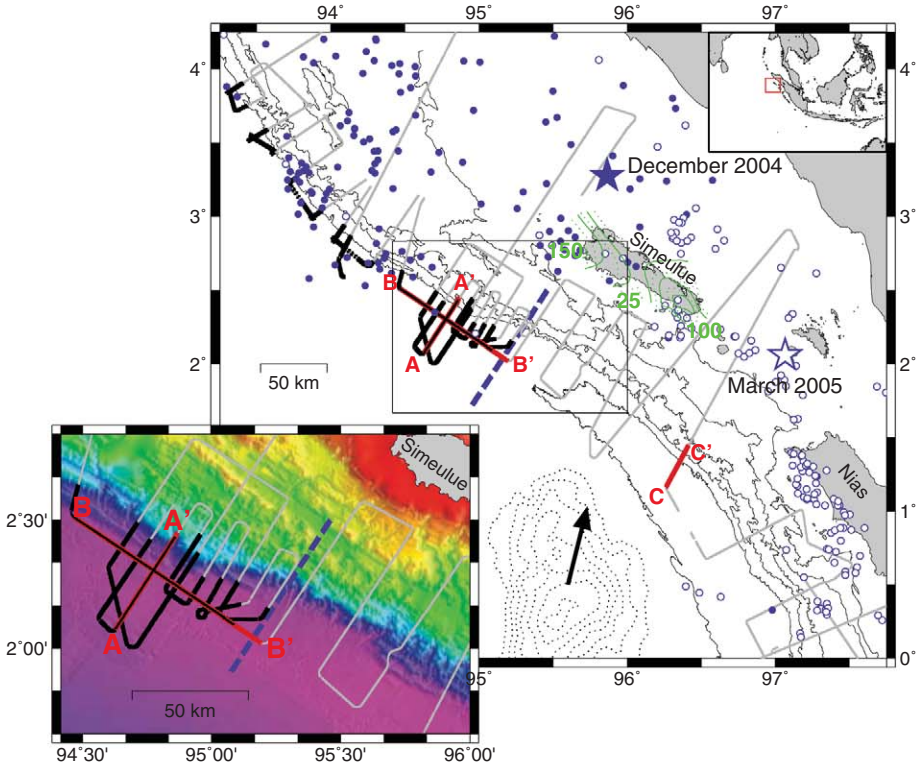

Fig. 1. Multichannel seismic profiles (gray lines) and study area. Blue circles: December 2004 (solid) and March 2005 (open) Sumatra ISC earthquakes (*17*) during 1 month after earthquake. Thick black lines indicate seismic reflector observations; red lines locate study area of Fig. 2 (A-A′), Fig. 3 (B-B′), and Fig. 4 (C-C′). Dashed blue line: change in aftershock distribution and southeastern boundary of distinct reflector. Green contours: 2004–2005 coseismic uplift (in centimeters) on Simeulue Island (*3*); thin black lines: 1000-m bathymetry contours; dotted black contours indicate oceanic fracture zone from satellite-derived gravity data (*27*); convergence vector is from (*28*). (**Inset**) Multibeam bathymetry data (*12*, *13*, *29*).

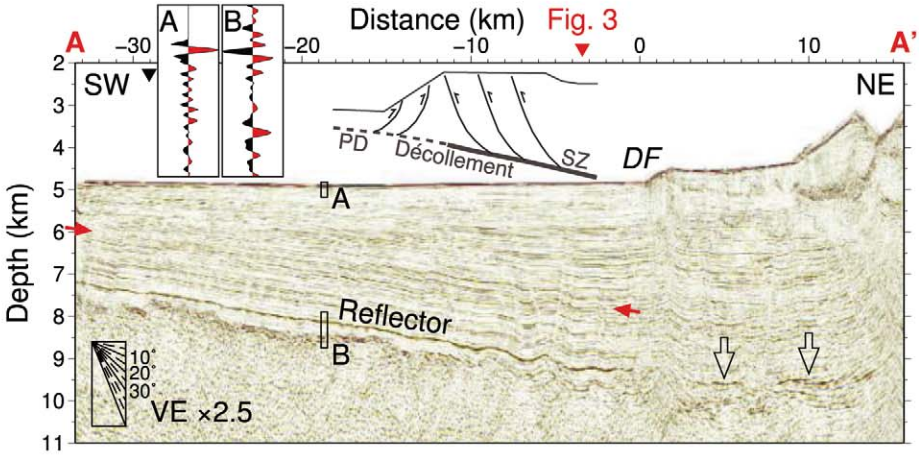

Fig. 2. Depth-migrated seismic profile A-A′ (DF: distance from deformation front; VE: vertical exaggeration). The reflector continues from 7.25-km depth in the southwest as a continuous negative-polarity event 0.2 to 0.5 km above oceanic basement and discontinuously beneath the outer prism (open arrows). Red arrows: unconformity between trench fill and underlying deep-ocean sediment. Boxes show reflected wave forms: (A) Seabed. (B) Reflector (negative polarity); top of oceanic basement is near trace base (positive polarity); wave forms are aligned at peak amplitude. **(Inset)** Schematic of prism structure and relation to predécollement (PD), décollement, and seismogenic zone (SZ) northwest of the 2004–2005 rupture boundary; seismic sections shown represent the outermost prism and oceanic plate.

northwest of the basement high, and stratigraphically we would expect the base of the sediments to be close to the depth of the HA-NP reflector observed to the northwest. However, no reflector with similar characteristics is observed, and thus our data tightly constrain the southward limit of the HA-NP reflector. Stratigraphy of the deepest oceanic sediments seaward of Simeulue indicate that basement topography is preexisting, probably related to an oceanic fracture zone (*12*).

The area where we observe the HA-NP reflector coincides with distinct accretionary prism properties and seismogenic behavior, implying links to both long- and short-term deformation. The morphology and structure of the prism in this region are unusual: A steep outer slope and broad plateau extend up to 150 km from the trench to the outer edge of the forearc basin (*13*). In contrast, the region to the southeast has a more uniform prism taper and reduced prism width of 100 km (*14*). The southeastern termination of the reflector, close to the 2004–2005 rupture boundary, also corresponds to a change in trend of the deformation front. The outer prism northwest of this change has well-developed landward-vergent fold ridges up to 80 km long (*13*) compared with 20- to 30-km-long mixed-vergence folds to the southeast (*14*). Forearc islands are absent in the northwest even though free-air gravity values are as high at the outer prism as in locations to the southeast. The southern 2004 rupture propagated seaward beneath the prism from its deep initiation point (*1*, *2*) and may have reached the seabed, rupturing faults within the prism (*13*, *15*, *16*). In contrast, the 2005 rupture largely occurred beneath the forearc basin and islands, with limited extent further seaward (*2*, *3*). Finally, the aftershock distribution changes, consistent with the mainshock slip (*1*–*3*); aftershocks for the 2004 and 2005 events from the International Seismological Centre (ISC) catalog (*11*, *17*) and from local networks (*18*) show epicenters extending to the trench where the reflector is present, whereas epicenters are rare in the seaward forearc where the reflector is absent (Fig. 1). The aftershock distribution suggests that the reflector termination corresponds to the southern edge of 2004 seismicity within the outer prism.

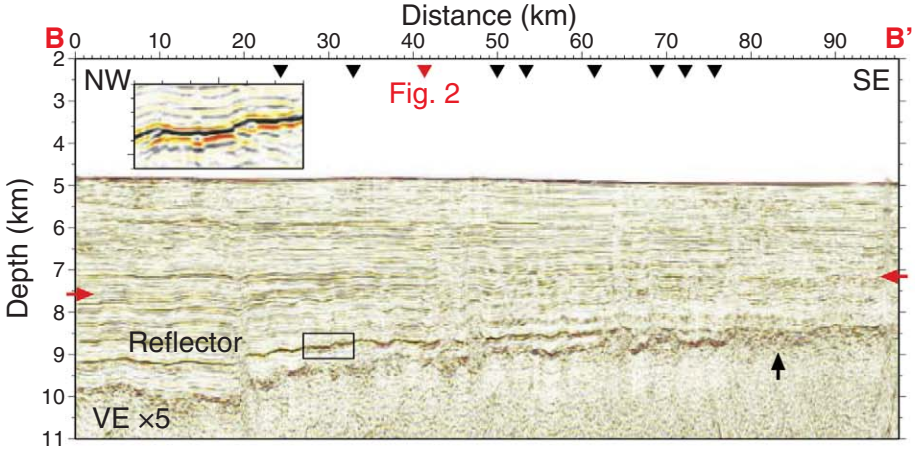

Fig. 3. Depth-migrated trench-parallel seismic profile B-B′ seaward of deformation front (VE: vertical exaggeration). The HA-NP reflector is at 9.2-km depth, and oceanic basement is ~10 km in the northwest. Oceanic basement shallows by ~1.5 km to the southeast, and reflector merges at 80 to 85 km along the profile (black arrow). Red arrows indicate unconformity from Fig. 2. **(Inset)** Enlarged section of reflector (black box).

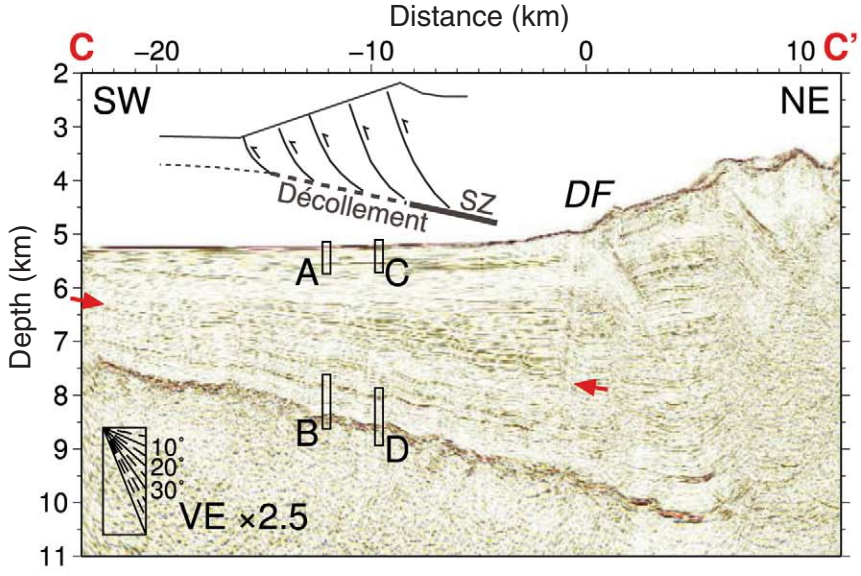

Fig. 4. Depth-migrated seismic profile C-C′ (DF: distance from deformation front; VE: vertical exaggeration). Oceanic basement reflector has a higher amplitude and overlying oceanic sediment is thinner than in Fig. 1. Red arrows indicate unconformity from Fig. 2. A reflector, ~0.5 km above oceanic basement, is superficially similar to the reflector identified in Figs. 2 and 3 but has appreciably lower amplitude and variable polarity. Boxes A to D locate reflected wave forms shown in fig. S6. **(Inset)** Schematic of prism structure southeast of the 2004–2005 rupture boundary.

High-amplitude, negative-polarity décollement and predécollement (the seaward extension of the décollement) reflectors are identified on several other convergent margins, most notably northern Barbados [e.g., (*10*, *19*–*21*)], Nankai [e.g., (*9*, *22*–*24*)], and Central Cascadia [e.g., (*25*)]. In north Barbados, the décollement is locally HA-NP and traceable ~70 to 100 km across the prism. Drilling and MCS data show reduced density, high porosity at the predécollement and décollement, resulting from high fluid content and underconsolidation and coincident with a weak radiolarian-rich claystone (*19*–*21*). In the Nankai Trough (Muroto transect), the predécollement has a low amplitude and normal polarity, but the décollement is consistently HA-NP beneath the outer prism (*9*). Drilling and MCS data show high pore-fluid content reducing velocity and density and increasing porosity at and below the décollement, with fractures potentially enhancing porosity (*23*, *24*). Shallow décollements with HA-NP reflections are weak faults [e.g., (*20*, *21*)] that can be traced beneath the prism and into the seismogenic zone [e.g., (*9*)].

Comparison with these other margins suggests that the horizon offshore North Sumatra is a zone of low density and elevated pore pressure relative to overlying sediments. Such a layer, intrinsically weaker than surrounding sediments, would therefore be the likely locus for initiating the décollement fault, an interpretation consistent with the thickness of the frontally accreted sediment package. We infer that the landward extension of this horizon ultimately influences prism geometry and megathrust rupture. In North Sumatra, the reflector has distinct properties up to 35 km seaward of the deformation front, with a weaker negative-polarity extension beneath the prism, rather than a strong negative reflector beneath the prism, and a weaker, variable-polarity reflector seaward of the deformation front as observed on other margins. The reflector properties seaward of the deformation front imply a lithological origin on the North Sumatra margin, rather than arising solely from structural or hydrogeological

processes within the prism. Three changes could explain contrasting observed reflector properties southeast of the rupture boundary (Fig. 4): The stratigraphic section here postdates the particular horizon; an equivalent stratigraphic section is present but has different lithologies; or the horizon properties differ as a result of combined differences in lithology and forearc deformational and hydrogeological processes across the rupture boundary. The deepest sediments in the northwest likely derive from the early Nicobar Fan (*26*), and the observed contrast in properties may be a result of oceanic basement highs limiting southward fan turbidite transport.

Multiple lines of evidence support interpretation of the distinct reflector as the predécollement/décollement on the North Sumatran margin, and we thus hypothesize that its landward extension acts as the focus of plate boundary slip as the seismogenic décollement. Given the coincident changes in structure, seismic velocity, and seismogenic behavior, the lithological and rheological properties of the lowermost sediments shown by the predécollement likely differ on either side of the 2004–2005 rupture boundary (Fig. 1). Similarities between the structure and dynamics of the 2005 rupture segment and many other forearcs [e.g., (*5*)] emphasize the atypical nature of the southern 2004 rupture segment.

Thus, sediment properties may have a substantial impact on earthquake rupture and tsunamigenesis by influencing décollement behavior from the trench deep into the seismogenic zone.

References and Notes

1. T. Lay *et al.*, *Science* **308**, 1127 (2005).
2. C. J. Ammon *et al.*, *Science* **308**, 1133 (2005).
3. R. W. Briggs *et al.*, *Science* **311**, 1897 (2006).
4. D. E. Byrne, D. M. Davis, L. R. Sykes, *Tectonics* **7**, 833 (1988).
5. R. E. Wells, R. J. Blakeley, Y. Sugiyama, D. W. Scholl, P. A. Dinterman, *J. Geophys. Res.* **108**, 2507 (2003).
6. G. Plafker, *J. Geophys. Res.* **77**, 901 (1972).
7. D. Davis, J. Suppe, F. A. Dahlen, *J. Geophys. Res.* **88** (B2), 1153 (1983).
8. K. L. Wang, Y. Hu, *J. Geophys. Res.* **111**, (B6), B06410 (2006).
9. N. L. Bangs *et al.*, *Geology* **32**, 273 (2004).
10. T. H. Shipley, G. F. Moore, N. L. Bangs, J. C. Moore, P. L. Stoffa, *Geology* **22**, 411 (1994).
11. Materials and methods are available as supporting material on *Science* Online.
12. D. Franke *et al.*, *Earth Planet. Sci. Lett.* **269**, 118 (2008).
13. T. J. Henstock, L. C. McNeill, D. R. Tappin, *Geology* **34**, 485 (2006).
14. H. Kopp *et al.*, *Basin Res.* **20**, 519 (2008).
15. E. Araki *et al.*, *Earth Planets Space* **58**, 113 (2006).
16. J.-Y. Lin, X. Le Pichon, C. Rangin, J.-C. Sibuet, T. Maury, *Geochem. Geophys. Geosyst.* **10**, Q05006 (2009).
17. International Seismological Centre, On-line Bulletin, www.isc.ac.uk (International Seismological Centre, Thatcham, UK, 2001).
18. F. Tilmann *et al.*, *Geophys. J. Int.* **181**, 1261 (2010).
19. N. L. Bangs, T. H. Shipley, J. C. Moore, G. F. Moore, *J. Geophys. Res.* **104**, 20399 (1999).
20. J. C. Moore *et al.*, *Geology* **26**, 811 (1998).
21. J. C. Moore, A. Klaus, Eds., *Proc. Ocean Drill. Prog. Sci. Results* **171A** (2000).
22. G. F. Moore, T. H. Shipley, *Proc. Ocean Drill. Prog. Sci. Results* **131**, 73 (1993).
23. H. Mikada *et al.*, *Proc. Ocean. Drill. Prog. Init. Rep.* **196** (2002).
24. G. F. Moore, H. Mikada, J. C. Moore, K. Becker, A. Taira, *Proc. Ocean Drill. Prog. Sci. Results* **190/196**, 1 (2005).
25. G. R. Cochrane, J. C. Moore, M. E. MacKay, G. F. Moore, *J. Geophys. Res.* **99**, 7033 (1994).
26. J. R. Curray, F. J. Emmel, D. G. Moore, *Mar. Pet. Geol.* **19**, 1191 (2003).
27. D. T. Sandwell, W. H. F. Smith, *J. Geophys. Res.* **114**, (B1), B01411 (2009).
28. C. Vigny *et al.*, *Nature* **436**, 201 (2005).
29. D. Graindorge *et al.*, *Earth Planet. Sci. Lett.* **275**, 201 (2008).

30. We thank the master and crew of the *F/S Sonne* and all those involved in SO198-2 for their assistance, and our partners BPPT, Jakarta, for their logistical assistance. This work was funded by Natural Environment Research Council (NE/D004381/1) and NSF (OCE-0623165).

Supporting Online Material

www.sciencemag.org/cgi/content/full/329/5988/207/DC1
Materials and Methods
Figs. S1 to S6
Table S1
References

9 March 2010; accepted 18 May 2010
10.1126/science.1189373

Seismic Evidence for Active Underplating Below the Megathrust Earthquake Zone in Japan

Hisanori Kimura,[1]* Tetsuya Takeda,[1] Kazushige Obara,[1,2] Keiji Kasahara[2]

Determining the structure of subduction zones is important for understanding mechanisms for the generation of interplate phenomena such as megathrust earthquakes. The peeling off of the uppermost part of a subducting slab and accretion to the bottom of an overlying plate (underplating) at deep regions has been inferred from exhumed metamorphic rocks and deep seismic imaging, but direct seismic evidence of this process is lacking. By comparing seismic reflection profiles with microearthquake distributions in central Japan, we show that repeating microearthquakes occur along the bottom interface of the layer peeling off from the subducting Philippine Sea plate. This region coincides with the location of slow-slip events that may serve as signals for monitoring active underplating.

Underplating is a process through which the uppermost part of the subducting plate is peeled off and accreted to the bottom of the overlying plate. In association with underplating, the active plate boundary moves downward from the top interface of the accreting materials to its bottom interface. Deep ocean drilling and three-dimensional seismic imaging has revealed this "step-down" from the top of the subducting soft sediments to the bottom (*1*–*3*), which suggests that active underplating occurs at shallow depths. Underplating at deep regions has been inferred from exhumed high-pressure/low-temperature metamorphic rocks (*4*–*7*) and deep seismic imaging (*8*–*11*), but both of these provide indirect evidence of underplating. Hence, any reliable example of active deep underplating and its details, such as the behavior on shorter time scales and exact location, remain unknown.

Off the Kanto region, in the central part of Japan, the Philippine Sea plate (PHS) is now subducting below the continental plate (Fig. 1), and the Izu-Bonin arc is colliding with the continent (*12*, *13*). The plate boundary and structure of the PHS have been clearly imaged by deep seismic imaging (*13*) (P1 in Figs. 1 and 2). The PHS plate is thought to have a crustal thickness of 15 to 20 km at the entrance of subduction (Sagami trough) (*14*, *15*). The uppermost layers of the crust consist of a thin sedimentary layer hundreds of meters thick and a layer of volcaniclastic and volcanic rock (VCR) several kilometers thick (*14*, *15*). At the trench, the soft sediment is scraped off and the VCR layer subducts (*13*).

Along this boundary, various seismic and aseismic interplate phenomena have been observed. Megathrust earthquakes occur in the upper locked section (*13*), followed by slow-slip events (SSEs) (*16*, *17*) and repeating microearthquakes (RQs) (*13*, *18*) at greater depth (Fig. 1). Because RQs rupture small fault patches on the plate boundary and are indicators of this interface (*18*, *19*), obtaining the precise locations of RQs may contribute to the detection of the active step-down. However, direct comparison between seismic imaging and natural earthquakes on the small scale (~1 km) has been difficult. To overcome this limitation, we have made a series of relative comparisons. We used converted phases of natural earthquakes to image a plane at the base of a low velocity layer with high resolution. Waveform analyses link the conversion plane to reflector images from a seismic profile. Precise location of the interface involved determining high-precision hypocenters of the earthquakes, including the

[1]National Research Institute for Earth Science and Disaster Prevention (NIED), 3-1 Tennodai, Tsukuba, Ibaraki 305-0006, Japan. [2]Earthquake Research Institute, University of Tokyo, 1-1-1, Yayoi, Bunkyo, Tokyo 113-0032, Japan.

*To whom correspondence should be addressed. E-mail: kimura@bosai.go.jp

RQs, using converted wave analysis and precise relative hypocenter determination.

We processed profile P2 just above the RQs (Fig. 1), in which two major deep subhorizontal reflectors, R1 and R2, emerge (Fig. 2) (*20*). These reflectors have clear reverse and normal polarities, respectively, suggesting that a low-velocity layer lies between the boundaries having strong velocity contrasts. Analysis of the relative amplitude of R1 reveals the *P*-wave velocity (Vp) of the intervening layer as 5.5 ± 0.2 km/s (fig. S2), which translates to a thickness of 3.1 to 3.6 km (*22*). Moreover, a substantial imbricated reflection zone was imaged in the northern half of P2 (Fig. 2).

Such a strong velocity boundary is expected to generate converted waves. To detect such waves, we systematically examined seismograms of ~2000 microearthquakes with magnitude 2 to 4 around the RQs region (Off-Kanto cluster, Fig. 1) from 1979 to 2003 based on the National Research Institute for Earth Science and Disaster Prevention (NIED) seismographic network database. We cross-correlated radial components of seismograms with the vertical direct *P* wave, stacked seismograms to enhance the signal-to-noise ratio, and plotted record sections (*22*) (fig. S4). Clear later phases are observed for microearthquakes below the RQs (i.e., deeper than 35 km). These phases (i) arrive later than the direct *P* wave and are faster than the direct *S* wave, (ii) are dominant in the radial component, (iii) can be traced coherently over a wide depth range, with almost constant travel-time differences from the direct *P* arrival, and (iv) have polarities that correspond to the transmission from the high to the low velocity layer (Fig. 3A). These characteristics indicate that the later phase in the radial component is generated by *P-S* conversion at a plane above the Off-Kanto cluster.

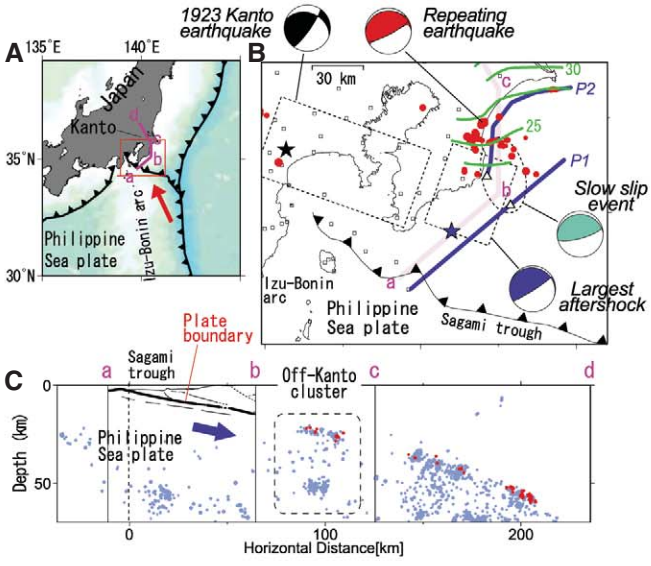

Fig. 1. (**A**) Plate geometry of the PHS, which subducts below Kanto from the Sagami trough. The arrow represents the plate convergence direction relative to Kanto (*25*). (**B**) Map of Kanto. Blue lines denote deep seismic survey lines. Small triangles denote the nearest points between P1 and P2. Small red circles denote repeating earthquakes on the PHS, with the representative focal mechanism (*13*, *18*). Green lines represent isodepth contours of the PHS; numbers denote depths in kilometers (*18*). The epicenter, focal mechanism, and source fault are shown for the 1923 Kanto earthquake (*12*, *26*), its largest aftershock (*13*), and the SSE (*16*, *17*), respectively. Small squares represent seismographic stations. (**C**) The cross section along a line a-b-c-d. The plate boundary of the PHS revealed by P1 (*13*) is shown as a thick line. Small blue circles denote background earthquakes.

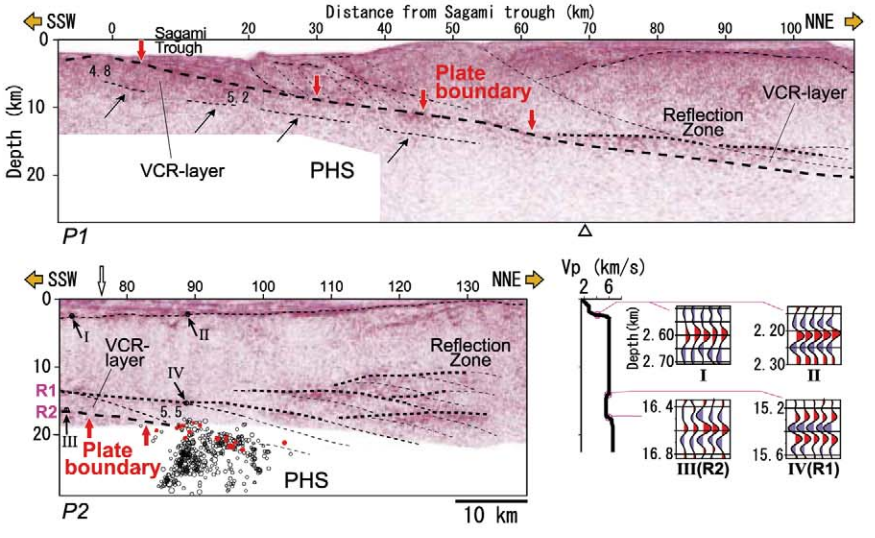

Fig. 2. Deep seismic reflection profiles. Horizontal distance from the Sagami trough is shown on top. P2 is projected onto the N30°E direction. Red arrows show the plate boundary. Numbers denote *P*-wave velocities (km/s). Small triangles denote the nearest point between P1 and P2. In P2, the final hypocenters of the Off-Kanto cluster for which depths were adjusted by the *P-S* wave are projected (red, RQs; black, background microearthquakes). The original sections are shown in fig. S1. The velocity profile at the location indicated by an open arrow is displayed to the right, with enlargements of waveforms at major deep reflectors (R1 and R2) at locations shown by black arrows (III, IV) that are convolved by reflectors at the basement of the surface sedimentary layer just above each region (I, II). P1 data are from (*13*).

To detect the location of the conversion plane, we then compared seismic profiles with microearthquake data. The seismic profiles show that the base of the low-velocity layer in P2 (R2) is the most apparent velocity boundary above the Off-Kanto cluster. Moreover, there is no strong discontinuity 10 km above and below reflector R2 at the southern end of P2 or at the location along P1 closest to P2, except R1 (Fig. 2). R2 corresponds to a change from high to low velocity for a seismic wave from the hypocenter, which can explain the polarities of the *P-S* wave; therefore, the *P-S* wave originates at R2. The layer structure is also imaged in P1 with estimated Vp values of 4.8 and 5.2 km/s at the Sagami trough and a thickness of 2.6 to 4.2 km (*13*). Compared with seismic surveys at the Izu-Bonin arc, the layer structures in P1 and P2 are the deeper extension of the VCR layer (*22*).

The converted (*P-S*) wave allows us to estimate the relative location between the Off-Kanto cluster and the conversion plane by using travel-time differences between the *P-S* wave and the direct *S* wave (*22*). The advantage of such an analysis is that both the *S* and *P-S* waves propagate as *S* waves above the conversion plane, and effects of heterogeneity on their paths through complex shallow structures are cancelled out. Hence, the relative location can be determined accurately (Fig. 3B). We picked arrival times of the *P-S* waves from six earthquakes (35 to 40 km depth) that exhibit a clear onset and are as close as possible to the conversion plane. Travel times calculated by the finite difference method (*23*) revealed the relative location between the Off-Kanto cluster and the conversion plane with travel time residuals less than 0.16 s, which corresponds to a 1.6-km depth uncertainty (*22*) (fig. S5).

Precise relative hypocenters in the Off-Kanto cluster, determined using the double-difference method (*24*) incorporating waveform correlations, shows that RQs are located at the top of the cluster and define a sharp planar distribution (*22*) (fig. S3). Finally, combination of all the results shows that RQs are distributed along the conversion plane, that is, the bottom interface of the VCR layer, and not along its upper interface (Fig. 2). This result is also supported by the fact that the dip angle of the

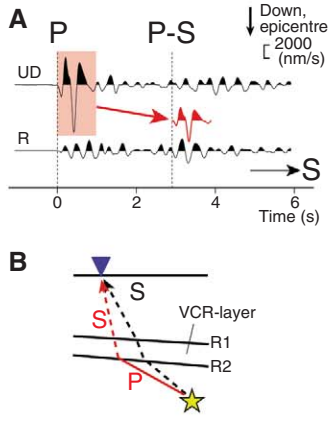

Fig. 3. (**A**) Stacked seismograms for microearthquakes in the Off-Kanto cluster. Vertical (UD) and radial (R) components are shown. A dashed vertical line indicates the arrival time of the *P-S* wave determined from cross-correlation analysis (*22*). (**B**) Schematic ray paths of direct *S* and *P-S* waves are shown. Solid and dashed lines denote *P* and *S* waves, respectively. A star and an inverted triangle denote a hypocenter and a station, respectively.

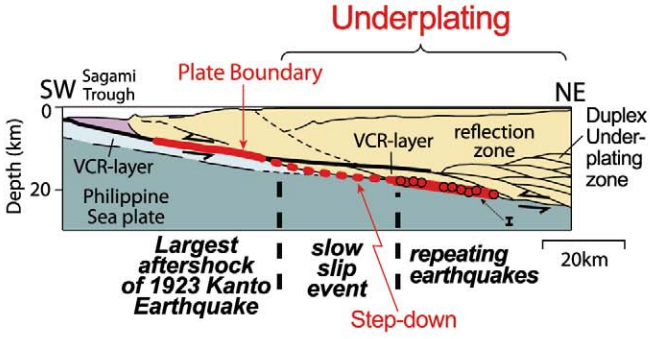

Fig. 4. Schematic illustration of subsurface structure, the plate boundary (red line), and underplating off the Kanto region of the Philippine Sea plate. The depth uncertainty of the RQs is also shown.

RQ plane is 12 ± 1°, which is about twice as large as the dip angle of the upper interface of the VCR layer (~5°) (fig. S3), which suggests that RQs are not distributed along the upper interface. The final result indicates that the plate boundary corresponds to the bottom interface of the VCR layer, showing that the zone of active slip steps down from its upper interface (Fig. 4). Such a step-down will cause accumulation of VCR. A characteristic imbricated structure called a duplex has been widely observed in association with underplating (*8*–*11*, *13*). Here, the reflection zone in P2 resembling such a structure is located northward of the active underplating region (Figs. 2 and 4).

Off Kanto, source areas of the megathrust earthquake [the largest aftershock, moment magnitude (M_w) 7.5, of the 1923 great Kanto earthquake (M_w 7.9) (*13*)], the SSE, and RQs are distributed in sequence from the trench axis to deeper regions (Fig. 4), with the region of the active step-down coinciding with the SSE. Because the SSE off Kanto repeats about every 6 years, with durations of about 10 days (*16*, *17*), underplating may also occur intermittently. In such cases, SSEs may serve as indicators of active step-down of plate boundaries and intermittent formation of duplex structures by underplating.

References and Notes

1. J. C. Moore *et al.*, *Geol. Soc. Am. Bull.* **100**, 1578 (1988).
2. B. A. Housen, H. J. Tobin, P. Labaume, E. C. Leitch, A. J. Maltman; Ocean Drilling Program Leg 156 Shipboard Science Party, *Geology* **24**, 127 (1996).
3. N. L. Bangs *et al.*, *Geology* **32**, 273 (2004).
4. G. Kimura, J. Ludden, *Geology* **23**, 217 (1995).
5. Y. Isozaki, S. Maruyama, F. Furuoka, *Tectonophysics* **181**, 179 (1990).
6. B. R. Hacker, in *Subduction: Top to Bottom* (American Geophysical Union, 1996), pp. 337–346.
7. M. Aoya, S. Uehara, M. Matsumoto, S. R. Wallis, M. Enami, *Geology* **31**, 1045 (2003).
8. J. C. Moore *et al.*, *Geology* **19**, 420 (1991).
9. A. J. Calvert, *Nature* **428**, 163 (2004).
10. G. S. Fuis *et al.*, *Geology* **36**, 267 (2008).
11. T. Ito *et al.*, *Tectonophysics* **472**, 124 (2009).
12. H. Sato *et al.*, *Science* **309**, 462 (2005).
13. H. Kimura, K. Kasahara, T. Takeda, *Tectonophysics* **472**, 18 (2009).
14. S. Asano *et al.*, *J. Phys. Earth* **33**, 173 (1985).
15. K. Suyehiro *et al.*, *Science* **272**, 390 (1996).
16. S. Ozawa, H. Suito, M. Tobita, *Earth Planets Space* **59**, 1241 (2007).
17. H. Hirose, S. Sekine, H. Kimura, K. Obara, *Eos Trans. AGU* **89**, U32A (2008).
18. H. Kimura, K. Kasahara, T. Igarashi, N. Hirata, *Tectonophysics* **417**, 101 (2006).
19. R. M. Nadeau, T. V. McEvilly, *Science* **285**, 718 (1999).
20. This is a reprocessing of (*21*) because only the depth range where commercial drilling can reach was processed previously. For processing, see (*22*).
21. Japan National Oil Corporation (JNOC), "Shallow ocean off the Boso Peninsula" (Report of the Marine Fundamental Geophysical Survey, JNOC, 2000).
22. Materials and methods are available as supporting material on *Science* Online.
23. C. A. Zelt, P. J. Barton, *J. Geophys. Res.* **103**, (B4), 7187 (1998).
24. F. Waldhauser, W. L. Ellsworth, *Bull. Seismol. Soc. Am.* **90**, 1353 (2000).
25. T. Seno, S. Sakurai, S. Stein, *J. Geophys. Res.* **101**, (B5), 11305 (1996).
26. H. Kanamori, *Bull. Earthq. Res. Inst. Univ. Tokyo* **49**, 13 (1971).

27. We thank the Japan National Oil Company (JNOC) for providing the industry seismic reflection data. The manuscript benefited from useful comments and discussions by P. Davis and N. Hirata. We also thank the anonymous reviewers for their valuable comments. This work is supported by the project entitled "Research Project for Crustal Activity Based on Seismic Data" at NIED and Special Project for Earthquake Disaster Mitigation in Tokyo Metropolitan Area from the Ministry of Education, Culture, Sports, Science, and Technology of Japan.

Supporting Online Material

www.sciencemag.org/cgi/content/full/329/5988/210/DC1
Materials and Methods
Figs. S1 to S5
References

15 January 2010; accepted 14 May 2010
10.1126/science.1187115

Adaptation via Symbiosis: Recent Spread of a *Drosophila* Defensive Symbiont

John Jaenike,[1]* Robert Unckless,[1] Sarah N. Cockburn,[2] Lisa M. Boelio,[1] Steve J. Perlman[2]

Recent studies have shown that some plants and animals harbor microbial symbionts that protect them against natural enemies. Here we demonstrate that a maternally transmitted bacterium, *Spiroplasma*, protects *Drosophila neotestacea* against the sterilizing effects of a parasitic nematode, both in the laboratory and the field. This nematode parasitizes *D. neotestacea* at high frequencies in natural populations, and, until recently, almost all infections resulted in complete sterility. Several lines of evidence suggest that *Spiroplasma* is spreading in North American populations of *D. neotestacea* and that a major adaptive change to a symbiont-based mode of defense is under way. These findings demonstrate the profound and potentially rapid effects of defensive symbionts, which are increasingly recognized as major players in the ecology of species interactions.

The ancient origin (*1*–*3*) yet ongoing rapid evolution (*4*–*6*) of genes involved in defense against pathogens and parasites indicate that infective agents have been and continue to be major selective factors for virtually all organisms. In addition to the arsenal of nuclear genes encoding diverse and sophisticated mechanisms of defense, some organisms carry symbiotic microbes that provide defense against natural enemies (*7*, *8*). In insects, for example, maternally

transmitted symbionts have recently been shown to provide protection against parasitoid wasps, fungal pathogens, and RNA viruses (*9*–*13*).

Nematodes are probably the most abundant, diverse, and destructive macroparasites of plants and animals (*14*–*17*). Nematodes commonly attack *Drosophila* (*18*), and at least 10 mushroom-feeding species of *Drosophila* are parasitized by the nematode *Howardula aoronymphium* (Allantonematidae, Tylenchida) (*18*). Mated female *Howardula* infect *Drosophila* larvae, persist to the adult stage of flies, and release offspring that are passed from the fly via the gut and ovipositor into mushrooms, where the nematodes mate to renew the cycle (fig. S1). In the eastern United States, the most commonly infected *Drosophila* species is *D. neotestacea*, with a mean prevalence of parasitism of 0.23 around Rochester, New York (fig. S2) (*19*). Infections are severe, generally rendering females completely sterile, as well as reducing adult survival and male mating success (*18*). Given the high frequency and virulence of infection, there must be strong selective pressure on *D. neotestacea* to evolve defenses against these nematode parasites.

D. neotestacea is also infected with two maternally transmitted bacterial endosymbionts, *Spiroplasma* and *Wolbachia*, neither of which acts as a reproductive parasite in this species (*20*). To test whether the endosymbionts confer defense against nematode parasites, we exposed replicate iso-female lines of *D. neotestacea* to parasitism by *H. aoronymphium* in the laboratory, using lines co-infected with *Spiroplasma* and *Wolbachia* (*SW*), infected with *Spiroplasma* only (*S*), infected with *Wolbachia* only (*W*), or uninfected (*U*) (*21*). The fertility of nematode-parasitized females was greater if they were infected with *Spiroplasma*, but not *Wolbachia*, indicating that such flies have greater tolerance of parasitism [as defined in (*22*)] (Fig. 1A; nematode parasitism × *Spiroplasma* infection: $F_{1,723} = 239$, $P < 0.0001$; parasitism × *Wolbachia* interaction: $F_{1,723} = 0.04$, $P = 0.84$). We failed to detect any bacterial symbionts other than *Spiroplasma* in the *S* lines of *D. neotestacea* by cloning and sequencing 16*S* ribosomal DNA, suggesting that *Spiroplasma* alone is responsible for the fertility rescue.

To test whether *Spiroplasma* is associated with tolerance of nematode parasitism in the wild, we dissected *D. neotestacea* collected from natural populations and scored them for *Howardula* parasitism and the number of mature eggs per ovary. We then used polymerase chain reaction (PCR) to screen these flies for infection with *Spiroplasma* and *Wolbachia*. Female fertility was significantly affected by a nematode parasitism × *Spiroplasma* interaction ($F_{1,211} = 4.45$, $P = 0.036$; Fig. 1, B and C). Among nematode-parasitized flies, females infected with *Spiroplasma* had >10× greater fertility than those not infected with this symbiont (means = 11.13 ± 0.89 and 0.95 ± 0.35 eggs per ovary, respectively; $F_{1,129} = 19.34$, $P < 0.0001$). Among unparasitized flies, females harboring *Spiroplasma* carried a mean of 17.2 ± 0.8 eggs per ovary, and those without *Spiroplasma* carried 17.2 ± 1.5 ($F_{1,87} = 0$, $P = 0.99$), indicating that *Spiroplasma* has little effect on the fertility of unparasitized flies. All main effects and interactions involving *Wolbachia* were nonsignificant ($P > 0.5$), indicating that it does not play a role in defense against nematode parasitism.

To explore how *Spiroplasma* confers tolerance of nematode parasitism, we measured the sizes of motherworms (inseminated adult female worms within flies) in experimentally parasitized one-week-old *D. neotestacea* females. Using antibiotics, we selectively cured a doubly infected *SW* line of *D. neotestacea* from wild populations of either *Wolbachia* only or both *Spiroplasma* and *Wolbachia*; therefore, experimental flies had similar nuclear genetic backgrounds. At the motherworm stage, size is a good indicator of a nematode's potential reproductive output and impact on the host, as a *Howardula* motherworm is largely a sack of embryos and developing juveniles (*23*). As measured by surface area, motherworms were only half as large in flies infected with *Spiroplasma* as in those that were uninfected (means = 0.44 ± 0.04 mm^2 and 0.80 ± 0.04 mm^2, respectively; $F_{1,58} = 45.2$, $P < 0.0001$), indicating that *Spiroplasma* adversely affects motherworm growth and reproduction (Fig. 1F).

Thus, in both the wild and the laboratory, *Spiroplasma* is associated with tolerance of nematode parasites that would otherwise cause sterility in *D. neotestacea* females, and it appears to do so by impairing, through an unknown mechanism, the growth of *Howardula* within parasitized flies. To our knowledge, this is the first example of *Spiroplasma* acting as a mutualist. *Spiroplasma* are among the most widespread bacterial associates of arthropods (*24*), including

[1]Department of Biology, University of Rochester, Rochester, NY 14627, USA. [2]Department of Biology, University of Victoria, Victoria, British Columbia V8W 3N5, Canada.

*To whom correspondence should be addressed. E-mail: john.jaenike@rochester.edu

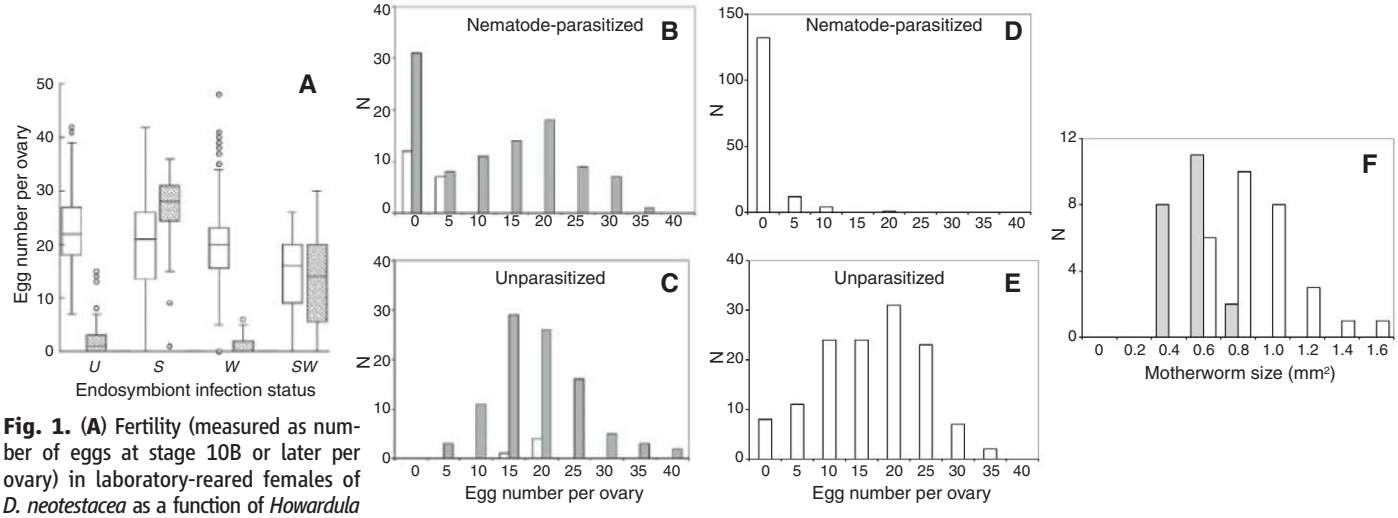

Fig. 1. (**A**) Fertility (measured as number of eggs at stage 10B or later per ovary) in laboratory-reared females of *D. neotestacea* as a function of *Howardula aoronymphium* parasitism, *Spiroplasma* infection, and *Wolbachia* infection. Hatched bars, nematode-parasitized flies; unhatched bars, unparasitized flies. *Spiroplasma* infection increases the fertility of females parasitized with *H. aoronymphium* (compare *U* to *S* and *W* to *SW*). In contrast, *Wolbachia* has no such effect (compare *U* to *W* and *S* to *SW*). (**B** and **C**) Fertility of 2008 field-collected *D. neotestacea* females parasitized (B) or not parasitized (C) by *Howardula*. Gray, infected with *Spiroplasma*; white, uninfected. The fertility of unparasitized flies was independent of *Spiroplasma* infection, whereas for parasitized flies, those carrying *Spiroplasma* were more fertile than uninfected flies. (**D** and **E**) Fertility of 1989 field-collected *D. neotestacea* females parasitized (D) or not parasitized (E) by *Howardula*. Mean number of eggs per ovary = 0.5 ± 0.2 and 14.5 ± 0.7 for parasitized and unparasitized flies, respectively. These flies were not scored for *Spiroplasma* infection, but note that the fertility of *Howardula*-parasitized flies in 1989 was similar to that of parasitized flies in 2008 that were not infected with *Spiroplasma*, suggesting a low level of *Spiroplasma* infection in 1989. (**F**) Nematode motherworms are significantly smaller in flies that harbor *Spiroplasma*. Motherworm size within one-week-old *Spiroplasma*-infected (gray) and uninfected (white) individuals of *D. neotestacea* experimentally parasitized with *Howardula*. *N*, number of flies (B to E) or motherworms (F).

Drosophila (*25*, *26*), but the role of *Spiroplasma* strains that experience solely vertical transmission has remained largely elusive. Although some *Spiroplasma* are reproductive parasites (*27*), mutualistic benefits may be responsible for the persistence of *Spiroplasma* in many host species. It is interesting to note that *Spiroplasma* occurs not only within cells of its invertebrate hosts but also within the hemocoel (*28*), where most parasitic nematodes, such as *Howardula*, reside (*29*).

Four lines of evidence independently suggest that the *Spiroplasma* infection is dynamic and spreading within natural populations of *D. neotestacea*. First, we PCR-screened museum specimens of *D. neotestacea* collected in the eastern United States in the early 1980s for *Spiroplasma*, *Wolbachia*, and, as a control for DNA quality, *Drosophila* cytochrome c oxidase subunit 1 (COI). Of the 20 flies, 18 (90%) were PCR-positive for *Wolbachia*, similar to current levels of *Wolbachia* infection in this species (*20*). In contrast, *Spiroplasma* was not detected, suggesting a prevalence in the 1980s in the range of 0 to 0.14 (the 95% confidence interval around 0 out of 20 *Spiroplasma*-infected flies). This is well below the current infection prevalence in eastern North America, which ranges from 0.5 to 0.8 at sites from Maine to Minnesota (*20*).

Second, almost all nematode-parasitized females of *D. neotestacea* collected in New York in the 1980s were sterile (*18*, *30*). The fertility distribution of nematode-parasitized flies collected in 1989 (Fig. 1D) was similar to that of nematode-parasitized flies that were uninfected with *Spiroplasma* in 2008 (Fig. 1B). A small fraction of parasitized flies in the 1980s carried 10 or more eggs, suggesting they may have been infected with *Spiroplasma*. Thus, in populations of *D. neotestacea* in Rochester, *Spiroplasma* appears to have increased from a low frequency in the 1980s to ~0.8 in less than 20 years (fig. S3 and table S6) (*20*).

Third, there is a continent-wide cline in the prevalence of *Spiroplasma* infection in *D. neotestacea* (Fig. 2A). In contrast, there is much less geographic variation in the infection prevalence of *Wolbachia*, suggesting that it is close to equilibrium across North America (Fig. 2B). *D. neotestacea* is parasitized by *Howardula* throughout its range, from Maine to British Columbia. *Howardula* infection frequencies in coastal British Columbia, where *Spiroplasma* is absent, were 0.21 in 2008 (n = 296 flies surveyed for parasitism) and 0.25 in 2009 (n = 132), similar to the long-term 0.23 prevalence of parasitism near Rochester, New York (*19*). Thus, nematode parasites probably impose selection in favor of *Spiroplasma* infection across the range of *D. neotestacea*.

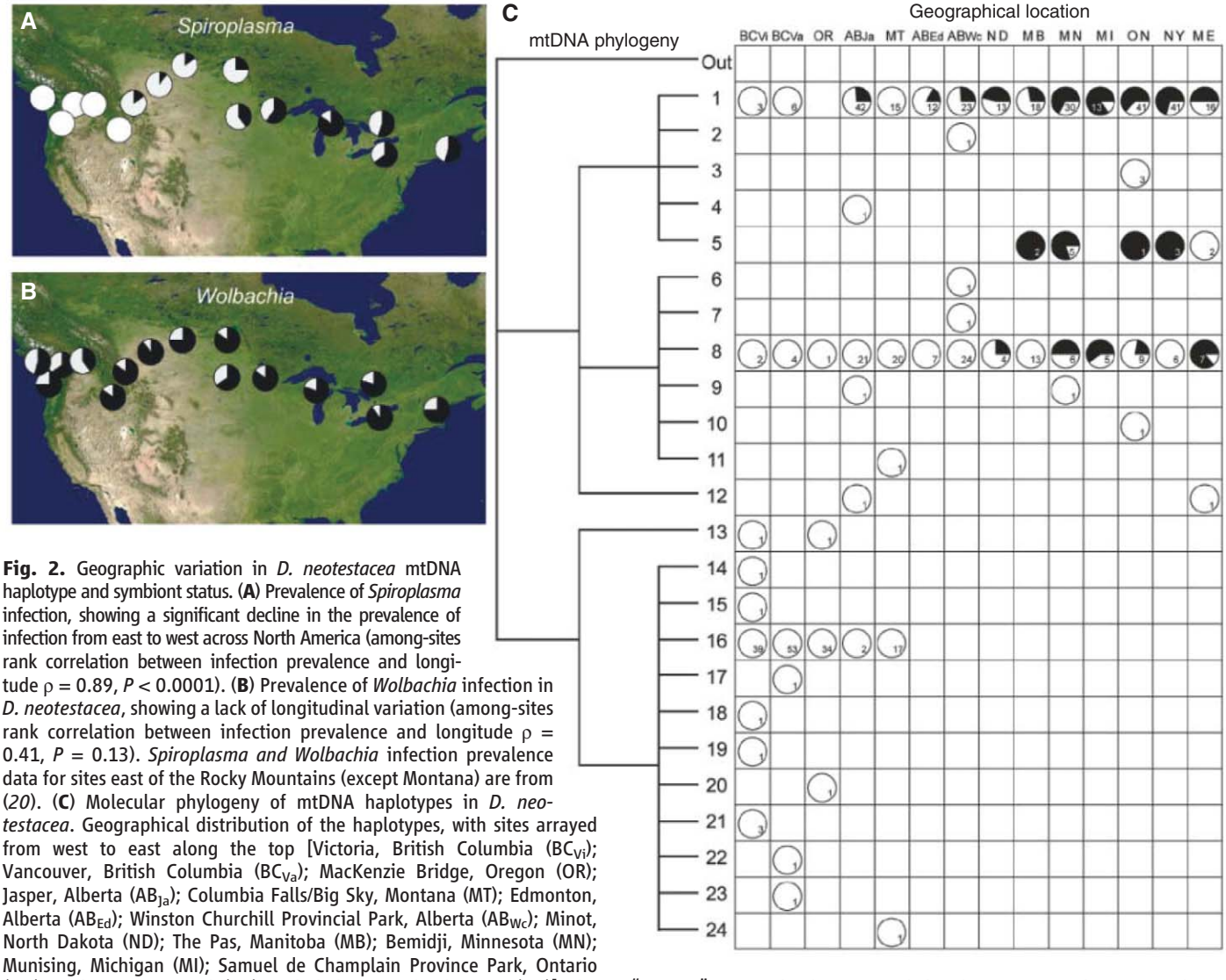

Fig. 2. Geographic variation in *D. neotestacea* mtDNA haplotype and symbiont status. (**A**) Prevalence of *Spiroplasma* infection, showing a significant decline in the prevalence of infection from east to west across North America (among-sites rank correlation between infection prevalence and longitude $\rho = 0.89$, $P < 0.0001$). (**B**) Prevalence of *Wolbachia* infection in *D. neotestacea*, showing a lack of longitudinal variation (among-sites rank correlation between infection prevalence and longitude $\rho = 0.41$, $P = 0.13$). *Spiroplasma and Wolbachia* infection prevalence data for sites east of the Rocky Mountains (except Montana) are from (*20*). (**C**) Molecular phylogeny of mtDNA haplotypes in *D. neotestacea*. Geographical distribution of the haplotypes, with sites arrayed from west to east along the top [Victoria, British Columbia (BC_{Vi}); Vancouver, British Columbia (BC_{Va}); MacKenzie Bridge, Oregon (OR); Jasper, Alberta (AB_{Ja}); Columbia Falls/Big Sky, Montana (MT); Edmonton, Alberta (AB_{Ed}); Winston Churchill Provincial Park, Alberta (AB_{Wc}); Minot, North Dakota (ND); The Pas, Manitoba (MB); Bemidji, Minnesota (MN); Munising, Michigan (MI); Samuel de Champlain Province Park, Ontario (ON); Rochester, New York (NY); and Chebeague Island, Maine (ME)]. The *Spiroplasma* infection prevalence for each site and haplotype is indicated by the proportion of black shading in the pie diagrams. Samples sizes are indicated by the numbers within each pie diagram. The clinal variation in *Spiroplasma* prevalence, the association of *Spiroplasma* infection with "eastern" mtDNA haplotypes, and the clines in *Spiroplasma* prevalence within haplotypes all suggest that *Spiroplasma* is spreading from east to west across North America. The lack of longitudinal variation in *Wolbachia* is consistent with a long-term infection and is close to equilibrium prevalence everywhere.

Finally, the *Spiroplasma* infection status of flies carrying different mitochondrial haplotypes reveals a *Spiroplasma* infection not yet at species-level equilibrium. We previously found a perfect association between *Spiroplasma* haplotype and mitochondrial DNA (mtDNA) haplotype within Rochester, New York, populations of *D. neotestacea*, indicating that horizontal transmission of *Spiroplasma* is rare or nonexistent (*20*). Consequently, mtDNA variation can be used to infer the history of *Spiroplasma* infection in *D. neotestacea*. At equilibrium between natural selection favoring *Spiroplasma* infection and imperfect maternal transmission resulting in loss of *Spiroplasma*, the prevalence of *Spiroplasma* infection should be similar among flies with different mtDNA haplotypes; flies carrying all major mtDNA haplotypes should be infected, and all individuals, whether infected or not, should be descended from infected females (*31*, *32*). This is not the case for *D. neotestacea*, as *Spiroplasma* is common in flies carrying certain mtDNA haplotypes (notably 1, 5, and 8) but absent from all flies carrying "western" haplotypes (e.g., haplotype 16; Fig. 2C). We identified 16 individuals, collected in Oregon and British Columbia, carrying the most common mitochondrial haplotypes in eastern North America, and none were infected with *Spiroplasma*, indicating that the absence of *Spiroplasma* in the west is not due to the absence of mitochondrial clades that elsewhere harbor *Spiroplasma*. Mean within-population mitochondrial diversity is greater in populations where *Spiroplasma* is absent ($\overline{\theta}$ = 0.0056 ± 0.0007) than where it is present ($\overline{\theta}$ = 0.0025 ± 0.0005; $F_{1,12}$ = 11.07, P = 0.006), consistent with theoretical expectations that *Spiroplasma* has not been present in western populations of *D. neotestacea* in the recent evolutionary past (*33*). Taken together, these four patterns suggest that *Spiroplasma* has recently increased in frequency in the eastern populations of *D. neotestacea* and may now be spreading from east to west across North America.

The equilibrium infection prevalence of maternally transmitted endosymbiont is $\hat{P} = 1 - \left(\frac{1-\beta}{s}\right)$, where β is the fidelity of maternal transmission of the symbiont, and s is the selective advantage of infected over uninfected cytoplasmic lineages (*31*). Using wild-caught females, we have estimated that β = 0.97 (*20*) and s = 0.17. The estimate of s is based on the fertility of wild females as a function of *Howardula* parasitism and *Spiroplasma* infection, weighted by the probability of nematode parasitism (*21*). The expected equilibrium prevalence, $\hat{P} \approx 0.8$, is similar to that observed in populations in eastern North America, suggesting that *Spiroplasma* prevalence is at or approaching an equilibrium based largely on a balance between imperfect maternal transmission and a selective advantage due to tolerance of nematode parasitism. Our estimates of β and s are also consistent with a hypothesized increase in *Spiroplasma* infection around Rochester from ~10% in the 1980s to ~80% today (fig. S4).

Does the apparent recent increase of *Spiroplasma* result from recent colonization of *D. neotestacea* by *Spiroplasma*, a recent favorable *Spiroplasma* mutation conferring tolerance to an existing parasite challenge, or the imposition of a new selective pressure? The occurrence of *Spiroplasma* in flies carrying three different mtDNA haplotypes (Fig. 2C) suggests that the colonization of *D. neotestacea* by *Spiroplasma* was not a recent event. We previously found a perfect match between two slightly different *Spiroplasma* variants and two closely related mtDNA haplotypes, indicating that sufficient time has elapsed since the original infection for mutations in both *Spiroplasma* and mtDNA to have accumulated in the infected cytoplasmic lineages (*20*). Thus, *Spiroplasma* was probably present within *D. neotestacea* long before its recent increase. We can also rule out a recent favorable mutation, as both of these *Spiroplasma* variants were associated with tolerance to nematode parasitism. Among nematode-parasitized flies collected in 2008 and for which *spoT* was sequenced, the mean egg numbers for flies carrying the two variants were 13.5 ± 1.0 and 17.2 ± 2.2, both of which were much greater than the 0.95 ± 0.35 eggs in parasitized flies that did not carry *Spiroplasma* ($F_{1,90}$ = 41.9 and $F_{1,29}$ = 83.2, respectively; both P values < 0.0001). Finally, we previously hypothesized that *H. aoronymphium* had recently colonized North America (*34*), based on our finding of no DNA sequence variation (mtDNA COI) among North American samples of *H. aoronymphium*, as well as sequence identity between North American and European samples of this species (*35*). Thus, the apparently rapid spread of *Spiroplasma* is most likely due to recently imposed selection on *D. neotestacea* to evolve tolerance of these sterilizing parasites. The presumed beneficial function of *Spiroplasma* in *D. neotestacea* before the arrival of *H. aoronymphium* is unknown.

Our results show that *Spiroplasma* rescues *D. neotestacea* females from the sterilizing effects of nematode parasitism and that this endosymbiont appears to have recently increased to high frequency in eastern North America and is now spreading from east to west across the continent. Thus, *D. neotestacea* is undergoing a major change to a symbiont-based mode of defense against nematode parasites. This is the first report of natural symbiont-mediated defense against nematodes, the most widespread macroparasites of plants and animals. From an applied perspective, these findings suggest novel measures for nematode control (*36*); for instance, river blindness and lymphatic filariasis are caused by nematodes that are transmitted by various species of flies (*37*). If *Spiroplasma* impaired the development of filarial nematodes within their insect vectors, this could reduce nematode transmission and, thus, incidence of disease in human populations. With respect to natural communities, this study demonstrates the profound and potentially rapid effects of defensive symbionts, which are increasingly recognized as major players in the ecology of species interactions (*7*–*13*).

References and Notes

1. M. F. Flajnik, L. Du Pasquier, *Trends Immunol.* **25**, 640 (2004).
2. G. W. Litman, J. P. Cannon, L. J. Dishaw, *Nat. Rev. Immunol.* **5**, 866 (2005).
3. P. Rosenstiel, E. E. R. Philipp, S. Schreiber, T. C. G. Bosch, *J. Innate Immunity* **1**, 291 (2009).
4. A. L. Hughes, *Mol. Biol. Evol.* **14**, 1 (1997).
5. T. B. Sackton *et al.*, *Nat. Genet.* **39**, 1461 (2007).
6. D. J. Obbard, K. H. J. Gordon, A. H. Buck, F. M. Jiggins, *Philos. Trans. R. Soc. London Ser. B* **364**, 99 (2009).
7. M. S. Gil-Turnes, M. E. Hay, W. Fenical, *Science* **246**, 116 (1989).
8. A. E. Arnold *et al.*, *Proc. Natl. Acad. Sci. U.S.A.* **100**, 15649 (2003).
9. K. M. Oliver, J. A. Russell, N. A. Moran, M. S. Hunter, *Proc. Natl. Acad. Sci. U.S.A.* **100**, 1803 (2003).
10. C. L. Scarborough, J. Ferrari, H. C. J. Godfray, *Science* **310**, 1781 (2005).
11. L. M. Hedges, J. C. Brownlie, S. L. O'Neill, K. N. Johnson, *Science* **322**, 702 (2008).
12. L. Teixeira, A. Ferreira, M. Ashburner, *PLoS Biol.* **6**, e1000002 (2008).
13. K. M. Oliver, P. H. Degnan, M. S. Hunter, N. A. Moran, *Science* **325**, 992 (2009).
14. J. Parkinson *et al.*, *Nat. Genet.* **36**, 1259 (2004).
15. A. Dobson, K. D. Lafferty, A. M. Kuris, R. F. Hechinger, W. Jetz, *Proc. Natl. Acad. Sci. U.S.A.* **105**, 11482 (2008).
16. D. M. Bird *et al.*, *Annu. Rev. Phytopathol.* **47**, 333 (2009).
17. W. R. Nickle, in *Insect Diseases*, vol. 2, G. E. Cantwell, Ed. (Dekker, New York, 1974), pp. 327–376.
18. J. Jaenike, S. J. Perlman, *Am. Nat.* **160** (suppl. 4), S23 (2002).
19. J. Jaenike, *Ecology* **83**, 917 (2002).
20. J. Jaenike, J. K. Stahlhut, L. M. Boelio, R. L. Unckless, *Mol. Ecol.* **19**, 414 (2010).
21. Materials and methods are available as supporting material on *Science* Online.
22. L. Råberg, D. Sim, A. F. Read, *Science* **318**, 812 (2007).
23. J. Jaenike, *Evolution* **50**, 2241 (1996).
24. L. B. Regassa, G. E. Gasparich, *Front. Biosci.* **11**, 2983 (2006).
25. M. Mateos *et al.*, *Genetics* **174**, 363 (2006).
26. T. S. Haselkorn, T. A. Markow, N. A. Moran, *Mol. Ecol.* **18**, 1294 (2009).
27. G. D. D. Hurst, F. M. Jiggins, *Emerg. Infect. Dis.* **6**, 329 (2000).
28. D. L. Williamson, *J. Invertebr. Pathol.* **7**, 493 (1965).
29. G. O. Poinar, *The Natural History of Nematodes* (Prentice-Hall, Englewood Cliffs, NJ, 1983).
30. J. R. Montague, J. Jaenike, *Ecology* **66**, 624 (1985).
31. K. A. Dyer, J. Jaenike, *Genetics* **168**, 1443 (2004).
32. K. A. Dyer, J. Jaenike, *Evolution* **59**, 1518 (2005).
33. R. A. Johnstone, G. D. D. Hurst, *Biol. J. Linn. Soc. London* **58**, 453 (1996).
34. S. J. Perlman, J. Jaenike, *Evolution* **57**, 1543 (2003).
35. S. J. Perlman, G. S. Spicer, D. D. Shoemaker, J. Jaenike, *Mol. Ecol.* **12**, 237 (2003).
36. Z. Kambris, P. E. Cook, H. K. Phuc, S. P. Sinkins, *Science* **326**, 134 (2009).
37. J. E. Allen *et al.*, *PLoS Negl. Trop. Dis.* **2**, e217 (2008).

38. This work was supported by NSF grants DEB-0542094 and DEB-0918872 to J.J. and a Natural Sciences and Engineering Research Council of Canada Discovery Grant to S.J.P. S.J.P. is a Scholar in the Canadian Institute for Advanced Research. We thank C. Cornish, P. Gibas, and K. Dyer for collecting some of the North American *D. neotestacea* used in this study; A. Marshall and L. Harris for technical assistance; N. Polet for the cloning work; D. Grimaldi for providing museum specimens of *D. neotestacea*; and J. Coyne, R. Minckley, K. Oliver, and D. Presgraves for comments on the manuscript. Sequences have been deposited in GenBank under accession numbers GU552299 to GU552304, HM126644 to HM126667, and HM133591 to HM133593.

Supporting Online Material

www.sciencemag.org/cgi/content/full/329/5988/212/DC1
Materials and Methods
SOM Text
Figs. S1 to S4
Tables S1 to S6
References

11 February 2010; accepted 25 May 2010
10.1126/science.1188235

Gamete Recognition in Mice Depends on the Cleavage Status of an Egg's Zona Pellucida Protein

Gagandeep Gahlay, Lyn Gauthier, Boris Baibakov, Olga Epifano, Jurrien Dean*

At fertilization, mouse sperm bind to the zona pellucida (which consists of glycoproteins ZP1, ZP2, and ZP3) that surrounds eggs. A ZP2 cleavage model of gamete recognition requires intact ZP2, and a glycan release model postulates that zona glycans are ligands for sperm. These two models were tested by replacing endogenous protein with ZP2 that cannot be cleaved ($Zp2^{Mut}$) or with ZP3 lacking implicated O glycans ($Zp3^{Mut}$). Sperm bound to two-cell $Zp2^{Mut}$ embryos despite fertilization and cortical granule exocytosis. Contrary to prediction, sperm fertilized $Zp3^{Mut}$ eggs. Sperm at the surface of the zona pellucida remained acrosome-intact for more than 2 hours and were displaced by additional sperm. These data indicate that sperm-egg recognition depends on the cleavage status of ZP2 and that binding at the surface of the zona is not sufficient to induce sperm acrosome exocytosis.

Mammalian fertilization requires successful recognition between ovulated eggs and acrosome-intact capacitated sperm. Most models of gamete recognition postulate that a single ligand in the extracellular zona pellucida (ZP1, ZP2, or ZP3) surrounding eggs interacts with a sperm surface receptor. Although individual zona proteins were initially considered as possible ligands, the absence of ZP1 or the replacement of ZP2 and ZP3 with human homologs does not affect the specificity of sperm-egg recognition (*1*–*3*). Carbohydrate side chains on mouse ZP2 and ZP3 that are released after fertilization have attracted greater investigative attention. Both N and O glycans have been implicated in sperm-egg recognition (*4*), but a particularly precise and widely embraced glycan release model proposes that O glycans attached at Ser^{332} and Ser^{334} on ZP3 act as ligands for a sperm-surface receptor (*5*, *6*).

A more-recent ZP2 cleavage model proposes that rather than sperm binding a single ligand, sperm binding is supported by a three-dimensional zona structure. This model is predicated on the cleavage status of ZP2, rendering the zona pellucida either permissive (uncleaved ZP2) or nonpermissive (cleaved ZP2) to account for sperm binding to the zona pellucida surrounding eggs, but not to that surrounding two-cell embryos (*3*). Both models remain controversial—the first over the presence and identity of the carbohydrate ligand (*7*–*13*) and the second for validation with human ZP2 that was fortuitously not cleaved in transgenic mice (*14*). To test the two models (fig. S1), transgenic mouse lines mutated to either pre-

Laboratory of Cellular and Developmental Biology, National Institute of Diabetes and Digestive and Kidney Diseases, National Institutes of Health, Bethesda, MD 20892, USA.

*To whom correspondence should be addressed. E-mail: jurrien@helix.nih.gov

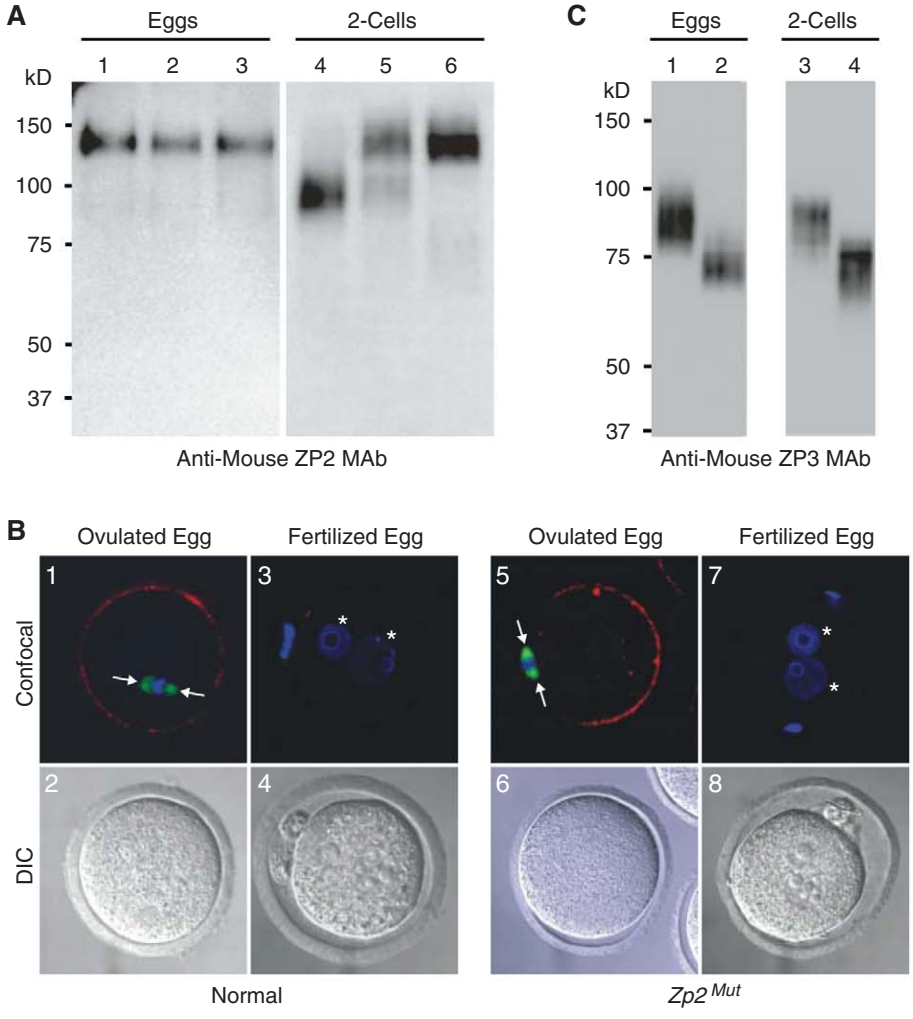

Fig. 1. Expression of mutant zona proteins. (**A**) Immunoblot of eggs (lanes 1 to 3) or embryos (lanes 4 to 6) from normal (lanes 1 and 4), $Zp2^{mut}$ transgenic (lanes 2 and 5), and $Zp2^{Mut}$ (lanes 3 and 6) mice using ZP2 antibodies (*3*). Molecular mass is at left. (**B**) Eggs and embryos from normal (1 to 4) or $Zp2^{Mut}$ (5 to 8) mice were stained with rhodamine-conjugated LCA to image cortical granules, which were present in ovulated (1 and 5) but not in fertilized (3 and 7) eggs. The metaphase spindle (arrows) was stained with a fluorescein-conjugated antibody to α-tubulin, and pronuclei were stained with 4′,6′-diamidino-2-phenylindole (DAPI) (asterisks). (**C**) Same as (A) but with eggs and embryos from normal (lanes 1 and 3) and $Zp3^{Mut}$ (lanes 2 and 4) mice using ZP3 antibodies (*19*).

vent cleavage of mouse ZP2 or the attachment of implicated O glycans on ZP3 (figs. S2 and S3) were back-crossed into appropriate null backgrounds (*3*, *15*) to establish $Zp2^{Mut}$ ($Zp1^{+/+}$, $Zp2^{tm/tm;mut/mut}$, $Zp3^{+/+}$) and $Zp3^{Mut}$ ($Zp1^{+/+}$, $Zp2^{+/+}$, $Zp3^{tm/tm;mut}$) lines, where *tm* indicates a null allele.

In ovulated eggs, ZP2 with a molecular mass of 120 kD is detected, reflecting uncleaved protein. After fertilization, normal ZP2 is cleaved, but mutant ZP2 is not. Thus, ZP2 was detected as a 90-kD (cleaved) protein in normal embryos and as a 120-kD (uncleaved) protein in $Zp2^{Mut}$ two-cell embryos. Both cleaved (endogenous) and uncleaved (mutant) ZP2 were present in mutant *Zp2* transgenic mice ($Zp1^{+/+}$, $Zp2^{+/+;mut}$, $Zp3^{+/+}$) (Fig. 1A). The inability to cleave ZP2 after fertilization could reflect the absence of cortical granule exocytosis. Therefore, ovulated and fertilized eggs were isolated from normal or $Zp2^{Mut}$ females and stained with *Lens culinaris* agglutinin (LCA) to detect cortical granules. In both normal and $Zp2^{Mut}$ mice, cortical granules were present at the periphery of ovulated eggs. Fertilization in the one-cell zygotes was confirmed by the presence of two pronuclei, and in each genotype, LCA staining was absent, reflecting post-fertilization cortical granule exocytosis (Fig. 1B). Thus, the inability to cleave ZP2 in embryos derived from $Zp2^{Mut}$ mice was independent of fertilization and cortical granule exocytosis.

No change in molecular mass was detected before and after fertilization in zonae from either normal or $Zp3^{Mut}$ mice. Although only Ser^{332} and Ser^{334} have been proposed as the binding sites for O glycan ligands that are required for sperm binding, the adjacent Ser^{329}, Ser^{331}, and Ser^{333} were also mutated to validate comparisons with

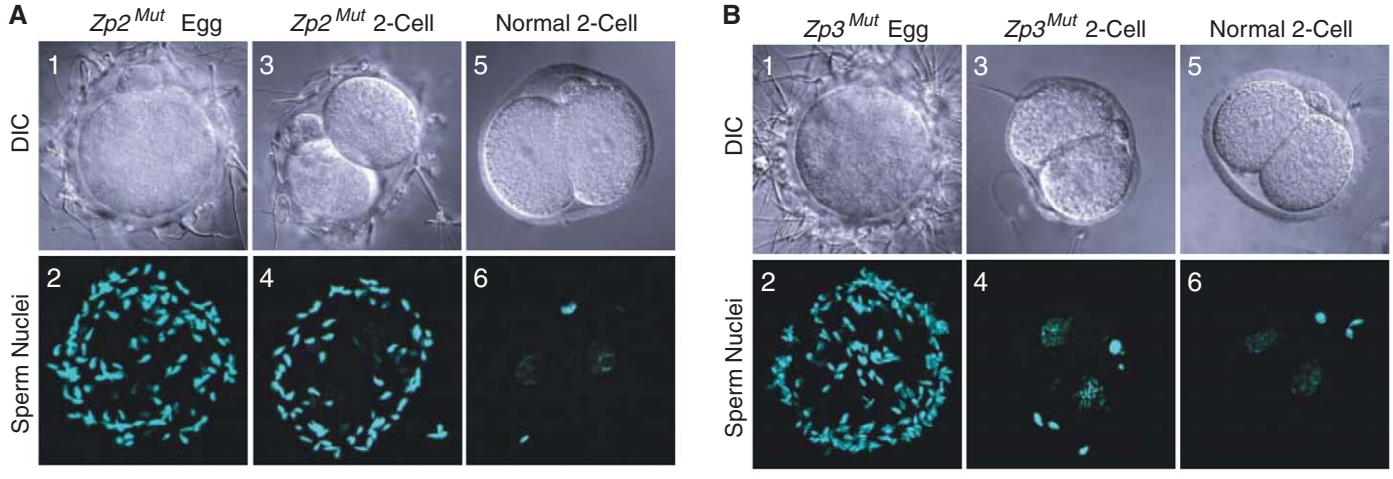

Fig. 2. Sperm binding to eggs and embryos. (**A**) Sperm binding to $Zp2^{Mut}$ eggs (1 and 2) and two-cell embryos (3 and 4) was assayed after 1 hour of incubation with normal capacitated sperm using normal two-cell embryos (5 and 6) as wash controls. The number of sperm bound to eggs and embryos was determined by confocal microscopy. (**B**) Same as (A) but with eggs and embryos from $Zp3^{Mut}$ females.

Fig. 3. Reversible sperm binding. (**A**) Normal (1), $Zp2^{Mut}$ (2), and $Zp3^{Mut}$ (3) eggs and $Zp2^{Mut}$ embryos (4) were incubated with capacitated sperm for 1 hour and stained with Hoechst before imaging by confocal microscopy. After a brief rinse, capacitated *Acr3*-EGFP sperm [5×10^5 ml^{-1} of human tubal fluid (HTF)] were added and incubated for an additional 1 hour. After washing with normal two-cell embryo controls (insets) to remove nonadherent sperm, eggs and embryos were stained with Alexa 568–SBTI before imaging by confocal microscopy (5 to 8). Acrosome-reacted and -intact sperm were labeled with Alexa 568 and EGFP, respectively. Images were modified in Adobe Photoshop to remove nuclear staining from EGFP-positive sperm; thus, Hoechst-positive, EGFP-negative sperm reflect those that were not displaced by EGFP sperm. (**B**) Quantification of the number of sperm bound to eggs and two-cell embryos before (blue bars labeled original) and after (green bars labeled displaced) the addition of *Acr3*-EGFP sperm. Residual sperm (blue bars) reflect those not displaced by *Acr3*-EGFP after 1 hour of incubation and removal of nonadherent sperm.

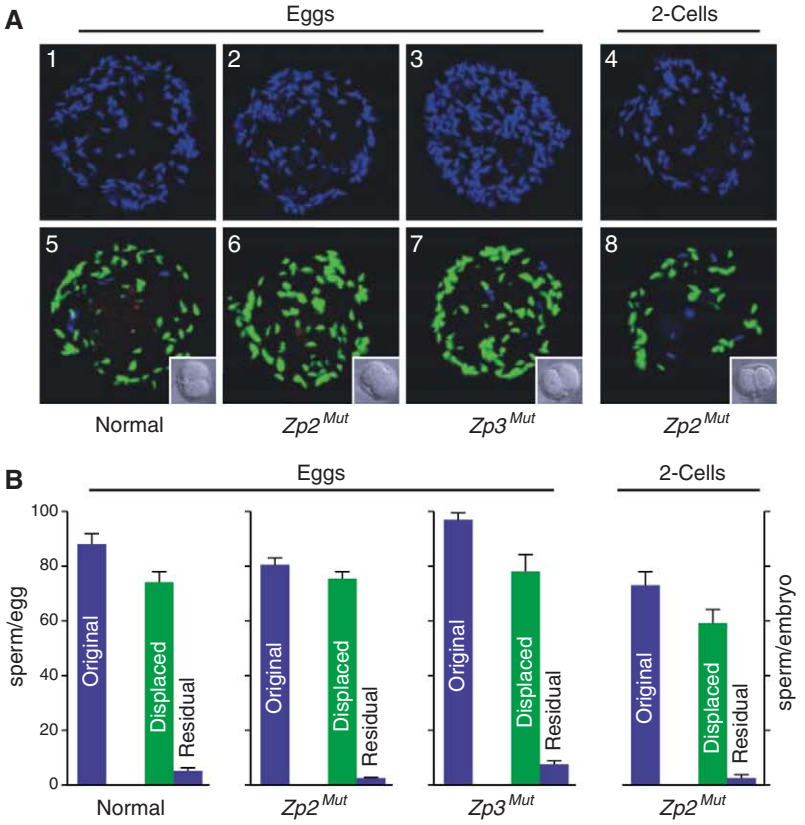

earlier investigations (*6*). The loss of Ser^{329} and Ser^{332} disrupted two attachment sites [$^{327}NCS^{329} \rightarrow {}^{327}NCA^{329}$ (where Ser^{329} is changed to Ala); $^{330}NSS^{332} \rightarrow {}^{330}NVG^{332}$ (where Ser^{331} is changed to Val and Ser^{332} is changed to Gly)] for N glycans that are occupied in native mouse ZP3 (*10*, *16*). Thus, $ZP3^{Mut}$ zonae lacking two of five N glycans had a lower average molecular mass (~75 kD) than was normal (~85 kD) (Fig. 1C).

To test sperm-egg recognition, eggs and two-cell embryos were isolated from normal, $Zp2^{Mut}$, and $Zp3^{Mut}$ mice. After insemination, sperm bound avidly to $Zp2^{Mut}$ eggs (67.2 ± 9.5, n = 12 eggs), as compared with normal two-cell embryos used as wash controls (7.0 ± 0.8, n = 13 embryos). However, sperm also bound (49.3 ± 5.5, n = 19 embryos) to two-cell embryos isolated from $Zp2^{Mut}$ females, in which ZP2 remained uncleaved (Fig. 2A). Contrary to prediction, sperm bound to $Zp3^{Mut}$ eggs (96.1 ± 1.9, n = 7 eggs) in assays using normal two-cell embryos as negative wash controls (Fig. 2B). Thus, sperm binding was unaffected by the ZP3 mutations ($Ser^{332} \rightarrow$ Ala; $Ser^{334} \rightarrow$ Ala), which preclude the attachment of O glycans at those sites. Rather, sperm binding to the surface of the zona pellucida required uncleaved ZP2, in a process that was independent of fertilization and cortical granule exocytosis.

To determine the reversibility of gamete interactions on the surface of the zona pellucida, eggs and embryos were inseminated for 1 hour with normal sperm labeled with Hoechst stain. The fertilized eggs and embryos were then rinsed to remove loosely adherent sperm and challenged with capacitated *Acr3*-enhanced green fluorescent protein (EGFP) sperm (1 hour) followed by washing, using normal two-cell embryos as controls (Fig. 3A). Although comparable numbers of total sperm bound normal, $Zp2^{Mut}$, and $Zp3^{Mut}$ eggs as well as $Zp2^{Mut}$ embryos, 91 to 97% of the initially bound sperm had been replaced with *Acr3*-EGFP sperm (Fig. 3B). These results indicate that the reversibility of sperm adherence to the zona pellucida for eggs (normal, $Zp2^{Mut}$, and $Zp3^{Mut}$) is also observed in $Zp2^{Mut}$ two-cell embryos in which ZP2 remains uncleaved.

Integral to current glycan release models of sperm-egg recognition is that a zona glycan also induces exocytosis of the acrosome, which is a subcellular organelle at the head of sperm (*6*, *17*). Using *Acr*-EGFP sperm to monitor acrosome status, $Zp2^{Mut}$ and $Zp3^{Mut}$ eggs were fertilized in vitro. Sperm were present at the surface of the zona pellucida for >2 hours after insemination. The number of sperm adherent to normal, $Zp2^{Mut}$, and $Zp3^{Mut}$ eggs was comparable among the genotypes at 1 hour (80.8 ± 5.6, 76.7 ± 4.5, and 77.6 ± 13.5, respectively) and 2 hours (39.8 ± 3.6, 45.8 ± 3.3, and 43.5 ± 7.5, respectively). Sperm also remained adherent to the surface of the zona matrix surrounding $Zp2^{Mut}$ embryos at 1 (98.4 ± 4.1) and 2 (25.7 ± 0.9) hours (Fig. 4A). During this time period, virtually all adherent sperm remained acrosome-intact. Thus, binding to the surface of the zona pellucida is not sufficient to induce acrosome exocytosis. However, only acrosome-reacted sperm

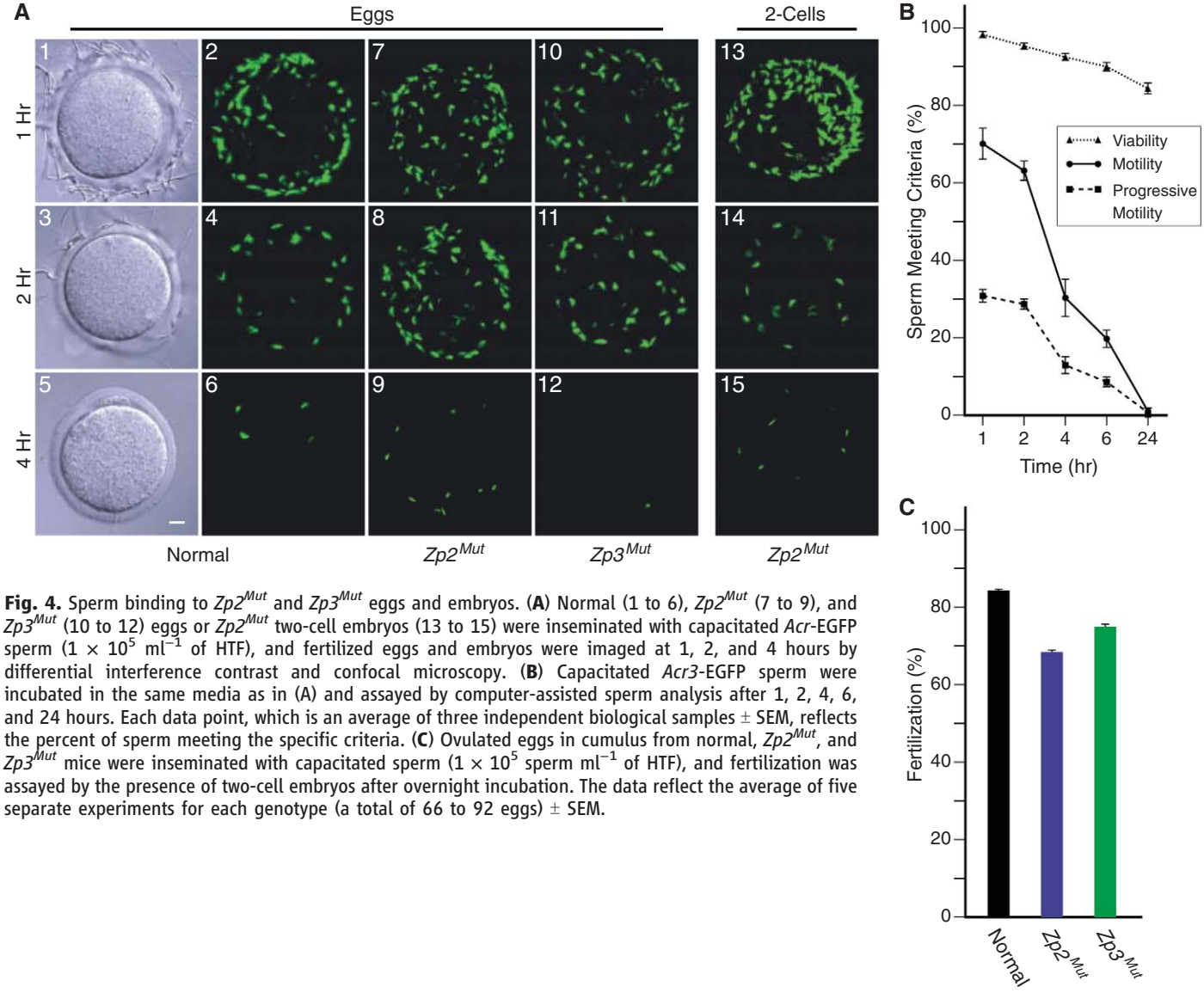

Fig. 4. Sperm binding to $Zp2^{Mut}$ and $Zp3^{Mut}$ eggs and embryos. (**A**) Normal (1 to 6), $Zp2^{Mut}$ (7 to 9), and $Zp3^{Mut}$ (10 to 12) eggs or $Zp2^{Mut}$ two-cell embryos (13 to 15) were inseminated with capacitated *Acr*-EGFP sperm (1×10^5 ml^{-1} of HTF), and fertilized eggs and embryos were imaged at 1, 2, and 4 hours by differential interference contrast and confocal microscopy. (**B**) Capacitated *Acr3*-EGFP sperm were incubated in the same media as in (A) and assayed by computer-assisted sperm analysis after 1, 2, 4, 6, and 24 hours. Each data point, which is an average of three independent biological samples ± SEM, reflects the percent of sperm meeting the specific criteria. (**C**) Ovulated eggs in cumulus from normal, $Zp2^{Mut}$, and $Zp3^{Mut}$ mice were inseminated with capacitated sperm (1×10^5 sperm ml^{-1} of HTF), and fertilization was assayed by the presence of two-cell embryos after overnight incubation. The data reflect the average of five separate experiments for each genotype (a total of 66 to 92 eggs) ± SEM.

are present in the perivitelline space, which suggests that acrosome exocytosis is initiated either before arrival at the surface of the zona pellucida or during penetration of the zona matrix (*18*).

By 4 hours after insemination, few *Acr*-EGFP sperm remained on the zona surface of normal, $Zp2^{Mut}$, and $Zp3^{Mut}$ eggs (1.8 ± 0.4, 12.0 ± 1.8, and 1.1 ± 0.3, respectively) or $Zp2^{Mut}$ embryos (10.9 ± 2.1). To determine whether release was secondary to acrosome exocytosis, sperm were stained with Alexa 568–conjugated soybean trypsin inhibitor (SBTI), which binds to the inner acrosomal membrane after the acrosome reaction. With rare exceptions (2 of 1929 sperm observed), no acrosome-reacted sperm were detected on the surface of the zona matrix. The disappearance of sperm from the zona surface of $Zp2^{Mut}$ eggs and embryos (which must be independent of ZP2 cleavage) as well as from normal and $Zp3^{Mut}$ eggs correlated with a pronounced decrease in progressive sperm motility (Fig. 4B), although causality has not been established.

In vitro fertilization was determined by the addition of capacitated sperm to ovulated eggs in cumulus obtained from normal, $Zp2^{Mut}$, and $Zp3^{Mut}$ female mice. Both rescue lines had fertilization rates that were comparable to those observed with normal controls (Fig. 4C). To assess in vivo fertilization, $Zp2^{Mut}$ or $Zp3^{Mut}$ females were paired with corresponding transgenic females as controls and mated with normal male mice that were proven to be fertile. The size of $Zp3^{Mut}$ litters was comparable to those of co-caged control female mice (table S1), indicating that $Zp3^{Mut}$ mice have normal fertility both in vitro and in vivo.

However, only half (3 out of 6) of the $Zp2^{Mut}$ females produced pups in vivo, with 36% as many litters, the size of which were significantly smaller than those of co-caged controls. Similar numbers of eggs and one-cell embryos were recovered from the oviducts of $Zp2^{Mut}$ and control females after gonadotrophin stimulation or in vivo fertilization, respectively (tables S1 and S2). There was no evidence of supernumerary sperm in the perivitelline space (0.05 ± 0.03 sperm per embryo, $n = 40$ embryos), indicating that an effective postfertilization block to polyspermy was imposed independently of ZP2 cleavage. After flushing oviducts at embryonic day 3.5 (E3.5), significantly fewer blastocysts were recovered from mutant as compared with control female mice, of which mating was confirmed by the presence of a copulatory plug (table S2). Thus, early embryonic loss rather than defects in fertility appears as the major contributor to the smaller litter sizes observed in $Zp2^{Mut}$ females.

The normal fertility of $Zp3^{Mut}$ mice is not consistent with glycan release models in which O glycans attached to ZP3 Ser^{332} or Ser^{334} play an essential role in sperm-egg recognition. More generally, the ability of sperm to bind to $Zp2^{Mut}$ embryos after cortical granule exocytosis does not support any zona ligand in a glycan release model. Mutant mouse ZP2, which differs in only three amino acids from the native protein, has the same extent of posttranslational modifications and reconstitutes a zona pellucida in *Zp2* null mice. The observed binding of sperm to $Zp2^{Mut}$ two-cell embryos is not consistent with glycan release models, in which a cortical granule glycosidase cleaves off a zona glycan to account for the inability of sperm to bind after fertilization. For sperm to bind to the zona pellucida after cortical granule exocytosis, the candidate glycan would have to remain accessible to sperm and yet have been inaccessible for cleavage by a cortical granule glycosidase. This inconsistency applies both to N and O glycan candidate ligands. We thus conclude that glycan release models, as currently formulated, do not offer an adequate explanation of sperm-egg recognition.

Rather, recent and accumulating data support a ZP2 cleavage model for sperm-egg recognition, in which sperm adhere to the surface of the zona pellucida if ZP2 is intact, independent of fertilization and cortical granule exocytosis. Thus, sperm bind to normal eggs but not to two-cell embryos in which ZP2 has been cleaved by a protease that is released during cortical granule exocytosis. However, mutant ZP2 protein cannot be cleaved, and sperm bind to two-cell embryos derived from $Zp2^{Mut}$ mice. A direct effect of ZP2 cleavage on the three-dimensional matrix provides a parsimonious explanation of these results, rendering the zona pellucida either permissive (intact ZP2) or nonpermissive (cleaved ZP2) for sperm-egg recognition.

References and Notes

1. T. L. Rankin *et al.*, *Development* **125**, 2415 (1998).
2. T. Rankin, P. Talbot, E. Lee, J. Dean, *Development* **126**, 3847 (1999).
3. T. L. Rankin *et al.*, *Dev. Cell* **5**, 33 (2003).
4. D. R. Tulsiani, H. Yoshida-Komiya, Y. Araki, *Biol. Reprod.* **57**, 487 (1997).
5. H. M. Florman, P. M. Wassarman, *Cell* **41**, 313 (1985).
6. J. Chen, E. S. Litscher, P. M. Wassarman, *Proc. Natl. Acad. Sci. U.S.A.* **95**, 6193 (1998).
7. S. Shi *et al.*, *Mol. Cell. Biol.* **24**, 9920 (2004).
8. S. A. Williams, L. Xia, R. D. Cummings, R. P. McEver, P. Stanley, *J. Cell Sci.* **120**, 1341 (2007).
9. L. C. Lopez *et al.*, *J. Cell Biol.* **101**, 1501 (1985).
10. E. S. Boja, T. Hoodbhoy, H. M. Fales, J. Dean, *J. Biol. Chem.* **278**, 34189 (2003).
11. A. D. Thall, P. Malý, J. B. Lowe, *J. Biol. Chem.* **270**, 21437 (1995).
12. J. B. Lowe, J. D. Marth, *Annu. Rev. Biochem.* **72**, 643 (2003).
13. M. Asano *et al.*, *EMBO J.* **16**, 1850 (1997).
14. M. K. Jungnickel, K. A. Sutton, H. M. Florman, *Cell* **114**, 401 (2003).
15. T. Rankin *et al.*, *Development* **122**, 2903 (1996).
16. Single-letter abbreviations for the amino acid residues are as follows: A, Ala; C, Cys; G, Gly; N, Asn; S, Ser; and V, Val.
17. L. Leyton, P. Saling, *J. Cell Biol.* **108**, 2163 (1989).
18. B. Baibakov, L. Gauthier, P. Talbot, T. L. Rankin, J. Dean, *Development* **134**, 933 (2007).
19. I. J. East, B. J. Gulyas, J. Dean, *Dev. Biol.* **109**, 268 (1985).

20. This research was supported by the Intramural Research Program of NIH, National Institute of Diabetes and Digestive and Kidney Diseases.

Supporting Online Material

www.sciencemag.org/cgi/content/full/329/5988/216/DC1
Materials and Methods
Figs. S1 to S3
Tables S1 and S2
References

10 February 2010; accepted 17 May 2010
10.1126/science.1188178

Ku70 Corrupts DNA Repair in the Absence of the Fanconi Anemia Pathway

Paul Pace,[1]* Georgina Mosedale,[2]* Michael R. Hodskinson,[1]* Ivan V. Rosado,[1] Meera Sivasubramaniam,[1] Ketan J. Patel[1]†

A conserved DNA repair response is defective in the human genetic illness Fanconi anemia (FA). Mutation of some FA genes impairs homologous recombination and error-prone DNA repair, rendering FA cells sensitive to DNA cross-linking agents. We found a genetic interaction between the FA gene *FANCC* and the nonhomologous end joining (NHEJ) factor *Ku70*. Disruption of both *FANCC* and *Ku70* suppresses sensitivity to cross-linking agents, diminishes chromosome breaks, and reverses defective homologous recombination. Ku70 binds directly to free DNA ends, committing them to NHEJ repair. We show that purified FANCD2, a downstream effector of the FA pathway, might antagonize Ku70 activity by modifying such DNA substrates. These results reveal a function for the FA pathway in processing DNA ends, thereby diverting double-strand break repair away from abortive NHEJ and toward homologous recombination.

Fanconi anemia (FA) proteins are components of a conserved metazoan DNA repair pathway that facilitates homologous recombination (HR) and DNA translesion synthesis (TLS) (*1*, *2*). Genetic and biochemical evidence point to an upstream role for the FA pathway in interstrand cross-link repair during replication (*3*, *4*). Consequently, FA knockout cell lines accumulate large numbers of chromatid breaks after exposure to cross-linking agents, indicating a crucial role for the FA proteins in resolving DNA double-strand breaks (DSBs) created at

[1]MRC Laboratory of Molecular Biology, Hills Road, Cambridge CB2 2QH, UK. [2]Weatherall Institute of Molecular Medicine, University of Oxford, Oxford OX3 9DS, UK.

*These authors contributed equally to this work.
†To whom correspondence should be addressed. E-mail: kjp@mrc-lmb.cam.ac.uk

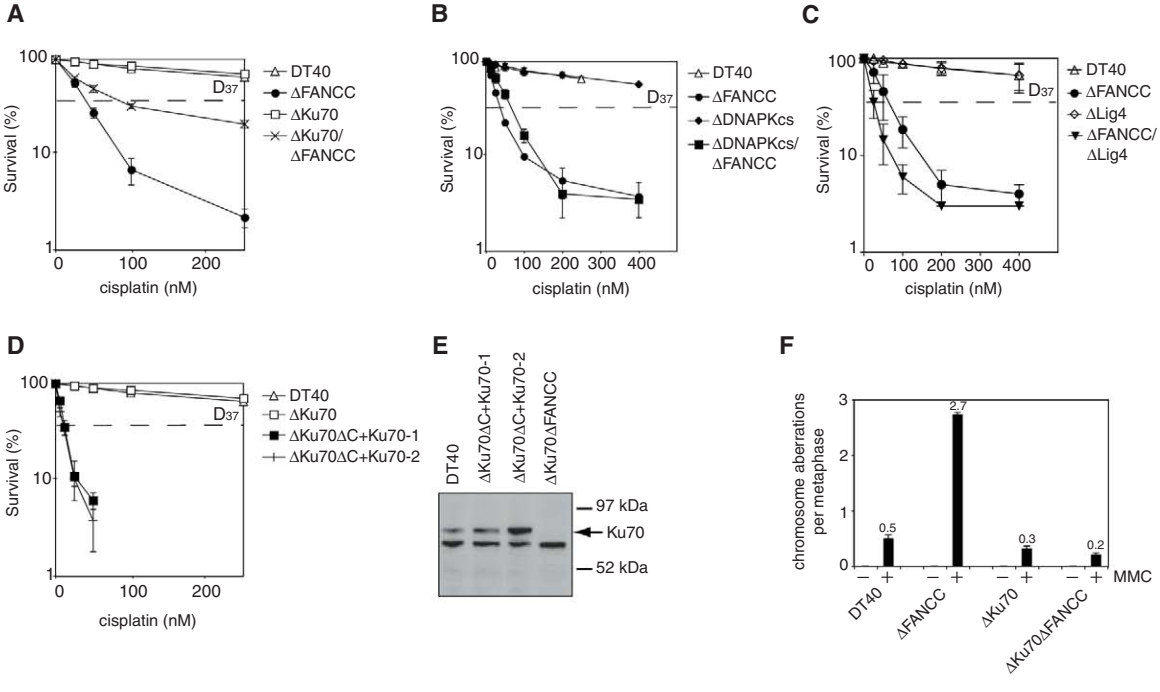

Fig. 1. Suppression of cross-linker sensitivity and chromosome breakage in *ΔKu70ΔFANCC* DT40 cells. (**A** to **C**) Cisplatin sensitivity of NHEJ DT40 mutants (*ΔKu70*, *ΔDNAPKcs*, *ΔLig4*) combined with FANCC (*ΔFANCC*) disruption, analyzed by modified proliferation assay (*3*). Each point represents the mean from three independent experiments ± SE. (**D**) Cisplatin sensitivity of *ΔKu70ΔFANCC* complemented with Ku70 cDNA (*ΔKu70ΔC+Ku70-1* *ΔKu70ΔC+Ku70-2*). (**E**) Immunoblot analysis for Ku70 expression in the indicated cell lines. (**F**) Chromosome breakage analysis of strains after exposure to a single dose of the cross-linking agent mitomycin C (MMC). Log-phase cultures were exposed to MMC (50 ng/ml) for 12 hours; bars represent means ± SE.

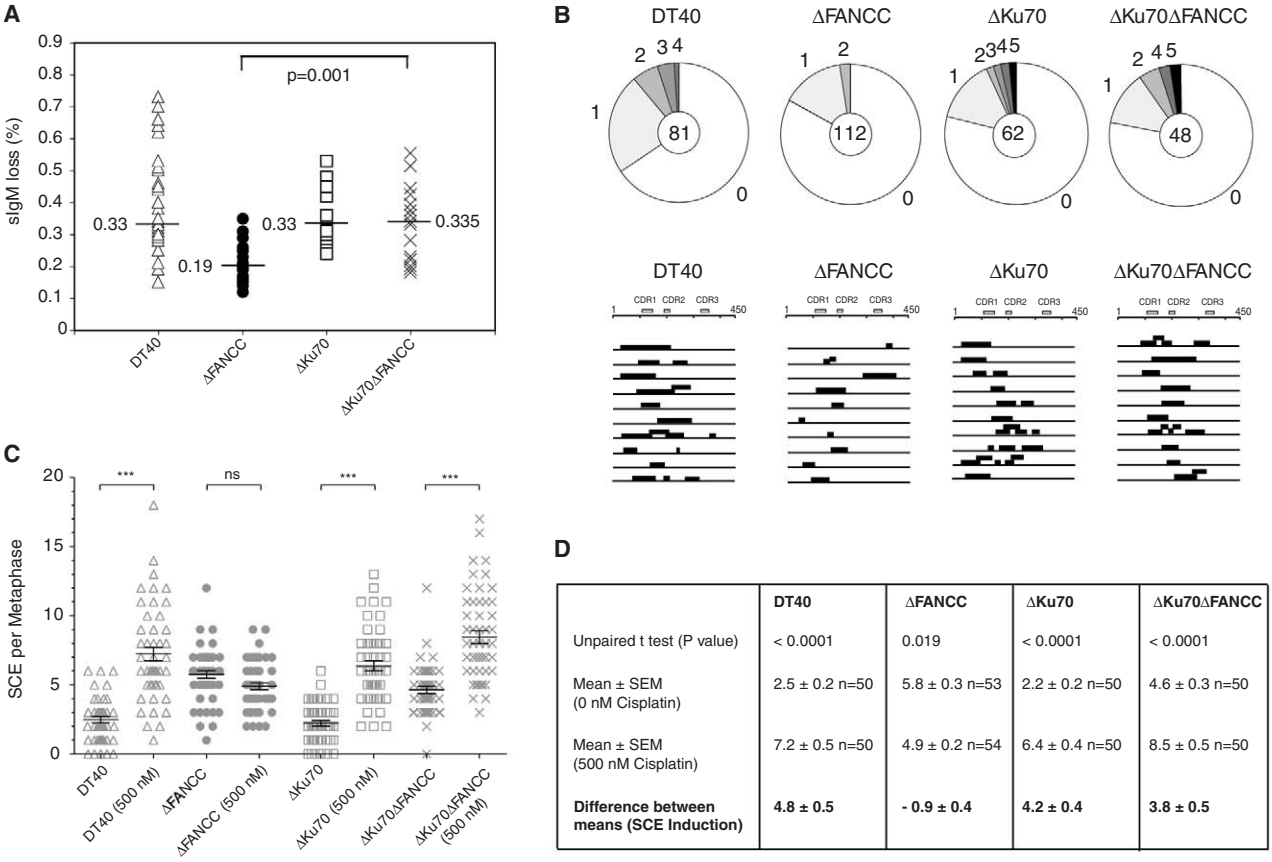

	DT40	ΔFANCC	ΔKu70	ΔKu70ΔFANCC
Unpaired t test (P value)	< 0.0001	0.019	< 0.0001	< 0.0001
Mean ± SEM (0 nM Cisplatin)	2.5 ± 0.2 n=50	5.8 ± 0.3 n=53	2.2 ± 0.2 n=50	4.6 ± 0.3 n=50
Mean ± SEM (500 nM Cisplatin)	7.2 ± 0.5 n=50	4.9 ± 0.2 n=54	6.4 ± 0.4 n=50	8.5 ± 0.5 n=50
Difference between means (SCE Induction)	**4.8 ± 0.5**	**- 0.9 ± 0.4**	**4.2 ± 0.4**	**3.8 ± 0.5**

Fig. 2. Improved HR repair of endogenous and cisplatin-induced DNA damage in the *ΔKu70ΔFANCC* strain. (**A**) $sIgM^+$ to $sIgM^-$ fluctuation assay to assess Ig gene conversion efficacy. $sIgM^+$ clones (each symbol denotes a single clone) were expanded from single cells up to 55 doublings and then assessed for sIgM by FACS. sIgM loss was expressed as a percentage of the total per clone and the median calculated. (**B**) Sequence analysis of amplified V genes obtained from sorted $sIgM^-$ cells. Pie charts depict the proportion of the total number of sequences (number at center) containing one to five distinct gene conversion tracts per locus. Gene conversion events (solid bars) are represented as 10 separate diversified V gene loci for each strain. (**C**) Inducible sister chromatid exchanges in response to cisplatin, scored as described previously (*3*). Each symbol depicts a single scored metaphase. (**D**) Statistical analysis of SCE data.

cross-links. DSBs are preferentially repaired by nonhomologous end joining (NHEJ) in the G_1 phase of the cell cycle, and by HR during replication (*5*). Although the selective use of either pathway shows clear associations with different phases of the cell cycle, little is known about the regulation of this specificity in cross-link repair.

The FA pathway has been implicated in the repair of some DSBs by HR but also in NHEJ fidelity (*6*, *7*). These apparent contradictions led us to examine the nature of the relationship between the FA pathway and NHEJ. We compared DT40 chicken B cells with combined disruption of the FA nuclear complex gene *FANCC* and the NHEJ genes *Ku70* (Δ*Ku70*), *DNA-PK$_{CS}$* (Δ*DNA-PK$_{CS}$*), or *Ligase IV* (Δ*Lig4*) (*8*). Strains were tested for their sensitivity to the DNA cross-linking agent cisplatin (Fig. 1, A to C) and to x-rays (fig. S1, B and C). Δ*FANCC* cells were very sensitive to cross-links but not to x-rays, in contrast to Δ*DNA-PK$_{CS}$* or Δ*Ku70* strains. However, combined ablation of *FANCC* with *Ku70*, but not with *DNA-PK$_{CS}$* or *Ligase IV*, caused suppression of the cisplatin sensitivity seen in the Δ*FANCC* strain [Fig. 1A; dose resulting in 37% population survival (D_{37}) values: Δ*FANCC* = 45 nM, Δ*Ku70*Δ*FANCC* = 95 nM; dose resulting in 10% population survival (D_{10}) values: Δ*FANCC* = 90 nM, Δ*Ku70*Δ*FANCC* = 400 nM]. The Δ*Ku70*Δ*FANCC* cells were complemented with *Ku70* cDNA and the marked sensitivity to cisplatin was restored (Fig. 1, D and E; *Ku70*-complemented Δ*Ku70*Δ*FANCC* lines Δ*Ku70*Δ*C*+*Ku70-1* and Δ*Ku70*Δ*C*+*Ku70-2*; D_{37} = 15 nM, D_{10} = 25 nM). To extend our finding to other vertebrates, we knocked down Ku70/80 in human *FANCC*-deficient cells, facilitating cross-linker resistance (fig. S1, D and E; D_{37} values: mock siRNA = 3 μM, Ku80 siRNA = 6 μM).

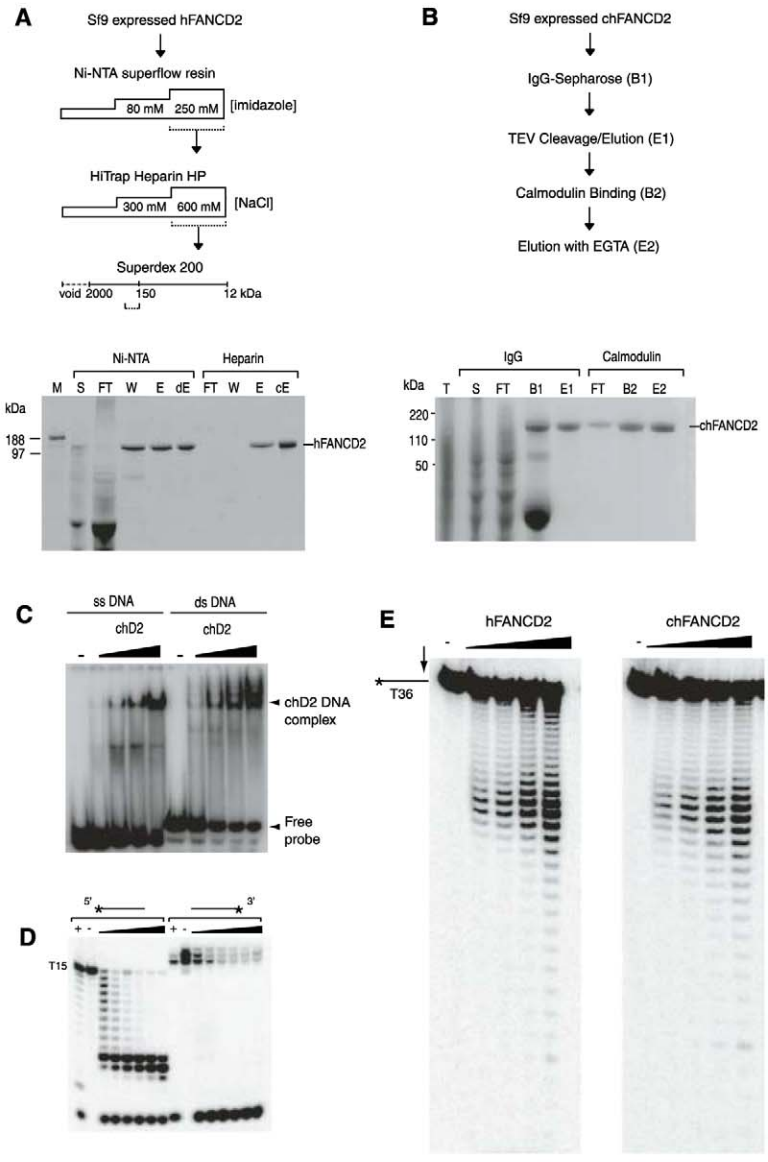

Fig. 3. Purified human and chicken FANCD2 possess 3′→5′ exonuclease activity. (**A**) Purification scheme (top) and Coomassie-stained SDS-PAGE analysis (bottom) for the purification of human FANCD2 (hFANCD2) containing a C-terminal His tag. M, marker; S, supernatant; FT, flowthrough; W, wash; E, eluate (d, dialyzed; c, concentrated). (**B**) Purification scheme (top) and Coomassie-stained SDS-PAGE analysis (bottom) for chicken FANCD2 (cFANCD2) carrying an N-terminal tandem affinity purification tag. T, total lysate; B, bound fractions. (**C**) Electrophoretic mobility shift assay to determine binding of cFANCD2 (ChD2) to radiolabeled ssDNA and dsDNA. (**D**) hFANCD2 (200 nM) was reacted with 5′- or 3′-radiolabeled single-stranded T15 oligonucleotide for increasing times (5 to 80 min at 37°C). +, mung bean nuclease was used as a positive control (10 min). (**E**) Purified equimolar hFANCD2 and cFANCD2 were compared for exonuclease activity (0, 5, 10, 25, and 50 nM protein reacted with 5′-labeled polyT 36-mer (T36) for 15 min at 37°C).

After exposure to cross-linking agents, Δ*FANCC* cells display higher levels of chromosome breakage than wild-type DT40 cells (*3*). Because *Ku70* appears to be required for increased cellular sensitivity to cross-linkers in Δ*FANCC* cells, we investigated whether *Ku70* ablation affects levels of chromosome breakage. Exposure to a single dose of the cross-linking agent mitomycin C (MMC) caused much less chromosome breakage in Δ*Ku70*Δ*FANCC* cells than observed in the Δ*FANCC* strain (Fig. 1F).

DT40 cells express immunoglobulin M on their surface (sIgM). The variable (V) loci of *IgM* undergo constant diversification by gene conversion (HR) or point mutation (TLS) (*9*, *10*); both processes are impaired in the Δ*FANCC* strain (*3*). We therefore used sIgM fluctuation analysis to determine whether *Ku70* contributes toward defective gene conversions and point mutations in the Δ*FANCC* strain (fig. S2A). The prevalence of sIgM loss was reduced in the Δ*FANCC* cells relative to the Δ*Ku70* and DT40 strains, yet this defect was largely reversed in the Δ*Ku70*Δ*FANCC* double-deficient strain (Fig. 2A). It is noteworthy that sIgM negative frequency in Δ*Ku70*Δ*FANCC* cells is lower than that reported for HR-deficient Δ*XRCC2* strains (in which increased TLS accounts for locus diversification) (*9*, *10*). To confirm that gene conversions, and not point mutations, are rescued at the *IgM* locus in Δ*Ku70*Δ*FANCC* cells, we used fluorescence-activated cell sorting (FACS) to separate the sIgM-negative populations from multiple clones and then amplified and sequenced their V gene loci. Gene conversion and point mutation events were identified and their frequency compared to our published database for DT40 and the Δ*FANCC* strain. These data clearly show that the number of gene conversion tracts per individual sequence was increased in the Δ*Ku70*Δ*FANCC* strain relative to the Δ*FANCC* strain (Fig. 2B). In contrast, no increase in point mutations was observed after *Ku70* ablation (Δ*FANCC*, 1/85 changes; Δ*Ku70*Δ*FANCC*, 0/30 changes). Two additional HR events were analyzed to confirm the rescue of HR-dependent repair: sister chromatid exchanges (SCEs) and gene targeting. DT40 and Δ*Ku70* cells induced SCEs when

exposed to cisplatin, but this response did not occur in Δ*FANCC* cells. However, Δ*Ku70*Δ*FANCC* was clearly capable of inducing SCEs in response to cisplatin (Fig. 2, C and D). The Δ*FANCC* strain also showed a defect in specific gene targeting, which was also reversed in the Δ*Ku70*Δ*FANCC* strain (fig. S2B).

These results indicate a pivotal role for the *Ku70* gene in inhibiting homologous recombination repair after inactivation of the FA pathway, and this role is not due to the NHEJ genes *DNA-PKcs* or *Ligase IV* (*11*). Ku70 binds DNA ends at DSBs (*12*) and can interfere with HR repair (*8*, *13*). DSBs generated as a by-product of replication-coupled repair could therefore be trapped by Ku70, causing them to be diverted from HR repair. Our data suggest that the FA pathway intervenes in this process. The FANCC protein regulates monoubiquitination of FANCD2, a key downstream effector of the FA pathway (*14*, *15*). It was therefore logical to test whether the purified FANCD2 protein (Fig. 3, A and B, Fig. 4B, and fig. S3C) might counteract Ku70 access to DNA. Both human (*16*) and chicken FANCD2 bound single-stranded DNA (ssDNA) and double-stranded DNA (dsDNA) in the absence of divalent cations (Fig. 3C). Addition of Mg^{2+}/Mn^{2+} resulted in degradation of ssDNA and 3′ overhangs (fig. S3, A and B). Degradation occurred with 3′→5′ polarity and was common to both human and chicken FANCD2 (Fig. 3, D and E). Despite extensive analysis of the FANCD2 primary sequence, an exonuclease domain remained elusive. We therefore established the specificity of this activity by several distinct approaches. First, the activity fractionated with FANCD2 (fig. S4A). Second, adsorption of purified FANCD2 by means of anti-FANCD2 columns removed exonucleolytic activity (Fig. 4A). Third, human FANCD2 expressed and purified from a different host specifically co-purified with exonuclease activity (Fig. 4B). Furthermore, exonuclease activity was coincident with purified FANCD2 renatured in SDS–polyacrylamide gel electrophoresis (PAGE) activity gels, whereas truncations abolished activity (fig. S4, B and C). Finally, we crystallized chicken FANCD2, washed the crystals, and reconstituted them in nuclease buffer (Fig. 4C). These preparations retained 3′→5′ exonuclease activity. These converging lines of evidence indicate that exonuclease activity is intrinsic to the FANCD2 polypeptide.

Our results indicate that the FA pathway promotes HR repair of DSBs created at cross-links or abasic sites by counteracting Ku70. We suggest that this is achieved by direct modification of DSBs. Recent work using *Xenopus* extracts showed that a DNA cross-link causes bidirectional replication fork arrest (fig. S5). Repair is initiated when one fork advances up to the cross-link; dual incisions combined with TLS then generate an intact chromatid, thereby enabling HR repair of DSBs, with the repaired chromatid acting as a template. FANCD2 depletion reduces incisions and TLS, although these steps do still occur inefficiently (*4*).

In addition to promoting incisions and TLS, we suggest that FANCD2 modifies the resulting DSBs to prevent Ku70 from binding and subverting HR. It is noteworthy that the polarity of

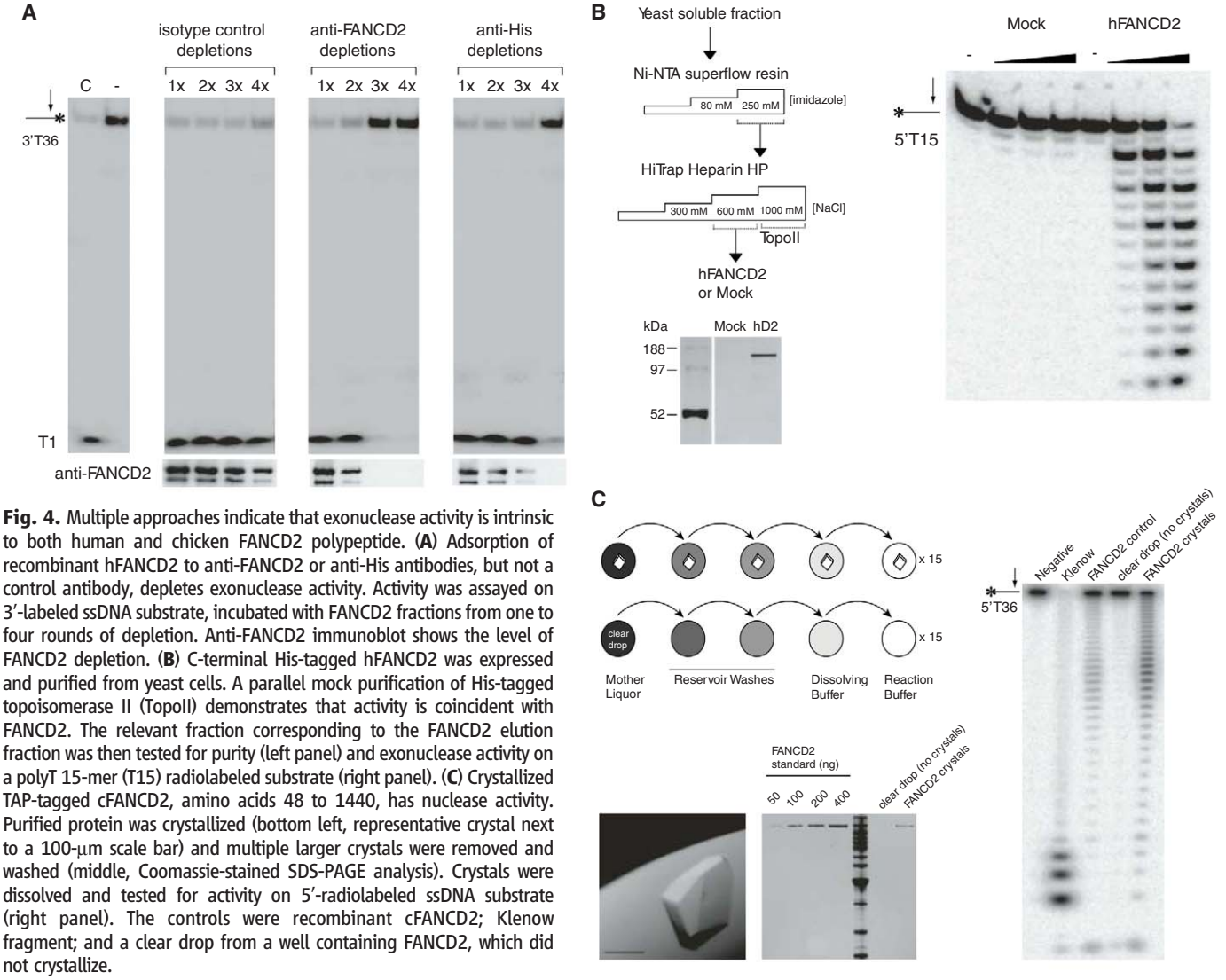

Fig. 4. Multiple approaches indicate that exonuclease activity is intrinsic to both human and chicken FANCD2 polypeptide. (**A**) Adsorption of recombinant hFANCD2 to anti-FANCD2 or anti-His antibodies, but not a control antibody, depletes exonuclease activity. Activity was assayed on 3′-labeled ssDNA substrate, incubated with FANCD2 fractions from one to four rounds of depletion. Anti-FANCD2 immunoblot shows the level of FANCD2 depletion. (**B**) C-terminal His-tagged hFANCD2 was expressed and purified from yeast cells. A parallel mock purification of His-tagged topoisomerase II (TopoII) demonstrates that activity is coincident with FANCD2. The relevant fraction corresponding to the FANCD2 elution fraction was then tested for purity (left panel) and exonuclease activity on a polyT 15-mer (T15) radiolabeled substrate (right panel). (**C**) Crystallized TAP-tagged cFANCD2, amino acids 48 to 1440, has nuclease activity. Purified protein was crystallized (bottom left, representative crystal next to a 100-μm scale bar) and multiple larger crystals were removed and washed (middle, Coomassie-stained SDS-PAGE analysis). Crystals were dissolved and tested for activity on 5′-radiolabeled ssDNA substrate (right panel). The controls were recombinant cFANCD2; Klenow fragment; and a clear drop from a well containing FANCD2, which did not crystallize.

the FANCD2 exonuclease (3′ to 5′) is predicted to generate 5′ ssDNA tails, contrary to a general view that only 3′ ssDNA tails stimulate recombination. However, recent biochemical work shows that the fungal ortholog of FANCD1/BRCA2 is able to promote HR by using 5′ ssDNA tails (*17*–*19*). We therefore speculate that FANCD2 may function with BRCA2 in a similar manner to repair DSBs generated during cross-link repair.

References and Notes

1. L. J. Niedernhofer, A. S. Lalai, J. H. Hoeijmakers, *Cell* **123**, 1191 (2005).
2. K. J. Patel, H. Joenje, *DNA Repair* **6**, 885 (2007).
3. W. Niedzwiedz *et al*., *Mol. Cell* **15**, 607 (2004).
4. P. Knipscheer *et al*., *Science* **326**, 1698 (2009); published online 12 November 2009 (10.1126/science.1182372).
5. S. C. West, *Nat. Rev. Mol. Cell Biol.* **4**, 435 (2003).
6. M. Escarceller *et al*., *J. Mol. Biol.* **279**, 375 (1998).
7. M. Escarceller, S. Rousset, E. Moustacchi, D. Papadopoulo, *Somat. Cell Mol. Genet.* **23**, 401 (1997).
8. T. Fukushima *et al*., *J. Biol. Chem.* **276**, 44413 (2001).
9. H. Arakawa, J. Hauschild, J.-M. Buerstedde, *Science* **295**, 1301 (2002).
10. J. E. Sale *et al*., *Philos. Trans. R. Soc. London Ser. B* **356**, 21 (2001).
11. S. Houghtaling *et al*., *Hum. Mol. Genet.* **14**, 3027 (2005).
12. Z. Zhang *et al*., *J. Biol. Chem.* **276**, 38231 (2001).
13. A. J. Pierce, P. Hu, M. Han, N. Ellis, M. Jasin, *Genes Dev.* **15**, 3237 (2001).
14. I. Garcia-Higuera *et al*., *Mol. Cell* **7**, 249 (2001).
15. N. Matsushita *et al*., *Mol. Cell* **19**, 841 (2005).
16. W. H. Park *et al*., *J. Biol. Chem.* **280**, 23593 (2005).
17. N. Mazloum, W. K. Holloman, *Mol. Cell* **33**, 160 (2009).
18. N. Mazloum, W. K. Holloman, *Mol. Cell* **36**, 620 (2009).
19. N. G. Howlett *et al*., *Science* **297**, 606 (2002); published online 13 June 2002 (10.1126/science.1073834).

20. We thank M. Takata for the anti-Ku70 antibody and the *Ku70* cDNA expression vector; H. Koyama and S. Takeda for *ΔLig4*, *ΔKu70*, and *ΔDNA-PKcs* DT40 cell lines; H. Joenje and J. DeWinter for human *FANCC* cell lines; and W. Niedzwiedz and J. Sale for help with *IgM* sequence analysis. Supported by the Children's Leukaemia Trust (G.M.), the Leukaemia and Lymphoma Research Fund (M.R.H.), and a FEBS fellowship (I.V.R.).

Supporting Online Material

www.sciencemag.org/cgi/content/full/science.1192277/DC1
Materials and Methods
Figs. S1 to S5
References

13 May 2010; accepted 28 May 2010
Published online 10 June 2010;
10.1126/science.1192277
Include this information when citing this paper.

Genomic Analysis of Organismal Complexity in the Multicellular Green Alga *Volvox carteri*

Simon E. Prochnik,[1]* James Umen,[2]*† Aurora M. Nedelcu,[3] Armin Hallmann,[4] Stephen M. Miller,[5] Ichiro Nishii,[6] Patrick Ferris,[2] Alan Kuo,[1] Therese Mitros,[7] Lillian K. Fritz-Laylin,[7] Uffe Hellsten,[1] Jarrod Chapman,[1] Oleg Simakov,[8] Stefan A. Rensing,[9] Astrid Terry,[1] Jasmyn Pangilinan,[1] Vladimir Kapitonov,[10] Jerzy Jurka,[10] Asaf Salamov,[1] Harris Shapiro,[1] Jeremy Schmutz,[11] Jane Grimwood,[11] Erika Lindquist,[1] Susan Lucas,[1] Igor V. Grigoriev,[1] Rüdiger Schmitt,[12] David Kirk,[13] Daniel S. Rokhsar[1,7]†

The multicellular green alga *Volvox carteri* and its morphologically diverse close relatives (the volvocine algae) are well suited for the investigation of the evolution of multicellularity and development. We sequenced the 138–mega–base pair genome of *V. carteri* and compared its ~14,500 predicted proteins to those of its unicellular relative *Chlamydomonas reinhardtii*. Despite fundamental differences in organismal complexity and life history, the two species have similar protein-coding potentials and few species-specific protein-coding gene predictions. *Volvox* is enriched in volvocine-algal–specific proteins, including those associated with an expanded and highly compartmentalized extracellular matrix. Our analysis shows that increases in organismal complexity can be associated with modifications of lineage-specific proteins rather than large-scale invention of protein-coding capacity.

Multicellularity and cellular differentiation evolved independently in diverse lineages, including green and red algae, animals, fungi, plants, Amoebozoa, and Chromalveolates (*1*) (fig. S1A), yet the genetic changes that underlie these transitions remain poorly understood. The volvocine algae, which include both unicellular and multicellular species with various levels of morphological and developmental complexity, are an appealing model for studying such an evolutionary transition (*2*) [fig. S2 and supporting online material (SOM) text]. Multicellular *Volvox carteri* (hereafter *Volvox*) has two cell types: ~2000 small biflagellate somatic cells that are embedded in the surface of a transparent sphere of glycoprotein-rich extracellular matrix (ECM), and ~16 large reproductive cells (termed gonidia) that lie just below the somatic cell monolayer (*2*) (Fig. 1A and figs. S1B and S3). The somatic cells resemble those of *Chlamydomonas reinhardtii*, a model unicellular volvocine alga (*3*) (Fig. 1B). The changes that are associated with the evolution of *Volvox* from a *Chlamydomonas*-like unicellular ancestor have clear parallels in other multicellular lineages but took place more recently than in land plants and animals (*4*).

To begin to characterize the genomic features that are associated with volvocine multicellularity, we sequenced the 138–mega–base pair (Mbp) *Volvox* genome to ~11.1× redundant coverage (~2.9 million reads) using a whole-genome shotgun strategy (*5*). The assembly captures over 98% of known mRNA sequences and expressed sequence tags (ESTs) (*5*). The *Volvox* nuclear genome is 19.6 Mbp (17%) larger than the *Chlamydomonas* genome (Table 1), primarily because of increased repeat content in *Volvox* relative to *Chlamydomonas* (*5*) (table S1). Whereas a few repeat families show bursts of expansion in the *Volvox* and *Chlamydomonas* lineages, most have changed gradually (fig. S4) (*5*).

The sequence divergence between *Volvox* and *Chlamydomonas* is comparable to that between human and chicken [which diverged ~310 million years ago (Ma)], human and frog (~350 Ma), and *Arabidopsis* and poplar (~110 Ma), based on the frequency of synonymous transversions at fourfold-degenerate sites (4DTV distance) (*5*, *6*) (table S2). Although conserved synteny between *Volvox* and *Chlamydomonas* genomes is evident, these volvocine algae show higher rates of genomic rearrangement than vertebrates and eudicots do (tables S2 to S4 and fig. S5).

We predicted 14,566 proteins (at 14,520 loci) in *Volvox* (*5*) (Table 1 and tables S5 to S7). *Volvox* and *Chlamydomonas* have similar numbers of genes (Table 1) (*3*) and more genes than most unicellular organisms (table S8). Genes in both algae are intron-rich (Table 1), like those of most multicellular organisms (table S8), and introns are longer, on average, in *Volvox* (fig. S6) (*5*). Novel protein domains and/or combinations are proposed to have contributed to multicellularity in metazoans (*7*), and such expansions are evident in both the plant and animal lineages (Fig. 2A and table S9). In contrast, the numbers of domains and combinations in *Volvox* are very similar

[1]U.S. Department of Energy, Joint Genome Institute, Walnut Creek, CA 94598, USA. [2]The Salk Institute for Biological Studies, La Jolla, CA 92037, USA. [3]University of New Brunswick, Department of Biology, Fredericton, New Brunswick E3B 5A3, Canada. [4]Department of Cellular and Developmental Biology of Plants, University of Bielefeld, D-33615 Bielefeld, Germany. [5]Department of Biological Sciences, University of Maryland Baltimore County, Baltimore, MD 21250, USA. [6]Biological Sciences, Nara Women's University, Nara-shi, Nara Prefecture 630-8506, Japan. [7]Center for Integrative Genomics, Department of Molecular and Cell Biology, University of California at Berkeley, Berkeley, CA 94720, USA. [8]European Molecular Biology Laboratory, Meyerhofstrasse 1, 69117 Heidelberg, Germany. [9]Faculty of Biology, University of Freiburg, 79104 Freiburg, Germany. [10]Genetic Information Research Institute, 1925 Landings Drive, Mountain View, CA 94043, USA. [11]HudsonAlpha Institute for Biotechnology, Huntsville, AL 35806, USA. [12]Department of Genetics, University of Regensburg, D-93040 Regensburg, Germany. [13]Department of Biology, Washington University in St. Louis, St. Louis, MO 63130, USA.

*These authors contributed equally to this work.
†To whom correspondence should be addressed. E-mail: umen@salk.edu (J.U.); dsrokhsar@gmail.com (D.S.R.)

to those in *Chlamydomonas* and other unicellular species (Fig. 2A and table S9) (*5*). microRNAs (miRNAs) have been identified in *Chlamydomonas*, most of which have no homologs in *Volvox* (*8*, *9*). It is likely that *Volvox* also has miRNAs, but these have yet to be characterized.

To investigate protein evolution in *Chlamydomonas* and *Volvox*, we constructed families containing both orthologs and paralogs from 20 diverse species, including animals, plants, fungi, protists, and bacteria (*5*) (table S10). We assigned 9311 (64%) *Volvox* and 9189 (63%) *Chlamydomonas* protein sequences to 7780 families (Fig. 2B), of which 80% (5423) contain one ortholog from each alga (table S11). 1835 families (26%) contain orthologs only from *Volvox* and *Chlamydomonas* (that is, they are volvocine-specific) (Fig. 2B). Only 32 EST-supported *Volvox* gene models lack detectable homologs in *Chlamydomonas* or other species (*5*) (tables S12 and S13), suggesting that limited protein-coding innovation occurred in the *Volvox* lineage.

Gene-family expansion or contraction is an important source of adaptive variation (*10*, *11*). In a density plot of proteins per family in *Volvox* versus *Chlamydomonas* (Fig. 2C), most points lie on or near the diagonal, showing that the majority of families have approximately equal membership from each alga. Exceptions include the gametolysin/VMP (*Volvox* matrix metalloprotease) family, whose substrates are cell-wall/ECM proteins (*12*) (Fig. 2C, g), and a family containing leucine-rich repeat proteins (LRRs), whose functions in green algae have not been well defined (Fig. 2C, L). Conversely, families containing core histones and ankyrin repeats have more members in *Chlamydomonas* (Fig. 2C, a). In contrast, the subset of 1835 volvocine algae–specific families (*5*) shows a strikingly different distribution (Fig. 2D), with a significant bias toward more members in *Volvox* ($P = 2 \times$

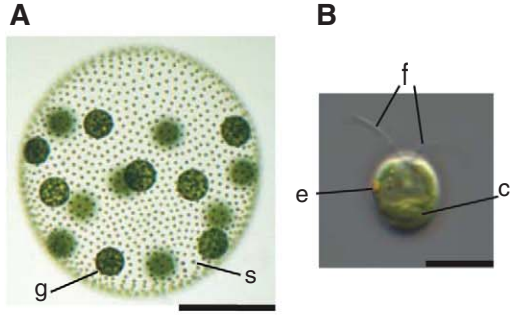

Fig. 1. *Volvox* and *Chlamydomonas*. (**A**) Adult *Volvox* is composed of ~2000 *Chlamydomonas*-like somatic cells (s) and ~16 large germline gonidia (g) (scale bar, 200 μm) (fig. S1B). (**B**) *Chlamydomonas* cell showing apical flagella (f), chloroplast (c), and eyespot (e) (scale bar, 10 μm). The microscopy used is described in (*5*).

Table 1. Comparison of the *Volvox* and *Chlamydomonas* genomes.

Species	Genome size (Mbp)	Number of chromosomes	% G and C	Protein-coding loci	% coding	% of genes with introns	Introns per gene	Median intron length (bp)
V. carteri	138	14*	56	14,520	18.0	92	7.05	358
C. reinhardtii	118	17	64	14,516	16.3	91	7.4	174

*See (*15*).

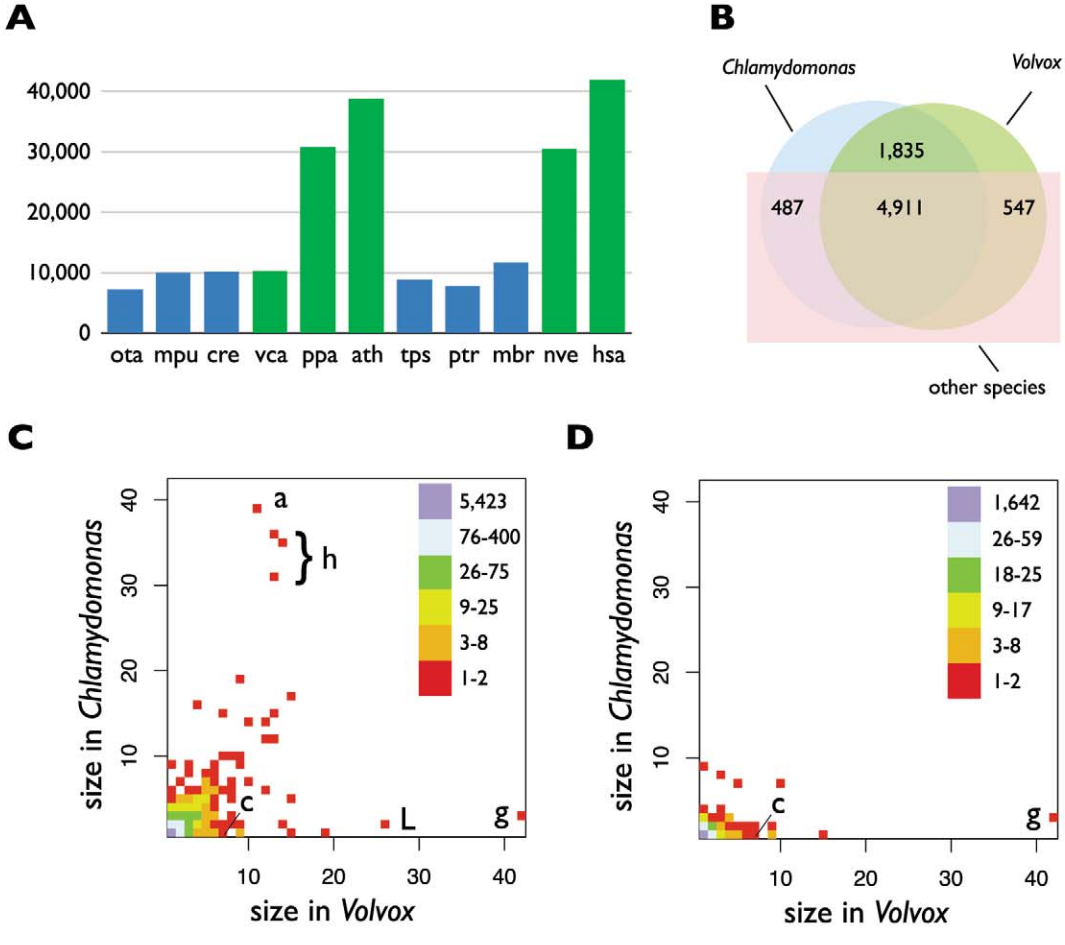

Fig. 2. Comparisons of protein domains and families. (**A**) Total number of Pfam domains in the multicellular (green) and unicellular (blue) species: *Ostreococcus tauri* (ota); *Micromonas pusilla* (mpu); *Chlamydomonas reinhardtii* (cre); *Volvox carteri* (vca); *Physcomitrella patens* (ppa); *Arabidopsis thaliana* (ath); *Thalassiosira pseudonana* (tps); *Phaeodactylum tricornutum* (ptr); *Monosiga brevicollis* (mbr); *Nematostella vectensis* (nve); and *Homo sapiens* (hsa). (**B**) The numbers of protein families from *Volvox*, *Chlamydomonas*, and other species (*5*) are shown in a Venn diagram. The numbers of *Volvox* and *Chlamydomonas* members per protein family are plotted for all families (**C**) and for the volvocine algae–specific subset (**D**). In these density plots, the position of each square represents the number of family members in *Volvox* (*x* axis) and *Chlamydomonas* (*y* axis), with coloring to indicate the total number of families plotted at each position. The Pfam domains for outlier families are abbreviated as follows: a, ankyrin repeat; c, cysteine protease; g, gametolysin; h, histone; L, LRR.

10^{-120}, heterogeneity chi-squared test). These families include ECM proteins such as VMPs and pherophorins that both participate in ECM biogenesis (*12*), and an algal subgroup of cysteine proteases (Fig. 2D, c).

Although some of the genomic differences between *Volvox* and *Chlamydomonas* may reflect environmental adaptations that have not been extensively investigated (*5*), we expected many of the changes to be in protein families that are associated with the large differences in organismal complexity. Therefore, we investigated in detail pathways related to key developmental processes that are either novel or qualitatively different in *Volvox* relative to *Chlamydomonas* (*2*). These include the following: protein secretion and membrane trafficking [potentially involved in cytoplasmic bridge formation via incomplete cytokinesis (*13*, *14*)]; the cytoskeleton [potentially involved in *Volvox*-specific basal body rotation, inversion, and asymmetric cell division (*15*)]; ECM and cell-wall proteins [involved in ECM expansion, sexual differentiation, and morphogenesis (*12*) (fig. S2)]; and cell-cycle regulation (potentially involved in cell division patterning or asymmetric cell division). The components of these pathways are nearly identical in *Volvox* and *Chlamydomonas* (table S14). Transcription-related proteins also have highly similar repertoires in the two species (fig. S7 and table S15) (*5*). Thus, with three exceptions (see below), we found little difference in the complements of proteins that might underlie developmental complexity in *Volvox*.

The ECM composes up to 99% of an adult *Volvox* spheroid and is larger and more structurally complex than the ancestral *Chlamydomonas*-like cell wall from which it was derived (*12*) (fig. S3 and SOM text). These changes are mirrored by at least two dramatic changes in ECM protein family size in *Volvox* as compared with *Chlamydomonas*: pherophorins (49 versus 27 members) and VMPs (42 versus 8 members) (Fig. 3A, fig. S8, and table S14). We found expanded *Volvox*-specific clades of pherophorins and VMPs as well as species-specific duplications in both algae (Fig. 3A and fig. S8). Besides their role in ECM structure, *Volvox* pherophorins have evolved into a diffusible sex-inducer glycoprotein that has replaced nitrogen deprivation (used in *Chlamydomonas* and other volvocine algae) as the trigger for sexual differentiation (*16*). The co-option of an ECM protein for sexual signaling shows parallels in the sexual agglutinins of *Chlamydomonas* that are themselves related to cell-wall/ECM proteins (*17*). The *Volvox* ECM proteins, pherophorins, and VMPs diversified and then presumably were recruited to novel developmental roles in *Volvox*, thus representing a source of adaptive plasticity that is specific to the volvocine algae.

The *Volvox* and *Chlamydomonas* cell cycles are fundamentally similar, but *Volvox* has evolved additional regulation of timing, number, and types of cell divisions (symmetric and asymmetric) among different subsets of embryonic cells (*2*). The division program of males and females is further modified during sexual development to produce sperm and eggs (*18*). Whereas most of the core cell-cycle proteins of *Volvox* and *Chlamydomonas* have a 1:1 orthology relationship, the cyclin D family is notably larger in *Volvox*. In addition to three D cyclins that have *Chlamydomonas* orthologs (Cycd2, Cycd3, and Cycd4), *Volvox* has four D1-related cyclins (Cycd1.1 to Cycd1.4), whereas *Chlamydomonas* has only one (Fig. 3B). D cyclins bind cyclin-dependent kinases and target them to phosphorylate retinoblastoma (RB)–related proteins (*19*). In *Chlamydomonas*, the RB-related protein MAT3 controls the timing and extent of cell division (*20*), so it is plausible that the expanded D-type cyclin family in *Volvox* plays a role in regulating its cell division program during development.

The genetic changes that brought about the evolution of multicellular life from unicellular progenitors remain obscure (*2*, *21*, *22*). For example, many proteins associated with animal multicellularity, such as cadherins and receptor tyrosine kinases (*23*), evolved in the unicellular ancestor of animals and are specific to its descendants. Other critical components of metazoan multicellularity, including key transcription factors and signaling molecules, are absent from the closest unicellular relatives of animals (*22*), suggesting that animal multicellularity also involved protein-coding innovation. Our comparisons of *Volvox* and *Chlamydomonas* indicate that, with the interesting exceptions of pherophorins, VMPs, and D cyclins, the developmental innovations in the *Volvox* lineage did not involve major changes in the ancestral protein repertoire. This is consistent with previous observations indicating co-option of ancestral genes into new developmental processes without changes in copy number or function (*24*–*26*). However, our analyses do suggest that the expansion of lineage-specific proteins occurred preferentially in *Volvox* and provided a key source of developmental innovation and adaptation. Further studies of gene regulation (*27*) and the role of noncoding RNAs (*28*) will be

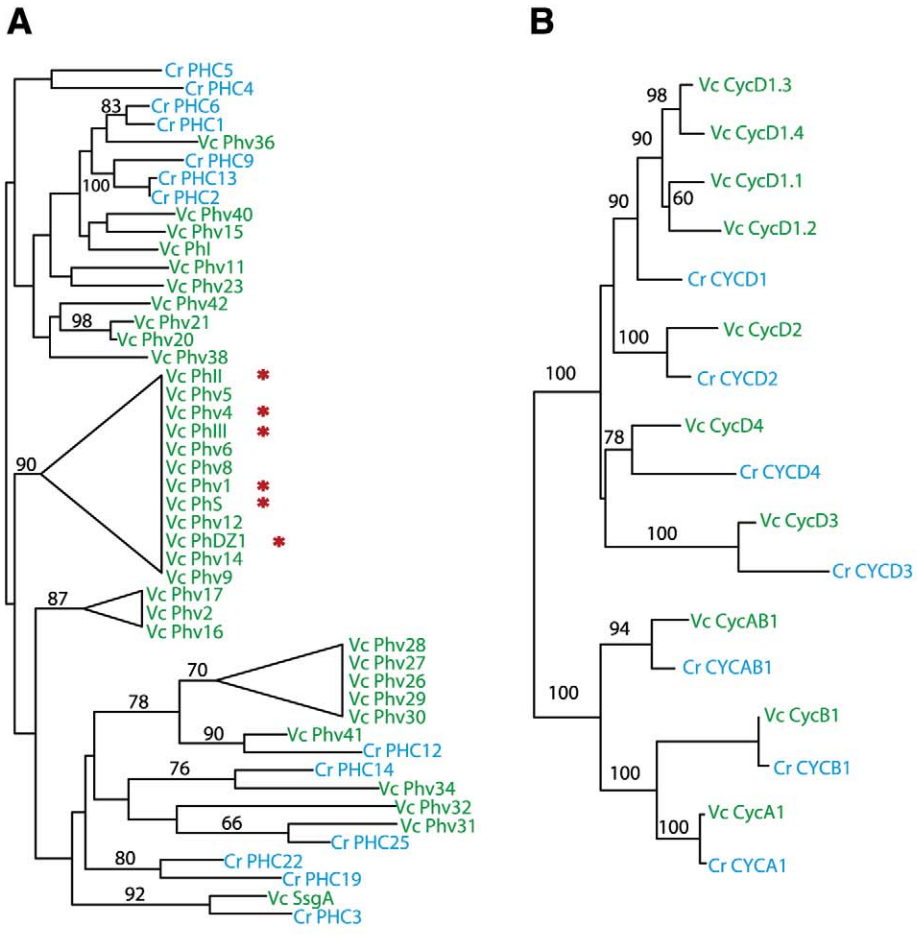

Fig. 3. Diversification of key protein families with known or predicted roles in *Volvox* development. Unrooted maximum likelihood trees (*5*) are shown for pherophorins (**A**) and cyclins (**B**). Protein sequences are from *Volvox* (Vc, green) and *Chlamydomonas* (Cr, blue). Incomplete gene models were not included; *Volvox*-specific clades with poorly resolved branches are collapsed into triangles; bootstrap support ≥50% is indicated on branches. Red asterisks indicate pherophorins whose mRNA levels are up-regulated by a sex inducer (*16*).

enabled by the *Volvox* genome sequence, allowing a more complete understanding of the transformation from a cellularly complex *Chlamydomonas*-like ancestor to a morphologically and developmentally complex "fierce roller."

References and Notes

1. S. L. Baldauf, *Science* **300**, 1703 (2003).
2. D. L. Kirk, *Bioessays* **27**, 299 (2005).
3. S. S. Merchant *et al.*, *Science* **318**, 245 (2007).
4. M. D. Herron, J. D. Hackett, F. O. Aylward, R. E. Michod, *Proc. Natl. Acad. Sci. U.S.A.* **106**, 3254 (2009).
5. Materials and methods are available as supporting material on *Science* Online.
6. R. R. Reisz, J. Müller, *Trends Genet.* **20**, 237 (2004).
7. N. H. Putnam *et al.*, *Science* **317**, 86 (2007).
8. T. Zhao *et al.*, *Genes Dev.* **21**, 1190 (2007).
9. A. Molnár, F. Schwach, D. J. Studholme, E. C. Thuenemann, D. C. Baulcombe, *Nature* **447**, 1126 (2007).
10. O. Lespinet, Y. I. Wolf, E. V. Koonin, L. Aravind, *Genome Res.* **12**, 1048 (2002).
11. J. Zhang, *Trends Ecol. Evol.* **18**, 292 (2003).
12. A. Hallmann, *Int. Rev. Cytol.* **227**, 131 (2003).
13. K. J. Green, D. L. Kirk, *J. Cell Biol.* **91**, 743 (1981).
14. K. J. Green, G. I. Viamontes, D. L. Kirk, *J. Cell Biol.* **91**, 756 (1981).
15. D. Kirk, *Volvox: Molecular-Genetic Origins of Multicellularity and Cellular Differentiation* (Cambridge Univ. Press, Cambridge, 1998).
16. A. Hallmann, *Plant J.* **45**, 292 (2006).
17. P. J. Ferris *et al.*, *Plant Cell* **17**, 597 (2005).
18. P. Ferris *et al.*, *Science* **328**, 351 (2010).
19. L. De Veylder, T. Beeckman, D. Inzé, *Nat. Rev. Mol. Cell Biol.* **8**, 655 (2007).
20. S.-C. Fang, C. de los Reyes, J. G. Umen, *PLoS Genet.* **2**, e167 (2006).
21. L. W. Buss, *The Evolution of Individuality* (Princeton Univ. Press, Princeton, NJ, 2006).
22. N. King *et al.*, *Nature* **451**, 783 (2008).
23. N. King, C. T. Hittinger, S. B. Carroll, *Science* **301**, 361 (2003).
24. S. M. Miller, D. L. Kirk, *Development* **126**, 649 (1999).
25. I. Nishii, S. Ogihara, D. L. Kirk, *Cell* **113**, 743 (2003).
26. Q. Cheng, R. Fowler, L. W. Tam, L. Edwards, S. M. Miller, *Dev. Genes Evol.* **213**, 328 (2003).
27. S. B. Carroll, *Cell* **134**, 25 (2008).
28. K. J. Peterson, M. R. Dietrich, M. A. McPeek, *Bioessays* **31**, 736 (2009).

29. The work conducted by the Joint Genome Institute of the U.S. Department of Energy is supported by the Office of Science of the U.S. Department of Energy under contract number DE-AC02-05CH11231 and by NIH grant R01 GM078376 and a Coypu Foundation grant to J.U.; a grant from the Natural Sciences and Engineering Research Council–Canada to A.M.N.; NSF grants IBN-0444896 and IBN-0744719 to S.M.M.; Japan Society for the Promotion of Science Grant-in-Aid for Scientific Research numbers 20247032 and 22570203 to I.N.; and NIH grant 5 P41 LM006252 to J.J. We thank M. Cipriano for Pfam annotations; E. Hom, E. Harris, and M. Stanke for Augustus u9 gene models; and R. Howson for artwork. Sequence data from this study are deposited at the DNA Databank of Japan/European Molecular Biology Laboratory/GenBank under the project accession no. ACJH00000000.

Supporting Online Material

www.sciencemag.org/cgi/content/full/329/5988/223/DC1
Materials and Methods
SOM Text
Figs. S1 to S8
Tables S1 to S16
References

25 February 2010; accepted 3 June 2010
10.1126/science.1188800

A Molecular Clock for Malaria Parasites

Robert E. Ricklefs† and Diana C. Outlaw*

The evolutionary origins of new lineages of pathogens are fundamental to understanding emerging diseases. Phylogenetic reconstruction based on DNA sequences has revealed the sister taxa of human pathogens, but the timing of host-switching events, including the human malaria pathogen *Plasmodium falciparum*, remains controversial. Here, we establish a rate for cytochrome b evolution in avian malaria parasites relative to its rate in birds. We found that the parasite cytochrome b gene evolves about 60% as rapidly as that of host cytochrome b, corresponding to ~1.2% sequence divergence per million years. This calibration puts the origin of *P. falciparum* at 2.5 million years ago (Ma), the initial radiation of mammalian *Plasmodium* at 12.8 Ma, and the contemporary global diversity of the Haemosporida across terrestrial vertebrates at 16.2 Ma.

The rate of nucleotide substitution in DNA sequences can provide a molecular clock useful for inferring absolute times in phylogenetic trees (*1*). This rate can be estimated by direct observation over reasonable time periods, as with several viral parasites of humans (*2*, *3*) and experimental populations of *Drosophila* (*4*). Relatively slow nucleotide substitution precludes this approach for malaria parasites, for which calibration is indirect. For some specialized parasites, phylogenetic analyses have revealed codivergence of host and parasite evolutionary lineages, which permits calibration of genetic distance in one relative to the other (*5*–*7*). In contrast, *Plasmodium* and other haemosporidian parasites of terrestrial vertebrates exhibit widespread host switching, often across considerable host taxonomic distance (*8*–*11*). Cospeciation cannot, therefore, provide a means of clock calibration.

In spite of evident host switching, biologists have used the ages of host phylogenetic ancestral nodes to calibrate the rate of nucleotide substitution in *Plasmodium* and to estimate the ages of *Plasmodium* lineages. For example, Ollomo *et al.* (*12*) suggested that a *Plasmodium* lineage newly discovered in chimpanzees diverged from another chimpanzee pathogen, *Plasmodium reichenowi*, 21 ± 9 million years ago (Ma) on the basis of placing the *P. reichenowi*–*P. falciparum* divergence coincident with the human-chimp divergence 4 to 7 Ma. In another analysis, Hayakawa *et al.* (*13*) calibrated amino acid substitutions in three mitochondrial genes based on host-parasite codivergence of *P. gonderi* (a parasite of African primates) and a clade of malaria parasites of southeast Asian primates, including humans. This calibration yielded a divergence time of either 2.5 ± 0.6 million years (My) or 4.0 ± 0.9 My for *P. falciparum* and *P. reichenowi*, depending on the dating of the split between lineages of Asian and African macaques, on one hand, and Asian and African colobine monkeys, on the other hand. However, as Rich *et al.* (*14*) point out, humans could have acquired *P. falciparum* any time after the split of the human-chimpanzee lineage "by a single host transfer, which may have

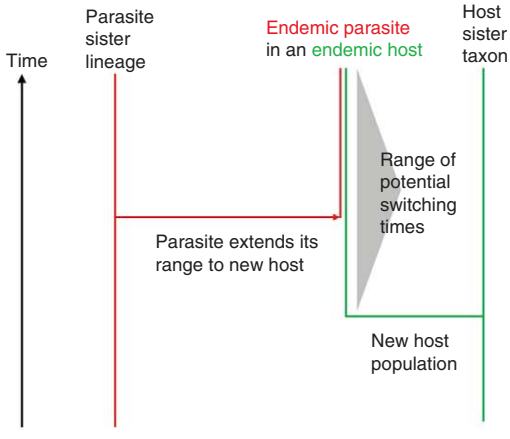

Fig. 1. An approach to estimating a calibration for the rate of haemosporidian nucleotide substitution. We assume that a parasite can switch to a new host at any point with equal probability during the host's independent evolutionary history. Although the range of switching times corresponds to the age of the contemporary host taxon, the range of genetic distances relative to the host is equal to the ratio of the parasite-to-host nucleotide substitution rate. Endemic parasites limited to a single host are suitable for analysis because their divergence from their sister taxon in a different host represents the historical event of host switching (for alternatives, see appendix S1).

Department of Biology, University of Missouri–St. Louis, One University Boulevard, St. Louis, MO 63121–4499, USA.

*Present address: Department of Biological Sciences, Mississippi State University, 130 Harned Hall, Lee Boulevard, Mississippi State, MS 39762, USA.
†To whom correspondence should be addressed. E-mail: ricklefs@umsl.edu

occurred as early as 2 to 3 million years ago, or as recently as 10,000 years ago."

Here, we calibrate the mitochondrial cytochrome b nucleotide substitution rate in haemosporidian parasites of birds, relating it to the rate of cytochrome b evolution in avian hosts (*15*). We assume that nucleotide substitution is clocklike, so that the number of substitutions is binomially distributed, and that the distribution of switching times is uniform over the age of the endemic host taxon (Fig. 1) (supporting online text, appendix S1). Our approach requires identification of endemic parasite lineages, which in turn depends on thorough sampling. In our survey of avian haemosporidians in the West Indies (*16*–*19*), we have screened extensive samples of small land birds from all the major islands, except Cuba. Moreover, many host species are endemic to individual islands. We identified seven endemic parasite lineages (appendix S2) and measured the genetic distances, based on cytochrome b, between these parasite lineages and their sister lineages, and between their hosts and the sister taxon of each host (Fig. 1). The variable of interest is the ratio (k) of the rates of nucleotide substitution between the pairs of parasite and host sequences.

The probability (p) of a nucleotide substitution at a single position over time is equal to the rate of substitution (r) × time (t), or $p = rt$. The mean number of substitutions is the number of nucleotides (n) times the probability, or np, and the variance is $np(1 - p)$; for small numbers of nucleotide substitutions (p near 0), this approaches a Poisson distribution with variance np; the probability of multiple events is low enough to be ignored (*20*).

Because we assume that a parasite can switch to a new host any time after the ancestral host lineage splits, the expected mean for the number of substitutions separating the parasite sequences (N) is

$$N = \frac{1}{t}\int_{i=0}^{t} knridi \qquad (1)$$

where k is the ratio of the rate of substitution (parasite/host). Accordingly, $N = knrt/2$ and $k = 2N/nrt$.

For the seven comparisons of host and parasite genetic divergence considered in this analysis, nrt is the estimated number of host substitutions [average 48.94 base pairs (bp), with correction for within-species variation]; the corrected parasite distances (N) averaged 15.23 bp; thus, $k = 2 \times 15.2/48.9 = 0.62$ (appendix S3). According to this estimate, the rate of substitution in the parasite lineages is 62% of that in the host lineages. The average ratio of the parasite divergence to the host divergence for each of the seven comparisons was 0.292 ± 0.119 SD (0.048 SEM; 95% confidence limits, 0.197 to 0.387). The value

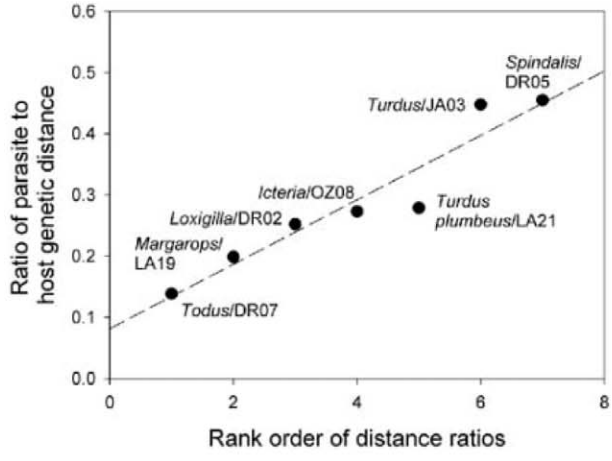

Fig. 2. Rank-ordered ratios of parasite-to-host genetic distances are consistent with a uniform distribution.

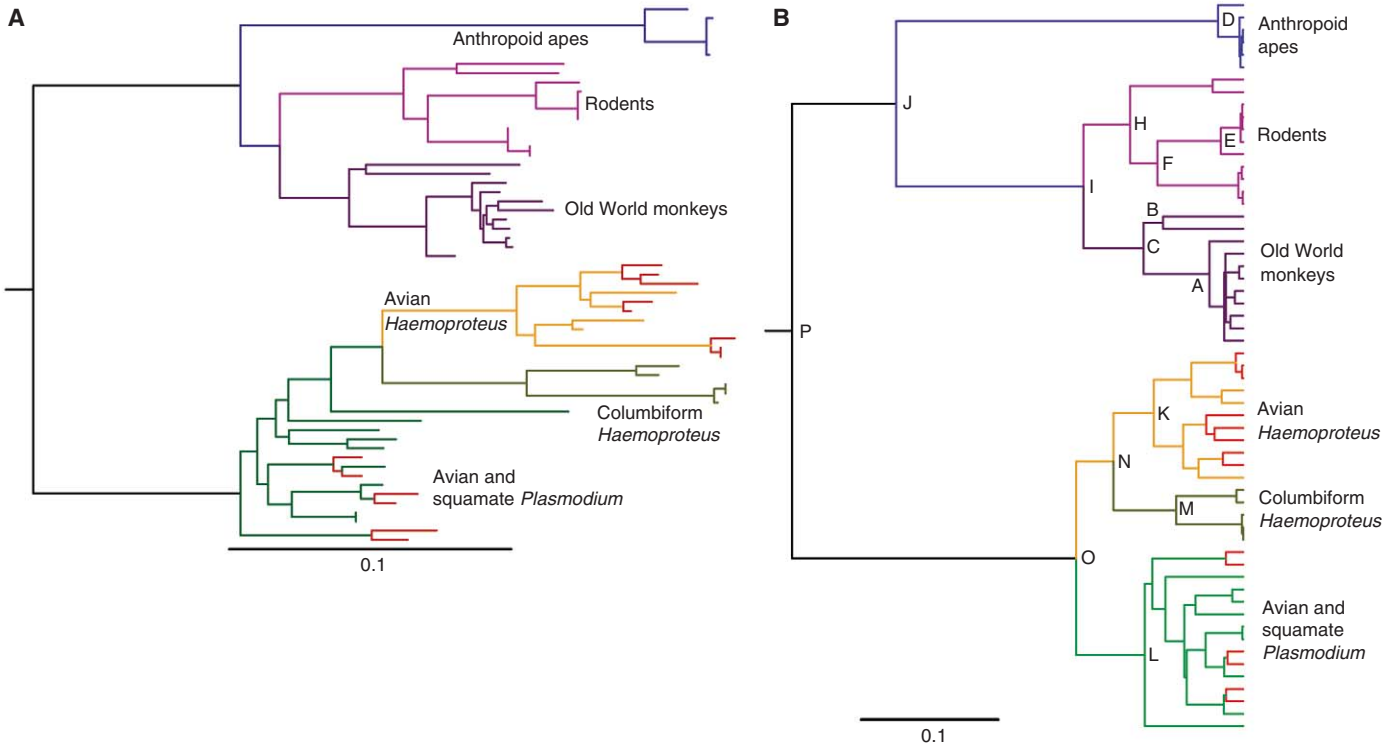

Fig. 3. Phylogenetic trees for representative haemosporidian cytochrome b sequences. (**A**) Tree produced by maximum likelihood optimization under a GTR + Γ model of nucleotide evolution. (**B**) Tree produced under a GTR + Γ model of nucleotide evolution using a strict clock. Letters in (B) indicate aged nodes (see Table 1). Calibration pairs in both panels are indicated in red.

of k estimated from these parasite/host ratios was $2 \times 0.292 = 0.584 \pm 0.096$ SEM [95% confidence interval (CI), 0.394 to 0.774]. Thus, in seven comparisons of genetic distance in avian haemosporidian cytochrome b sequences, ranging from 1 to 3% sequence divergence, the estimated rate of nucleotide substitution was close to 60% of the host rate. (See appendix S4 for an analysis of the variance in genetic distances among pairs of host and parasite taxa.)

An important assumption in our calibration is that switching times are distributed uniformly over the age of the host lineage. Alternatively, new host lineages might be available immediately for "colonization," and parasites switch quickly to the new host. In this case, the ages of endemic parasite lineages would be skewed toward the host age, with few host/parasite genetic distance ratios at low values. In our data, the ratios of parasite to host genetic distances are broadly spread between 0.14 and 0.45 (Fig. 2) and are consistent with an even distribution of switching times (appendix S5).

Assuming the rate of nucleotide substitution in Haemosporida is 0.584 times that of their avian hosts, the parasite rate can be obtained directly from calibrations of the host rate. In the case of birds, a generally agreed-upon average value for the rate of nucleotide divergence in cytochrome b is ~0.021 My^{-1} (*21*, *22*). Fifty-eight percent of this rate is ~0.012 (1.2%) genetic divergence My^{-1} (0.002 SEM, 0.0079 to 0.0155 CI), which is equivalent to 0.83 My per 0.01 (1%) sequence divergence.

To calculate absolute divergence times for the major clades of the Haemosporida, we used two estimates of the depths of the major nodes. First, we produced DNA distance matrices for subsets of lineages using the F84 model of nucleotide substitution (appendices S6 and S7). Clades were identified on the basis of a maximum likelihood (ML) phylogenetic tree of 54 species, or lineages, of representative haemosporidian parasites, including the sister pairs analyzed here (Fig. 3A). Ages of the basal nodes within designated clades were calculated as the means of the distances between all pairs of species or lineages descending from the two branches emanating from the node. Second, we produced a phylogenetic tree under a strict clock assumption, which resulted in branch lengths proportional to time. The resulting phylogeny is rooted between the clades of mammalian and avian-reptilian parasites and has a topology similar to that of the ML tree rooted at this point (Fig. 3B).

The estimated node depths in the clock-enforced (ultrametric) tree match reasonably well those calculated independently from sequence distances (Table 1), particularly with respect to the origins of the major clades: rodent versus Old World monkey (OWM) (ultrametric, 9.3 My, and F84, 8.7 My); basal node in mammalian *Plasmodium* (11.9 and 12.8, respectively); avian *Haemoproteus* versus *Plasmodium* (9.3 and 9.0); avian-reptilian versus mammalian Haemosporida (16.9 and 16.2). Although the estimated age of the split between *P. gonderi* and the *Plasmodium* parasites of Asian Old World monkeys was similar (2.8 and 2.8), estimated ages for many of the other mammalian nodes were younger in the clock-enforced tree, including nodes within the rodent malarias and the node ancestral to *P. falciparum* and *P. reichenowi* (1.2 and 2.5) (appendix S7).

The divergence of the human *P. falciparum* from the chimpanzee *P. reichenowi* dates to either 2.5 Ma (F84 distance) or 1.2 Ma (ultrametric distance), which is considerably more recent than the estimated divergence time of their hosts, on the basis of fossil evidence and corroborated by molecular dating (4 to 7 Ma) (*23*). The divergence times between the parasites of African and Asian Old World monkeys, estimated—if we assume codivergence—from primate fossil evidence at 6 and 10 My (*24*) and used by Hayakawa *et al*. (*13*) to calibrate age on their parasite phylogenetic tree, date to 2.8 Ma with both F84 and ultrametric distances.

The basal node in the phylogeny of contemporary haemosporidian parasites in the genera *Plasmodium* and *Haemoproteus* can be dated to between 16 and 17 Ma, well after the evolutionary diversification of their hosts, as well as fossil evidence of the parasites in dipteran vectors preserved in amber (appendix S8). Thus, the history of the contemporary Haemosporida is one of rapid diversification and spread through the terrestrial vertebrate classes (*10*, *25*). In addition, both the avian-reptilian and mammalian parasite clades have long stems, indicative of considerable pruning (extinction) of lineages since their origin. With respect to cytochrome b [but not other genes such as the mitochondrial cytochrome oxidase I and the apicoplast caseinolytic protease C (ClpC)], the divergence between bird-reptile and mammal parasite clades involved substantial protein evolution (i.e., nonsynonymous nucleotide substitution) possibly associated with the shift between nucleated and nonnucleated erythrocytes (*26*). Shifts between avian and reptilian hosts have occurred more recently and likely several times (*27*, *28*); birds and reptiles both have nucleated erythrocytes.

The age estimates for nodes in the parasite phylogeny emphasize that a new disease might emerge in a host soon after its origin and at any time thereafter. The lineage of *Plasmodium falciparum* evidently has infected the ancestors of humans for several million years and likely was relatively benign through much of that period, as is

Table 1. Genetic distances based on the mitochondrial cytochrome b gene and estimated ages of principal nodes in a phylogenetic tree of the Haemosporida. Genetic distances were obtained in Phylip-3.69 (program dnadist.exe) using the following default settings: F84 model, Ts/Tv = 2.0, homogeneous substitution rate. The depth of each node was calculated as the average pairwise distance between sequences on either side of the node. Upper and lower confidence limits are based on the 95% CI calculated for the ratio of parasite-to-host nucleotide substitution. No standard deviation (SD) is available for (B) and (G) because only a single sequence from each side of the split was used to estimate the genetic distance.

Comparison	Genetic distance			Age (My), 95% CI		
	Sample	Mean	SD	Mean	Lower	Upper
A. African (*P. gonderi*) versus Asian Old World monkeys (OWM)	1,8	0.033	0.005	2.76	2.14	4.19
B. Between *P. ovale* and *P. malariae*	1,1	0.072		6.03	4.67	9.16
C. Between *P. ovale* or *P. malariae* and sister OWM clade	2,9	0.074	0.006	6.19	4.79	9.41
D. *P. falciparum* versus *P. reichenowi* (human-chimp)	3,1	0.030	0.001	2.49	1.93	3.79
E. *P. berghii* versus *P. yoellii* (rodent pathogens)	1,3	0.032	0.001	2.67	2.07	4.06
F. *P. chabaudi* versus (D) (rodent pathogens)	3,4	0.066	0.007	5.51	4.27	8.38
G. *P. vinckii* versus *P. atheruri* (rodent pathogens)	1,1	0.061		5.07	3.93	7.71
H. Basal split in rodent *Plasmodium*, (G) versus (F)	2,9	0.081	0.006	6.77	5.25	10.29
I. Rodent versus OWM	4,6	0.105	0.008	8.73	6.76	13.26
J. Basal split in mammal *Plasmodium*	2,6	0.154	0.011	12.82	9.93	19.49
K. Basal split in avian *Haemoproteus*	5,6	0.076	0.015	6.37	4.93	9.68
L. Basal split in avian P*lasmodium*	3,11	0.085	0.011	7.06	5.47	10.74
M. Basal split within dove *Haemoproteus*	2,2	0.094	0.005	7.85	6.08	11.92
N. *Haemoproteus* versus *Parahaemoproteus*	5,10	0.131	0.007	10.93	8.46	16.60
O. Avian *Haemoproteus* versus *Plasmodium*	10,6	0.108	0.015	9.01	6.98	13.70
P. Avian versus mammalian haemosporidians	7,7	0.195	0.018	16.21	12.56	24.64

the case of most haemosporidian parasites (*29*, *30*). The recent expansion of the *P. falciparum* population, evidenced by its low genetic diversity (*31*), and the emergence of malaria as a major disease in humans, almost certainly was associated with the origins of agriculture and increasing population density, as well as large-scale movements of humans and introduction of the parasite to susceptible human populations (*29*, *30*, *32*).

The haemosporidian parasites of terrestrial vertebrates apparently began to diversify ~20 Ma, possibly displacing other types of parasites in the phylum Apicomplexa and, through host switching, bridging several hundred million years of vertebrate evolution. Because of their prevalence and broad distribution among terrestrial vertebrates, haemosporidian parasites make an excellent model system for investigating host-parasite coevolutionary relationships, host switching, and emerging diseases. A time calibration for the evolution of the group now provides a context for haemosporidian evolution with respect to host diversification, biogeographic distribution, and environmental change.

References and Notes

1. E. Zuckerkandl, L. Pauling, in *Horizons in Biochemistry: Albert Szent-Györgyi Dedicatory Volume*, M. Kasha, B. Pullman, Eds. (Academic Press, New York, 1962), pp. 189–225.
2. A. Rambaut, D. Posada, K. A. Crandall, E. C. Holmes, *Nat. Rev. Genet.* **5**, 52 (2004).
3. B. Korber *et al.*, *Science* **288**, 1789 (2000).
4. C. Haag-Liautard *et al.*, *PLoS Biol.* **6**, e204 (2008).
5. R. D. M. Page, Ed., *Tangled Trees: Phylogeny, Cospeciation, and Coevolution* (Univ. of Chicago Press, Chicago, 2003).
6. R. D. M. Page, M. S. Hafner, in *New Uses for New Phylogenies*, P. H. Harvey, A. J. L. Brown, J. Maynard Smith, S. Nee, Eds. (Oxford Univ. Press, Oxford, 1996), pp. 255–270.
7. A. Rector *et al.*, *Genome Biol.* **8**, R57 (2007).
8. M. J. Martin, J. C. Rayner, P. Gagneux, J. W. Barnwell, A. Varki, *Proc. Natl. Acad. Sci. U.S.A.* **102**, 12819 (2005).
9. J. Waldenström, S. Bensch, S. Kiboi, D. Hasselquist, U. Ottosson, *Mol. Ecol.* **11**, 1545 (2002).
10. R. E. Ricklefs, S. M. Fallon, *Proc. R. Soc. London B Biol. Sci.* **269**, 885 (2002).
11. L. Z. Garamszegi, *Malar. J.* **8**, 110 (2009).
12. B. Ollomo *et al.*, *PLoS Pathog.* **5**, e1000446 (2009).
13. T. Hayakawa, R. Culleton, H. Otani, T. Horii, K. Tanabe, *Mol. Biol. Evol.* **25**, 2233 (2008).
14. S. M. Rich *et al.*, *Proc. Natl. Acad. Sci. U.S.A.* **106**, 14902 (2009).
15. Materials and methods are available as supporting material on *Science* Online.
16. S. M. Fallon, E. Bermingham, R. E. Ricklefs, *Evolution* **57**, 606 (2003).
17. S. M. Fallon, E. Bermingham, R. E. Ricklefs, *Am. Nat.* **165**, 466 (2005).
18. S. M. Fallon, R. E. Ricklefs, S. Latta, E. Bermingham, *Proc. R. Soc. London B Biol. Sci.* **271**, 493 (2004).
19. S. C. Latta, R. E. Ricklefs, *J. Avian Biol.* **41**, 25 (2010).
20. B. S. Arbogast, S. V. Edwards, J. Wakeley, P. Beerli, J. B. Slowinski, *Annu. Rev. Ecol. Syst.* **33**, 707 (2002).
21. I. J. Lovette, *Auk* **121**, 1 (2004).
22. J. T. Weir, D. Schluter, *Mol. Ecol.* **17**, 2321 (2008).
23. S. Kumar, A. Filipski, V. Swarna, A. Walker, S. B. Hedges, *Proc. Natl. Acad. Sci. U.S.A.* **102**, 18842 (2005).
24. C. B. Stewart, T. R. Disotell, *Curr. Biol.* **8**, R582 (1998).
25. J. S. Beadell *et al.*, *Mol. Ecol.* **13**, 3829 (2004).
26. D. C. Outlaw, R. E. Ricklefs, *Mol. Biol. Evol.* **27**, 537 (2010).
27. E. S. Martinsen, S. L. Perkins, J. J. Schall, *Mol. Phylogenet. Evol.* **47**, 261 (2008).
28. S. L. Perkins, J. J. Schall, *J. Parasitol.* **88**, 972 (2002).
29. A. G. Nerlich, B. Schraut, S. Dittrich, T. Jelinek, A. R. Zink, *Emerg. Infect. Dis.* **14**, [letter] (2008); www.cdc.gov/EID/content/14/8/1317.htm.
30. R. Sallares, A. Bouwman, C. Anderung, *Med. Hist.* **48**, 311 (2004).
31. S. M. Rich, F. J. Ayala, *Proc. Natl. Acad. Sci. U.S.A.* **97**, 6994 (2000).
32. D. A. Joy *et al.*, *Science* **300**, 318 (2003).

33. We thank S. S. Renner and two anonymous reviewers for constructive comments on the manuscript. The study was supported by NSF DEB 0542390 to R.E.R., who also acknowledges the generous support of the Curators of the University of Missouri and the Alexander von Humboldt Foundation.

Supporting Online Material

www.sciencemag.org/cgi/content/full/329/5988/226/DC1
Materials and Methods
SOM Text
Figs. S1 and S2
References

1 March 2010; accepted 13 May 2010
10.1126/science.1188954

An Autophagy-Enhancing Drug Promotes Degradation of Mutant α_1-Antitrypsin Z and Reduces Hepatic Fibrosis

Tunda Hidvegi, Michael Ewing, Pamela Hale, Christine Dippold, Caroline Beckett, Carolyn Kemp, Nicholas Maurice, Amitava Mukherjee, Christina Goldbach, Simon Watkins, George Michalopoulos, David H. Perlmutter*

In the classical form of α_1-antitrypsin (AT) deficiency, a point mutation in AT alters the folding of a liver-derived secretory glycoprotein and renders it aggregation-prone. In addition to decreased serum concentrations of AT, the disorder is characterized by accumulation of the mutant α_1-antitrypsin Z (ATZ) variant inside cells, causing hepatic fibrosis and/or carcinogenesis by a gain–of–toxic function mechanism. The proteasomal and autophagic pathways are known to mediate degradation of ATZ. Here we show that the autophagy-enhancing drug carbamazepine (CBZ) decreased the hepatic load of ATZ and hepatic fibrosis in a mouse model of AT deficiency–associated liver disease. These results provide a basis for testing CBZ, which has an extensive clinical safety profile, in patients with AT deficiency and also provide a proof of principle for therapeutic use of autophagy enhancers.

The classical form of α_1-antitrypsin (AT) deficiency is caused by a point mutation (substitution of lysine for glutamate at residue 342) that alters the folding of an abundant liver-derived plasma glycoprotein during biogenesis and also renders it prone to polymerization (*1*). In addition to the formation of insoluble aggregates in the endoplasmic reticulum (ER) of liver cells, there is an 85 to 90% reduction in circulating concentrations of AT, the predominant physiologic inhibitor of neutrophil elastase. Liver fibrosis and carcinogenesis are caused by a gain–of–toxic function mechanism. Indeed, AT deficiency is the most common genetic cause of liver disease in childhood but can also present for the first time with cirrhosis and/or hepatocellular carcinoma in adulthood (*1*).

Genetic and/or environmental modifiers determine whether an affected homozygote is susceptible to liver disease (*2*). Two general explanations for the effects of such modifiers have been postulated: variation in the function of intracellular degradative mechanisms (*3*, *4*) and/or variation in the signal transduction pathways that are activated to protect the cell from protein mislocalization and/or aggregation. As for degradation, the proteasome is responsible for degrading soluble forms of α_1-antitrypsin Z (ATZ) (*5*), and macroautophagy is specialized for disposal of the insoluble polymers and aggregates (*6*, *7*). However, disposal of ATZ may involve other degradative mechanisms, as yet not well defined (*8*, *9*). In terms of cellular response pathways, accumulation of ATZ activates nuclear factor κB (NF-κB)

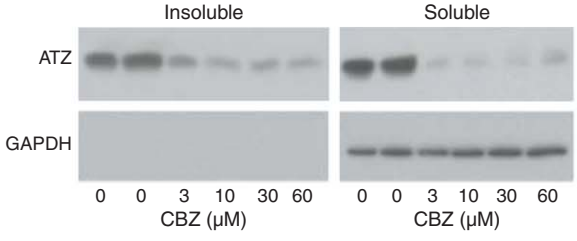

Fig. 1. Effect of CBZ on steady-state levels of ATZ in the HTO/Z cell line. Immunoblot analysis of HTO/Z cells treated with various concentrations of CBZ, separated into soluble and insoluble fractions, and then probed with antibodies to AT (**top**) and to GAPDH (**bottom**).

Departments of Pediatrics, Pathology, Cell Biology and Physiology, University of Pittsburgh School of Medicine, Pittsburgh, PA 15261 USA.

*To whom correspondence should be addressed. E-mail: david.perlmutter@chp.edu

and autophagy but not the unfolded protein response (*6*, *9*, *10*).

Because the autophagic response participates in both degradation of ATZ and in the cellular response to accumulation of ATZ in the ER, we examined whether a drug that enhances autophagy could ameliorate hepatotoxicity in this disorder. From a list of drugs that have been recently shown to enhance autophagic degradation of aggregation-prone proteins with polyglutamine repeats (*11*–*13*), we selected carbamazepine (CBZ) for detailed studies of its effect on ATZ because it has the most extensive safety profile in humans.

First, we found that CBZ mediated a marked decrease in steady-state levels of ATZ in both the insoluble and soluble fractions in the HeLa inducible cell line HTO/Z (Fig. 1). The effect of CBZ was also specific because rapamycin, a drug that activates autophagy by inhibiting target of rapamycin (TOR) kinase, had no effect on ATZ levels (fig. S1). CBZ was dose dependent in the range of 1 to 60 μM (fig. S2) and did not affect wild-type AT levels in the HTO/M cell line or BiP levels in the HTO/Z line (fig. S3).

To further characterize the effect of CBZ on ATZ, we carried out pulse labeling and pulse-chase labeling experiments in the HTO/Z line. CBZ did not affect synthesis of ATZ (Fig. 2A), and disappearance of ATZ from the intracellular compartment was more rapid in cells treated with CBZ than in the untreated cells (Fig. 2, B and C). A statistically significant increase in disappearance of ATZ from the intracellular compartment was mediated by CBZ ($P = 0.0007$ by two-way analysis of variance with Bonferroni adjustment), with a half-time of 130 min compared to 200 min

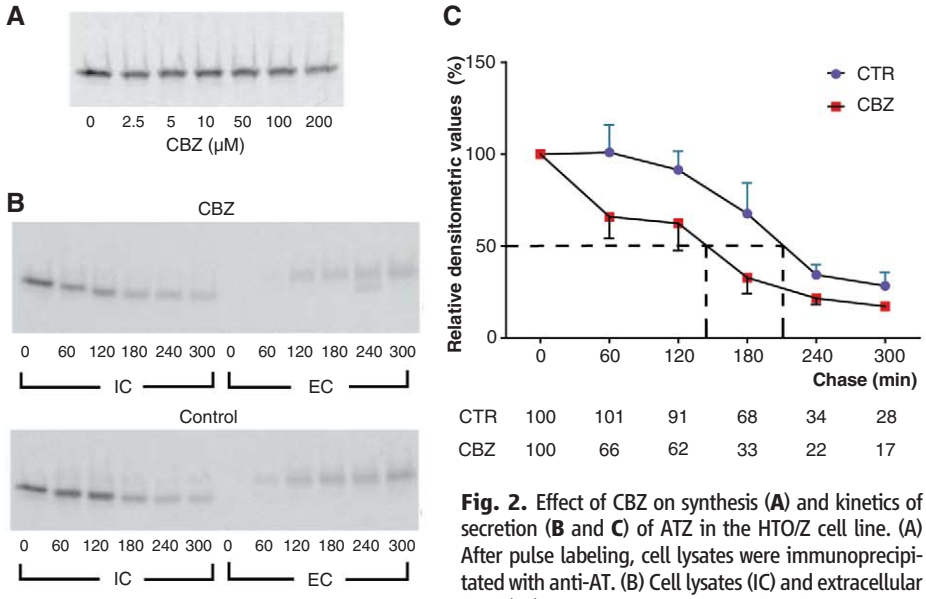

Fig. 2. Effect of CBZ on synthesis (**A**) and kinetics of secretion (**B** and **C**) of ATZ in the HTO/Z cell line. (A) After pulse labeling, cell lysates were immunoprecipitated with anti-AT. (B) Cell lysates (IC) and extracellular fluid (EC) were immunoprecipitated with anti-AT after pulse-chase labeling. (C) Kinetics of disappearance from IC was determined by densitometric scanning of fluorograms from five separate experiments. Data are shown as the mean ± SE. Dashed lines show the half-time for disappearance. Raw densitometric values for each time point are shown below the figure.

Fig. 3. (**A**) Effect of CBZ on LC3 conversion in the HTO/Z cell line by immunoblot. Densitometric values are shown at the bottom. (**B** and **C**) Effect of CBZ on ATZ in autophagy-deficient ($Atg5^{-/-}$) (B) versus wild-type ($Atg5^{+/+}$) (C) cell lines. (**D**) Effect of CBZ on levels of the AT Saar variant in the HTO/Saar cell line compared to ATZ in the HTO/Z line. (**E**) Effect of CBZ on ATZ levels in the presence of proteasomal inhibitors. For the last 6 hours of incubation with CBZ (30 μM) or control, proteasomal inhibitors were added to some of the monolayers. The experiments were done as in Fig. 1. For loading control, immunoblots for GAPDH are shown in the lower panels. Similar results were obtained in three separate experiments.

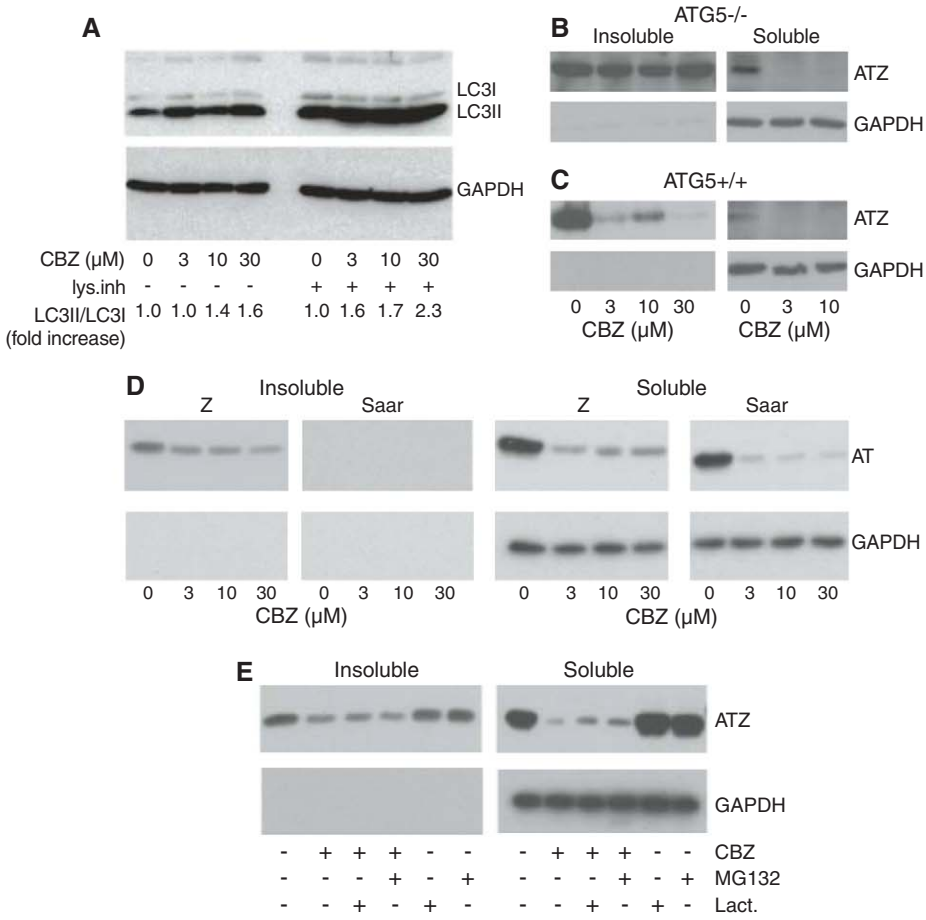

in untreated cells. The increase in intracellular disappearance of ATZ mediated by CBZ could not be attributed to enhanced secretion (Fig. 2B and fig. S4). Thus, CBZ appears exclusively to change the rate of intracellular degradation.

To determine whether CBZ enhances autophagy in the HTO/Z line, we examined its effect on isoform conversion of autophagosomal membrane-specific protein LC3, an indicator of autophagosome formation (Fig. 3A). The LC3-II to LC3-I ratio increased in a dose-dependent manner and was greater in the presence of lysosomal enzyme inhibitors, indicating that CBZ elicits increased autophagic flux. This effect of CBZ on autophagic flux exceeded the increase that results from intracellular accumulation of ATZ (fig. S5). Thus, CBZ stimulates autophagy in cells that have already activated the autophagic pathway in response to ER accumulation of ATZ.

To determine whether the effect of CBZ on ATZ degradation involved enhanced autophagy, we examined its effect on ATZ levels in an autophagy (Atg5)–deficient cell line (Fig. 3, B and C). CBZ mediated a decrease in levels of insoluble ATZ in the wild-type mouse embryonic fibroblast (MEF) cell line but not in the Atg5-deficient cell line. CBZ also mediated a decrease in levels of soluble ATZ in both wild-type and Atg5-deficient cells. Thus, CBZ enhances the disposal of insoluble ATZ by autophagy and has an independent action on the disposal of soluble ATZ by mechanism(s) that do not involve the conventional autophagic pathway.

To determine whether the effects of CBZ were specific for the Z variant of AT, we investigated its effect on disposal of AT Saar, a variant of AT that accumulates in the ER but does not aggregate and is predominantly degraded by a proteasomal mechanism (*9*). AT Saar was present only in the soluble fraction, but it was degraded by CBZ in a manner almost identical to that of ATZ (Fig. 3D), suggesting an effect of CBZ also on the proteasome.

Thus, we examined the effect of CBZ on steady-state levels of ATZ in the presence of proteasomal inhibitors (Fig. 3E). Although they had no effect on levels of insoluble ATZ, lactacystin and MG132 partially reversed the effect of CBZ on levels of soluble ATZ [lactacystin: reversal of 23.1 ± 14.0% (mean ± SD), $n = 3$ experiments; MG132: reversal of 12.3, average of n = two experiments]. Increased levels of ATZ in the presence of lactacystin and MG132 alone provided validation for proteasome inhibitory activity under the conditions of these experiments. Thus, CBZ mildly enhances proteasomal degradation of ATZ and has an independent action on nonproteasomal mechanisms for disposal of soluble ATZ.

Next, we examined the effect of CBZ on hepatic load of ATZ in vivo using PiZ × GFP-LC3 mice. The PiZ mouse was created with the human *ATZ* gene as transgene. Although it differs from the human disorder in having normal circulating levels of the endogenous murine ortholog of AT, the PiZ mouse is a robust model of liver disease associated with AT deficiency, as characterized by intrahepatocytic ATZ-containing globules, inflammation, and increased regenerative activity, dysplasia, and fibrosis (*14*, *15*). It has been bred onto the GFP-LC3 background to monitor autophagy (*6*). When administered at 250 mg kg^{-1} day^{-1} for 2 weeks by gavage, CBZ mediated a marked decrease in total, insoluble, and soluble ATZ in the liver (Fig. 4A). The treatment was also associated with a marked decrease in intrahepatocytic ATZ-containing globules (Fig. 4, B and C). Quantitative morphometry showed a decrease in globule-containing hepatocytes by a factor of 3.36 ($P < 0.001$ by Mann-Whitney rank sum test). Serum concentrations of human AT were not significantly affected by CBZ treatment (fig. S6), arguing against any effect on secretion of ATZ in vivo.

Using indirect immunofluorescence, an increase in number of hepatic green fluorescent autophagosomes was detected in areas of liver that lacked AT-stained globules after CBZ treatment (Fig. 4D), and this was confirmed by quantitative morphometry (mean ± SD: 565.7 ± 185.7 μm^2 in control versus 1055.3 ± 139.7 μm^2 in CBZ; $P = 0.049$ by t test). The increase in autophagosomes mediated by CBZ superseded the increase that occurs predominantly in globule-containing hepatocytes from ATZ expression alone (*6*) (figs. S7 and S8). The effect of CBZ in vivo was specific in that rapamycin had no effect on hepatic ATZ levels (fig. S9). Next, we ex-

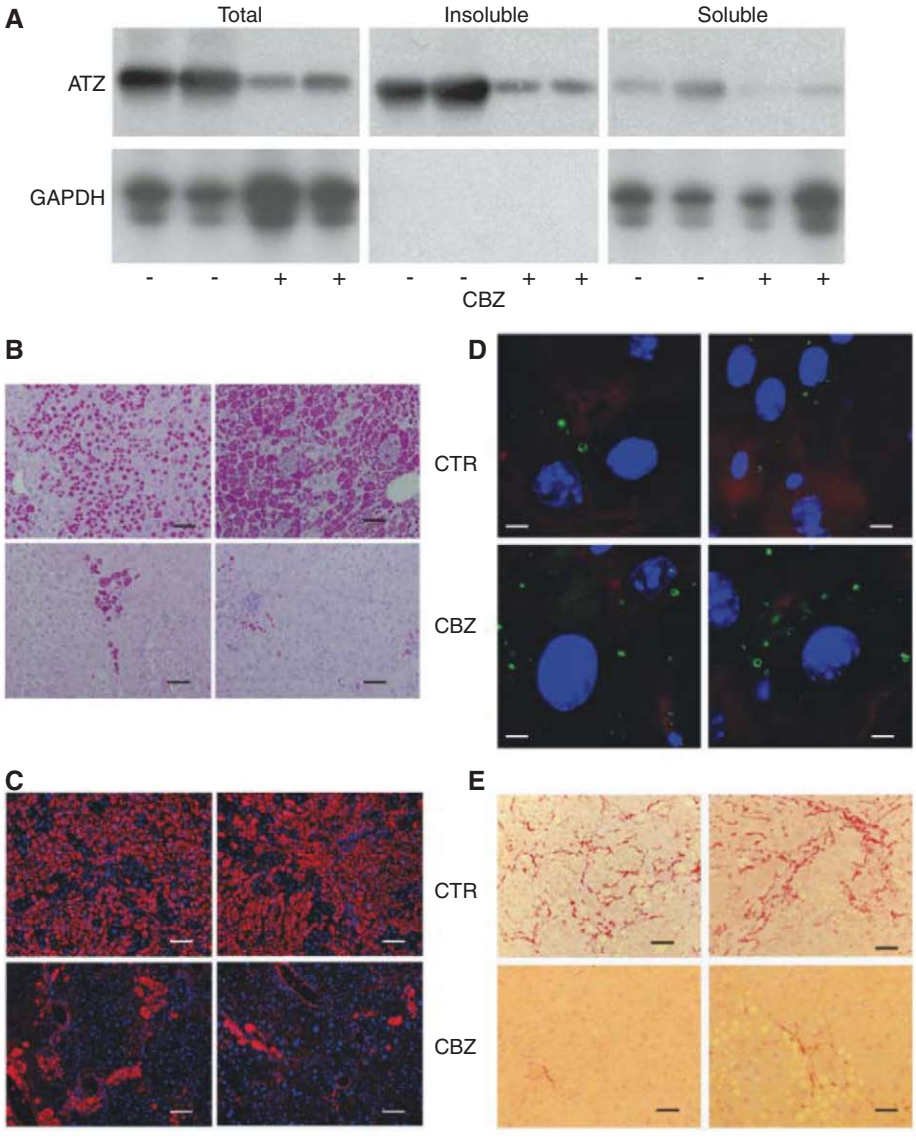

Fig. 4. In vivo effect of CBZ on (**A**) hepatic AT load, (**B** and **C**) globules, (**D**) autophagosomes, and (**E**) hepatic fibrosis in PiZ × GFP-LC3 mice. Male mice at 5 months of age were treated for 2 weeks with CBZ (250 mg kg^{-1}) or solvent (dimethyl sulfoxide) by gavage. Samples from two control and two CBZ-treated mice are shown. (A) Immunoblot; (B) histochemical staining with periodic acid-Schiff and diastase; (C) immunostaining with anti-AT; (D) immunostaining with anti-GFP; (E) histochemical staining with Sirius red. Globules are purple in (B). Globules are red and nuclei blue in (C). Autophagosomes are green in (D). Scale bars, 100 μm.

amined the effect of CBZ on hepatic fibrosis because it is a key feature of the liver disease associated with AT deficiency (*14*). CBZ mediated a marked decrease in fibrosis (Fig. 4E). Furthermore, there was a marked and statistically significant reduction in hepatic hydroxyproline concentration in PiZ mice treated with CBZ (mean ± SD: 1.21 ± 0.7 in CBZ versus 2.27 ± 1.02 μg per milligram of dry weight in control, $P = 0.0074$ by t test with Welch modification). Hepatic hydroxyproline content was decreased 46.7% by CBZ, reaching a level that was indistinguishable from that of the background FVB/N strain (fig. S10). CBZ also mediated a decrease in hepatic hydroxyproline concentration in the PiZ × IKKβΔhep mouse model (fig. S11). On this hepatocyte-specific NFκB-deficient background, there is more severe liver damage as reflected by hydroxyproline concentrations that are >150% of the levels in the PiZ mouse on the FVB/N background (fig. S10). CBZ treatment decreased levels of stellate cell activation markers, including smooth muscle actin, collagen 1A, and transforming growth factor β, but only the decrease in actin reached statistical significance (table S1).

To determine whether lower doses of CBZ for more prolonged time intervals could reduce hepatic fibrosis, we examined the effect of CBZ at lower doses for 6 weeks. Hepatic hydroxyproline concentrations decreased at the dose of 200 mg kg^{-1} day^{-1} but not at doses of 50 and 100 mg kg^{-1} day^{-1} (fig. S10). Although the lowest effective dose of CBZ (200 mg kg^{-1} day^{-1}) was considerably higher than the doses used in humans (10 to 20 mg kg^{-1} day^{-1}), effective doses of drugs can be 10 to 20 times as high in mice because of the higher ratio of surface area to body weight when compared to humans.

Thus, CBZ reduces the hepatic load of mutant ATZ and hepatic fibrosis in the PiZ mouse. Mechanistic studies indicate that CBZ increases both autophagic and proteasomal degradation of ATZ. That rapamycin does not enhance autophagic disposal of ATZ may mean that a TOR-independent pathway is involved in the effect of CBZ. The effect of CBZ on ATZ disposal cannot be fully accounted for by the proteasomal and conventional macroautophagic pathways. The capacity to enhance disposal of both insoluble and soluble ATZ could represent an important characteristic of CBZ as a potential therapeutic in that it might provide for elimination of the putative hepatotoxic form of ATZ, whether it is soluble monomeric, soluble oligomeric, and/or insoluble polymeric ATZ species.

Because it is theorized that clinically significant liver damage occurs only in AT-deficient patients who also have a "second" defect in quality control and that these second defects are heterogeneous among the affected population, one might conclude that CBZ would be effective only in individuals in whom the "second" defect is related to the specific mechanism of CBZ action. However, our results suggest that CBZ can enhance autophagy beyond the extent to which it has already been activated by the pathological state. CBZ also appears to affect several mechanisms of intracellular disposal and therefore may not require mechanistic specificity for a beneficial effect. It is also encouraging that CBZ reduced hepatic fibrosis in the PiZ × IKKβΔhep mouse model, which could be viewed as a mouse with a type of "second" defect—in this case, reduced functioning of the hepatocyte NF-κB signaling pathway.

In addition to its potential for the treatment of liver disease due to AT deficiency, CBZ should be considered for its ability to enhance intracellular disposal pathways for the treatment of other diseases in which tissue damage involves gain–of–toxic function mechanisms caused by misfolded or aggregation-prone proteins (*13*). Our results also provide further evidence for the concept that the endogenous protein homeostasis machinery can be used to prevent tissue damage from mutant proteins (*16*).

References and Notes

1. D. H. Perlmutter, *Cell Death Differ.* **16**, 39 (2009).
2. E. Piitulainen, J. A. Carlson, K. Ohlsson, T. Sveger, *Chest* **128**, 2076 (2005).
3. Y. Wu *et al.*, *Proc. Natl. Acad. Sci. U.S.A.* **91**, 9014 (1994).
4. S. Pan *et al.*, *Hepatology* **50**, 275 (2009).
5. D. Qu, J. H. Teckman, S. Omura, D. H. Perlmutter, *J. Biol. Chem.* **271**, 22791 (1996).
6. T. Kamimoto *et al.*, *J. Biol. Chem.* **281**, 4467 (2006).
7. K. B. Kruse, J. L. Brodsky, A. A. McCracken, *Mol. Biol. Cell* **17**, 203 (2006).
8. C. M. Cabral, P. Choudhury, Y. Liu, R. N. Sifers, *J. Biol. Chem.* **275**, 25015 (2000).
9. T. Hidvegi, B. Z. Schmidt, P. Hale, D. H. Perlmutter, *J. Biol. Chem.* **280**, 39002 (2005).
10. T. Hidvegi *et al.*, *J. Biol. Chem.* **282**, 27769 (2007).
11. S. Sarkar *et al.*, *J. Cell Biol.* **170**, 1101 (2005).
12. L. Zhang *et al.*, *Proc. Natl. Acad. Sci. U.S.A.* **104**, 19023 (2007).
13. B. Ravikumar, S. Sarkar, D. C. Rubinsztein, *Methods Mol. Biol.* **445**, 195 (2008).
14. D. A. Rudnick *et al.*, *Hepatology* **39**, 1048 (2004).
15. Further description of the mouse model is available as supporting material on *Science* Online.
16. E. T. Powers, R. I. Morimoto, A. Dillin, J. W. Kelly, W. E. Balch, *Annu. Rev. Biochem.* **78**, 959 (2009).

17. We are indebted to J. Englert for the hydroxyproline assay and to G. Silverman and J. Brodsky for critical review of the manuscript. The work was partially supported by NIH grants HL037784, DK076918, and RR022241.

Supporting Online Material

www.sciencemag.org/cgi/content/full/science.1190354/DC1
Materials and Methods
Figs. S1 to S10
Table S1
References

1 April 2010; accepted 21 May 2010
Published online 3 June 2010;
10.1126/science.1190354
Include this information when citing this paper.

AAAS is here – helping scientists achieve career success.

Every month, over 400,000 students and scientists visit ScienceCareers.org in search of the information, advice, and opportunities they need to take the next step in their careers.

A complete career resource, free to the public, *Science* Careers offers a suite of tools and services developed specifically for scientists. With hundreds of career development articles, a grants and scholarships database, webinars and downloadable booklets filled with practical advice, a community forum providing real-time answers to career questions, and thousands of job listings in academia, government, and industry, *Science* Careers has helped countless individuals prepare themselves for successful careers.

As a AAAS member, your dues help AAAS make this service freely available to the scientific community. If you're not a member, join us. Together we can make a difference.

To learn more, visit **aaas.org/plusyou/sciencecareers**

AAAS + U = Δ

NEW PRODUCTS

VARIABLE-SPEED MIXER

The variable-speed VX-200 Vortex Mixer offers smooth, fast, and efficient mixing with minimal vibration across all speeds. Unlike vortex mixers that use elliptical orbits, the VX-200 deploys a true circular orbit mixing technique that facilitates uniform sample vortexing, even at low speeds. The standard CombiCup head accepts many different tube sizes, while the unique technology used in its manufacture provides a robust, sturdy core that fits optional heads for microplates, polymerase chain reaction strip tubes, 15-ml tubes, 30-ml tubes, and blood vials. The VX-200 can be used in "touch" or "continuous" mode. Touch mode is activated by depressing the sample head and stopped by releasing the pressure. Other features include an optimized counter-balance system that minimizes vibration and movement of the mixer during operation.

Cleaver Scientific

For info: +44-1788-565-300 | www.cleaverscientific.com

ELECTROPHORESIS GELS

The Mini-Protean TGX precast gels provide researchers with fast-running, long-shelf-life precast gels for protein electrophoresis using the standard Laemmli buffer system. The TGX gels can be run to completion in as little as 12 minutes. The gels are based on a modification of the Laemmli buffer system that significantly increases gel matrix stability and performance over time. The modification extends the gel shelf life to more than 12 months and offers consistent, superior resolution and reproducibility while delivering unprecedented electrophoresis run speeds. Compared with other long-shelf-life products, these gels have the advantage of using the standard and inexpensive tris/glycine/sodium dodecylsulfate buffers that researchers have preferred over other buffer systems for more than 30 years.

Bio-Rad

For info: 800-424-6723 | www.bio-rad.com

ENVIRONMENTAL SAMPLE CONCENTRATION

The proprietary SampleGenie flask technology helps scientists eliminate handling of samples by concentrating them, without loss of volatile components, directly into a small gas chromatography or high-performance liquid chromatography vial. SampleGenie technology enables samples in Genevac Rocket series, EZ-2 series, or HT series centrifugal evaporators to be concentrated directly into a single vial, eliminating the need for reformatting of samples after drying. Along with the automation featured in Genevac evaporators, this concentration helps deliver uniform results every time, thereby increasing productivity in environmental analysis.

Genevac

For info: +44-1473-240-000 | www.genevac.co.uk

WATER FOR ION CHROMATOGRAPHY

The ICW-3000 water purification system produces a constant and reliable source of ultrapure water for Dionex IC (ion chromatography) systems. Ultrapure water from the ICW-3000 can increase the precision of IC analyses. The system provides a continual flow of ultrapure water to the eluent generator and regenerant lines of the suppressor. This reduces the carbonate content in the water, which sharply decreases contamination risks and improves experiment reproducibility, while also eliminating the need for helium. The water system also eliminates the need for eluent preparation and the instrument downtime that occurs when filling eluent bottles.

Millipore

For info: 978-762-5170 | www.millipore.com/icw3000

PEPTIDE LIBRARY SYNTHESIZER

The Overture Robotic Peptide Library Synthesizer can run syntheses from 0.005 to 24 mmol scales. It features six reaction blocks capable of holding 96 (10 ml) or 24 (40 ml or 45 ml) reaction vessels, 49 amino acid positions, six solvent bottle positions, variable-speed vortex mixing, automatic robotic arm calibration, and a full-color, chemical-resistant touchscreen. Amino acid deliveries are performed from individual dispensers, which do not require rinsing in between deliveries, saving the user time and money. These dispensers are capable of infinitely variable delivery volumes accurate to 50 µl. The Overture's flexible, easy-to-use software features easy sequence importing, automatic sequence placement, automatic library generation, automated cleaning routines, and report and log-file generation.

Protein Technologies

For info: 520-629-9626 | www.peptideinstruments.com

LABORATORY INFORMATION MANAGEMENT

A new laboratory information management system (LIMS), the LIMS-on-Demand allows organizations of varying types and sizes to leverage all the benefits of an industry-leading LIMS solution without the time and cost associated with on-premise software installation. LIMS-on-Demand can reduce the capital investment associated with traditional LIMS implementation and validation by eliminating the need for extensive software testing and installation. For the cost of a monthly subscription fee, a laboratory can easily, affordably, and securely access a fully functional, validated solution through a standard web browser. This on-demand access provides a flexible alternative to conventional LIMS that allows organizations to cost-effectively adapt technology as needs change.

Thermo Fisher Scientific

For info: 781-933-4689 | www.thermofisher.com

Electronically submit your new product description or product literature information! Go to **www.sciencemag.org/products/newproducts.dtl** for more information.

Newly offered instrumentation, apparatus, and laboratory materials of interest to researchers in all disciplines in academic, industrial, and governmental organizations are featured in this space. Emphasis is given to purpose, chief characteristics, and availability of products and materials. Endorsement by *Science* or AAAS of any products or materials mentioned is not implied. Additional information may be obtained from the manufacturer or supplier.

POSITIONS OPEN

FOREST ECOLOGIST AT THE APPALACHIAN LABORATORY

The Appalachian Laboratory (AL) of the University of Maryland Center for Environmental Science (UMCES) seeks to fill a new full-time, tenure-track **ASSISTANT PROFESSOR** position in forest ecology. The successful candidate should address questions at broad spatial scales and complement our strengths in landscape and watershed ecology. We are especially interested in expertise such as biogeochemistry, stable isotopes, phylogeography, and advanced statistical methods that will be used to assess the effects of environmental change on temperate forest ecosystems.

Excellent research, computing, and teaching facilities are available, including plant, soil, water, and molecular analysis laboratories with state-of-the-art analytical instrumentation, a new stable isotope facility, growth chambers, and a greenhouse. UMCES faculty are expected to participate in graduate education in addition to research, outreach, and application. Applicants should send an electronic copy of curriculum vitae; statement of research interests and a brief discussion of how their research would complement ongoing research at AL and UMCES; selected reprints; and names of four references (including title, mailing address, telephone and fax numbers, and e-mail address) to **e-mail: pisearch@al.umces.edu**. Review of applications will begin on September 1, 2010, and will continue until the position is filled. Information about AL and UMCES and this search can be found at **website: http://www.al.umces.edu/**. *UMCES is an Affirmative Action/Equal Opportunity Employer. Women and minorities are strongly encouraged to apply.*

RESEARCH ASSISTANT PROFESSOR

The Division of Metabolism, Endocrinology, and Nutrition in the Department of Medicine at the University of Washington is recruiting a full-time faculty member at the Research Assistant Professor level. The appointment requires a Ph.D. or equivalent degree and a record of research publications in the area of pathogenesis of pancreatic beta cell failure in diabetes. The applicant is expected to have expertise in insulin secretion and partial support for his/her research. Interested applicants should submit a letter of interest, curriculum vitae, and a brief summary of research capabilities and funding to:

Jerry Palmer, M.D.
Search Committee Chair
VA Puget Sound Health Care System (111)
1660 S. Columbian Way
Seattle, WA 98108

Review of applications will begin immediately and continue until the position is filled. University of Washington faculty engage in teaching, research, and service. *The University of Washington is an Affirmative Action, Equal Opportunity Employer.*

POSTDOCTORAL RESEARCH POSITIONS
San Diego State University
Heart Institute–SDSU Research Foundation

The San Diego State University Heart Institute is recruiting **POSTDOCTORAL FELLOWS** to work in a dynamic, state-of-the-art cardiovascular cell and molecular biology research setting in the laboratory of the Institute Director **Dr. Chris Glembotski,** studying roles for heart-derived secreted cytokines (cardiomyokines) on cardiac protection and repair. Applicants should have a Ph.D. in a relevant field, demonstrated expertise in basic cell and molecular biology, including methods to examine gain- and loss-of-gene-function in culture and animal models of heart disease, excellent communication skills, a record of peer-reviewed journal publications, and the desire and ability to write and submit competitive research grant applications. Salary is commensurate with experience; excellent benefits. Applicants should submit a cover letter, curriculum vitae, and a description of research experience and professional goals with the application for **Job #100120** at **website: https://jobsfoundation.sdsu.edu** or call **telephone: 619-594-5703.** *Equal Employment Opportunity/Affirmative Action/Title IX Employer.*

POSITIONS OPEN

SENIOR FACULTY POSITION
Rutgers Laboratory for Surface Modification

The Laboratory for Surface Modification (LSM) at Rutgers University, a world-class research center focused on interdisciplinary research in the basic science and technology of interfaces, nanostructures, and surfaces, seeks an experimental scientist with exceptional credentials for a tenured faculty appointment at the **FULL PROFESSOR** level. The appointment may be in the Department of Physics, Chemistry, Materials Science, Electrical Engineering, or BioMedical Engineering or it may be a joint appointment. The successful candidate will have an outstanding record of achievement in science and/or technology and is expected to establish a world-class research program at Rutgers and to interact with industry. Submit applications electronically (preferred) to **e-mail: lsm_search@physics.rutgers.edu**, or by surface mail to: **LSM Search Committee, Rutgers University, 136 Frelinghuysen Road, Piscataway, NJ 08854.** Additional details may be found at **website: http://www.lsm.rutgers.edu**. *Rutgers, the State University of New Jersey, is an Equal Opportunity Employer, which encourages applications from underrepresented groups.*

Argonne NATIONAL LABORATORY

ASSOCIATE LABORATORY DIRECTOR PHYSICAL SCIENCES AND ENGINEERING DIRECTORATE

ARGONNE NATIONAL LABORATORY

Argonne National Laboratory seeks applications from highly qualified candidates for the position of Associate Laboratory Director, Physical Sciences and Engineering (ALD-PSE). Argonne is one of the preeminent multi-disciplinary research facilities in the country located about 25 miles southwest of Chicago, Illinois and is operated by the University of Chicago for the U.S. Department of Energy's Office of Science. The ALD-PSE is an executive position that reports to the Laboratory Director and provides leadership for five divisions: Center for Nanoscale Materials, Chemical Sciences and Engineering, High Energy Physics, Materials Science, and Physics. Major initiatives under the direction of PSE include Alternative Energy and Efficiency, Energy Storage, and Materials and Molecular Design and Discovery.

The ALD-PSE will: (1) provide primary basic science vision, identify new research opportunities, and be a force for the integration of basic and applied science and engineering throughout the laboratory; (2) be a leading interface with the U.S. Department of Energy and UChicago Argonne LLC for mission-based science issues; (3) act as a member of Argonne's senior management team in setting strategic goals and in developing collaborations among stakeholders, scientific, academic and industrial entities to achieve those goals.

The successful candidate should have an internationally recognized research stature in one of the disciplines within PSE and experience in managing large multi-disciplinary science programs.

Argonne offers an excellent compensation and benefits package. For more information and to apply, see job # 316179 at www.anl.gov/jobs. For full consideration, apply promptly; we aim to have an appointment to this position by the start of our fiscal year on October 1, 2010.

Argonne National Laboratory is a multi-program laboratory managed by UChicago Argonne, LLC for the U.S. Department of Energy. We are an equal opportunity employer and value diversity in our workforce. For additional information about Argonne, visit us online at www.anl.gov

www.uni-frankfurt.de

GOETHE UNIVERSITÄT FRANKFURT AM MAIN

The Faculty of Computer Science and Mathematics at the Goethe University Frankfurt together with the Frankfurt Institute for Advanced Studies invites applications to fill the position of a

Associate Professorship (W2) in Computational Neuroscience/Computational Vision (tenure track)

Applicants must have an excellent track record in Computational Neuroscience with emphasis on modeling the visual system. Successful acquisition of third party funding and collaborations in interdisciplinary project consortia are expected. This research professorship is part of the Bernstein Focus Neurotechnology Frankfurt and the successful applicant shall collaborate actively within the Focus (http://fias.uni-frankfurt.de/bernstein). Opportunities for collaborations in additional research areas of FIAS are strongly desired.

The teaching obligations for this research professorship are 2 hours per week. The successful candidate will also be member of the Faculty of Computer Science and Mathematics or the Faculty of Physics.

The designated salary for the position is based on "W2" on the German university scale or equivalent. The Goethe University is committed to a pluralistic campus community through affirmative action and equal opportunity. For further information regarding the general conditions for professorship appointments, please see: http://www.uni-frankfurt.de/aktuelles/ausschreibung/professuren/index.html

Qualified academics are invited to submit their applications accompanied by the usual documents (CV, degrees and certificates, list of publications, details on teaching and international experience, information on successful grant applications, a statement about your research goals in the context of the Bernstein Focus Neurotechnology within **three weeks** after publication of this advertisement to: **Frau Gaby Schmitz, Frankfurt Institute for Advanced Studies, Ruth-Moufang-Str. 1, D-60438 Frankfurt am Main, E-Mail: schmitz@fias.uni-frankfurt.de**

PENNSTATE University Park

Systems & Computational Genomics: Faculty Cluster Hiring

The Pennsylvania State University is embarking on a comprehensive and transformative investment in systems genomics, complex traits and biological variation. This cross-college endeavor coordinates faculty recruitments and team-building efforts to address critical problems in the life sciences affecting agriculture, energy production and healthcare. Development of computational and informatics systems for the analysis of genomic data is an integral part of the strategic plan. The PSU Systems Genomics Initiative is a concerted effort to bring predictive power to our understanding of biological systems and realize the potential of biology-based tools.

We seek to appoint multiple tenure-track professors at all levels from Assistant and Associate Professor through to Full Professors and Endowed Chairs who will further Penn State's leadership role in the fields of Systems Genomics and Bioinformatics. We seek faculty interested in analyzing genomic data, undertaking systems and functional genomics and in applying these results to a broad range of biological problems. These will include Computer and Information Scientists, Social Scientists, Life Scientists, Physicists, Mathematicians, Statisticians and Biomedical researchers. Appointments will be made both at the main campus at University Park in Central Pennsylvania and also in the College of Medicine, located at the Penn State Medical Center in Hershey, PA. We seek interactive faculty who can work across disciplines and in a team to provide novel insights into current and future issues. We anticipate that many candidates will have joint appointments and join one of our centers of excellence in genomics, such as the Center for Comparative Genomics and Bioinformatics (http://www.bx.psu.edu/) or Center for Medical Genomics (http://www.huck.psu.edu/institutes-and-centers/medical-genomics).

These positions feature outstanding research space and competitive start-up packages and state-of-the-art shared instrumentation for sequencing (http://www.huck.psu.edu/) and computational analysis (http://www.ics.psu.edu/). Penn State has achieved great successes in the field of genomics and bioinformatics with an impressive collection of publications and analysis software, including Galaxy (http://galaxy.psu.edu/), a universal platform that can continuously adapt and gain new capabilities to serve the needs of experimental and computational scientists.

Please electronically submit a cover letter, including future research plans, curriculum vitae and the contact information of three references to Deb Stauffer at dsg3@psu.edu

Review will start in August and continue until multiple positions have been filled.

Penn State is committed to affirmative action, equal opportunity and the diversity of its workforce.

Opportunities as **limitless** as **Penn State**.

www.psu.jobs

Eidgenössische Technische Hochschule Zürich
Swiss Federal Institute of Technology Zurich

Assistant Professor (Tenure Track) of Computational Biology
Assistant Professor (Tenure Track) of Bioinformatics

ETH Zurich is strengthening its involvement in the area of computational science. The initiative is aimed to foster concerted interdisciplinary research and teaching collaborations, in particular in the life sciences.

Applications from candidates with internationally recognized research credentials and proven teaching abilities are invited for two professorial positions:

Assistant Professor (Tenure Track) of Computational Biology
The Department of Biology (www.biol.ethz.ch) at ETH Zurich invites applications for a position of Assistant Professor (Tenure Track) in the area of Computational Biology. Life Science Zurich and the Department of Biology offer outstanding scientific opportunities to participate in interdisciplinary research projects, including close interactions with SystemsX.ch, the Swiss initiative for systems biology, the Functional Genomics Center Zurich and the ETH Laboratory of Computational Science and Engineering. Involvement in the biology teaching program, including teaching within an inter-departmental Master's curriculum in bioinformatics, is expected. Candidates are expected to build a strong, independent research program in theoretical or applied computational biology. Research areas include but are not limited to the development and implementation of novel algorithms for the analysis of complex biological questions, molecular and developmental networks and their dynamic changes in cells, using information available from genomic, proteomic, imaging, and metabolomic data. The successful candidate will be a member of the Institute of Molecular Systems Biology. The future professor will be expected to teach undergraduate level courses (German or English) and graduate level courses (English).

Assistant Professor (Tenure Track) of Bioinformatics
The Department of Computer Science (www.inf.ethz.ch) at ETH Zurich invites applications for a position of Assistant Professor (Tenure Track) of Bioinformatics. Applicants should have an excellent record of internationally recognized research which demonstrates a strong knowledge and link of computer science with computational methods and bioinformatics. The expertise of the successful candidate may encompass areas such as Computational Biology or Modelling and Uncertainty Quantification for the simulation of challenging biological problems. Background in interdisciplinary, innovative research bridging Computer Science with scientific fields such as the Life Sciences and in particular Computational Biology, the Social Sciences, Engineering, Medicine, and Finance while contributing to the development of fundamental Computer Science concepts is highly desirable. The candidate is expected to establish and lead a research group within the Department of Computer Science at ETH Zurich. A strong background in Computer Science is required for this position. Moreover, the successful candidate shall supervise graduate students and teach courses in Computational Science and core courses of Computer Science. The professorship is expected to be instrumental in the participation of joint activities with the departments of Biology and the Department of Biosystems Science and Engineering as well as with the Swiss Institute for Bioinformatics.

Assistant professorships have been established to promote the careers of younger scientists. The initial appointment is for four years with the possibility of renewal for an additional two-year period and promotion to a permanent position.

Please submit your application together with a curriculum vitae, a list of publications, the names of at least three referees, and a short overview of the research interests to the **President of ETH Zurich, Prof. Dr. Ralph Eichler, Raemistrasse 101, ETH Zurich, 8092 Zurich, Switzerland, (or via e-mail as one single pdf to faculty-recruiting@sl.ethz.ch) no later than August 31, 2010.** With a view toward increasing the number of female professors, ETH Zurich specifically encourages qualified female candidates to apply.

PENN SCHOLARS IN MOLECULAR MEDICINE

Penn Medicine

The Department of Medicine at the University of Pennsylvania School of Medicine seeks candidates for several Assistant, Associate, and/or Full Professor positions in the tenure track. Rank will be commensurate with experience. Applicants must have an M.D or M.D./Ph.D. degree. B/C B/E in Internal Medicine.

The University of Pennsylvania School of Medicine Department of Medicine announces the Penn Scholars in Molecular Medicine.

Through this program, we seek to recruit outstanding physician scientists interested in the interface between basic investigation and translational medicine. Faculty members in the Penn Scholars in Molecular Medicine will have appointments in both the Department of Medicine and the basic science department that most closely corresponds to the investigator's area of research. In addition to providing an environment rich in scientific mentorship and collaboration, appointees to the Penn Scholars in Molecular Medicine program will receive generous start up packages to support the establishment of a robust research program.

The successful applicant will direct a productive, independent basic or translational research program in addition to complementary clinical service and teaching. Applicants are being considered for all Internal Medicine disciplines; however, we are particularly seeking those with specialty in Hematology-Oncology, Renal, Electrolyte and Hypertension, or Pulmonary, Allergy and Critical Care. Applicants with a strong record of independent funding and peer-reviewed publications will be given preference.

The University of Pennsylvania is an equal opportunity, affirmative action employer. Women and minority candidates are strongly encouraged to apply.

Apply for this position online at:
http://www.med.upenn.edu/apps/faculty_ad/index.php/g323/d2347

UCDAVIS SCHOOL OF MEDICINE

UCDAVIS School of Veterinary Medicine

FACULTY POSITION

THE CENTER FOR COMPARATIVE MEDICINE
Schools of Medicine and Veterinary Medicine
University of California, Davis

Candidates are sought for a tenure-track position at the level of **ASSISTANT** or **ASSOCIATE PROFESSOR/ASSISTANT** or **ASSOCIATE PROFESSOR IN RESIDENCE** in the Center for Comparative Medicine, a research center at the University of California, Davis, co-sponsored by the Schools of Medicine and Veterinary Medicine and a relevant Instructional and Research (I&R) academic department. The center is engaged in investigative research involving animal models of human disease. We seek individuals with D.V.M and/or Ph.D. degrees or equivalent, postdoctoral experience and a record of publication in high-quality journals. We are soliciting applications from candidates who have enthusiasm for the investigation of human infectious diseases in animal models and the concepts of "One Health". Candidates are expected to have or to establish and maintain a strong extramurally funded research program and to participate in professional and graduate education in their fields. Ample office and laboratory space is available in the Center (including access to BSL2 and BSL3 laboratory space), with state-of-the art facilities, instrumentation, and administrative support. Center research and teaching programs interdigitate with other campus-wide programs and resources in the Schools of Medicine and Veterinary Medicine, the Mouse Biology Program, the California National Primate Research Center, and the Cancer Center. Faculty members will hold an academic appointment in the commensurate department of the School of Veterinary Medicine. The position will provide 0.5 salary support. Review of applications will commence immediately until the position is filled. Priority will be given to applications received by October 1, 2010.

Submit applications with letter of interest, curriculum vitae, concise statement of present and future research plans, summary of teaching experience, up to three representative reprints, and names of four references (including addresses, telephone numbers and e-mail addresses) to: **Recruitment Committee Chair, c/o Center for Comparative Medicine, University of California, Davis, CA 95616**.

The University of California is an Equal Opportunity/Affirmative Action Employer.

Executive Director of the North Pacific Research Board

The North Pacific Research Board (NPRB) is seeking exceptional candidates for the position of Executive Director. Congress created the NPRB in 1997 to recommend marine research initiatives to the US Secretary of Commerce, who makes final funding decisions. More information about NPRB and the position is available at **http://www.nprb.org/**.

Candidates should submit a letter of application, curriculum vitae, and a two-page summary of their philosophy on guiding collaborative research. Please send paper and electronic versions of these documents with contact information for four references to:

Cindy L. Ecklund
Senior Human Resource Manager
Alaska SeaLife Center
PO Box 1329
Seward, AK 99664-1837
cindy_ecklund@alaskasealife.org

Applications will be accepted until **August 30, 2010** and review of applications will take place in September with an anticipated start date of January 1, 2011.

NPRB is committed to Affirmative Action, Equal Opportunity and the diversity of its workforce.

Lamont-Doherty Earth Observatory
COLUMBIA UNIVERSITY | EARTH INSTITUTE

Faculty Position in Biogeoscience in the Department of Earth & Environmental Sciences and the Lamont-Doherty Earth Observatory of Columbia University

The Department of Earth and Environmental Sciences seeks applicants for a faculty position in biogeoscience, at the tenure track or tenured level. We seek applicants engaged in process-oriented research who will bring crucial new skills, such as use of molecular-level tools, innovative remote sensing techniques, new insight or methodology for understanding biogeochemical cycles, specialist knowledge of ecosystem energetics, and/or application of nano-scale techniques. Our ongoing research in fields related to biogeoscience includes study of biogeochemistry and geochemistry, paleoecology, ecophysiology, climate and paleoclimate, oceanography and paleoceanography, geologic carbon capture and storage, fluid-rock interaction, and the human dimensions of environmental change. Preference will be given to strong applicants who can integrate their work within this spectrum.

Minimum requirements for the position are demonstrated scientific creativity, specialist knowledge in both biology and geoscience, a Ph.D. in a biogeoscience-related field, and capability to teach at the undergraduate and graduate level. Application review will commence immediately and continue until the position is filled. For more information and to apply for this position please visit our online site at:

https://academicjobs.columbia.edu/applicants/Central?quickFind=53131

Questions can be addressed to Peter Kelemen (peterk@LDEO.columbia.edu), Chair of the Search Committee.

Columbia University is an Equal Opportunity/Affirmative Action employer.

OLD DOMINION UNIVERSITY

CHAIR/PROFESSOR, DEPARTMENT OF CHEMISTRY AND BIOCHEMISTRY

Old Dominion University (**http://www.odu.edu**) invites applications and nominations for the position of Chair, Department of Chemistry and Biochemistry, in the College of Sciences. We seek an outstanding scholar with demonstrated excellence in research, international recognition, consistent peer-reviewed research grant funding, and a strong commitment to educational programs at the undergraduate and graduate level. The successful candidate will have a Ph.D. in Chemistry, Biochemistry or some related discipline, will provide leadership to further enhance the Department's excellent research and educational programs and will have a strong commitment to teaching and mentoring junior faculty, post-doctoral fellows, and graduate and undergraduate students.

Old Dominion University is a state supported, Carnegie doctoral research-extensive institution enrolling more than 24,000 students of which 6,000 are graduate students. The Department of Chemistry and Biochemistry has 17 faculty members with research strengths in physical and analytical chemistry, biochemistry, computational chemistry, geochemistry and materials chemistry, and strong programs in undergraduate and graduate education. There is a commitment to build a strong energy-related research and teaching program. The department offers Ph.D. and M.S. degrees in Chemistry and Biochemistry. Departmental faculty also participate in joint Ph.D. programs with the Department of Biological Sciences (Biomedical Sciences) and with the Department of Ocean, Earth & Atmospheric Sciences (Chemical Oceanography). Currently a total of 45 graduate students are enrolled (34 Ph.D. and 11 M.S.).

Candidates should submit a curriculum vitae, a statement of research and teaching interests, and arrange for four letters of reference to be sent electronically to **chemchairsearch@odu.edu** or to **Dr. J. Mark Dorrepaal, Chemistry and Biochemistry Search Committee Chair, Department of Mathematics and Statistics Chair, 2300 E&CS Bldg., Old Dominion University, Norfolk, VA 23529.** The review of applications will begin immediately and continue until the position is filled.

Old Dominion University is an Affirmative Action/Equal Opportunity institution and requires compliance with the Immigration Reform and Control Act of 1986.

GRANT FOR POSTDOCTORAL POSITIONS IN SWEDEN

This grant enables researchers with doctorates (PhDs or equivalent) to work at Swedish higher education institutions or research establishments. The programme spans two years. Research areas:

- Natural Sciences
- Engineering Sciences
- Medicine
- Humanities
- Social Sciences
- Educational Sciences
- Artistic research and development

Call for applications opens early July.
Submission deadline is August 26, 2010.

Further information at www.vr.se

Vetenskapsrådet

Scientist Positions at Novo Nordisk China R&D Center

Zhongguancun Life Science Park, Beijing, China

Novo Nordisk is a world leader in diabetes care. Novo Nordisk China R&D (NNST) is an integrated part of Novo Nordisk R&D organization. Our newly formed Diabetes Research Department is expanding rapidly and we therefore have the following 4 positions open for highly qualified scientists planning to advance a career in China.

For all positions, excellent communication skills in English, flexibility and the desire to work within a multidisciplinary team are required. Industry and patent experience is strongly preferred. Title and compensation will be based on qualifications. For full job advertisements, please visit **http://www.ebiotrade.com/jobf/readall1.asp?cmpidn=y2003527103359.**

For application or further information, please send e-mail with job code in the header to **InfoNNST@novonordisk.com**.

Principal Scientist – Diabetes and Obesity Biology [Job Code: DR-Biol]

Responsibility:
Defining and performing biological evaluations in research projects.

Requirements:
- Ph.D. within biological sciences and excellent scientific background with proved expertise in diabetes and/or obesity biology.
- Minimum 5 years working experience within diabetes/obesity research (*in vitro* and/or *in vivo* biology and pharmacology) at principal scientist or professor level.

Scientist – Computational Biology [Job Code: DR-CompBiol]

Responsibility:
Start up the use of expression profiling technology, providing systems biology and bioinformatics expertise in our diabetes research projects in collaboration with colleagues in the US and in Denmark.

Requirements:
- Ph.D. within computational biology, focus on expression profiling and a high degree of biological understanding.
- Solid hands-on experience and in-depth knowledge in bioinformatics: Developing methodologies to analyze large datasets of microarray or sequencing-based expression profiling, using statistical analysis and integrating results with relevant large scale datasets.
- Experience in programming and ability to transform conclusions into biology.

Scientist – *In vivo* Pharmacology [Job Code: DR-Pharmacol]

Responsibility:
Defining and performing *in vivo* evaluations in research projects.

Requirements:
- Ph.D. within experimental animal science, *in vivo* pharmacology, veterinary medicine, medicine, pharmacy or other relevant area. >2 years of postdoctoral experience is preferred.
- Excellent scientific background within diabetes and/or obesity pharmacokinetics and/or pharmacodynamics.

Scientist - Molecular Biology/Protein Expression [Job Code: DR-MB]

Responsibility:
Developing and optimizing recombinant protein expression systems, especially *E.coli.*

Requirements:
- Ph.D. in Molecular Biology, Biochemistry or relevant biological science, 2-5 years experience in protein expression and engineering.
- Solid theoretical basis and hands-on experience within molecular biology, special focus on *E.coli.*
- Knowledge within process development, fermentation and protein separation processes is an advantage.

Furthermore, we have 2 positions within our biopharmaceutical research departments:

- Senior/Principal Scientist in Protein Chemistry
- Scientist in Cell Biology

Novo Nordisk is an international healthcare company, the world leader in diabetes care and has leading positions within haemophilia management, growth hormone therapy and hormone replacement therapy. For more information, see ***www.novonordisk.com*** *.*

Nontraditional Careers:

Opportunities Away From the Bench

Webinar

Want to learn more about exciting and rewarding careers outside of academic/industrial research? View a roundtable discussion that looks at the various career options open to scientists across different sectors and strategies you can use to pursue a nonresearch career.

Now Available
On Demand
www.sciencecareers.org/webinar

Participating Experts:

Dr. Lori Conlan
Director of Postdoc Services,
Office of Intramural Training and Education
National Institutes of Health

Pearl Freier
President
Cambridge BioPartners

Dr. Marion Müller
Director, DFG Office North America
Deutsche Forschungsgemeinschaft
(German Research Foundation)

Richard Weibl
Director, Center for Careers in Science and Technology
American Association for the Advancement of Science

Produced by the
Science/AAAS Business Office.

Science Careers
From the journal *Science* AAAS

UNIVERSITY OF LIVERPOOL

School of Biomedical Sciences and MRC Human Genetics Unit, Edinburgh

Postdoctoral Researcher in Adult Tissue Homeostasis

£30,747 pa

This project will study the important area of adult tissues maintenance and regulation of tissue homeostasis. Preliminary data from the Hastie and the Wilm laboratories, serve as strong basis for the analysis of mesothelial cells and the Wilms' tumour gene (Wt1) in tissue maintenance/homeostasis. This joint project starts at the MRC (Hastie laboratory) in Edinburgh (first 6-9 months), and continues at the University of Liverpool (Wilm laboratory). You should have a PhD in cell biology or mouse genetics. Experience in any aspect of this work is desirable. The post is funded by the Wellcome Trust and is available for 3 years.

Job Ref: R-572658/S **Closing Date: 6 August 2010**

For full details, or to request an application pack, visit www.liv.ac.uk/working/job_vacancies/ or e-mail jobs@liv.ac.uk Tel 0151 794 2210 (24 hr answerphone) please quote job ref in all enquiries.

COMMITTED TO DIVERSITY AND EQUALITY OF OPPORTUNITY

Stonewall DIVERSITY CHAMPION

POSITIVE ABOUT DISABLED PEOPLE

E A M **ENGINEERING OF ADVANCED MATERIALS**

The Friedrich-Alexander-Universität Erlangen-Nürnberg with its 26,000 students and 12,000 employees is one of the leading European research universities with a strong focus on engineering, natural sciences and medicine. The university is committed to excellent research and interdisciplinary academic education.

The research cluster of excellence „Engineering of Advanced Materials – Hierarchical Structure Formation for Functional Devices" is supported by the German Excellence Initiative and focuses on the science and engineering of hierarchical materials organised from the molecular to the macroscopic levels and the related process technologies. Based on a coherent methodological approach the following research areas are explored:

- **Cross-cutting topics: particle technology, nanomaterials characterization and multiscale modeling and simulation**
- **engineering of nanoelectronic materials**
- **engineering of photonic and optic materials**
- **engineering of catalytic materials**
- **engineering of lightweight materials**

The vision of the cluster is to bridge the gap between fundamental research and real-world applications of modern high-performance materials in key scientific and engineering areas.

As part of the cluster's **Rising Star Program** leadership positions are available for independent, interdisciplinary, and fundamental research. The Cluster invites applications for

1 Junior Professorship (W1, tenure track)

Candidates with an excellent track record in at least one of the mentioned research areas are eligible to apply. As fellows of the programme they will be granted flexible resources for three years and will be expected to establish a research group within the cluster. The successful candidate is expected to develop an internationally recognized fundamental research program strongly interlinked with the cluster's research areas.

Applicants should be exceptional junior researchers with outstanding university undergraduate and doctoral degrees in natural sciences or engineering as well as excellent teaching skills. Applicants with post-doctoral employment in Germany should not exceed the maximum employment period of six years according to German law. Appointments are for three years initially with the possibility of a further extension for another three years, following a positive evaluation. Assuming success during this six year period and subject to the fulfillment of certain legal requirements, candidates will be offered promotion to the rank of a W2 Professor (tenure track).

The Universität Erlangen-Nürnberg actively encourages applications from female candidates in an effort to increase female representation in research and teaching.

Given equal suitability for the appointment the applications of disabled candidates will be given priority.

The position is available immediately.

Application documents (curriculum vitae, photograph, copies of degree certificates and a selection of the most important publications) and a brief statement of research interests (not more than 3 pages) must be submitted before **2010-08-20** by e-mail to:

Friedrich-Alexander-Universität Erlangen-Nürnberg
Cluster of Excellence Engineering of Advanced Materials
Prof. Dr.-Ing. Wolfgang Peukert
Nägelsbachstr. 49b
D-91052 Erlangen
e-mail: administration@eam.uni-erlangen.de
www.eam.uni-erlangen.de

Friedrich-Alexander-Universität Erlangen-Nürnberg

www.uni-erlangen.de

UCL

UCL Division of Biosciences
Research Department of Genetics, Evolution and Environment

Chair in Evolutionary and Population Biology

The appointment will be full time on the UCL Professorial grade. The salary range will be negotiable on the professorial scale but not less than £61,713 per annum, inclusive of London Allowance.

We invite applications from world class research scientists using theoretical or experimental approaches, with no restriction on organism or level of biological organisation studied. The appointment is part of a major initiative to strengthen and diversify research activity in evolutionary, population and environmental biology in newly refurbished laboratories within UCL.

The successful candidate will be expected to play a leadership role in this initiative and promote interaction across the diverse disciplines represented in the Department, the Division of Biosciences and across UCL, as well as co-ordinate efforts to respond to national and international funding initiatives. Furthermore, the successful candidate will play an important part in developing existing and new postgraduate training programmes and contribute to undergraduate teaching.

The successful candidate will have an international reputation in an area of Evolutionary and Population Biology and a track record of running a successful research group, securing competitive funding over a number of years and publishing high impact original research articles.

For further details about the vacancy and how to apply online please go to http://www.ucl.ac.uk/hr/jobs/ and search on Reference Number 1127113.

Informal enquiries may be made to Professor Andrew Pomiankowski, tel: +44 (0)20 7679 7413; email: a.pomiankowski@ucl.ac.uk. Queries regarding the application process should be addressed to Nick McGhee, tel: +44 (0)20 7679 8878; email: n.mcghee@ucl.ac.uk.

Closing Date: 3rd September 2010.

Interview Date: Week commencing 11th October 2010.

We particularly welcome female applicants and those from an ethnic minority, as they are under-represented within University College London at this level.

Ri.MED FOUNDATION

Fondazione Ri.MED

Call for applications for the awarding of

5 Postdoctoral Fellowships

for training and research in the field of biotechnology and biomedicine in laboratories of the University of Pittsburgh

(Ref. Ri.MED – Ric/10)

The Ri.MED Foundation was created in 2006 as an international partnership between the Italian Government, the Region of Sicily, the National Research Council, the University of Pittsburgh, and the University of Pittsburgh Medical Center (UPMC) with the mission of improving health through research in Sicily and worldwide.

The Foundation also focuses on supporting regional economic growth through creating job opportunities as well as promoting basic and translational research.

The Foundation will contribute to developing biomedical research and a biotechnology industry in Sicily by establishing the Biomedical Research and Biotechnology Center (BRBC). The Center, housed in a state-of-the-art laboratory complex soon to be constructed near Palermo, is designed to undertake biomedical research that may ultimately lead to new drugs, vaccines, other biological products, and technologies.

In preparing the scientific workforce that will populate the BRBC, the Foundation is calling for applications for the assignment of five (5) one-year fellowships (renewable on an annual basis) to be awarded on the basis of qualifications and interviews.

Selected candidates will undertake their training and research activities in the laboratories of the University of Pittsburgh in the fields of Structural Biology, Computational Biology, Drug Discovery, Vaccine Development, Biomedical and Tissue Engineering/Regenerative Medicine, Molecular Imaging, and Neuroscience.

Eligible fellowship candidates must meet the following requirements: **Degree in Medicine and Surgery, OR other doctoral Degree relevant to biomedical research. The Degree should already have been achieved or to be obtained by December 31, 2010.**

Also required: excellent (spoken/written) **English and Italian language** and good knowledge of main software applications. Preferred: previous research experience in one of the aforementioned areas.

Candidates of both sexes are requested to submit their on-line applications by **July 30, 2010** at **www.fondazionerimed.com**

Ri.MED Foundation – Piazza Sett'Angeli 10, 90134 Palermo.

PCR Products

Evolutionary qRT-PCR begins with One-Step

One-Step SYBR® *Ex Taq*™ qRT-PCR Kit

Takara's One Step SYBR® *Ex Taq*™ qRT-PCR Kit combines a new RTase with increased speed and exceptional elongation capability with Takara's high-specificity, high-sensitivity *Ex Taq*™ Hot Start DNA Polymerase. This combination provides excellent amplification rates and reaction specificity for detection of even low abundance samples like RNA viruses. The one-step, single tube format is simple to assemble, reduces user error and minimizes risk of contamination. Takara's One-Step SYBR® *Ex Taq*™ qRT-PCR Kit provides a superior solution for any qPCR application.

One Step SYBR® qRT-PCR Kit

Three easy steps!

Step 1

Create a MasterMix with
- 2X One Step SYBR RT-PCR buffer
- *Ex Taq* HS
- RTase Enzyme Mix

Add:
- RNase free dH_2O
- Primers

Step 2

Add:
- Template RNA

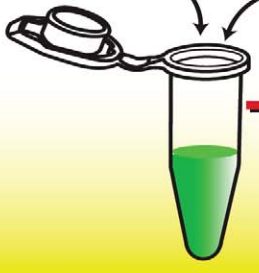

Step 3

Place Tube in Real Time PCR Machine

Use standard protocols:
- RT-PCR
- Melt Curve Analysis

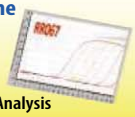

- **Efficient:** Uses new RT with strong elongation activity and high-performance *Ex Taq*™ Polymerase.
- **High Specificity:** Optimized buffer system and antibody mediated hot start.
- **Highly Sensitive:** Accurate quantification of low abundance samples such as RNA viruses.
- **Simple Protocol:** One step qRT-PCR reduces pipetting steps and risk of contamination.

SAMPLE Available

Also available without SYBR®, see our website for details.

TaKaRa

For more information
www.takara-bio.com

Japan:
Takara Bio Inc.
+81 77 543 7247
www.takara-bio.com

USA:
Takara Bio USA
A Division of Clontech Laboratories, Inc
888-251-6618
www.takara-bio.us

Europe:
Takara Bio Europe S.A.S.
+33 1 3904 6880
www.takara-bio.eu

China:
Takara Biotechnology (Dalian) Co., Ltd.
+86 411 8764 1681
www.takara.com.cn

Korea:
Takara Korea Biomedical Inc.
+82 2 2081 2525
www.takara.co.kr

R&D Systems High Quality Reagents for Developmental Biology Research

R&D Systems offers a wide range of high quality products for developmental biology research. We are proud to offer premium quality active cytokines, growth factors, and morphogens. Our high performance antibodies and ELISA kits can be used for the study of axon guidance, angiogenesis, pattern formation, and cell fate. Our catalog also includes primary cells, culture media, and kits for the expansion and differentiation of embryonic, neural, mesenchymal, and hematopoietic stem cells.

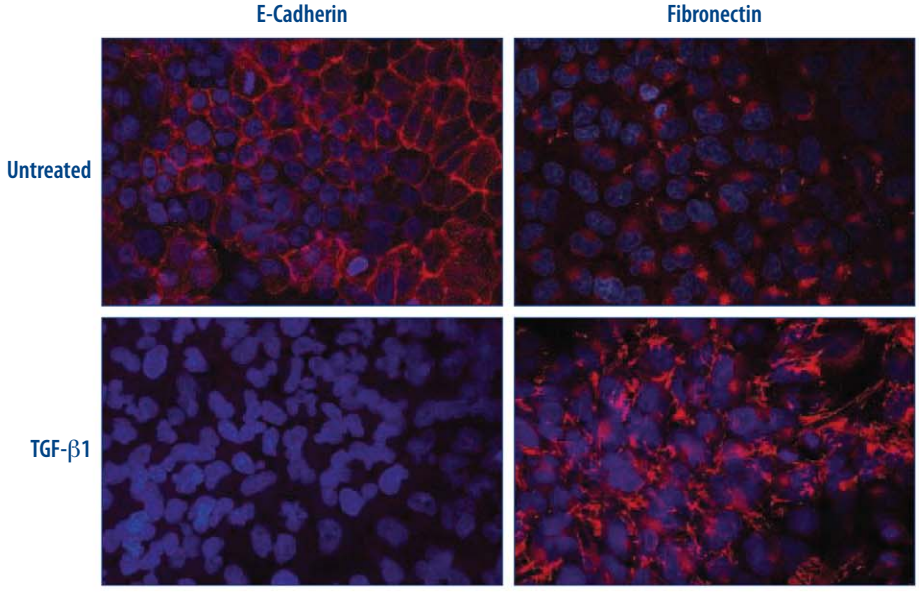

Induction of Epithelial to Mesenchymal Transition by TGF-β1. A549 human lung carcinoma cells were treated with 10 ng/mL TGF-β1 (Catalog # 240-B) for 24 hours to induce epithelial to mesenchymal transition (EMT), a process which is essential for gastrulation and neural crest cell migration. R&D Systems antibodies reveal downregulation of the epithelial marker E-Cadherin (Catalog # AF648) and concurrent upregulation of the mesenchymal marker Fibronectin (Catalog # AF1918).

For more information visit our website at www.RnDSystems.com/go/Development

R&D Systems, Inc. www.RnDSystems.com

R&D Systems Europe, Ltd. www.RnDSystems.co.uk

R&D Systems China Co., Ltd. www.RnDSystemsChina.com.cn

R&D SYSTEMS®